The role of windblown dust from ephemeral river valleys in the fertilisation of the Benguela Upwelling System



Andrew Dansie

Clarendon Scholar

School of Geography and the Environment

Linacre College

University of Oxford

Thesis submitted Michaelmas Term 2016-17 for the degree of

Doctor of Philosophy

Supervisors:

Prof. David Thomas, Professor of Geography

School of Geography and the Environment at the University of Oxford

Prof. Giles Wiggs, Professor of Aeolian Geomorphology

School of Geography and the Environment at the University of Oxford

Abstract

The deposition of dust on the global ocean provides essential nutrients for biological primary production. Research into aeolian dust has focused on dust sources identified at the global scale by the emission of mineral aerosols a minimum of one kilometre into the atmosphere. The deflation origins of these global hot-spots of dust are major topographical pan features providing paleolacustrine sources of fine, desiccated sediment that is highly susceptible to wind erosion. However, small-scale geomorphological features are being increasingly identified as significant emitters of dust. Namibia's twelve western ephemeral river valleys are known to regularly produce dust but have remained largely overlooked as a regionally significant source of dust and as a contributor to ocean fertilisation. The depositional area of the river valley dust is the adjacent marine Benguela Upwelling System which hosts one of the highest primary production rates in the world's oceans. In this research correlation between terrestrial airborne dust concentrations, aeolian dust and oceanic chlorophyll levels is assessed and the fertilisation potential of dust from three river valleys is investigated. The results provide the first direct evidence of the contribution of river valley dust to ocean fertilisation within the highly productive Benguela upwelling system. The research further shows that Namibia's river valleys provide an enriched source of aeolian nutrients, most importantly for bioavailable iron, with windblown dust and source sediments having a higher fertilisation potential than either of southern Africa's major pan dust source areas. These enriched sediments in the dust-emitting lower regions of the three river valleys are shown to occur irrespective of upper catchment rainfall, land use or geology. This suggests that similarly enriched dust source sediments would be common to all twelve valleys, resulting from comparable geomorphological processes, and the river valleys are therefore a regionally significant source of ocean fertilising dust. This research demonstrates the impact that small-scale dust sources can have and that riverine dust sources can be a source of highly fertile mineral aerosols that warrant increased research attention.

Acknowledgements

I would like to thank first and foremost my supervisors Dave and Giles for whose tremendous support, patience and perseverance I am forever indebted. Their knowledge and passion is something I will carry with me throughout my professional and personal life. My DPhil at Oxford would not have been possible without the support of the Clarendon Fund and the Oxford University Press and for their generous provision of my four-year scholarship I will be forever thankful. The research would not have been possible without the valued and meaningful support of the Dust Observation for Models (DO4 Models) research project, the Natural Environment Research Council grant NE/H021841/1 and the John Fell Fund that provided partial support of fieldwork activities. The Namibian Ministry of Environment and Tourism is thanked for their support and assistance, especially with access to field sites permitted under permit number 1788/2013.

The fieldwork for this research was an adventure in itself and the staff at the Gobabeb Research and Training Centre are thanked for their assistance, friendship and welcoming arms after weeks out in the desert. Their responsive and selfless assistance after the car accident during fieldwork is especially noted as is the support of Ed Humphry, Honorary Consul at the Australian Consulate in Namibia, Ian Livingstone and Rob Bryant whilst in hospital.

Kelly Munkittrick and Kendra McLaughlan are gratefully thanked for supporting large parts of the nutrient analyses with further support from Dave Thomas for BSNE sample analysis. Mona Edwards and Hong Zhang's assistance in the SOGE Geolabs is also gratefully acknowledged. Chris Doherty is deeply thanked for his time and training in the use for the SEM with in the Oxford Research Laboratory for Archaeology. Ian Ashpole's tireless efforts to instill remote sensing analytical abilities in me are tremendously thanked as is Jerome Mayaud for his advice and support in statistical analyses. James King, Sebastian Engelstädter and Richard Washington are thanked for their support and advice both in the field and during the subsequent analyses. Robert Bryant and Michael Fettweis are thanked for their advice on remote sensing tools and data.

Linacre College has provided me with more than I could have ever imagined and I thank the College and its community for making my time in Oxford so rewarding. The 'Linacore' are thanked for being there in both the good times and the hard times and I look forward to the rest of our life-long friendships.

Laura, the one who I owe so much, thank you for your support, patience, assistance and for being there for me in every way. I am so lucky to be sharing all of our upcoming adventures with you. Lastly my parents, Sylvia and Phil, and brother Mark who have supported me in everything I have done. I would not be here without you, thank you for each and every support you have provided along the way and up to this very day.

Table of Contents

SECTION 1

1 Introduction 1

1.1 The ephemeral valleys of Namibia as sources of ocean fertilising dust 1

1.2 Research Question and Aims 7

1.3 Thesis Scope and Structure 9

2 The World of Dust and Ocean Fertilisation 15

2.1 Introduction 15

2.2 Global dust sources 16

2.2.1 River dust sources 19

2.2.2 Ephemeral Rivers 22

2.3 Dust flux to the ocean 24

2.3.1 Global ocean productivity, biochemistry and nutrients 26

2.3.2 Phytoplankton response to aeolian deposition events 33

2.3.3 Atmosphere-Ocean nutrient cycling 39

2.4 Dust nutrient loading – importance of source 46

2.4.1 Nutrient loading of dust sources 48

2.4.2 Rivers and aeolian dust research 52

2.5 Southern African Dust 54

2.5.1 Dust Sources 54

2.5.2 Dust from Namibian River Valleys 58

SECTION 2

3 Regional Setting 67

3.1 Wind patterns 69

3.2 The Dry River Valleys of Western Namibia 70

3.2.1 Catchment landscape 72

4 Methodology 77

4.1 Introduction 77

4.2 Monitoring stations 79

4.3 Sample collections 86

4.3.1 Windblown Dust 86

4.3.2 Surface Sediments 87
4.4 Laboratory Analysis 92
4.4.1 Chemical Analyses 92
4.4.2 Field and Laboratory Quality Assurance and Quality Control 94
4.4.3 Grain Size Distribution Analysis 98
4.4.4 Grain Size Analyses Quality Assurance and Quality Control 100
4.4.5 Scanning Electron Microscope 104
4.5 Remote sensing 105
4.5.1 Data acquisition 105
4.5.2 Data analyses 109

SECTION 3

5 Paper 1 - Iron and nutrient content of wind-erodible sediment 115
5.1 Introduction 117
5.2 Research Design and Methods 121
5.2.1 Regional setting 121
5.2.2 Research Design 122
5.2.3 Methods 125
5.3 Results 127
5.3.1 Grain size characteristics 127
5.3.2 Bioavailable Fe, N and P content 130
5.4 Discussion 134
5.4.1 Sediment size and suitability for aeolian transport 135
5.4.2 Nutrient content of sediments within southern Africa 135
5.4.3 Ocean fertilisation 142
5.5 Conclusions 142
6 Paper 2 - Spatial variability of river catchment nutrients 145
6.1 Introduction 147
6.2 Study Sites 150
6.2.1 Regional Setting 150
6.3 Research Design 154
6.3.1 Field Sites 154
6.3.2 Sampling strategy 156
6.4 Methods 158
6.4.1 Chemical Analyses 159

6.4.2 Grain Size 159
6.5 Results 160
6.5.1 Nutrient concentrations along the hydrological system 160
6.5.2 Spatial distribution of nutrients across the upper catchments 164
6.6 Discussion 171
6.6.1 Nutrients and sedimentary units 171
6.6.2 Catchment-wide controls on nutrient patterns 174
6.7 Conclusions 175
7 Paper 3 - Windblown dust characteristics and fertilisation potential ... 177
7.1 Introduction 179
7.2 Regional setting 181
7.3 Methods 182
7.3.1 Field stations 182
7.3.2 Sample collection 186
7.3.3 Sample analysis 187
7.3.4 Chemical analyses 188
7.3.5 Grain size analysis 188
7.3.6 Identification of dust plumes over the ocean 189
7.4 Results and Discussion 190
7.4.1 Dust emission events 190
7.4.2 Grain size of windblown dust 196
7.4.3 Nutrient content of windblown dust 200
7.4.4 The regional fertilisation potential of windblown 203
7.5 Conclusion 206
7.6 SEM investigation of windblown dust samples 208
8 Paper 4 - Plumes and Blooms 215
8.1 Methods 225
8.1.1 Remote sensing 225
8.2 Extended Data 228
9 Conclusion 237
9.1 Research Aim and Objectives 237
9.2 Implication of findings within the Benguela Upwelling System 242
9.3 Global relevance and application 244
9.4 Prioritising future dust source research 248
10 Bibliography 253

List of Appendices

Appendix 1 – Paper 5 ……... 300

Appendix 2 – Windblown dust BSNE samples ……... 333

Appendix 3 – Laboratory analyses data …….. 339

Appendix 4 – Sample ID, collection location and maps ……. 346

Appendix 5 – Standard deviation table for duplicate samples …… 357

List of Figures

Figure 1 | Dust plumes emitted from Namibia's ephemeral river valleys. 5

Figure 2 | Schematic diagram of research components. 8

Figure 3 | Global distribution of major dust source areas. 17

Figure 4 | Map of riverine dust sources. 22

Figure 5 | Global map of dust flux to the ocean. 26

Figure 6 | Annual average global ocean surface concentrations of N and P. 30

Figure 7 | Spatial distribution of nutrient limitation in the global ocean. 32

Figure 8 | Global distribution of dust-phytoplankton studies. 34

Figure 9 | Nutrient uptake pathways following aeolian deposition. 41

Figure 10 | Weathering and solubility of Fe in desert soils. 51

Figure 11 | The major dust emission sites of southern Africa. 56

Figure 12 | Dust plumes off the coast of Namibia. 59

Figure 13 | Southern African dust plume source locations and frequency. 61

Figure 14 | Seasonal variations of wind direction in the central Namib Desert. 63

Figure 15 | Regional ocean and atmosphere circulation patterns. 69

Figure 16 | Namibia's ephemeral river catchments and topographical elevation. 72

Figure 17 | Monitoring station site locations. 80

Figure 18 | Meteorological monitoring mast and measurement equipment. 82

Figure 19 | DustTrak^{TM} DRX Aerosol Monitor 83

Figure 20 | DRX schematic diagram. 84

Figure 21 | Example of erected monitoring station instrumentation. 85

Figure 22 | a) Big Spring Number Eight (BSNE) aeolian sediment samplers. 87

Figure 23 | Sampling locations in the Huab, Kuiseb and Tsauchab catchments. 91

Figure 24 | Field duplicates nutrient analyses (Meh.P, Fe, NH_4^+, NO_3^-). 95

Figure 25 | Field duplicate analyses (Total N, Total P and pH). 96

Figure 26 | Laboratory duplicate analyses (Meh.P, Fe, NH_4^+, NO_3^-). 97

Figure 27 | Laboratory duplicate analyses (Total N, Total P and pH). 98

Figure 28 | Wet grain size distribution analysis sample duplicates. 101

Figure 29 | Dry grain size distribution analysis sample duplicates. 102

Figure 30 | Dry grain size analysis of dry-sieved sediment. 103

Figure 31 | Remote sensing area of investigation. 110

Figure 32 | Cross section sampling locations. 124

Figure 33 | Geomorphological units targeted along cross sections. 125

Figure 34 | Grain size of river valley, Etosha and Makgadikgadi Pan sediments. 128

Figure 35 | Classifications of river valley, Etosha and Mak. Pan sediments. 130

Figure 36 | Nutrient content of river valley, Etosha and Mak. Pan sediments. 132

Figure 37 | Grain size and nutrient scatter plots. 137

Figure 38 | Reduced Major Axis Regression analysis of TP and bioavailable P. 140

Figure 39 | Ephemeral river watersheds. 151

Figure 40 | Catchment characteristics and sampling locations. 153

Figure 41 | Overview of hydrological system sampling classification. 158

Figure 42 | Mean nutrient content of in-channel deposited fine materials. 161

Figure 43 | Nutrient enrichment ratios of lower-system fine channel deposits. 163

Figure 44 | Nutrient content of in-channel deposited coarse material. 164

Figure 45 | Catchment annual rainfall ($mm.yr^{-1}$) and sediment nutrients. 166

Figure 46 | Catchment geology and sediment nutrients. 167

Figure 47 | Catchment vegetation type and sediment nutrients. 169

Figure 48 | Catchment cattle densities and sediment nutrient concentrations. 171

Figure 49 | River hydrological sections and TN and TP. 172

Figure 50 | River hydrological sections and Mehlich P, Fe, NH_4^+, NO_3^-. 173

Figure 51 | Monitoring stations in the Huab, Kuiseb and Tsauchab. 184

Figure 52 | Typical monitoring station set up and instrumentation. 186

Figure 53 | Average two-minute TSP concentrations in the river valleys. 191

Figure 54 | Dust plumes emitted off the coast from the Huab and Kuiseb. 195

Figure 55 | Windblown dust grain size (individual and aggregated particles). 197

Figure 56 | Nutrient content of dust along entrainment profile. 202

Figure 57 | Bioavailable nutrient content of river valley dust and source sediment. 204

Figure 58 | Total N and Total P content of river valley dust and source sediment. 205

Figure 59 | Scanning electron of windblown dust samples. 211

Figure 60 | The Benguela Upwelling System location and annual cycles. 218

Figure 61 | Daily dust and chlorophyll correlations in the Benguela. 221

Figure 62 | Huab/Tsauchab dust measurements and daily dust/chlorophyll. 223

Figure 63 | Monthly dust and chlorophyll correlations in the Benguela. 228

Figure 64 | In-valley dust measurements and daily dust/chlorophyll/SST. 229

Figure 65 | In-valley dust and chlorophyll correlations in adjacent waters. 232

Figure 66 | Dust plume and chlorophyllic response plots (5 May). 233

Figure 67 | Dust plume and chlorophyllic response plots (17 June). 234

Figure 68 | Distinct upwelling-induced phytoplankton bloom on 10 December. 235

Figure 69 | Valley fill sampling sites for age determination. 240

List of Tables

Table 1 Identified dust sources of riverine origin. 20

Table 2 Chlorophyllic responses to dust deposition. 36

Table 3 Ocean fertilisation classification of Fe in depositional mineral aerosols. 45

Table 4 Station instrumentation. 81

Table 5 Volume weighted means of dry-sieved samples. 104

Table 6 Mean grain size variance of surface sediment classifications. 128

Table 7 Mean grain size fractions (%) of sediment units related to dust. 129

Table 8 Fine channel deposit enrichment ratio calculations. 131

Table 9 Mean bioavailable Fe concentrations river and pan dust source areas. 138

Table 10 Namibia ephemeral river catchment overview. 152

Table 11 Catchment land use variability according. 152

Table 12 River catchment sample classifications. 157

Table 13 Catchment classifications as defined by the Digital Atlas of Namibia. 158

Table 14 Deployed instrumentation. 185

Table 15 River valley airborne TSP concentrations. 192

Table 16 Average grain size class distribution of dust samples. 199

Table 17 Multi-day correlations of AOD and chlorophyll. 231

Table 18 Average dust concentration along river valleys during dust events. 231

List of Acronyms and Abbreviations

AAI - absorbing aerosol index

AAS - Atomic Absorption Analysis AAS

AOD - Aerosol Optical Depth

BUS - Benguela Upwelling System

Chl-a - chlorophyll *a*

CO_2 - carbon dioxide

DO4 Models - Dust Observation for Models research project

EBUS - eastern boundary upwelling systems

EOSDIS - Earth Observing System Data and Information

Fe - iron

GOCART - Goddard Global Ozone Chemistry Aerosol Radiation and Transport model

HNLC - High Nutrient, Low Chlorophyll Zone

LNLC - low nutrient low chlorophyll LNLC

MODIS - Moderate Resolution Imaging Spectroradiometer

N - nitrogen

P - phosphorus

SeaWiFS - Sea-Viewing Wide Field-of-View Sensor

SEM - Scanning Electron Microscopy SEM

SEVIRI - Spinning Enhanced Visible and InfraRed Imager

SRINTARS - Spectral Radiation-Transport Model for Aerosol Species

TN - total nitrogen

TOMS - Total Ozone Mapping Spectrometer

TP - total phosphorus

TSP – total suspended particulates

SECTION 1

- Research Context -

CHAPTER 1

1 Introduction

1.1 The ephemeral river valleys of Namibia as replenishing sources of ocean fertilising dust

Airborne dust is a critical component of Earth System behaviour, affecting atmospheric, oceanic, biological, terrestrial and human processes. Wind erosion in deserts is the major source of this dust (Mahowald et al., 2005) that, once airborne, can be transported for thousands of kilometres from its source across oceans and continents (Neff & Bertler, 2015; Middleton & Goudie, 2001), even circumnavigating the globe (Uno et al., 2009). Global estimates of dust emission to the atmosphere range between 1018 to 3000 Tg per year (Zender et al., 2004), or 1-3 billion tons. This mass of suspended sediment influences climate and biogeochemical cycles in a variety of ways. Individual dust particles can enhance atmospheric ice nucleation (Slater et al., 2015) thereby increasing cloud formation (Toon, 2003), with the potential to influence rainfall patterns far from their source (Creamean et al., 2013; DeMott et al., 2003). Conversely, desert dust has also been shown to cause smaller atmospheric droplets to form in clouds, thereby hindering the onset of precipitation (Rosenfeld et al., 2001). Atmospheric dust affects air temperature through the absorption and scattering of solar radiation (Liao & Seinfeld, 1998; Tegen & Lacis, 1996), which affects mean global temperature (Hansen et al., 1997). The dust's mineral and macronutrient composition is both defined by the source

material (Claquin et al., 1999) and influenced by atmospheric chemistry (Schulz et al., 2012; Shi et al., 2011; Hand et al., 2004) and, ultimately, contributes these atmospherically-processed minerals and nutrients to depositional environments. To date the role of dust deposition as a source of nutrient input has been recognized for terrestrial systems (Okin et al., 2004) and both freshwater (Reche et al., 2009; Tamatamah et al., 2005) and marine (Cassar et al., 2007; Prospero, 1996) aquatic environments.

The biological response of the marine environment to mineral aerosols plays a major role in atmospheric and oceanic systems. Aeolian inputs to the marine environment provide biologically essential iron (Fe) and macronutrients (namely Phosphorus (P) and Nitrogen (N)) to phytoplankton communities. These macronutrients and minerals are deposited on the light-abundant and oxygen-rich surface waters and influence primary production and thus carbon dioxide uptake, affecting atmospheric CO_2 levels (Ridgwell, 2003). The depositional dust input of nutrients and minerals are especially important in oceanic areas of high-nutrient-low-chlorophyll (HNLC) (Jickells et al., 2005), where aquatic nutrients required for photosynthetic growth are generally in abundance but with critical exceptions. While many challenges remain in understanding the complex biogeochemical interactions between atmosphere and ocean systems (Achterberg, 2014), it is mineral aerosols from dryland environments that are the predominant and most important sources of aeolian fertilisation material (Mahowald et al., 2008; Jickells et al., 2005).

To date the majority of research investigating dryland dust emission hot-spots has focused on formerly inundated lacustrine environments that are now dry (e.g. (McGowan & Clark, 2008; Todd et al., 2007; Washington et al., 2006)). The common geomorphology of these dust sources is a deep and extensive source of lacustrine material deposited during Quaternary wet phases (Prospero et al., 2002), with the now-dry lake

beds serving as a source of fine, desiccated material that is prone to deflation (Bryant et al., 2015; Vickery, 2014). The most eminent example of this is the world's largest dust emission source, the Bodélé Depression (Washington et al., 2009; Koren et al., 2006; Washington et al., 2003). Research on dust source areas has also included ephemeral lakes and pans, namely Owens Lake in the USA (Gillette et al., 1997), Lake Eyre in Australia (Bullard et al., 2008), the Makgadikgadi Pan system of Botswana (Haustein et al., 2015), Etosha Pan in Namibia (Bryant, 2003) and ephemeral lakes in Iran (Rashki et al., 2013). Modern ephemeral inflows may also serve to replenish sediment supply, and are then similarly susceptible to deflation once desiccated (Bryant et al., 2007). Further, the wetting and drying cycles of ephemeral systems lead to changes in ground-surface roughness upon drying that facilitate turbulence and surface disturbance (Nield et al., 2011) and crust break-up (Baddock et al., 2011; Reynolds et al., 2007). These seasonal geomorphological processes have been shown to enhance dust emission in ephemeral pan and lake systems but have not yet been widely investigated in ephemeral rivers.

Exposed riverine sediments have been known as a source of sediment fines that, upon desiccation, serve as beds of wind-erodible sediment (Nickling, 1978). Most recently this has been investigated in the glacial river systems of Iceland (Arnalds et al., 2016) and Alaska (Crusius et al., 2011), the midwest of the United States (Brungard et al., 2015), the dry valleys of Antarctica (Bhattachan et al., 2015b) as well as Iraq, Kuwait and the UAE (Jish Prakash et al., 2015). The high-latitude systems were shown to be notably rich in bioavailable Fe. Temperate and equatorial rivers are also well understood to concentrate and transport sediment and nutrients from the terrestrial to ocean realms. Yet ephemeral and drying rivers as sources of desiccated river fines have not yet received anywhere near the research attention of their pan and lake counterparts. Aeolian research is just now

beginning to recognise river valleys as productive dust source areas but little has been done to understand their potential regional and global importance.

A prime example is the reality that southern African dust research has largely focused on two such pan sites, the remnants of previously extensive inland water bodies that are now the Makgadikgadi Pan System in Botswana (Burrough et al., 2009) and Etosha Pan in Namibia (Brook et al., 2007), both which now see some ephemeral flooding (Bryant et al., 2007; Bryant, 2003). These sources have been hypothesised as a potentially important source of minerals for ocean fertilization (Piketh et al., 2000). It is now known that the dust source sediments in Makgadikgadi and Etosha Pans, prior to deflation, have enriched concentrations of phosphorus and nitrogen in the fine fraction (<45μm) compared to the larger-grained parent soil, but, in contrast, lower (bioavailable) iron concentrations are found in the finer fraction (Bhattachan et al., 2015a).

The ephemeral river valleys are consistent seasonal producers of dust, emitting ribbon-like plumes from their coastal valleys over the adjacent ocean (Figure 1). High-resolution remote sensing investigations have shown that the coastal regions of the ephemeral river valleys of Namibia are more frequent emitters of dust than either Makgadikgadi or Etosha Pans (Vickery et al., 2013; Eckardt & Kuring, 2005), with the total annual mass flux of dust likely being smaller than the pans. It is noted that dust emissions from the ephemeral rivers are in close proximity to the ocean in comparison to dust originating from Etosha Pan (400 km distant) and Makgadikgadi Pans (1200 km distant), and so their potential impact on ocean primary production is likely to be greater, dependant on the fertilisation potential of the deflated aerosols.

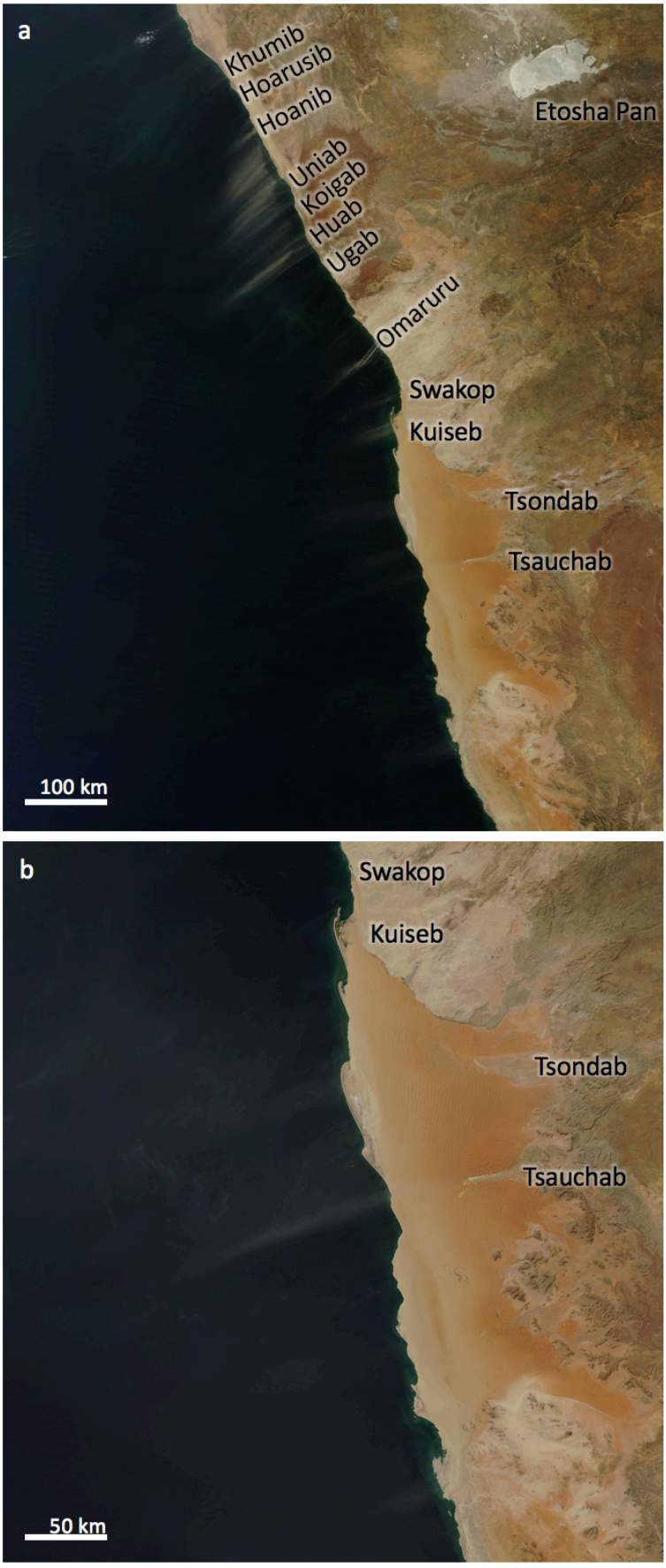


Figure caption over page

Figure 1 | Dust plumes emitted from the Huab and Kuiseb on (a) 05 May and (b) the Tsauchab on 04 May 2013 due to localised differences of wind strength between river valleys (discussed in Section 7.4.1). Additional plumes can also be seen emanating from other river valleys and coastal sabkas. While it appears that Etosha Pan is emitting dust westwards (light-coloured patch extending almost 100 km west from Pan edge) this is not dust but the terrain itself, coloured from deposited previously-deflated Pan sediments. Images from Earth Observing System Data and Information System (EOSDIS), NASA (2016).

Intermittent fluvial flows in dryland rivers are known to transport and deposit large volumes of sediment, including a high fraction of fines, from suspended sediment loads (Tooth, 2000). The dry river channels of Namibia's ephemeral rivers have been shown to contain enriched nitrogen and phosphorus alluvial sediments essential for desert biota (Jacobson & Jacobson, 2013; Jacobson et al., 2000). However, there has been limited assessment of the sedimentary characteristics of ephemeral river fluvial fines, and no quantification of the potential nutrient content with regards to the aeolian fertilisation on marine systems. This research provides the first analysis of the characteristics of both airborne dust and emission source material from Namibia's ephemeral rivers. Further, field-collected meteorological and airborne dust concentration data allows synchroneity between dust emission events and oceanic phytoplankton concentrations to be investigated using remote sensing.

The research presented in this thesis has been carried out in association with, but independently from, the Dust Observation for Models (DO4 Models) research project led by the School of Geography and the Environment at the University of Oxford in partnership with the University of Sheffield, Imperial College London and the University of Southampton and in collaboration with the Natural Environment Research Council

grant NE/H021841/1 and the John Fell Fund that provided partial support of fieldwork activities.

1.2 Research Question and Aims

Given the above context, this thesis aims to fill a significant research gap by investigating the properties of dust emitted from the Namibian valleys and its potential contribution to other environmental systems. The overarching aims are to determine the sediment characteristics, nutrient content and deflation dynamics of dust plumes from the ephemeral river valleys of Namibia, and secondly, to investigate whether chlorophyll concentrations in the southern Atlantic respond to observed dust events.

To address these aims a combination of meteorological measurement, dust monitoring, surface sample collection, laboratory analysis, and remote sensing analysis were undertaken (Figure 2). The research design and specific techniques are described in the methodology section and are used to complete the research objectives, which are to:

1. determine the sediment physical characteristics and nutrient content of surficial sediment in the dust-emitting dry river valleys along the coast of Namibia
2. investigate the spatial distribution of surficial sediment nutrient content along the river channels and upper catchments accounting for changes in and identify any relationships with climate, geology, and land use.
3. determine the physical characteristics and nutrient load of near-surface windblown sediment associated with large dust events derived from the ephemeral valleys.
4. investigate the potential response of phytoplankton in the Southern Atlantic Ocean to observed dust emission events.

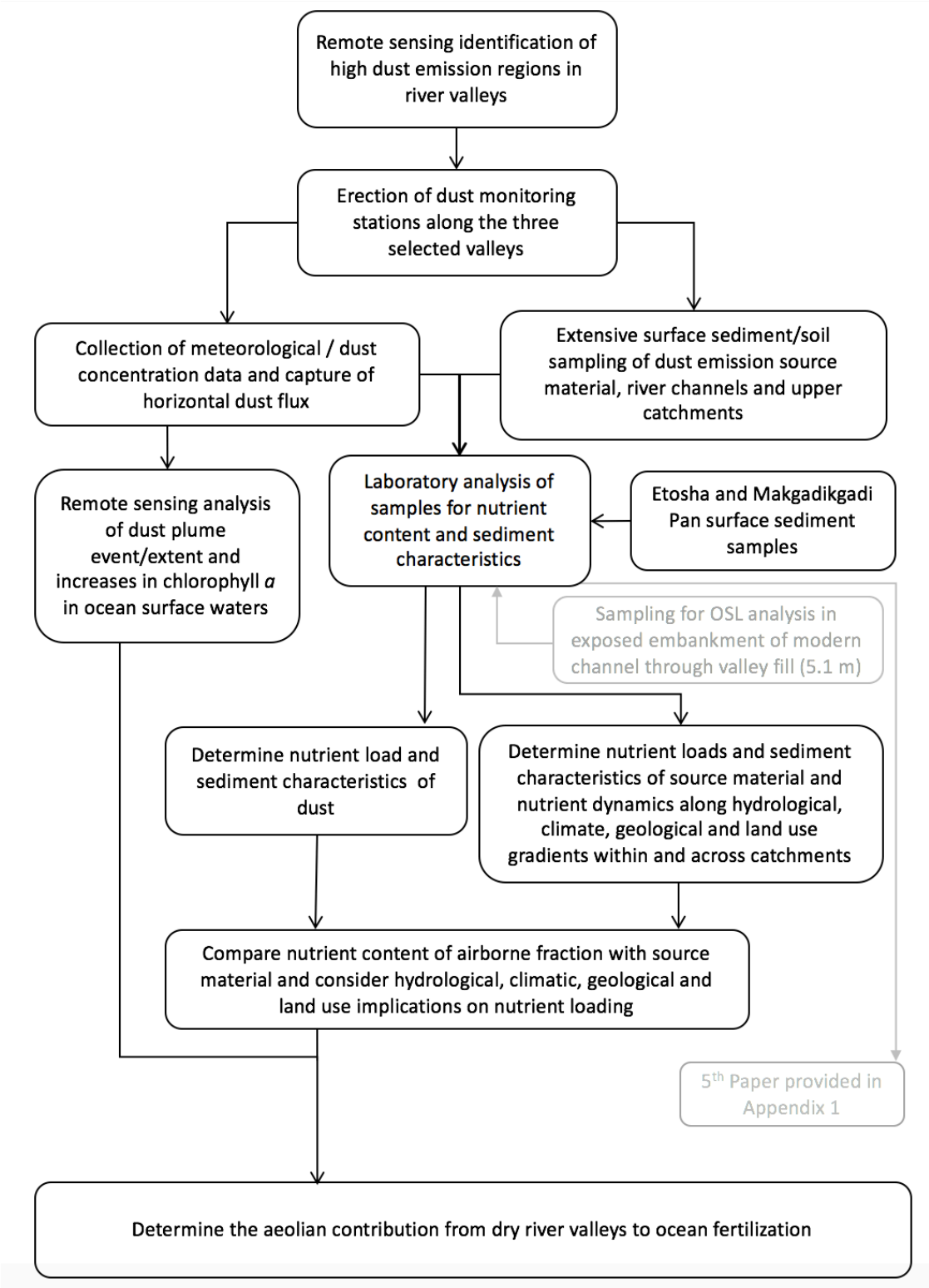


Figure 2 | Schematic diagram of research components.

1.3 Thesis Scope and Structure

This thesis comprises three sections; the first introducing the topic and presenting the research aims and objectives in Chapter 1 and providing the research context within the current state of knowledge in the literature in Chapter 2; the second section provides the regional context in Chapter 3 and the methodology in Chapter 4; the third section presents the research findings in Chapters 5-8 and the conclusion given in Chapter 9. This research has been prepared and submitted following the papers route with the four papers in Chapter 5-8 presented in their submitted format. Due to the nature of submission via the papers route some repetition in the context and methodology is seen between these chapters. This satisfies the requirements for the submission of a DPhil thesis. In addition to this, a fifth paper is provided as Appendix 1. This paper considers the temporal replenishment cycle of the dust source sediment and was contributed to in the forms of sample collection, additional laboratory analyses, data presentation/analyses and input to the draft under the direction of the lead author. A summary of the chapters within each section of the thesis is provided here.

SECTION 1 – RESEARCH CONTEXT

This section frames the importance of this research topic within the Earth System and introduces the particular relevance of dust on the global ocean in Chapter 1 with the research question and aims and thesis structure then provided. Chapter 2 then offers an in-depth review of the literature and the gap in knowledge that exists for atmosphere-ocean interactions that involve dust. The research need is framed within the increasingly studied association of nutrient content with mineral aerosols but highlighting that many uncertainties remain. This is explained by a paucity of data on the bioavailable suite of nutrients found in dust emission source areas and knowledge gaps on the cause and

attenuation of primary production constraints in nutrient limited regions of the global ocean. The relevance, knowledge gaps and understanding of global dust and deposition in the context of marine chemistry and nutrient limitations then leads into a southern African and, ultimately, Namibian ephemeral river focus of dust, nutrients and adjacent ocean environment considerations. This context is used to frame the importance of dust research and highlight the obscurities in the terrestrial-ocean feedbacks present off the coast of Namibia.

SECTION 2 – REGIONAL SETTING AND METHODOLOGY

This section comprises the Regional Context (Chapter 3) and Methodology (Chapter 4). It explains the overall research design and the rationale for the methods employed for field sampling, laboratory analysis, and remote sensing analysis. Standard operating procedures for laboratory analyses are also described to ensure the validity and reproducibility of results.

SECTION 3 - INVESTIGATION

This section provides the results of the research with Chapters 5-8 presented as journal-submitted papers that sequentially addresses one of each of the four research objectives. Chapter 9 is the concluding chapter that answers the overarching research aims and presents the global relevance and importance of the findings of this research.

Chapter 5 (Paper One) Iron and nutrient content of wind-erodible sediment in the dry river valleys of Namibia: The aim of this paper is to determine the nutrient content and grain size characteristics of sediments in the river valleys which are known to emit dust (Vickery et al., 2013). Further to this, a comparison of nutrient characteristics is made with other major dust emission sources of southern Africa, the pans of Etosha and

Makgadikgadi. Results show that the grain size of the sediment in the valleys (especially in-channel fines and valley fill) is suitable for deflation and aeolian transport with grain size distributions closely resembling those of Etosha and Makgadikgadi Pans. The major finding is that the ephemeral river valleys show a significantly higher level of bioavailable iron compared to Etosha and Makgadikgadi Pans. This, combined with the proximity of the river dust sources to the coast, suggest that the ephemeral river valleys should be considered as an important source of dust with a potential impact on ocean fertilisation.

Chapter 6 (Paper Two) Spatial variability of ocean fertilising nutrients in the dust-emitting ephemeral river catchments of Namibia: This paper builds on the fluvial and other geomorphological processes that are shown in Paper 1 to be important in the production of nutrient-rich fines. The aim is to investigate the spatial distribution of nutrients from the upper catchments to the river termini in three river catchments; the Huab, Tsauchab and Kuiseb. The three catchments are used to assess whether landscape characteristics (land use, geology, rainfall, vegetation type) influence the nutrient content of downstream fluvial sediments between river valleys. Downstream fluvial sediments were shown to be higher in nutrients than upper catchment surface sediments. In the upper catchments correlations were found between rainfall, vegetation and nitrogen, and between geology and phosphorus. However, no evidence was found suggesting that the nutrient content of sediments varied between catchments. A key finding was that concentrations of bioavailable Fe were consistently higher in the downstream river valley samples. The common geomorphological processes behind this enrichment would suggest that all twelve of Namibia's ephemeral river valleys are likely sources of bioavailable Fe-enriched sediment and could therefore potentially form a significant source of mineral aerosols important for ocean fertilisation.

Chapter 7 (Paper 3) Measurements of windblown dust characteristics and ocean fertilization potential: the ephemeral river valleys of Namibia: This paper aims to time the aerosol concentration, sediment characteristics and nutrient content of windblown dust emitted from Namibia's dry river valleys. The results provide the first TSP concentration measurements of dust-plumes from the river valleys that have only previously been defined in terms of emission frequency from remote sensing observations. The frequency of over-ocean dust plumes observed using remote sensing during the field season, with a focus on identifying those observed to terminate over the South Atlantic. Visually confirmation on satellite imagery is made for 18 dust plumes from the Huab, Kuiseb and Tsauchab off the coast in association with in-valley recorded dust events. Sedimentary characteristics (grain size of individual particles and sediment aggregates) of windblown dust in the valleys is shown to be highly suitable for long-range atmospheric transport and deposition over the ocean. The nutrient content of the emitted-material is shown to preserve the elevated nutrient content identified in the fine material of the contemporary channel and valley fill deposits discussed in Paper 1. The findings show that deflated sediment in the river valleys is both nutrient-rich and has the potential for long-range transport over the South Atlantic. This suggests that the deflated sediments are likely to be of regional significance with regards to ocean fertilisation potential.

Chapter 7 (addendum) SEM investigation of windblown dust samples: In addition to the analyses of grain size and nutrient content submitted in Paper 3, further investigation of grain shape and sediment aggregate characteristics of windblown dust was undertaken using SEM analyses and is presented here. Characterisation of grain shape provides insight into the aerodynamics, and therefore transport potential, of dust particles. The findings of the SEM investigation show the prevalence of plate-like flat particles in

captured dust that are characteristic of ephemeral river systems. The abundance of fluvially-derived crust fragments and assemblages in the deflated material provides explanation, by way of reduced chemical weathering of Fe-oxides, for the observed enrichment of bioavailable Fe seen in both the source material and deflated dust as presented in Papers 1, 2 and 3. Consideration is also given to the grain size fractions of seafloor sediments collected off the coast of Namibia. These aeolian fraction of these sediments, disaggregated upon dissolution in the seawater, are characterised as being finer than the in situ dust-particle size findings presented in this research and therefore not taking into account increased nutrients loading associated with deposition of aggregated aerosols.

Chapter 8 (Paper 4) Plumes and Blooms – Aeolian dust fertilises phytoplankton in the Benguela Upwelling System: This paper investigates the chlorophyllic response to aeolian dust over the depositional waters of the South Atlantic that are significantly influenced by the Benguela Upwelling System. The aim is to determine whether there is a phytoplankton growth response to deposition of the enriched windblown sediments identified in the previous findings. Remote sensing is used to determine the loading of mineral aerosols over the ocean and compare these with the concentrations of chlorophyll in the receiving waters. Sea surface temperature is also monitored using remote sensing to identify upwelling events of cold, nutrient-rich waters. Correlation of ocean chlorophyll levels is then investigated with the in-valley concentrations of windblown dust using field equipment measurements. The results show that a significant relationship exists between in-valley dust and chlorophyll at the daily scale and that rapid nutrient uptake is occurring of the highly bioavailable nutrients found in the river valley dust. Further correlation is shown with atmospheric aerosol concentrations and chlorophyll at the monthly scale. Both relationships show significance disconnected to sea surface temperature

demonstrating that aeolian fertilisation is a significant, and until now, overlooked component of the highly productive Benguela Upwelling System.

Chapter 9 - Conclusion: This chapter summarises the results and findings of Chapters 5-8 and assesses the degree to which they satisfy the research aims. Careful consideration of the Namibian ephemeral river valleys as significant dust emitters and an important source of nutrients for ocean fertilisation in a southern African and global context is proposed. Further, the global consideration of dry and ephemeral rivers as under-represented sources of nutrient-enriched dust is made. Both naturally dry rivers as well as drying rivers due to changing pluvial regimes and upstream damming are reflected on. The importance of the research findings on the ephemeral river valleys of Namibia as sources of nutrient-rich dust is framed within the importance of considering small-scale dust sources globally and the context of future research needs and priorities. The results showing that the Namibian sources serve as a regionally significant higher-nutrient emission source of dust, most notably bioavailable Fe, is used to underscore this importance.

CHAPTER 2

2 The World of Dust and Ocean Fertilisation

2.1 Introduction

In order to discuss the impacts of the deposition of windblown fluvial sediments on the waters of the South Atlantic, the context of both source and sink must be framed. This chapter provides that setting, beginning with an overview of dust sources first at the global scale and then at the regional scale of southern Africa. The technological constraints that have until recently precluded adequate identification and investigation of small-scale dust sources are outlined. Research that has been undertaken to-date of dust from riverine sources is summarised, followed by an explanation of ephemeral river geomorphology. A brief overview of the processes driving transport of dust from source to sink (ocean) then provides the context to review ocean fertilisation in detail. The current state of knowledge is synthesised using examples to highlight the common findings of importance, which are the roles of the key nutrients; nitrogen (N), phosphorus (P) and iron (Fe). The role in primary production of the two macronutrients (N, P) and micronutrients (Fe) is presented to provide an understanding of the biological response to depositional nutrients. This understanding of the receiving environment then allows the nutrient assemblage of dust sources to be examined in the context of the key nutrients. Global nutrient loading of dust sources are reviewed, first within the framework of N, P and Fe and then the role of rivers as nutrient-transport corridors through the landscape.

Finally, the regional context of dust and nutrient loadings in southern Africa and the Namibian ephemeral rivers are discussed.

2.2 Global dust sources

The estimated dust flux from different source regions varies considerably among global dust emission and transport models[1]. Ginoux et al. (2012) provides the highest resolution mapping of dust source areas and estimates global dust emission to comprise 1536 $Tg.yr^{-1}$, with the northern hemisphere understood to emit significantly more dust than the southern hemisphere (Mahowald et al., 2008; Jickells et al., 2005). An estimated 51-69% (Miller et al., 2004; Ginoux et al., 2004) of global annual emissions originate in the 'dust belt', a region that spans the Sahara, eastern Africa, the Arabian Peninsula and into Asia (see Figure 3). This region includes the world's largest individual dust source, the Bodélé Depression (Figure 3), which emits an estimated 400-700 Tg of dust annually (Washington et al., 2003). Outside of the dust belt four other dust source regions and their major emission source areas are North America (Western United States and Mexico), Australia (Lake Eyre and the Great Artesian Basin), Southern Africa (Makgadikgadi Depression and Pans, Botswana; Etosha Pan, Namibia), and South America (Altiplano, Bolivia; Patagonia and Western Argentina) as shown in Figure 3. These regions have been classified as 'modest' sources using aerosol data from the Total Ozone Mapping Spectrometer (TOMS) (Prospero et al., 2002).

[1] The Georgia Tech/Goddard Global Ozone Chemistry Aerosol Radiation and Transport model (GOCART) see Chin et al. (2000), Spectral Radiation-Transport Model for Aerosol Species (SPRINTARS) see Takemura et al. (2005). See Huneeus et al. (2001) for comparative review.

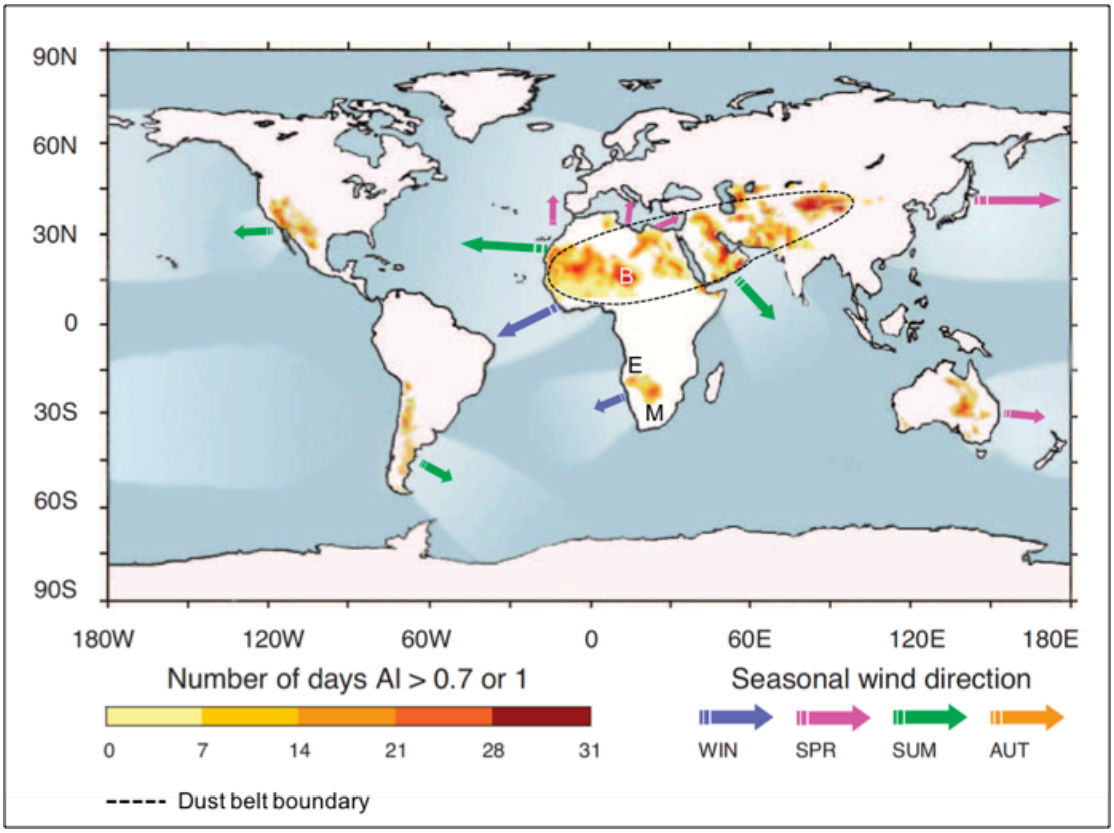


Figure 3 | Global distribution of major dust source areas (based on absorbing aerosol index (AI) thresholds of 1.0 in dust belt and 0.7 elsewhere from TOMS identification by Prospero et al. (2002)) with seasonal emissions and dominant transport pathways highlighted. The predominant global dust source, the Bodélé Depression is highlighted (B) as well as the southern African major pan sources, Etosha (E) and Makgadikgadi (M). Seasons are relevant to the hemisphere in which the source area is located. Adapted from Engelbrecht & Derbyshire (2010).

The term dust belt was coined by Prospero et al. (2002) using 13 years (1980-1992) of TOMS absorbing aerosol index (AAI) data to identify persistent global dust sources. Using this methodology the southern hemisphere was classified as devoid of major dust activity as detected by TOMS AAI index, noting "modest" dust sources in each of Australia, South Africa and South America. However, the reliance on TOMS only identifies dust at a minimum of 1km above the earth's surface, excluding any dust aerosols at lower altitudes. The global dust source investigation using Moderate

Resolution Imaging Spectroradiometer (MODIS) data by Ginoux et al. (2012) provides a much higher resolution analysis to include small-scale features and identifies the Namib Desert as a regionally important emitter of dust. It was noted that knowledge of global dust emissions is inhibited by a lack of information about dust sources, particularly for small-scale features that may account for a large fraction of global emissions (Ginoux et al., 2012). This would include sources such as Namibia's ephemeral valleys that are the major emission sites of the Namib Desert (Vickery et al., 2013).

Dust source areas are constrained by the availability of erodible surface sediments and erosive surface winds (Bullard et al., 2011; Gillette et al., 1980). Model estimates of dust producing regions address this through the use of emission thresholds subject to physical factors such as soil texture, topographic depressions, and vegetation cover (Prospero et al., 2002; Ginoux et al., 2001). This results in a modelling bias in predicting emission scenarios from large pan and lacustrine source areas, which meet the relatively static criteria of fine sediments, long-term absence of surface water and little to no vegetation cover. Models do not yet adequately incorporate dust emission from fluvially extant and dynamic systems such as ephemeral rivers where frequent reworking and replenishing of surface fines is taking place during flood events (Breshears et al., 2003; Tooth & Nanson, 2000). Until recently, the reliance on low-resolution satellite data for identifying global hot-spots of dust emission has resulted in southern African dust research and modelling scenarios being focused on the Makgadikgadi Pan system in Botswana and Etosha Pan in Namibia.

2.2.1 River dust sources

Sediment transport is driven by both aeolian and fluvial processes, yet these are almost always studied independently (Field et al., 2009). Pluvial and fluvial processes are primary drivers of sediment mobility though the landscape (Breshears et al., 2003; Howard et al., 1994), with modern day rivers serving as sediment transport conduits thorough the terrestrial sphere. The instances where riverine dust sources have been noted, through either remote sensing, site-based fieldwork, or a combination of both are listed in Table 1 and Figure 4. Direct connection between extant fluvial and aeolian activity has been made in several cases. In the case of the Senegal River, deforestation of the watershed has caused increased erosion and sediment transport along the river (Niang et al., 2008). The increased sediment load transported and then deposited in the inland delta has led to increased dustiness in the delta during dry periods (Ginoux et al., 2012; Niang et al., 2008). Seasonal flooding in the inland delta of the Niger River is similarly known to provide the alluvial source sediment for dust emission (Gillies et al., 1996). In Australia, fluvial erosion of fine particles in the wetter uplands and Channel Country are transported to arid regions where they form one of the continent's major dust sources, Lake Eyre (Li et al., 2008; Hesse & McTainsh, 2003).

Further supporting evidence of extant rivers contributing to enhanced dust production can be found in South America. Rivers identified there as dust sources by Ginoux et al. (2012) matched those that have been identified as having significantly decreased discharge from the early 20th century to the beginning of the 21st as a result of changing climate patterns (Pasquini et al., 2006). The ephemeral river valleys of Namibia have been subject to remote sensing investigation of dust emissions and are described in detail within the regional context in Section 3.2.

Table 1 Identified dust sources of riverine origin

Map Reference	Dust Source	Country	Geomorphological context	Reference
1	Copper and Alsek Rivers	Alaska	River delta of glacial fines observed to emit dust and rich in bioavailable Fe	(Crusius et al., 2011)
2	Slims River Valley	Canada	In-valley analysis of sediment transported by wind	(Nickling, 1978)
3	Snake, (Pecos, Rio Grande and Big Sioux)* Rivers	U.S.A.	*Basin-scale only and distinction not made between alluvial sediment and exposed soils from land clearing and agriculture. Snake valley has seen further ground-based investigation by (Brungard et al. 2015) identifying the significant contribution of alluvial fans to dust emission in the valley	(Brungard et al., 2015; Ginoux et al., 2012; Lee et al., 2009)
4	Rio Negro and Chico River	Argentina	MODIS identification only	(Ginoux et al., 2012)
5	Numerous	Iceland	Glacio-fluvial sediments and river plains shown to be major sources of dust storms and rich source of bioavailable Fe	(Arnalds et al., 2016)
6	Senegal River Basin	Senegal	Water erosion causes gullying and bank erosion that is observed to increase dust production in downstream fluvial-deposition areas	(Ginoux et al., 2012)
7	Inland delta of the Niger River	Mali	Aeolian source material known to be sediments deposited by seasonal flooding	(Gillies et al., 1996)
8	Ephemeral rivers	Namibia	High resolution remote sensing source identification of fluvial fill in river valleys as dust emission sources	(Vickery et al., 2013; Eckardt & Kuring, 2005)
9	Jordan River	Jordan	Mixture of anthropogenic and hydrological sources noted, predominantly on the eastern bank	(Ginoux et al., 2012)

Map Reference	Dust Source	Country	Geomorphological context	Reference
10	Al Batin, Al-Rimah and Al Sahba wadis	Saudi Arabia	Mixture of anthropogenic and hydrological sources around the three wadis (Arabic term for dry riverbed), Fryberger et al. (1983) observed aeolian erosion by sand abrasion	(Ginoux et al., 2012; Fryberger et al., 1983)
11	Sub-escarpment river fans	Yemen	Large dust sources associated with river fans at the base of coastal escarpment	(Ginoux et al., 2012)
12	Tigris and Euphrates Rivers	Iraq	Identification through combination high-resolution modelling and ground-based and satellite observations of aerosols	(Jish Prakash et al., 2015; Prospero et al., 2002)
13	Atrek River	Turkmenistan	Increasing dust emission in drying delta associated with upstream over-extraction of water for agriculture	(Ginoux et al., 2012)
14	Karram River	Pakistan	Fluvial plain	(Ginoux et al., 2012)
15	Ghaggar River	India	River sediments deflated in ephemeral system, intermittent flow only during the monsoon season	(Ginoux et al., 2012)
16	Numerous	China and southern Mongolia	Fluvial fans on edge of Gobi Desert providing dust source material	(Wang et al., 2008)
17	Numerous, Queensland	Australia	Dry channels of braided streams observed to emit dust	(Nickling et al., 1999)
18	Murray-Darling River	Australia	Fluvial transport of fines from active pluvial headwater regions to arid lowlands that are then emitted as dust	(Ginoux et al., 2012)
19	McMurdo Dry Valleys	Antarctica	Dry river valley sediment with enriched bioavailable Fe levels compared to surrounds	(Bhattachan et al., 2015b)

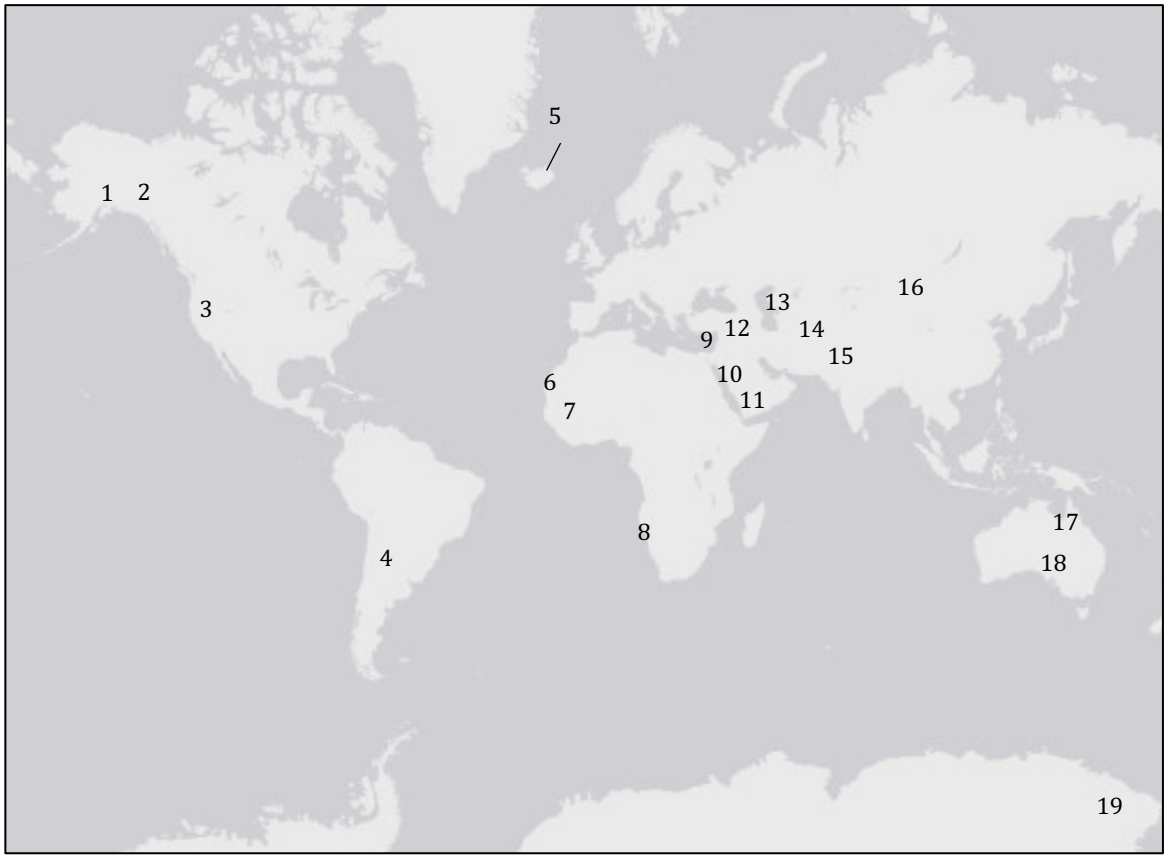


Figure 4 | Map of the identified riverine dust sources presented in Table 1.

2.2.2 Ephemeral Rivers

The prerequisite conditions for significant dust emission sources are most commonly the presence of historical or extant fluvial activity in modern dryland environments (Ginoux et al., 2012; Prospero et al., 2002). Despite the aridity, drylands often host ephemeral rivers (Tooth, 2000) with their flows a result of either infrequent pluvial activity or seasonal precipitation in highlands beyond the borders of the dryland environment. Such flow events are known to cause significant fluvial erosion and deposition along the hydrological system (Reid & Frostick, 1987).

Deposited sediments also contain nutrients (Harms & Grimm, 2010; Skoulikidis & Amaxidis, 2009; Laronne, 1993) that support microbiological activity (Belnap et al.,

2005) and primary biomass production (Steward et al., 2012) in otherwise arid landscapes. These fluvial sediments, macronutrients and minerals are representative of the geochemical and physical properties of the upstream river and watershed environment (Haddadchi et al., 2013), even sub-catchments (Franz et al., 2013).

Ephemeral rivers can transport large quantities of sediment during flow events, as both suspended sediment and bedload, compared to their perennial counterparts (Reid & Laronne, 1995; Sharma & Murthy, 1994). Sediment transported and deposited along ephemeral rivers is derived from two main processes: the high erosional potential of dryland soils in the catchment (Breshears et al., 2003; Rodier, 1985), and the mobilisation of sediment due to bank erosion and bed scouring (Tooth, 2000). The mobility of sediment in these ephemeral systems results in high transport rates even during moderate to low flows (Laronne, 1993). The episodic and often short-lived nature of flood events restrict fluvial sorting and the removal of finer particles from the riverbed sediment load (Tooth, 2000), thereby serving to enrich the sediment with a fine fraction of particles. Yet, even while exhibiting all of the precursor conditions for significant dust emission, ephemeral rivers are lagging behind in the world of dust research. Compounding the need to address this gap, the increasing alteration of hydrological systems, through dam construction and water extraction (Nilsson & Berggren, 2000; Vorosmarty et al., 2000), combined with shifting precipitation regimes due to anthropogenic climate change (Flato et al., 2013) is resulting in the increased exposure of previously inundated riverine sediments. Both naturally dry rivers and those now dry or drying due to anthropogenic forces could be expected to be significant contributors to global atmospheric loadings into the future.

2.3 Dust flux to the ocean

Dust emitted from the continents ultimately descends back to earth, a large component of which lands on the global ocean with the total flux to the marine environment being estimated at 450 $Tg.yr^{-1}$ (Jickells et al., 2005). The depositional process is classified as either dry deposition, with gravitational forces acting directly on the particle, or wet deposition, where suspended particles are removed from the atmosphere during precipitation events (Mahowald et al., 2005). Estimates of dry versus wet deposition vary greatly, with the wet deposition being estimated between 30 – 95% of total deposition globally, but explicit measurements are rare (Hand et al., 2004). The depositional process is thought to influence to bioavailability of nutrients, with increased bioavailability associated with wet deposition (Stockdale et al., 2016; Fan et al., 2006).

The transport of dust is controlled by prevailing winds and seasonal cycles, which influence the duration, transport pathways and spatial extent of deposition events. For example, the spring transport of Saharan dust towards Europe versus the western pathways prevalent in summer and winter (Figure 3). Once airborne, deflated dust can travel great distances with deposition occurring on oceans and landmasses far from the source. Spring emissions of Saharan dust (Figure 3) have been recorded over 3000 km from their source in fallout over the United Kingdom (Middleton & Goudie, 2001). Dust from Asia has more recently been discovered to have travelled the full circumference of the globe (Uno et al., 2009) and even large particles (>150 μm) have been shown to travel hundreds of kilometres offshore (Schroeder, 1985; Glaccum & Prospero, 1980).

Where perseverance and regularity of these aeolian pathways exist, it can lead to ecosystems in depositional areas becoming dependent on the external input of nutrients. For example, it has been proposed that the Amazon rainforest is dependent on mineral

aerosol phosphorus input from the Sahara (Yu et al., 2015; Bristow et al., 2010; Koren et al., 2006; Swap et al., 1992). Without the external P input the massive biological productivity of the Amazon during winter (Figure 3) would not be self-sustaining. Similarly, primary production in nutrient-limited oceanic regions derive nutritional input from dust (Fan et al., 2006; Jickells et al., 2005; Herut et al., 2002). The input of new, bioavailable nutrients to the ocean from dust is essential for marine productivity and the basis of the ocean food chains. Reduced levels of oceanic trace elements, derived from terrestrial sources, have even recently been hypothesized as contributing to major global marine mass extinction events (Long et al., 2015).

Accounts of dust falling on ships while crossing the Atlantic were first compiled by Darwin (1846) with sediment transport by wind theorised as a considerable ocean-delivery pathway at the turn of the 20th Century (Woodruff, 1909). It is now widely understood that Saharan dust is transported across the Atlantic (e.g. Gross et al (2015), Bristow et al (2010), Swap et al. (1992)). The depositional impact of this pathway is clearly observed in the distribution of globally averaged dust deposition (Figure 5). Oceanic regions adjacent to dust emission sources (Figure 3) are seen to receive greater quantities of dust, which is a result of the gravitation settling of mineral aerosols close to source, (Maring et al., 2003). The major contribution of the dust belt to the North Atlantic is clearly visible (Figure 5), as is the predominance of dust deposition in the northern hemisphere. Dust deposition research has therefore largely focused on the North Atlantic (e.g. Gross et al. (2015), Moulin et al. (1997), Schütz et al. (1981)) and the Mediterranean (e.g. Herut et al. (2002), Prospero (1996)) as well as the Arabian (e.g. The Red Sea (Jish Prakash et al., 2015)) and Asian (e.g. Yellow Sea, Sea of Japan and the Pacific (Sun et al., 2001)) marine environments. In the Southern Hemisphere South America, southern Africa and Australia are of particular importance for their contributions to the Southern

Ocean (Li et al., 2008) yet investigations of deposition and ocean fertilisation have been historically less common.

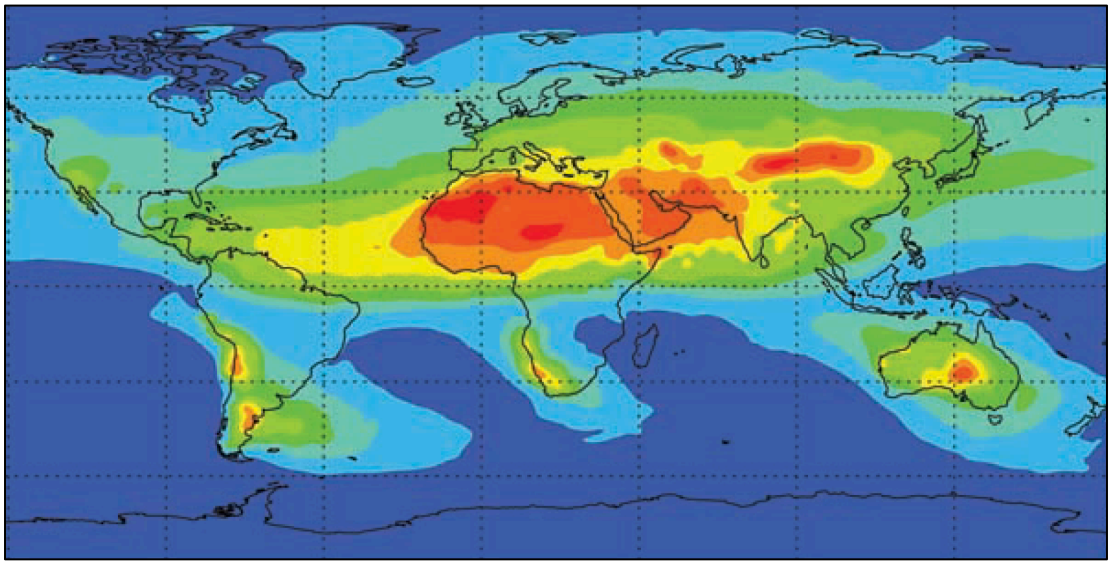


Figure 5 | Global dust flux to the ocean, a composite of three models matched with depositional observations as prepared by Jickells et al. (2005). Deposition into each ocean basin calculated as being: North Atlantic, 43%; South Atlantic, 4%; North Pacific, 15%; South Pacific, 6%; Indian, 25%; and Southern Ocean, 6%.

2.3.1 Global ocean productivity, biochemistry and nutrients

The world's oceans are responsible for half of global primary production (Behrenfeld et al., 2001) with microbial phytoplankton utilizing dissolved carbon dioxide and sunlight for photosynthetic growth while also requiring essential minerals (Moore et al., 2013), classified broadly as nutrients. There is consensus that dust-delivered nutrients alleviate phytoplankton growth inhibition (e.g. Jickells & Moore (2015), Mahowald et al. (2005)), where the limitation is caused by the lack of a key mineral, or minerals, in waters otherwise abundant in photosynthetic-life required compounds. Termed high nutrient low chlorophyll (HNLC) zones, these areas cover 30% of the world's ocean surface (De Baar & Boyd, 2000). Conversely, approximately 60% of the world's ocean surface are low

nutrient low chlorophyll (LNLC) (Longhurst et al., 1995), or oligotrophic, zones. The impact of dust and nutrient deposition on these waters is much less understood (Guieu et al., 2014a) and only beginning to see detailed research attention (e.g. (Louis et al., 2015; Guieu et al., 2014b; Ridame et al., 2014).

The biochemical interplay of nutrients limiting biological productivity in the ocean has long been recognized (Redfield, 1958). Yet the specific mechanism(s) of nutrient limitation is governed by complexities of planktonic community composition that determine nutrient uptake abilities (Hecky & Kilham, 1988; Tilman et al., 1982), and is further influenced by regional and temporal variations in marine biochemistry (Cetinić et al., 2015; Edwards et al., 2013). Of the ca. 30 essential elements for life (Moore et al., 2013), the growth-limiting nutrients of primary importance are widely agreed to be the micronutrient iron (Quéguiner, 2013; Cassar et al., 2007; Aumont & Bopp, 2006; Jickells et al., 2005; Coale et al., 1996b) as well as nitrogen (Bracken et al., 2015; Herut et al., 2002; Falkowski, 1997) and phosphorus-based (Gross et al., 2015; Filippelli, 2008; Codispoti, 1989) macronutrients. Other examples of trace metals and minerals that have been shown to limit phytoplankton growth are silicate (Nelson et al., 1995; Egge & Aksnes, 1992), broadly considered the fourth-most important nutrient, as well as copper (Coale, 1991), cobalt (Sunda & Huntsman, 1995), zinc (Morel et al., 1991) and, more recently, vitamin B12 (Sañudo‐Wilhelmy et al., 2006). The relative balance between the supply and removal of nutrients determines which one is limiting phytoplankton growth (Beman et al., 2005). It is by far, however, the macronutrients nitrogen and phosphate and micronutrient iron that most frequently limit primary production across vast areas of the world's oceans (Guieu et al., 2014a; Kanakidou et al., 2012; Jickells & Spokes, 2001). These are considered the chief limitation nutrients and are subsequently selected for the focus of this work.

The difficulties found to date in connecting dust-delivered-nutrients to increases in primary production are complicated by knowledge gaps of the role and uptake of a suite of macro and micronutrients in triggering phytoplanktonic growth once deposition has occurred. Broadly speaking, the subarctic Pacific Ocean, the Eastern Pacific equatorial waters and the Southern Ocean are the largest HNLC zones on the planet. These areas can be seen to have abundant nitrate and phosphorous-based nutrients (Figure 6). The levels of N and P macronutrients are never depleted because of the limitation on phytoplankton primary production caused by a lack of bioavailable Fe (Pitchford & Brindley, 1999).

In addition to these three HNLC regions, there are four major coastal upwelling regions, termed eastern boundary upwelling systems (EBUS), that play an important role in the global ocean. These are on the west of North and South America along the coasts of California and Peru and similarly for the west of Africa, along the coasts of Mauritania and Namibia-South Africa (Figure 6). Upwelling of deep nitrogen and phosphorus-rich waters is most visible in the southern African system (Figure 6a and b, Figure 7a and b) and is named the Benguela Upwelling System (BUS) after the northerly flowing Benguela Current along the same coast. The four systems share wind-driven upwelling of cold, nitrogen and phosphorus-rich water into the light-abundant surface waters that then supports tremendous planktonic photosynthesis activity (Capone & Hutchins, 2013; Chavez & Messié, 2009). These coastal upwelling regions make up only 1% of the ocean's surface area but are responsible for the highest primary production rates in the ocean (Toggweiler & Carson, 1995; Chavez & Barber, 1987). Fe maintains its essential role in these upwelling regions, where it can be nearly as critical as in HNLC zones (Capone & Hutchins, 2013). It is known that Fe limitation affects productivity in both the Californian and Peruvian systems because of limited Fe input during the upwelling season (Hutchins et al., 2002; Bruland et al., 2001). The vertical transport of

macronutrient-rich waters can create near-shore Fe-limited conditions as are found in the HNLC waters of the open ocean (Capone & Hutchins, 2013). Aeolian deposition is hypothesised here to provide essential Fe, as well as additional minerals and nutrients, to the photosynthetic surface waters off the coast of Namibia. Further, upwelling could cause longer residence times of aeolian-delivered nutrients near the surface and contribute to the highly productive Benguela ecosystem.

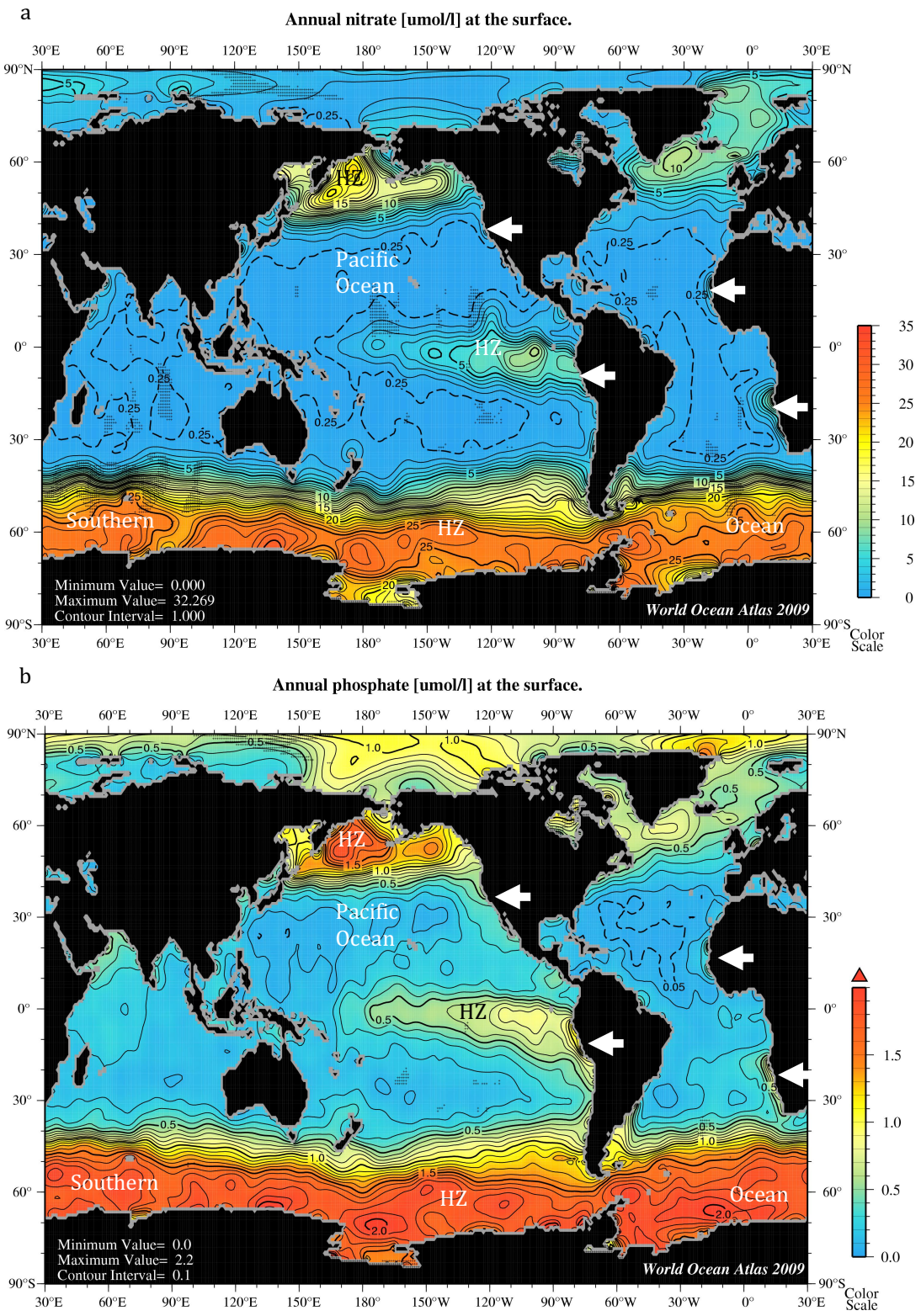


Figure 6 | Annual average global ocean surface concentrations of (a) nitrate and (b) phosphate showing HNLC zones (HZ) and location of the four global EBUS (arrows). Maps obtained from the World Ocean Atlas (Garcia et al., 2009).

A synthesis of experimental data by Moore et al. (2013) provides a global map, Figure 7, of the limiting nutrient(s) in ocean surface waters whilst demonstrating a robust agreement between a wide-range of laboratory and in situ approaches from the incorporated studies. The resulting global findings fell into two broad classifications of nutrient limitation. First, throughout the low latitudes (between 30°N/S), in areas lacking subsurface nutrient supply, nitrogen was the most frequent limiting nutrient, Figure 7a. The absence of the vertical transport of deep-water nutrients is also identifiable as the low phosphate regions, shown in Figure 7b, as both N and P are found in higher concentrations in cold, deep ocean waters (Tyrrell, 1999; Redfield, 1934). In contrast to this are the areas of oceanic upwelling, already rich in N and P nutrients (HNLC zones, Figure 6), where Fe was the limiting nutrient (Figure 7). In addition to the broad distinction of nitrogen versus iron-limitation in the world's oceans, P and micronutrients other than Fe were also identified (Figure 7), however the importance of co-limitation and spatial relevance remained unclear (Moore et al., 2013). The waters off the coast of northern Namibia (-13.3 °N, 0.0 °E), the geographically closest available study to the ephemeral rivers and which are supplied

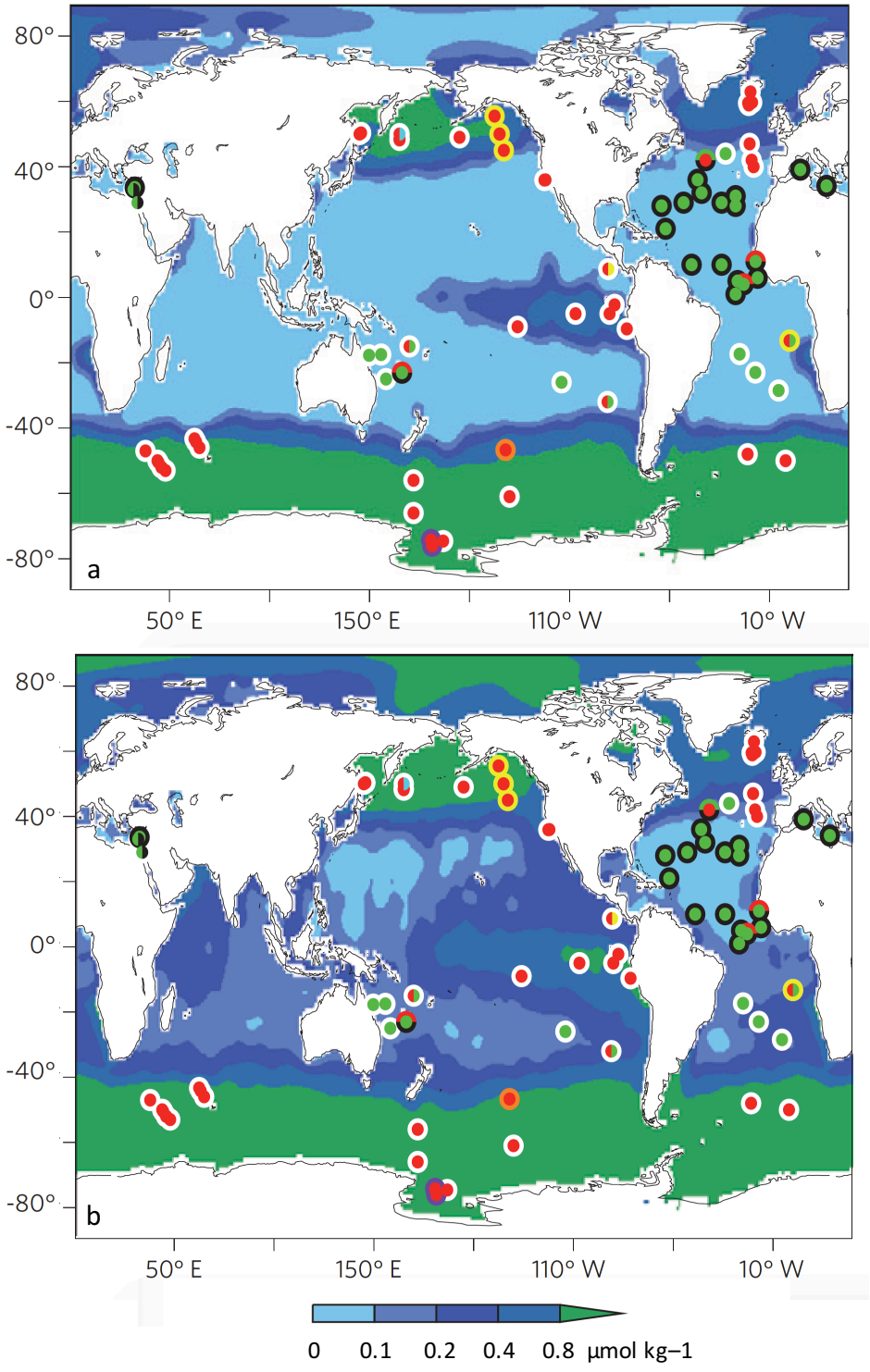


Figure 7 | Spatial distribution and pattern of nutrient limitation in the global ocean, from Moore et al. (2013). Backgrounds show annual average surface concentrations of (a) nitrate and (b) phosphate in µmol.kg^{-1}. As described by Moore et al. (2013), symbols indicate the primary (central circles) and secondary (outer circles) limiting nutrients as inferred from chlorophyll

and/or primary productivity increases following artificial amendment of: N (green), P (black), Fe (red), Si (orange), Co (yellow), Zn (cyan) and vitamin B12 (purple). Divided circles indicate potentially co-limiting elements. White outer circles indicate that no secondary limiting nutrient was identified, which in many cases will be because of the lack of a test.

by upwelling nutrients of the Benguela Current, were shown to be co-limited by Fe and N (Figure 7). These are listed as unpublished results by Saito et al., a co-author of the Moore et al. (2013) review paper. No aeolian fertilisation research has taken place off the coast of Namibia.

2.3.2 Phytoplankton response to aeolian deposition events

The global impact of oceanic nutrient deposition from dust has been observed in paleo-records. These have shown that mineral aerosol deposition and fertilisation of the ocean can be correlated with increased global atmospheric CO_2 drawdown during glacial periods (Lambert et al., 2015; Lamy et al., 2014). Although the evidence behind the specific historical mechanisms, e.g. the role of iron fertilisation (Kienast et al., 2004), have been challenged. The modern-day fertilisation effect of desert-derived mineral aerosols has also been widely reported in the literature (Jickells et al., 2014; Mahowald et al., 2005; Ridgwell, 2002) and it is accepted that aeolian deposition fertilizes the ocean and increases phytoplanktonic biomass in HNLC regions (Guieu et al., 2014a). Yet evidence to understand the direct connection between dust deposition and ocean fertilisation remains limited (Schulz et al., 2012). Modelling supports the notion that atmospheric deposition provides biologically essential nutrients that stimulate primary production in HNLC regions (Moore et al., 2002; Archer & Johnson, 2000). Models also agree that deposition of Fe and P to LNLC regions stimulate N fixation and phytoplanktonic growth (Mahowald, 2011; Krishnamurthy et al., 2009). However, the model studies rely on mean depositional values and do not capture the highly episodic

nature of deposition events (Guieu et al., 2014a). Seasonal correlation between dusty periods and increased phytoplankton concentrations have been reported to occur on annual cycles globally (Gao et al., 2001).

Numerous studies have investigated phytoplanktonic response following the deposition of mineral aerosols in many of the world's oceans (Figure 8). The complexities of oceanic response and the difficulty in excluding non-depositional driving factors as also triggering phytoplankton growth (Schulz et al., 2012) has caused some correlations of modern day dust and phytoplankton response to be disputed, as summarised in the global review by Boyd et al. (2010b), (Figure 8).

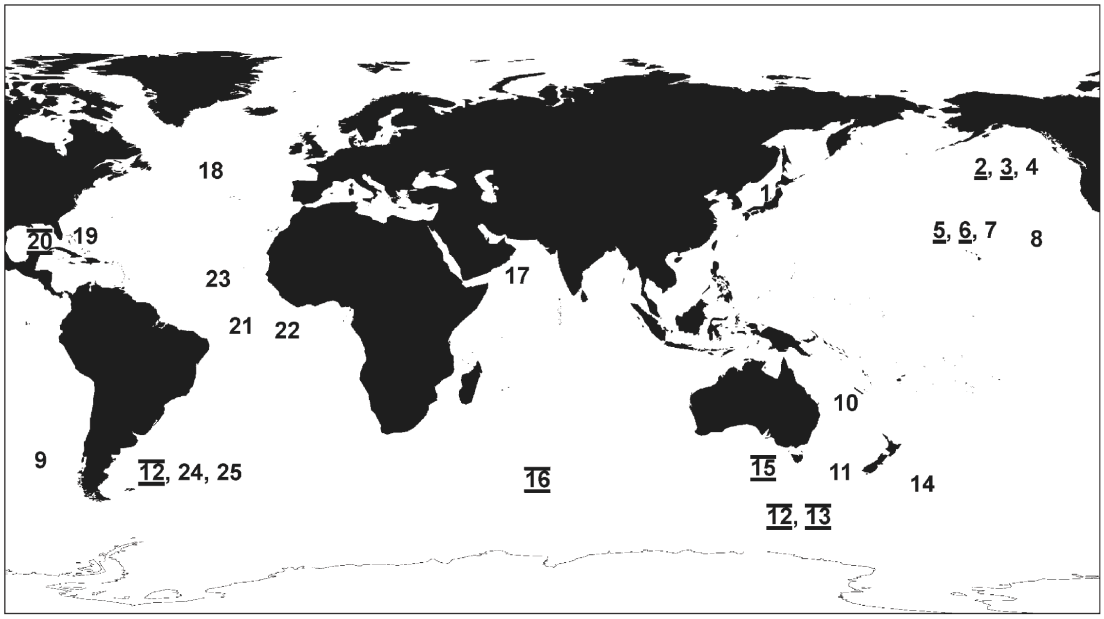


Figure 8 | Global distribution of studies to have directly or indirectly investigated the link between dust supply and phytoplanktonic response, from Boyd et al. (2010b). Underlined studies denote a relationship between dust and biota while those that are not underlined showed no reported relationship. Studies that are both underlined and overlined indicate that they have in subsequent re-analysis to be found to have misattributed the causes of the biological response to dust supply. 1 denotes Jo et al. (2007) ; 2 Bishop et al. (2002); 3 Boyd et al. (1998); 4 Crispo et al. (2005) ; 5 DiTullio and Laws (1991); 6 Young et al. (1991); 7 Wilson (2003); 8 Johnson et al.

(2003) ; 9 Bonnet et al. (2008); 10 Mackie et al. (2008); 11 Boyd et al. (2004a; 2004b); 12 Cassar et al. (2007); 13 Breviere et al. (2006); 14 Frew et al. (2006) ; 15 Gabric et al. (2002) ; 16 Ridgwell (2002); 17 Westberry and Siegel (2006); 18 Moore et al. (2006); 19 Sedwick et al. (2005); 20 Lenes et al. (2001); 21 Baker et al. (2007) ; 22 Tyrrell et al. (2003); 23 Mills et al. (2004); 24 Erickson et al. (2003) ; 25 Meskhidze et al. (2007).

The disconnect between dust deposition and a measurable fertilisation can be attributed to two reasons. Firstly, the response in nutrient-poor waters outside of the HNLC regions has proven more difficult to identify as phytoplankton growth appears limited by more factors than are remedied by the deposition of Fe and other nutrients (e.g. oligotrophic waters of the North Atlantic Gyre (Neuer et al., 2004)). Secondly, non-depositional factors can be the cause of limited nutrient remediation of HNLC waters, namely the subsurface transport of dissolved iron. A prime example of this is the lateral advection and vertical upwelling of dissolved Fe from the continental shelf observed in the HNLC North Pacific (Lam & Bishop, 2008). Of key relevance here, the upwelling of dissolved iron to surface waters occurred during the winter months when dust flux is at a minimum. Dust deposition (originating in the Gobi Desert) has also been shown to increase phytoplankton activity in those waters (Bishop et al., 2002).

In the Southern Ocean corroboration between dust input and phytoplankton response was made by Cassar et al. (2007), Cropp et al. (2005), and Gabric et al. (2002), yet other studies demonstrated no correlation was present (Meskhidze et al., 2007; Boyd et al., 2004b), suggesting other factors. Most recently the importance in considering seasonal and inter-annual cycles of local and long-range atmospheric dust, as sources of phytoplankton-sustaining Fe, was demonstrated in Antarctic waters (Winton et al., 2016) with temporal disparity between investigations providing an explanation for differing results. Understanding the temporal and spatial boundaries of investigation are therefore

vital in identifying fertilisation by mineral aerosols. Upwelling in the Benguela is the least seasonal of the four EBUS (Chavez & Messié, 2009) but still the largest biochemical determinant of the aquatic depositional-environment off the coast of Namibia and addressed in detail in Chapters 3 and 7.

Many studies have clearly shown increases in oceanic chlorophyll in response to individual dust deposition events (Table 2). An example of direct and measured increase in phytoplankton growth as a result of a dust storm was made during an expedition in the Mediterranean, which measured an in situ response of increased chlorophyll levels (Herut et al., 2005). In the Northwest Pacific, a detailed analysis of phytoplankton ecology demonstrated increased abundance following three separate deposition events of Asian dust (Chung et al., 2011). In-situ measurements during deposition events are less common than remotely sensed investigations due to feasibility and cost. Using this approach a SeaWiFS (Sea-Viewing Wide Field-of-View Sensor)/MODIS study off the eastern coast of Australia reported increased phytoplankton growth during and immediately following a dust storm (Shaw et al., 2008), building on previous findings that phytoplankton in those waters that showed an immediate response to nutrient input (Furnas et al., 2005).

Table 2 Chlorophyllic responses to dust deposition

Ocean / Sea	Sub-region	Description	Reference
Atlantic Ocean	Near Bermuda	Seasonal correlations of dust and phytoplankton abundance	(Orcutt et al., 2001)
	West Florida Shelf	Saharan dust event caused significant phytoplankton growth increase	(Lenes et al., 2001)
	Eastern subtropical gyre	Possible “feast and famine” association of dust deposition with phytoplankton response	(Neuer et al., 2004)
	Near Canary	Saharan dust events	(Franchy et al.,

Ocean / Sea	Sub-region	Description	Reference
	Islands	shown to increase primary production phytoplankton	2013)
Pacific Ocean	Southern region	Increased chlorophyll concentrations above seasonal average associated with Asian dust storm delivering co-limiting phosphate and iron in LNLC waters	(Tan et al., 2017; Calil et al., 2011)
	Northwestern region	Phytoplankton bloom observed 1 week following deposition of volcanic dust	(Lin et al., 2011)
	North, western and equatorial regions	10-year study of Asian dust showed significant correlation with increased chlorophyll a levels in the north, western and equatorial regions of the Pacific Ocean and the Sea of Japan	(Tan et al., 2013)
Southern Ocean	Between Tasmania and Antarctica	Evidence of large-scale fertilisation by Australian dust	(Gabric et al., 2010)
	Patagonia region	Strong correlation shown between atmospheric dust-Fe and chlorophyll levels over 24 month period (2000-2001)	(Erickson et al., 2003)
Mediterranean Sea		8-year investigation (2000-2007) found both positive and negative significant correlations between dust events and chlorophyll concentrations that varied by area and times of the year	(Gallisai et al., 2014)
		Dust pulses shown to provide P to surface waters and enhance biological activity through rapid, same day, uptake.	(Pulido‐Villena et al., 2010)
		Direct and measured	(Herut et al., 2005)

Ocean / Sea	Sub-region	Description	Reference
		increase in chlorophyll levels as the result of a dust storm	
Yellow Sea		Observed phytoplankton bloom 10-13 days after dust event.	(Tan & Wang, 2014)
Japan Sea		Dust deposition found to be the cause of unseasonably early onset of annual phytoplankton blooms.	(Jo et al., 2007)
Arabian Sea		Episodic phytoplankton blooms observed following dust storms between 2002-2003 and 2010-2011.	(Banerjee & Prasanna Kumar, 2014)

It should be noted, however, that the correlation between remotely sensed chlorophyllic response and mineral aerosol deposition has been questioned. The reason for this was a remote sensing study, similarly in the Mediterranean, that showed strong positive correlations between dust and chlorophyll at the daily and weekly timescales (Volpe et al., 2009). Dust deposition-driven chlorophyll increases occurred within 0-2 days although Volpe et al. (2009) concluded that the results were an artefact of the SeaWiFS data used and could not be used to test dust-phytoplankton response in the LNLC Mediterranean. While this is noted it is taken within the context of a global investigation using five years of SeaWiFS data, which found that dust and chlorophyll correlations are not affected by widespread measurement artefacts and supported that the observed remotely sensed phytoplanktonic response to dust deposition was occurring (Cropp et al., 2005).

The deposition of dust garners differing biological responses depending on the complement of nutrients in both the mineral aerosols and depositional waters, i.e. the

biochemical conditions of the ocean determine the importance and role of external nutrient input in triggering or sustaining primary production. The geochemical supply ratio of N, P and Fe to biological demand is becoming increasingly seen as a central factor in global primary production limitation, with nitrogen fixation providing the mechanism for the nutrient cycles to interact (Hagstrom et al., 2016). These must be considered if fertilisation by aeolian deposition is to be investigated and understood.

2.3.3 Atmosphere-Ocean nutrient cycling

2.3.3.1 The macronutrients, nitrogen and phosphorus

Primary production in the ocean has been observed to be limited by N and P macronutrients (Vitousek & Howarth, 1991; Hecky & Kilham, 1988), with co-limitation of N and P being broadly applicable for primary production across marine, freshwater and terrestrial ecosystems (Elser et al., 2007). Historically N was considered the main limiting macronutrient in the ocean (Howarth, 1988), predominantly in the form of nitrate (NO_3^-) (Codispoti, 1989). However, the complexities of nutrient limitation and the factors of co-limitation are still being unravelled (e.g. Jickells & Moore (2015)). Broadly speaking, N is usually depleted first making it the 'proximate' limiting macronutrient but changes in P availability trigger corresponding changes in N availability, making P the 'ultimate' limiting macronutrient (Tyrrell, 1999).

Nitrogen limitation has been shown to be remedied directly through the addition of N as well as indirectly through the addition of P and Fe (e.g. Mills et al. (2004)) which alleviate biological limitations on N-fixing bacteria in the ocean waters, Figure 9. These nitrogen-fixing planktonic bacteria, termed diazotrophs, provide a major portion of the total nitrogen input to the ocean through the fixation of atmospheric gaseous nitrogen (N_2) (Capone & Carpenter, 1982). Atmospheric N_2 is converted into bioavailable

ammonium (NH_4^+), which is then also converted into the further bioavailable forms of nitrite (NO_2^-) and nitrate (NO_3^-) by ammonia-oxidising and nitrite-oxidising bacteria (Kowalchuk & Stephen, 2001). These forms of N are then utilised by photosynthetic phytoplankton for primary production (Karl et al., 2002; Michaels et al., 1996; Capone & Carpenter, 1982). The biological fixation process relies, at an enzymatic and energy production level, on Fe (Moore & Doney, 2007; Berman-Frank et al., 2007; Hood et al., 2004; Falkowski, 1997) and P (Graham & Vance, 2000; Arnon, 1956) and the availability of these nutrients therefore constrain N_2 fixation rates.

Limitation on primary production in nitrogen-deficient HNLC regions has been mitigated experimentally in waters ranging from the North Atlantic (Mills et al., 2004) to the Southern Ocean (Okin et al., 2011). In the case of the North Atlantic this was demonstrated experimentally using both laboratory N, P and Fe reagents as well as Saharan dust as the source of external Fe and P (Mills et al., 2004). The abundance of studies (e.g. review complied by Moore et al. (2013) undertaken to date show that an adequate supply of N and P is essential to facilitate phytoplanktonic growth in ocean waters worldwide and that Fe is of particular importance as a terrestrially-derived nutrient (Jickells et al., 2005; Boyd et al., 2000).

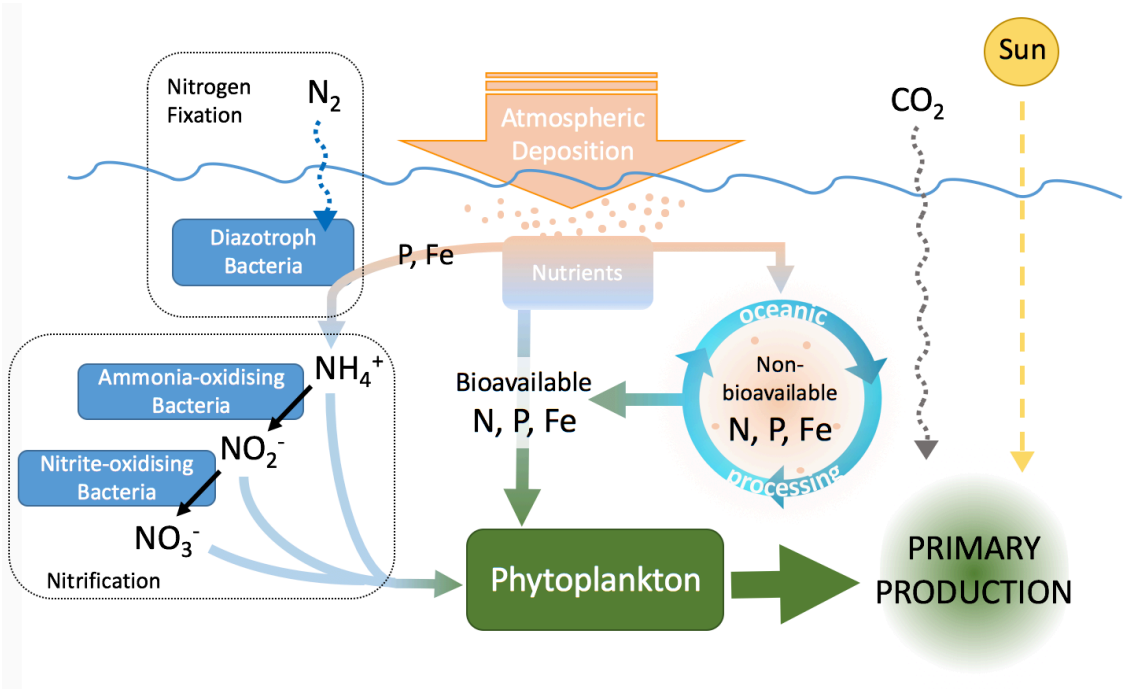


Figure 9 | Nutrient uptake pathways following aeolian deposition.

So while N limitation can be alleviated through either direct addition of N sources to surface waters or biological fixation of atmospheric N, the P and Fe sources are provided solely via external input to surface waters, be it via deposition, upwelling or coastal fluvial discharge. The primary oceanic input of P is from rivers that deliver continental, weathered P in both dissolved and particulate phases (Martin & Meybeck, 1979). Most of the riverine particulate phosphorus is retained within the continental shelf and does not reach the open ocean and associated marine biota. Aeolian deposition is the second most significant input of particulate phosphorus to the ocean (Krishnamurthy et al., 2010), with desert-derived mineral aerosols making up 82% of this airborne P source (Mahowald et al., 2008). There is however very little data on the solubility of aerosol P (Baker et al., 2006). An early study by Graham and Duce (1982) estimated a P solubility of 36% in aerosols collected over the northwestern Atlantic. Similar values have been reported in aerosol samples collected at coastal sites in Israel (Herut et al., 1999). Ridame and Guieu

(2002) reported that up to 15% of P in the <20 µm fraction of an Algerian soil (considered a proxy for Saharan aerosol) was soluble in seawater. Acidic atmospheric conditions encountered during aeolian transport has been shown to increase the bioavailable fraction of P from soil-derived minerals (Nenes et al., 2011), increasing the available P for marine phytoplankton uptake. Fe solubility, on the other hand, has seen much research attention.

2.3.3.2 The micronutrient, iron

Productivity in large areas of the ocean (ca. 25%) is undoubtedly and directly limited by the availability of iron (Schulz et al., 2012; Coale et al., 1996a; Martin & Fitzwater, 1988) and desert-derived dust is the major delivery mechanism to these areas, with mineral aerosols containing ~95% of the global averaged Fe budget (Mahowald et al., 2009). Research attention on Fe limitation of oceanic phytoplankton growth has increased dramatically since the first mesoscale experimental studies almost 30 years ago (Martin, 1990; Martin & Fitzwater, 1988). Subsequent experiments have demonstrated that the addition of Fe to HNLC regions promoted phytoplankton growth in each the northern hemisphere (Xiu et al., 2014; Tsuda et al., 2003), equatorial waters (Coale et al., 1996b; Martin et al., 1994) and southern hemisphere (Martin et al., 2013; Boyd et al., 2000). Consequently, the addition of iron to phytoplankton growth-limited regions of the world's oceans has been touted as a form of climate engineering to combat anthropogenically increased CO_2 levels (Vaughan & Lenton, 2011). Comparable studies have applied sediment collected from Saharan dust source locations to the ocean surface and similarly shown to trigger phytoplankton growth (Giovagnetti et al., 2013; Pulido-Villena et al., 2010).

The natural Fe cycle to, and within, the ocean remains full of complexities and uncertainties (Boyd & Ellwood, 2010; Jickells et al., 2005). Research to fill in the knowledge gaps has focused on the delivery of Fe to ocean surface phytoplankton communities by deposition of mineral aerosols (e.g. Aumont et al. (2008)), upwelling of deep waters containing dissolved iron (e.g. Coale et al. (1996a)) and, nearer the coast, fluvial discharge (e.g. Chase et al. (2007)). Fe delivery to the ocean surface by dust deposition presents unique challenges and complexities in understanding the cause and effect of fertilisation on phytoplankton communities. This is due to the composition and availability of the suite of nutrients and minerals in the dust as well as the aforementioned growth limiting factors of the receiving marine environment at the time of deposition. A number of well-referenced global reviews on the atmospheric transport of terrestrial Fe to the oceans exist (Jickells & Moore, 2015; Choobari et al., 2014; Jickells et al., 2014; Okin et al., 2011; Boyd et al., 2010b; Maher et al., 2010; Mahowald et al., 2009; Jickells et al., 2005; Mahowald et al., 2005; Gao et al., 2001). These widely agree that desert-derived mineral aerosols are the preeminent source of iron to the open ocean and that atmospheric processing increases the bioavailability of Fe between source and sink. It is further agreed that, following deposition, the process of phytoplanktonic uptake and Fe utilisation is governed by a complex and poorly-understood hierarchy of conditions including ocean acidity (Shi et al., 2010), phytoplankton community composition (Hutchins et al., 1999), limitation and co-limitation by other nutrients (Mills et al., 2004).

The bioavailability of iron when it is deposited on the ocean surface is especially not well understood (Mahowald et al., 2009) and is often reported as the fraction of Fe(II), or Fe^{2+}, (Mahowald et al., 2005; Zhu et al., 1997) in captured dust deposition sediments. Yet Fe(III), or Fe^{3+}, can also be bioavailable (Barbeau, 2006) and Fe^{3+} is the primary state of desert-derived mineral aerosols (Shi et al., 2009). Further, Fe^{3+} is converted into Fe^{2+} both

during atmospheric transport and then also by oceanic processing once suspended in ocean waters, Figure 9. Bioavailable Fe in dust as a fraction of total Fe (the sum of the three Fe types given in Table 3) has been reported in ranges from 0.01 – 80% (Mahowald et al., 2009) and is highly dependent on the laboratory techniques used, namely both the acidity of the leaching solution and digestion time increases the Fe dissolution (e.g. (Boyd et al., 2010a; Gaspari et al., 2006; Guieu & Thomas, 1996). The main impact of depositional iron supply is an initial rapid release of iron, followed by a secondary slower, sustained release of iron during its residence in the surface waters (Boyd et al., 2010b). The delayed response has been theorised to be due to the dissolving of non-bioavailable Fe into additional bioavailable fractions (Boyd et al., 2010b; Kraemer et al., 2005), drawing parallels with the similar observations of acidity and time increasing the dissolved bioavailable fraction in the laboratory. Further, microbial remediation of mineral Fe into phytoplankton-available forms is also likely to increase bioavailable Fe during residence time in surface waters (Boyd et al., 2010b). It has also been argued that all incoming Fe may be considered bioavailable if residence time and the breadth of nutrient-uptake abilities from diverse biological communities are considered (Weber et al., 2005).

For the purposes of depositional ocean fertilisation investigations it is therefore appropriate to classify three types of Fe, as shown in Table 3 based on a combination of the classification schemes of Visser et al. (2003) and Mackie et al. (2006)

The most bioavailable Fe form, the amorphous iron-(hydr)oxides, have the highest chemical reactivity (Visser et al., 2003) and are most easily dissolved in seawater (Kuma & Matsunaga, 1995; Zhuang et al., 1992), thereby being available for immediate biological uptake as would occur during dry deposition (Buck et al., 2006). Visser et al.

Table 3 Ocean fertilisation classification of Fe in depositional mineral aerosols

Fe type	**Mineralogy**	**Bioavailability**
Readily released, or instantaneously soluble, fraction	amorphous iron-(hydr)oxides	5-10 seconds upon contact with seawater
Acid-leachable	crystalline iron-(hydr)oxides	Hours to days
Refractory	structural elements of crystalline minerals	Not soluble under typical atmospheric conditions

(2003) and subsequent global reviews (e.g. Jickells & Moore (2015), Mahowald et al. (2009)) consider bioavailable Fe the most important Fe fraction of mineral aerosols. It is this fraction of Fe that is referred to as bioavailable Fe in this research.

In summary, while sole-nutrient limitation by N (Howarth & Marino, 2006) and P (Downing et al., 1999) has been reported in the oceans, primary production is intertwined with the availability of trace metals (Wu et al., 2000; Boyd et al., 2000; Falkowski et al., 1998), of which Fe is the most commonly limiting (Moore & Doney, 2007). Mineral dust typically contains substantial amounts of N, P and Fe and other potential micronutrients that are transported to the ocean surface through wet and dry deposition (Schulz et al., 2012; Duce & Tindale, 1991). During atmospheric transport the mineral and nutrient composition is altered through atmospheric processing, increasing the bioavailability of nutrients. This processing only serves to increase the bioavailable fraction of aerosol-bound nutrients (e.g. Zhuang et al. (1992)), not diminish it. Therefore, the first order determinant for the fertilisation potential of dust is defined by the source deposit and the nutrient composition of the deflated material, which may then be increased during transport.

2.4 Dust nutrient loading – importance of source

Investigation into the spatial variability of dust source mineral and nutrient composition is a current research need (Zhang et al., 2015) in order to better understand the impacts of mineral aerosols within the Earth System and feed into earth system models. Competing theories are presented in the literature on the relative importance of grain size (Baker et al., 2006), mineralogy of source material (Journet et al., 2008) and element speciation (Schroth et al., 2009) on the bioavailability of nutrients, most notably Fe, in dust. Irrespective of which plays the most important role, likely a combination of processes, it remains crucial to investigate the chemistry and bioactive potential of sediment in active dust source areas. In order to assess the major fertilisation potential of dust and its source the inclusion of N and P macronutrients in various forms of bioavailability as well as bioavailable Fe is essential.

Heterogeneity is known to exist between dust source areas that could be defined as 'hot-spots' of emission (e.g. across dust sites in China (Arimoto et al., 2004), northern Africa (López-García et al., 2017; Formenti et al., 2003; Eltayeb et al., 1993; Schütz & Sebert, 1987), South America (Gaiero et al., 2007), the USA (Desboeufs et al., 2005) and between the geomorphologically similar and regionally adjacent sources of Etosha and Makgadikgadi Pans (Bhattachan et al., 2015a)). A broad overview of the mineralogy of potential dust source regions was compiled by Claquin et al. (1999). This global study combined the mineralogical composition of characteristic arid soils, focusing on the minerals quartz, feldspar, the carbonates, gypsum, the iron oxides hematite and goethite and the clay minerals illite, kaolinite and smectite. Further estimates of the global spatial distribution and bioavailability of P and Fe in soils have been attempted (e.g. Yang et al.

(2013) and Zhang et al. (2015)) for incorporation in biogeochemical models but large degrees of uncertainty (50-60%) remain.

Studies with a focus on the N, P and Fe content of dust sources in the context of potential ocean fertilisation are considered here. Direct comparison of nutrient content, especially bioavailable fractions, between studies poses difficulties due to varying analytical methods[2] that produce varying results with differing detection limits and analytical errors (Formenti et al., 2011). Further, laboratory extraction methodology variations, such as the choice of extracting agent and the subsequent solution volume, pH, temperature, and mechanical agitation, also affect the results (López-García et al., 2017; Anderson et al., 2010). Call for the standardisation of the methodologies has been made previously to improve the data sets available to biogeochemical models (Boyd et al., 2010b), which would also greatly improve the inter-comparison of dust source nutrient content. Broadly, atmospheric loadings of N are mainly from agricultural sources or anthropogenic combustion while P and Fe loadings are mainly derived from desert dust and some anthropogenic sources (Guieu et al., 2014a; Mahowald et al., 2008). It is noted that bioavailable nutrients in dust source sediments are considered conservative in comparison to deposition-captured sediment that has undergone bioavailability enrichment via atmospheric transport (Zhang et al., 2015; Nenes et al., 2011).

[2] As described by Scheuvens et al. (2013) and Brown (1998), these include Spectrophotometer Colorimetric determination, Atomic Absorption Spectroscopy (AAS), Inductively Coupled Plasma Mass Spectrometry (ICP-MS), Inductively Coupled Plasma Optical (Atomic) Emission Spectroscopy (ICP-OES or ICP-AES), X-ray Fluorescence analysis (XRF), Instrumental Neutron Activation Analysis (INAA), Proton Induced X-ray Emission (PIXE), or traditional techniques as titration and gravimetry.

2.4.1 Nutrient loading of dust sources

2.4.1.1 Phosphorus

P availability for primary production in terrestrial systems has long been associated with pedogenesis (Walker & Syers, 1976), the weathering of rock providing the source of P in soils and, if not replenished, depletion can occur in very old soils (Vitousek et al., 2010). The Namib Desert may be the oldest in the world (Goudie, 2009) but weathering of rock outcrops in the Namibian escarpment, highlands and Namib Desert has occurred through the Pleistocene and continues to this day (Viles, 2005; Bierman & Caffee, 2001), ensuring P availability.

The global average soil concentration of total phosphorus (TP) is accepted as 700 ppm (Taylor & McLennan, 1995), with an average enriched P content of 720 ppm assumed in global dust models (Myriokefalitakis et al., 2016; Wang et al., 2015; Brahney et al., 2015), but significant geographical variation of this value exists, as synthesised in the global review by Mahowald et al. (2008). Saharan dust studies showed a typical concentration of 720 ppm but recent investigation highlighted the heterogeneity of P content from different Saharan source areas (Gross et al., 2016), the Mediterranean soil P ranges from 900 to 1300 ppm with fertilized agricultural regions in Asia reporting 1090 ppm (Mahowald et al., 2008; Carbo et al., 2005). In order to predict the P content of deflatable soils, the pedogenic processes, grain size and anthropogenic perturbations to the natural P cycles need to be identified (Mahowald et al., 2008). Yet the known terrestrial P enrichment corridors of rivers (see review of natural and anthropogenic pathways by Withers & Jarvie (2008)), which are increasingly being investigated as regular dust emitters, have had little research attention that connects riverine and aeolian nutrient fluxes.

2.4.1.2 Nitrogen

The nitrogen cycle differs from P and Fe in that it involves a stable gaseous phase, N_2. This abundant gas comprises 78% of the earth's atmosphere and becomes biologically available once converted into the reactive nitrogen (fixed nitrogen) compounds; nitrogen oxides, nitrate, ammonia. This is achieved naturally through marine microbial-fixation (as previously outlined, Figure 9) and similarly through soil microbial-fixation (Burns & Hardy, 2012). Reactive, or bioavailable N, therefore enters the ocean either through marine N-fixation or the transport of terrestrial reactive nitrogen by rivers or atmospheric deposition (Duce et al., 2008). These terrestrial reactive forms are immediately available for phytoplankton uptake compared to the diazotroph-dependant N-fixation. It is noted that major anthropogenic perturbations to the N cycle have occurred. This is due to industrial N-fixation which is then applied to agricultural lands as fertiliser and the production of reactive N compounds by internal combustion engines. Because both emission sources are associated with regions of high human density, the main emission sources are in Southeast Asia, North America, and Europe (Jickells & Moore, 2015). These are not directly applicable to Namibia, being one of the world's least densely populated countries (Population Division of the Department of Economic and Social Affairs of the United Nations Secretariat, 2009), allowing an assessment of the natural N contribution to mineral aerosol loading.

2.4.1.3 Iron

The mineral Fe makes up, on average, 3.5% of the earth's upper continental crust (Taylor & McLennan, 1995) yet is frequently limited in the world's oceans due to low solubility and high biological demand (Martin et al., 1994). Soils influenced by different geological origins and geomorphological processes can have varying amounts of Fe (Hand et al., 2004; Claquin et al., 1999). Fe is naturally found in numerous terrestrial minerals, notably

feldspars, clays, oxides, hydroxides and predominantly in desert soils as iron oxides, mainly hematite (Fe_2O_3) and goethite (FeOOH) (Lafon et al., 2004), which give the soils their characteristic yellow-red colour (Torrent et al., 1983). However, it is the solubility of iron, which determines the biotic availability, that is most pertinent for primary production (Jickells et al., 2005). Of particular note regarding the provenance of dust is that bioavailability is inversely related to chemical weathering exposure and the resulting concentration of Fe-oxide levels. As shown in Figure 10, fluvial sediments have a greater content of soluble Fe than the exposed, weathered surface sediment with sub-surface paleo sediments having the highest potential Fe solubility. The intermittent and endorheic flows of the Namibian ephemeral river valleys would provide an environment conducive to minimal weathering of Fe oxides, and therefore high solubility or bioavailable Fe in the valley fill as portrayed in Figure 10.

Much remains unknown with regards to the bioavailability and speciation of Fe within source environments (Schroth et al., 2009). The relative ratios and abundance of the Fe species are determined by environmental factors such as weathering and parent rock composition, which result in spatial variability of Fe species and solubility of soils, and consequently of dust sources (Cwiertny et al., 2008).

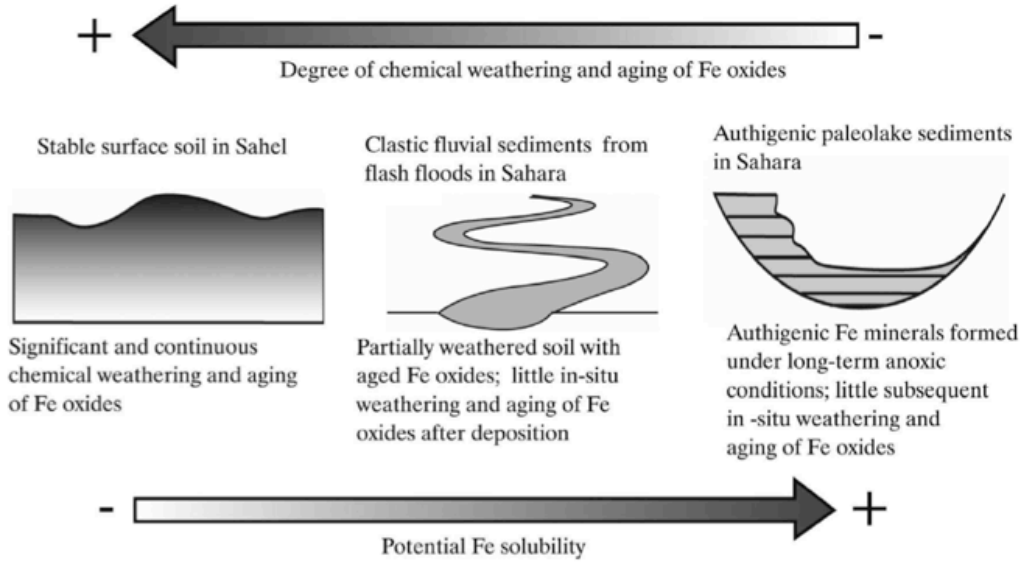


Figure 10 | Weathering and solubility of Fe in desert soils (Shi et al., 2011)

The bioavailability of Fe is further altered during aeolian transport. The fraction of depositional Fe that dissolves in seawater, becoming bioavailable, is influenced by atmospheric factors that remain poorly understood (Baker & Croot, 2010). This fraction of soluble iron on aerosols has been found to increase during aeolian transport in association with low pH conditions inside clouds (Mackie et al., 2005) and exposure to high UV levels in the atmosphere (Tagliabue & Arrigo, 2006). The bioavailable Fe fraction is known to correspondingly increase with transport distance and atmospheric residence time. Competing theories of dust particle size (Baker et al., 2006), source sediment geochemistry (Journet et al., 2008) and iron speciation (Schroth et al., 2009) exist as explanations for maximising the Fe bioavailability of dust. Both smaller grain size and higher clay content of dust material have been shown to relate to higher bioavailability. The broad classification 'atmospheric processing' is used to describe the bioavailable nutrient-enhancing processes during transport, which remains one of the least understood components of the global ocean cycle (Buck et al., 2010b). The combination of source sediment Fe bioavailability then being subject to atmospheric

processing would determine the ultimate Fe bioavailability of mineral aerosols that land on the ocean surface.

2.4.2 Rivers and aeolian dust research

Globally, aeolian transport and deposition is the second largest contributor of sediment and associated nutrients to the ocean (Mahowald et al., 2008; Jickells et al., 2005). Fluvial delivery provides the largest contribution of sediments (Syvitski, 2003), Fe (Poulton & Raiswell, 2002), and N and P derived from both natural processes and human activities (Glibert et al., 2006; Howarth & Marino, 2006) to the ocean. However, ocean fertilisation pathways that encompass both modern fluvial sources and atmospheric transport have yet to be thoroughly investigated.

River sediments have been known to possess fine fractions highly suitable for aeolian transport for decades (e.g. Nickling (1978)). However, research on riverine dust has traditionally been carried out to ascertain the human health impacts. Polluted rivers, when dry, emit aeolian particles with correspondingly elevated pollutant levels, notably heavy metals, that pose health risks to surrounding human populations. This has been investigated in response to long-term pollution in rivers, e.g. Taiwan (Kuo et al., 2010), as well as in direct response to industrial accidents, e.g. Hungary (Gelencsér et al., 2011).

The accumulation of anthropogenic pollutants in waterways and their attachments to riverine sediments is synonymous with P and N transport pathways, which are well understood (e.g. Meybeck (1982)). Phosphorus enrichment is known to occur in fluvial sediments (Welch & Cooke, 1995) as a result of P sorption to sediment grains (Lair et al., 2009; Barrow, 1980), and increased levels of both P and N in waterways is becoming widespread as a result of agriculture and intensifying land use (Downing & McCauley, 1992). Yet the connection between rivers as known nutrient accumulation corridors and

their potential for significant dust emission has not seen much research attention as a nutrient flux pathway within Earth System science. Only in the last few years has there been the beginnings of some thorough field-based and remote sensing investigation of river dust sources. These have been the Tigris and Euphrates rivers in Iraq (Jish Prakash et al., 2015), the eastern Great Basin in the United States (Brungard et al., 2015), and high latitude rivers in Alaska (Crusius et al., 2011), Iceland (Arnalds et al., 2016) and Antarctica (Bhattachan et al., 2015b). Yet research on river valleys as 'hot-spots' of dust emission have been the exceptions to the dominant paleolacustrine and ephemeral pan research foci.

Emergent research on the ocean fertilisation potential of riverine dust shows that the interest is justified, with promising results of enriched dust source sediments reported across geographically distant high-latitude source areas. Glacio-fluvial sediments and river plains have been shown to be major sources of Icelandic dust storms (Arnalds et al., 2016) and, importantly for ocean fertilization, glacial sediments are a known enriched source of bioavailable Fe. This is due to the glacial mechanical production of fines that have then been subject to little exposed weathering (Shi et al., 2012; Schroth et al., 2009; Journet et al., 2008). Similarly in Alaska river deltas comprised of fine, glacial-flour sediments were observed to emit plumes of dust over the Gulf of Alaska and shown to contain high levels of bioavailable Fe (Crusius et al., 2011). The only riverine dust study in the southern hemisphere to consider ocean fertilisation potential to-date, in dry river sediments in Antarctica, also showed elevated bioavailable Fe levels compared to non-riverine sediments (Bhattachan et al., 2015b). A recent review of the high-latitude dust source areas summarised that high-latitude dust source areas are associated with riverine floodplains, dry river valleys and glacial outwash deposits (Bullard et al., 2016), underlining the importance of these geomorphological features in global dust emissions.

The highly productive Amazon Rainforest ecosystem is reliant on external P inputs, much of this delivered from a single ancient lake bed in Africa. It is therefore feasible that many small yet nutrient rich sources of mineral aerosols from the world's ephemeral, dry and drying rivers provide a major combined input of aeolian nutrients to the world's ocean, that is an important yet underappreciated part of the Earth System. The ephemeral river valleys of Namibia, known to emit dust and located adjacent to the productive Benguela Current upwelling region of the South Atlantic, provide an ideal setting to investigate this.

Although the contribution of the Southern Hemisphere to the global dust budget is relatively small, Southern Hemisphere dust sources are expected to have a disproportionately large global impact on ocean fertilisation (Jickells et al., 2005). The primary production-limited southern oceans are especially reliant on aeolian dust deposition to deliver biologically-essential Fe and nutrients. There is also therefore a need to better understand these dust sources and the role they play in ocean productivity.

2.5 Southern African Dust

2.5.1 Dust Sources

Southern Africa is one of the three major sources of mineral aerosols in the Southern Hemisphere (Piketh et al., 1999), which compared to the northern hemisphere is significantly less dusty due to the configuration of source areas and a smaller land mass area (Mahowald et al., 2005; Prospero et al., 2002; Gao et al., 2001). Aerosol loading over southern Africa has been shown to be dominated by aeolian dust (Piketh et al., 1999), countering previous hypotheses of the dominance of particulates from biomass burning (Van Wilgen & Scholes, 1997; Levine, 1996). Dust export from this region to the ocean has largely focused on understanding paleoclimates (Lambert et al., 2015; Nakai et

al., 1993; Olivarez et al., 1991) with correlations made between aridity, wind regimes and aeolian transport off the western coast of Namibia (Stuut et al., 2002), with fertilisation of the South Indian Ocean by southern African dust having been hypothesised (Piketh et al., 2000). Modern dust departure from southern Africa has an estimated mass flux of 29 million tons of aeolian transport to the west over the Atlantic Ocean and 45 million tons eastward to the Indian Ocean (Tyson et al., 1996), with southern African dust occurring as far as 4000 km offshore in the tropical North Atlantic (Swap et al., 1996).

Four key southern African dust source areas are identified (Figure 11a), using both TOMS and MODIS remote sensing identification, as being the major contributors to southern African dust; the Makgadikgadi Pan system in Botswana, the south-western Kalahari in South Africa and Namibia, Etosha Pan in Namibia and the region of the ephemeral river valleys of Namibia (Ginoux et al., 2012; Engelstaedter & Washington, 2007; Washington et al., 2003). The most detailed and high-resolution regional analysis of southern African dust sources undertaken to date, by Vickery et al. (2013), corroborated the dominance of these four sources in southern African dust emission.

Of these regional dust emission sites, the Makgadikgadi Pan system in Botswana and Etosha Pan in Namibia have seen the most research attention. This is due to both their being major dust emission sites but also perhaps somewhat skewed in regional importance as a result of their early-on identification using TOMS lower-resolution

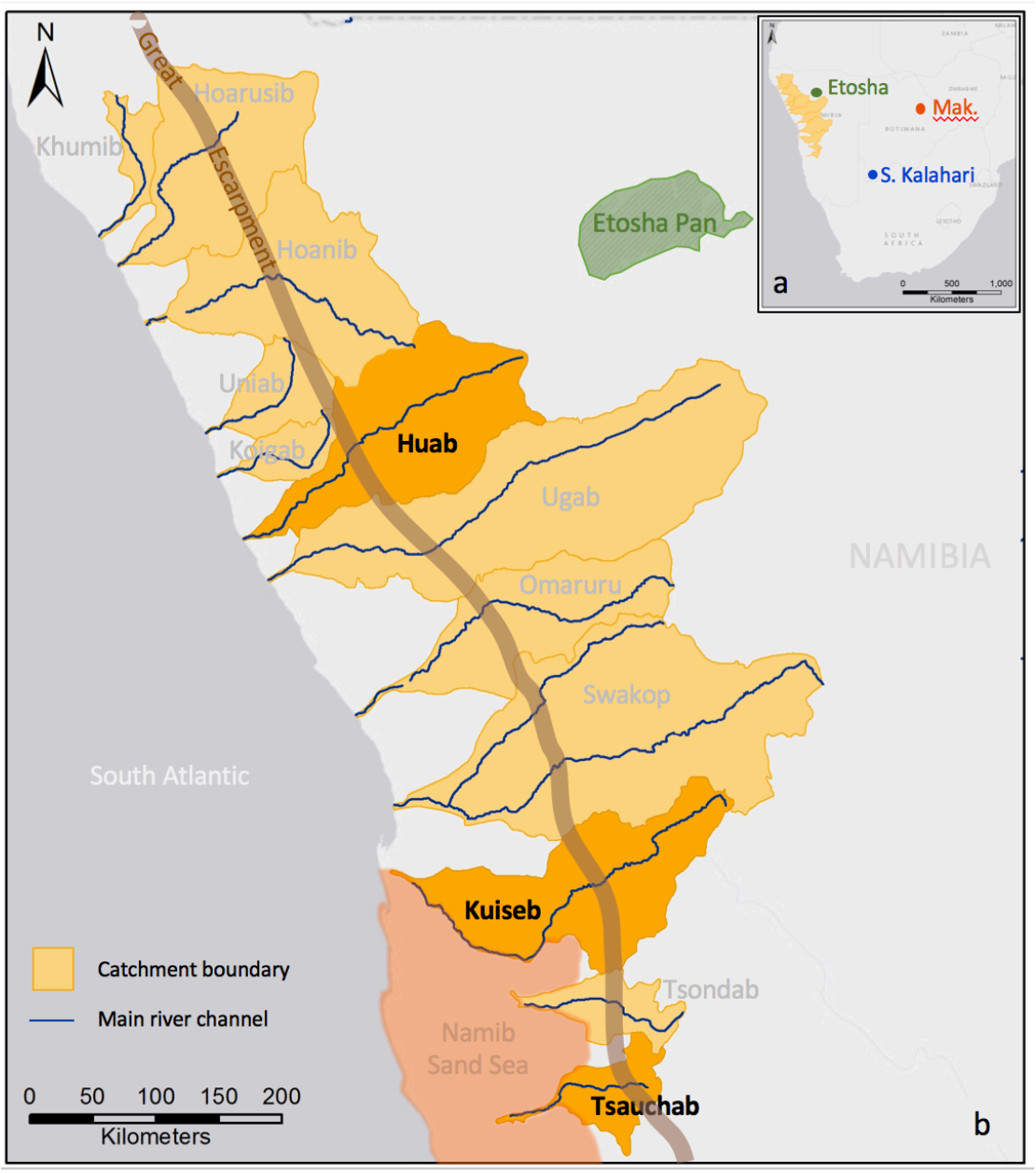


Figure 11 | (a) The major dust emission sites of southern Africa: Etosha Pan, Makgadikgadi Pan (Mak.), the southern Kalahari and the ephemeral river valleys of Namibia, (b) the twelve river valleys showing the three focused on in this research, the Huab, Kuiseb and Tsauchab.

global assessments (e.g. Prospero et al. (2002)). In the literature Makgadikgadi Pan is widely considered one of the world's major dust sources (Vickery, 2014; Bryant et al., 2007; Washington et al., 2003; Prospero et al., 2002) with emitted dust observed to be distributed across southern Africa (Resane et al., 2004) and models show contribution to

southern African dust loading over the Indian and Atlantic oceans (Ginoux et al., 2004). As part of the DO4 Models research project, intensive field-based investigation of Sua Pan, within the Makgadikgadi Pan system, was undertaken in 2011 and 2012. This used the dust and meteorological monitoring equipment subsequently deployed in the Namibian river valleys for the research presented in this thesis. The findings suggest that modelled dust emissions are significantly misjudged with horizontal flux overestimated by several orders of magnitude and vertical flux up to one order of magnitude (Haustein et al., 2015). Etosha Pan, as another TOMS-identified key dust source area (Washington et al., 2003), has also been shown to emit aerosols that are transported across southern Africa (Haywood et al., 2003) and similarly included in modelled emissions of dust over the Indian and Atlantic Oceans (see Tanaka & Chiba (2006), Ginoux et al. (2004)). This ephemeral pan has also been the focus of research into the impact of hydrological controls of dust emission (Bryant, 2003; Mahowald et al., 2003). Etosha Pan is the focus of DO4 Models investigation in 2015-2016.

The Kalahari dust sources are not associated with fluvial geomorphology, rather the dune and interdunes are subjected to aeolian erosion when the stabilising savannah vegetation is disturbed, with emissions reported to regularly reach the Southern Ocean (Bhattachan et al., 2012). There is potential for these dust emissions to increase should the largely inert, vegetated dunes be remobilised (see Wiggs et al. (1995)) due to vegetation degradation from overgrazing (Thomas & Twyman, 2004). In the long term Kalahari dune emissions are predicted to increase significantly through the 21st century due to climate change drivers mobilising the dunes (Thomas et al., 2005).

Only recently has the nutrient content for potential ocean fertilisation of these dust sources been investigated. Bhattachan (2015a) completed this first analysis for three of

the four major dust emission regions of southern Africa; the two pans and the Kalahari. Their results found that the fine fractions (<45 μm) of Makgadikgadi and Etosha pans were enriched in N and P compared to the parent material but not so for bioavailable iron. The Kalahari fine fraction was only enriched in N, with P and Fe higher in the parent material.

The biogeochemical analyses of southern African dust source sediments are the beginnings of being able to accurately constrain models of dust emission, transport and potential ocean fertilisation (Bhattachan et al., 2015a). As the investigation by Bhattachan et al. (2015a) targeted dust sources identified using TOMS aerosol optical thickness by Prospero et al. (2002) and Washington et al. (2003) the ephemeral river valleys of Namibia were once again overlooked.

2.5.2 Dust from Namibian River Valleys

The river valleys are known to emit ribbon-like dust plumes over the South Atlantic, Figure 12a and b, with contribution of aerosols also originating from coastal sabkas, most notably along the skeleton coast (Figure 12a).

Successive sub-regional studies within southern Africa have identified the importance of dust-emitting regions previously disregarded by global and regional TOMS investigations that were limited in their resolution. This is seeing a rise in research attention on the Namibian river valleys, the most recent and thorough of which are the intensive monitoring and dust capture field investigations of the Dust Observation for Models (DO4 Models) project to which this research is linked. First investigated as dust sources by Eckardt & Kuring (2005), the Namibian ephemeral river valleys were identified as reliable annual emitters of dust with the source sediments hypothesised as being supplied

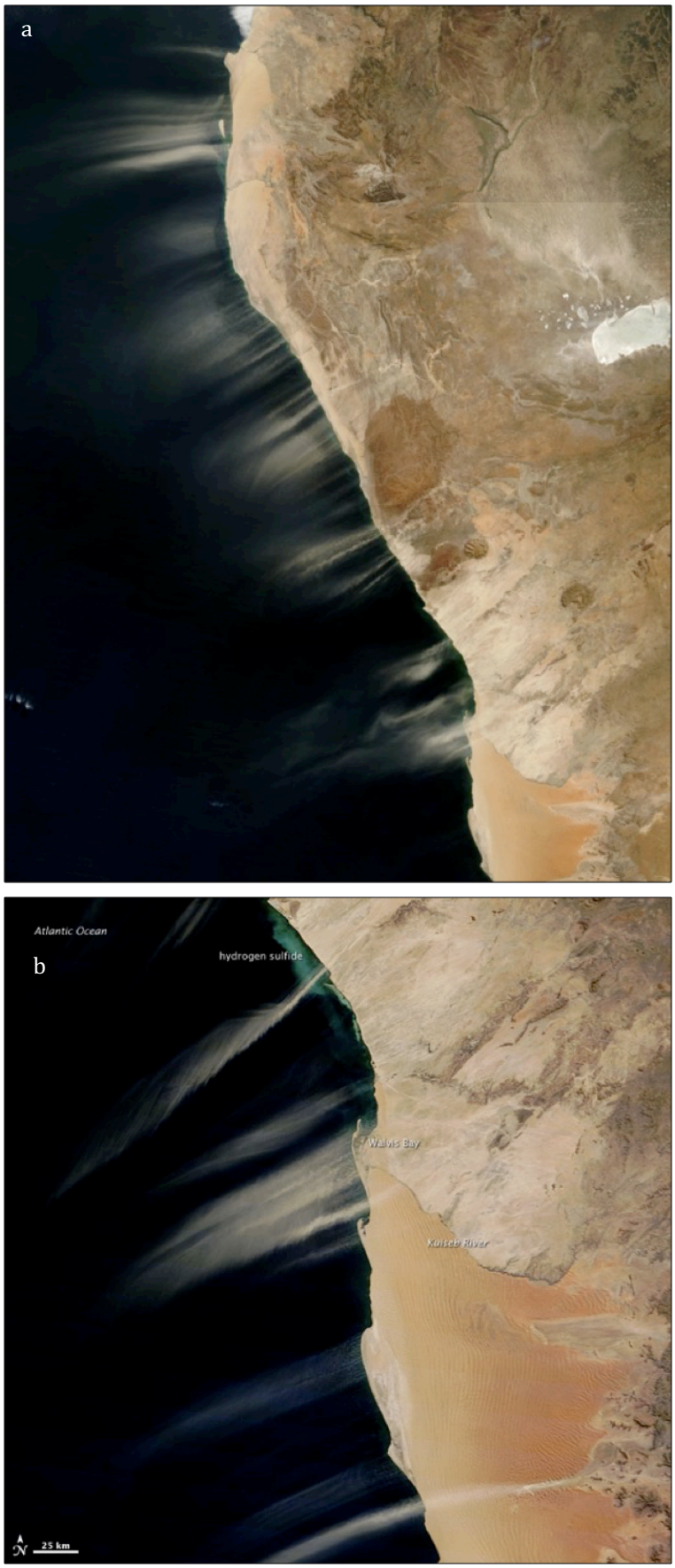


Figure 12 | True colour image from NASA's MODIS Terra satellite showing dust plumes extending from the coast of Namibia on a) 9 June 2004 (NASA, 2004) and b) 17 June 2010 (NASA, 2010).

by fluvial processes. The study reported 150 plumes from the river valleys and coastal sabkas between 1998-2001. In the same year two near-coastal, but non-riverine, dust source areas were modelled to emit a combined estimated 100,000 tonnes annually, with 4,437 tonnes estimated to contribute to ocean deposition (Tlhalerwa et al., 2005). No such estimates exist for dust plumes from the river valleys but intensive analysis of remotely sensed data by Vickery et al. (2013) provided the first high-resolution regional assessment of southern African dust sources. Dust events were identified by visual examination using multisensor imagery incorporating MODIS visible composite data from NASA Terra and Aqua platforms, and the Spinning Enhanced Visible and InfraRed Imager (SEVIRI) instrument on-board the Meteostat Second Generation (MSG) satellite utilizing the brightness temperature difference. Three images per day were analysed. This resulted in a much higher spatial and temporal resolution than is possible through TOMS dust plume identification methodologies. Regionally, Vickery et al. (2013) identified a total of 328 plumes between 2005 and 2008 originating from 101 source locations. Of these 101 source locations, 70 were located in the Namib Desert and it was ephemeral rivers that accounted for 55% of the plume sources in this region and 34% of total plumes in the entire study area. The Makgadikgadi Pan accounted for 16% of plumes and Etosha 10%. Thus, if the river valleys were considered a single source, as they could be regarding their ocean fertilization potential, then their emission frequency would be twice that of Makgadikgadi Pan (111 vs. 53 weighted emission frequency), see Figure 13. These findings propelled the Namibian ephemeral river valleys into the research spotlight of the DO4 project as significant emitters of dust.

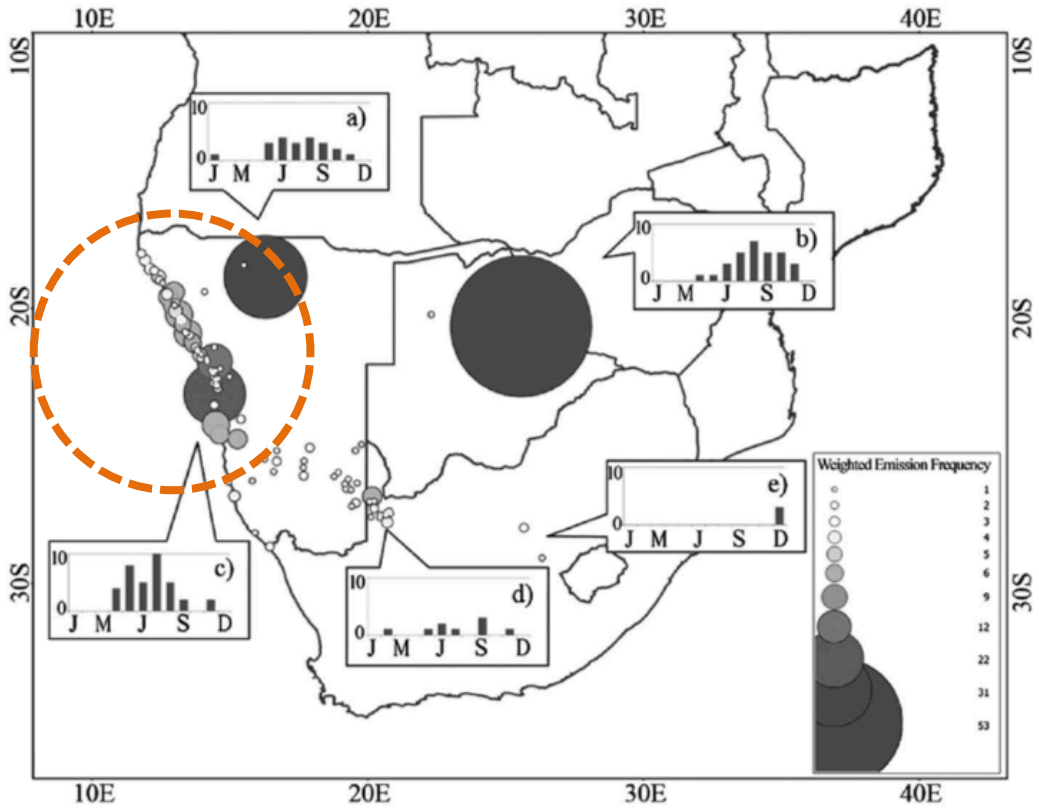


Figure 13 | Southern African dust plume source locations. Plume frequency and timing for the various regions: (a) Etosha Basin, (b) Makgadikgadi Basin, (c) Namib Coastal Sources, (d) South Western Kalahari Sources, (e) Free State Sources. Weighted emission frequency for combined ephemeral river plume count (111) shown with dashed-line. Adapted from Vickery et al. (2013).

The Kuiseb (see Figure 11b), identified as the dustiest river valley by Vickery et al. (2013), has also been the subject of further studies. Von Holdt (2013) determined that the surface sediments of the Kuiseb river valley increase in suitability for dust production towards the coast. The silt crust that is formed by evaporating flow and floodwaters provides the main source of appropriately sized material for deflation (Von Holdt, 2013). Vickery and Eckardt (2013) further investigated the dust emission control in the lower Kuiseb Valley, looking at 22 events that were identified on 15 days during 2005-2008. Of these events 19 originated from the Kuiseb main river channel and delta with three coming from tributary channels feeding into the Kuiseb across the gravel plain (Vickery

& Eckardt, 2013). The furthest plume inland was 100 km from the coast, with 41% of plumes coming from the river channel and tributaries. The delta produced 59% of identified plumes. The remote sensing studies to date demonstrate the importance of fluvial processes providing a highly-erodible source material that is consistently emitted from the river valleys as dust, with each valley on average emitting around five to eight major plumes each year.

Aeolian sediments have been identified off the Namibian coast in seabed sediment cores by Stuut et al. (2002) and used as a signature of terrestrial aridity in south western Africa over the last 300 kyr. Grain size analysis (undertaken in the range of 0.5 – 100 μm only) followed by end member modelling of results was used to distinguish fractions of fine and coarse aeolian sediments (modal grain size of 7 μm and 13 μm respectively) from the hemipelagic sediment. Pichevin et al. (2005) identified an aeolian component of coarser grains, between 50-60 μm, in the sediment cores using statistical modelling, which were considered to be transported by low-altitude winds. Dust collection was undertaken during the core sampling over an ~800 km ocean transect using a pump filter (dust sampler model GMWL 2000) and showed mean particle size of ca. 20 μm. During the collection period a 20-28 $km.h^{-1}$ SSW wind was present (Stuut et al., 2002) and no active dust emission was occurring from the coast.

In summary, Namibia's ephemeral river valleys adhere to the prerequisites to be considered dust emission 'hot-spots'. Observed to regularly emit dust (Vickery et al., 2013; Eckardt & Kuring, 2005), they possess a fluvial geomorphology within a dryland environment (Jacobson et al., 1995) that is subject to seasonal, strong winds (Lindesay & Tyson, 1990; Newell et al., 1972). These seasonal easterly winds occur during the austral winter months, as evident in Figure 14. Easterly and north-easterly winds are clearly

prominent from April – July. The north-easterly winds are also considered to demonstrate the topographic influence on wind direction close to ground level (Figure 14, caption), a further influence on dust emission from the E-W aligned river valleys.

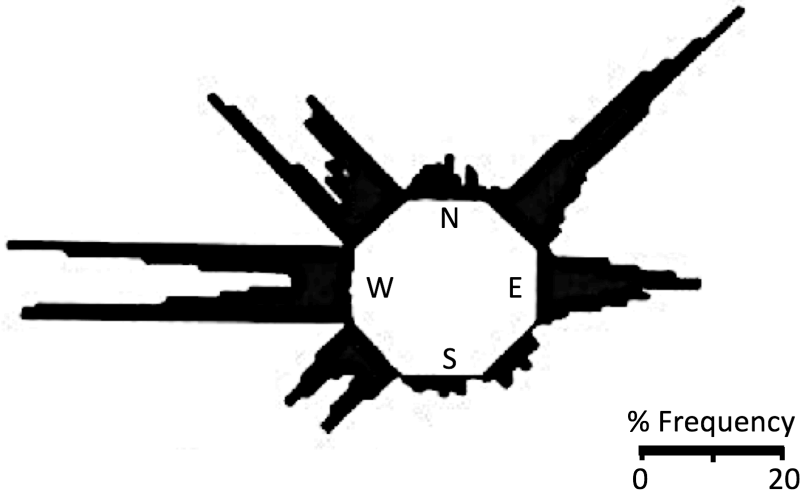


Figure 14 | Seasonal variations of wind direction in the central Namib Desert showing the proportion of winds from eight major compass directions in each month (Jan-Dec in a clockwise direction). Wind measured at a height of 3 m and recorded adjacent to a NE-SW-aligned portion of Namib Sand Sea border to the east of the Gobabeb Research and Training Centre and local topographic channelling, adapted from Lancaster (1989).

Further, the extant fluvial processes of the ephemeral systems would continuously replenish and rework the historical alluvial valley floor sediments (Heine & Völkel, 2010; Reid & Frostick, 1987) and thereby be expected to enhance emissivity. The limited work to-date on nutrients within the river valleys show that sediment associated with the extant channels is enriched in nutrients important for terrestrial photosynthetic biota (Jacobson & Jacobson, 2013; Jacobson et al., 2000). The dust-emitting lower-reaches of the river valleys lay within 100 km of the coast compared to the other major southern African sources; Etosha (400 km), Makgadikgadi Pan (1200 km), and the Southern Kalahari (650

km), Figure 11. The river valleys may therefore be potentially considered an especially important dust source for ocean fertilisation.

Of potential temporal importance for the South Atlantic Ocean, the strong dust-producing easterlies occur when the wind-driven Benguela Current upwelling is at its weakest (Andrews & Hutchings, 1980). While it is noted that the system is complex and many uncertainties remain (Flohr et al., 2014; Chen et al., 2012; Carr & Kearns, 2003), the addition of bioavailable Fe and macronutrients to ocean surface waters, when the vertical transport of cold nutrient rich waters is at the annual minimum (Capone & Hutchins, 2013), may contribute to sustaining productively through the year and is expected to play an important role in primary production.

SECTION 2

- Regional Setting and Methodology -

CHAPTER 3

3 Regional Setting

A large part of southern Africa is under the influence of the atmospheric subtropical high-pressure zone, resulting in the predominantly arid conditions of the region (Shi et al., 2000). The ephemeral river valleys of Namibia are located on southern Africa's west coast, crossing the 2000 km long coastal Namib Desert (Lancaster et al., 1984) between southern Africa's central plateau and the South Atlantic Ocean. In stark contrast to the hyper-arid Namib Desert the coastal waters are part of the highly productive Benguela Upwelling System (BUS), one of four globally significant upwelling regions[3] that cover 1% of the worlds ocean but provide the highest rates of primary production in the ocean (Toggweiler & Carson, 1995; Chavez & Barber, 1987) and support up to 20% of global fish catch (Fréon et al., 2009; Pauly & Christensen, 1995). Coastal upwelling brings cold, nutrient-rich waters from the ocean depths to the surface where the nutrients are then available to sunlight-harnessing photosynthetic plankton communities. This expanse of cold, upwelled surface water induces a strong temperature inversion that reduces convection and minimises precipitation over the adjacent land (Walker & Shillington, 1990), playing a significant role in the aridification of the region (Ward et al., 1983). The upwelling of the Benguela is wind-driven by the near-constant alongshore southeast trade winds that cause the surface and subsurface waters to be driven offshore, by the process

[3] The Benguela upwelling region is one of the world's four eastern boundary upwelling systems (EBUS) that also include northwest Africa, Peru and California.

of termed Ekman Transport (Cosmic, 1987), to be replaced by deep water then transported to the surface as the result (Shannon & Nelson, 1996).

Upwelling of the Benguela system is by far the least seasonal of the four global EBUS (Chavez & Messié, 2009). This has been correlated with the terrestrial steep topographical slope from the coast to the western Kalahari 2000 m above sea level that stabilizes the regional anticyclonic wind pattern and reducing the seasonal variability of upwelling (Hay & Brock, 1992). Though seasonal fluctuation is minimal on a global comparison, the BUS is often separated into three zones according to variations in upwelling regimes (Jury, 2012). The BUS is bounded to the north and south by the Angola and Agulhas Currents, Figure 15. These major currents influence the north and south upwelling zones, seeing increased winter upwelling of the northern zone (Gammelsrød et al., 1998) caused by the intrusion of tropical waters (Rouault, 2012), while the southern zone sees increased summer upwelling (Andrews & Hutchings, 1980). The central zone is the least fluctuating zone (Jury, 2012), often classified as continually upwelling (e.g. Goubanova et al. (2013)) due to perennially consistent SE Trade winds between 22-28°S (Shannon & Nelson, 1996), and is spatially relevant as the deposition region for the river valley dust investigation of this research.

The wind and sea environments of the region are thus explicitly linked, with the aeolian transport of desert-derived mineral aerosols hypothesised to further contribute to this inter-linkage.

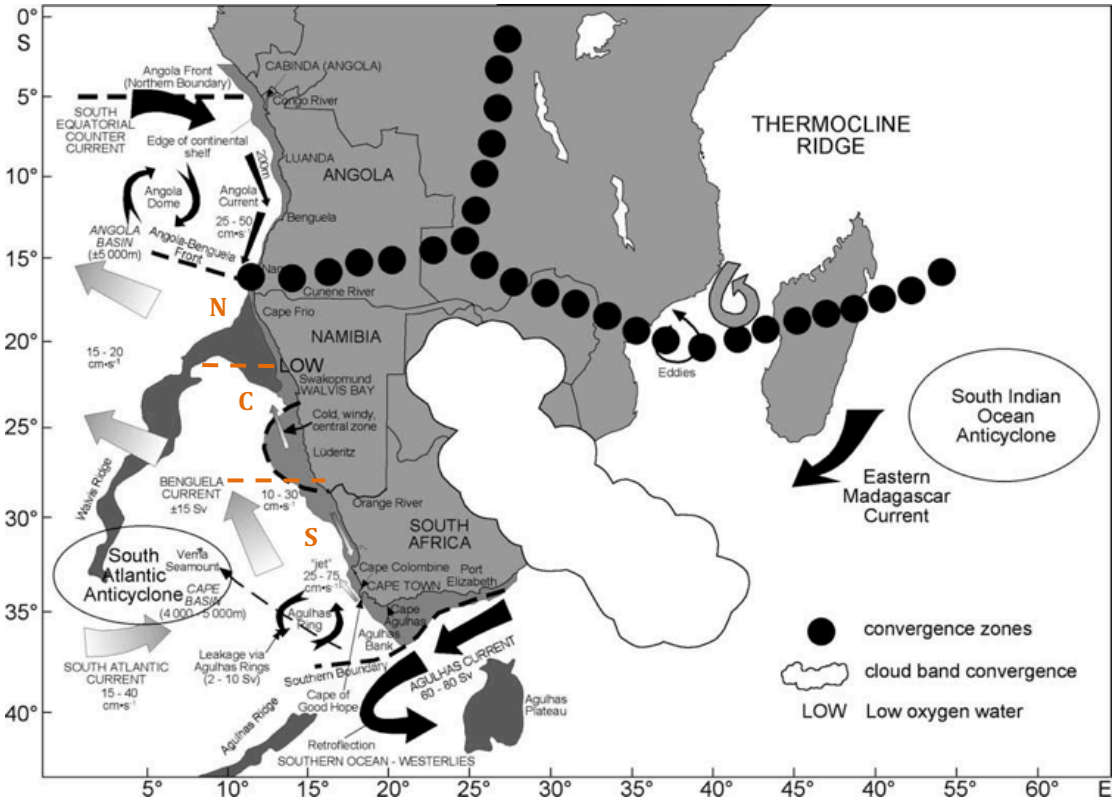


Figure 15 | Regional ocean and atmosphere circulation patterns with (N) northern, (C) central and (S) southern upwelling zones highlighted, adapted from Hutchings et al. (2009).

3.1 Wind patterns

The dust emitting regions of the river valleys lay within 100 km of the coast between the Great Escarpment and Atlantic Ocean. The regional atmospheric circulation patterns see predominantly south to southwesterly trade winds over South-western Africa (Lancaster, 1985). These patterns are generated by the pressure gradient between the South Atlantic Anticyclone (SAA) and the South African high-pressure cell (Shannon, 1985). As summarised by Pichevin et al. (2005), the centre of the SAA shifts seasonally from a southerly Namibian coastal location (30°S, 5°W) in summer to a northern offshore location (26°S, 10°W) during winter (van Loon, 1972), (Figure 15). This large-scale atmospheric shift influences the upwelling cells off the coast of Namibia and southern

Africa and provides the minor, in comparison to EBUS globally, seasonal influences that occur.

The notable exception to the regional patterns are episodic strong east to northeasterly 'berg' winds during the austral winter months (Fryberger et al., 1979), a result of a continental high associated with the seasonal semi-permanent subtropical anticyclonic circulation (Newell et al., 1972). These seasonal wind circulations also affect localised diurnal wind patterns that are produced by a strong thermo-topographic coupling (Lindesay & Tyson, 1990). This generates local nocturnal winds in winter that drain towards the coast (Tyson & Seely, 1980) where the river valleys of Namibia are located. The austral winter is also the known dust season of the river valleys (Vickery et al., 2013; Eckardt & Kuring, 2005). The E-W alignment of the Namibian valleys may additionally funnel the regional easterly and more local winds, enhancing their potential to entrain valley floor sediments, a potential noted by Wiggs et al. (2002).

3.2 The Dry River Valleys of Western Namibia

The Namib Desert runs N-S along the Namibian coast, extending from South Africa to Angola (Heine & Heine, 2002). The Central Namib Desert, from Walvis Bay to Lüderitz, comprises the extensive dune fields of the hyper-arid Namib Sand Sea (Lancaster, 1989). North of the Namib Sand Sea gravel plains occupy the 150-200 km coastal strip for 500 km until a smaller, northern sand sea begins near the Huab River mouth (Grünert, 2000). The coastal Namib receives almost zero precipitation with the non-river channel biota reliant on the frequent ocean fog.

Twelve ephemeral rivers run east-west along the western coast of Namibia, Figure 16. The river catchments extend inland for over 300 km, on to the 1000 m high Great

Escarpment (Morin et al., 2009), where aridity gives way to semi-arid savannah and average annual rainfall reaches 300 mm a year or more between January and March (Krapf et al., 2003; Jacobson et al., 1995). The Great Escarpment runs parallel to the coast, 100-150 km inland and serves as the eastern border for the Namib Desert and the expansive central plateau of southern Africa (Goudie & Eckardt, 1999). On the plateau and highlands above the escarpment, sufficient precipitation supports vegetation and the development of at least minimal colluvium on hill slopes (Bierman & Caffee, 2001). Below the escarpment, the river channels provide corridors of productivity through the arid landscape (Jacobsen et al., 1995). Ten of the river channels currently reach the South Atlantic, although endoreic flood events are commonplace, while the southern-most two terminate within the Namib Sand Sea, Figure 16. The dust-emitting regions are concentrated in the lower-reaches of the river valleys, within 100 km of the coast or 50 km inland of the sand sea termini (Vickery et al., 2013; Vickery & Eckardt, 2013). Detailed description of each ephemeral river individually can be found in Jacobson et al. (1995).

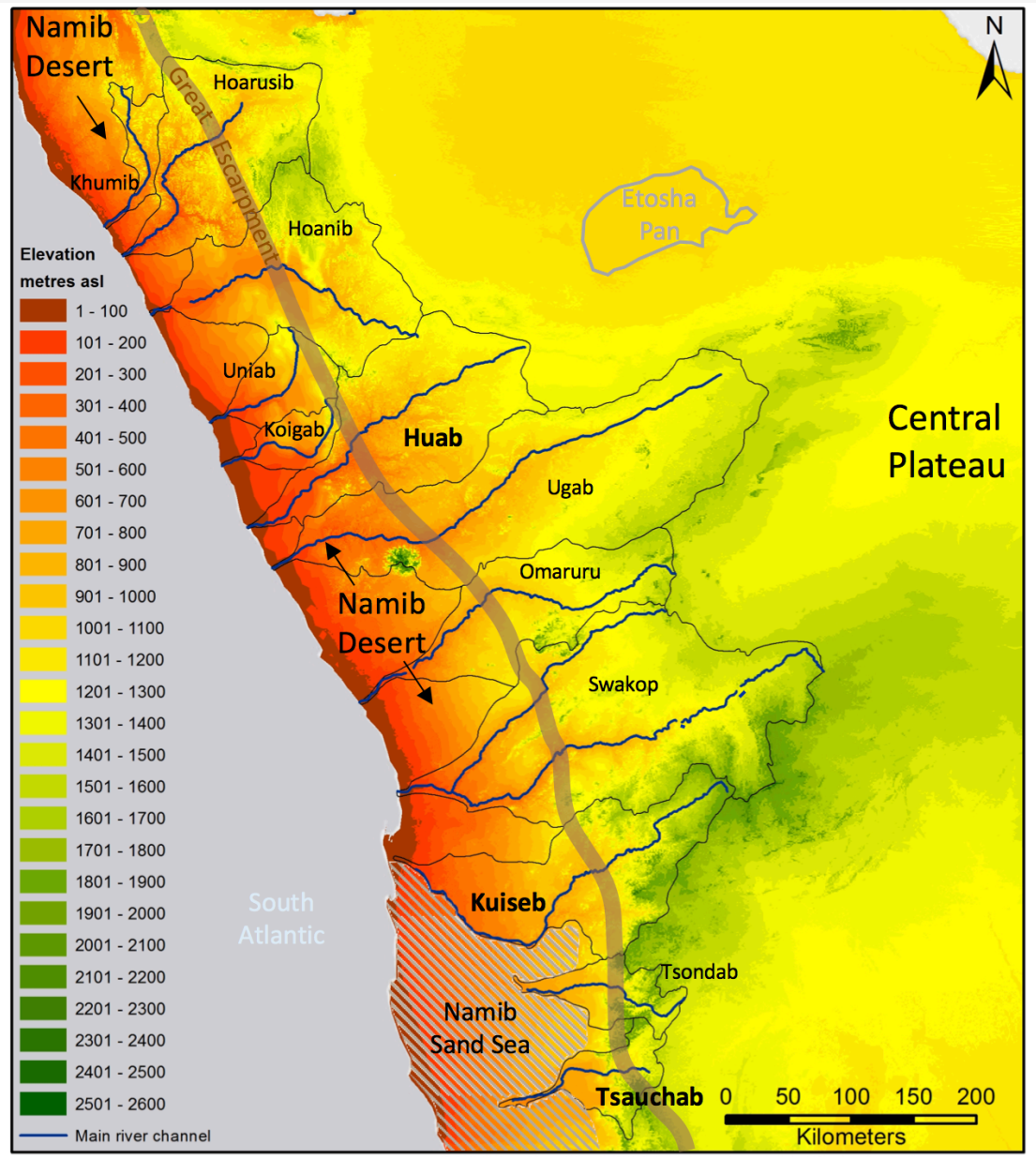


Figure 16 | Namibia's ephemeral river catchments and topographical elevation

3.2.1 Catchment landscape

The predominant geological sequence underlying the river catchments is the 850-500 Ma Damara Sequence comprised of Damaran Granites and Swakop Facies (Jacobsen et al., 1995). The oldest formations in the catchments are found in the Huab, the ancient granites and gneisses being over 2 billion years old (Jacobsen et al., 1995). The southern-most two river catchments, the Tsondab and the Tsauchab include more recent (570-500

Ma) Cambrian deposits of Nama Group sedimentary rock (Jacobsen et al., 1995). A period of extensive volcanic activity in the mid and late Jurassic ended with a regional uplift event, producing the Great Escarpment ±155.5 Ma (Light et al., 1992). The harsh climate of western Namibia, both previously and following the formation of the escarpment, has prevented vegetation growth and soil build up across the catchments resulting in a much older landscape than found further inland (Jacobsen et al., 1995). Atop the great escarpment, the poorly vegetated catchments have a relatively strong slope-channel coupling and a moderately abundant sediment supply. These conditions have resulted in a variety of confined bedrock and alluvial braided rivers across the E-W topographical gradient toward the coast (Jacobson et al. (1995) in (Thomas, 2011)). The 300-500 mm average annual rain fall experienced in the upper catchments provides the ideal semi-arid environment for maximum sediment erosion (Langbein & Schumm, 1958). Eroded sediment from the eastern catchment areas is then transported during ephemeral flow events to the Namib Desert. The clay mineral compositions of silts deposited in the river valleys below the escarpment has been shown to have characteristics that correspond with the geological and petrographic features of the associated catchment of the valley (Heine & Völkel, 2010). Correlation between modern flood events and subsequent dust emission of deposited sediment loads has been identified in the Kuiseb river valley (Vickery & Eckardt, 2013), an area of low topographical relief bounded on the south by the Namib Sand Sea and gravel plains of the Namib Desert to the north, Figure 16. Topography of the river valleys to the north sees the valleys situated within Karoo (Permo-Carboniferous to Jurassic) glacial sedimentary and volcanic units that form valley sides. This has seen the accumulation of historical alluvium, forming what is now the valley floor through which the extant channel is incised. The alluvium is continually eroded, transported and deposited down the

hydrological gradient of the rivers during flood events. Age determination of valley fill in the Huab (see Paper 5 provided as in Appendix 1) determined that valley fill sediments accumulated in the Late Holocene and remain an active contributor to modern dust events. More recent and modern flooding has been shown to maintain the transportation of eroded sediment from the upper catchments to the lower valleys. Major flood events have been identified every 30-40 years over the last millennium in the Kuiseb (Grodek et al., 2013). In the adjacent Swakop valley flood frequency had increased in recent centuries with a flood recorded every 7 years (Greenbaum et al., 2014). Further north, sediments in the Hoanib valley have similarly shown increased fluvial activity over the last 3k years (Eitel et al., 2006). The dust source sediments in the river valleys are therefore a combination of historical alluvium and extant flood-delivered material. Modern-day flood events would serve to replenish and rework valley fill during flood events by scouring and erosion (see Section 2.2.2 on ephemeral river geomorphology).

Flood events and sediment deposits are also known to transport nutrient-enriched material along the Namib river valleys (Morin et al., 2009; Jacobson et al., 2000), and below the escarpment the dry river channels support flora not found elsewhere in the desert (Jacobson et al., 2000; Cowlishaw & Davies, 1997). These nutrient corridors support enough biomass and biological activity to sustain an ecosystem that includes some of the planet's largest mammals and top predators (Leggett, 2006; Viljoen, 1989; Coetzee, 1970). Investigation of N and P macronutrients showed association with increased flora and primary production in the extant, dry river valley channels and adjacent flood water deposits (Jacobson et al., 2000). The spatial distribution of mineral iron in Namibia has only been a focus of research for the Namib Sand Sea, in relation to sand sea age, sand grain source origin, and climate gradient influences (White et al., 2007; Walden et al., 2000; Walden & White, 1997). In the Namib Sand Sea the gradient of yellow and red

sands from west to east has been linked to Hematite and Geothite Fe-oxides concentrations primarily derived from lithological providence with secondary influence from increased weathering from coastal fog (White et al., 1997). It is also known that the Namib Sand Sea is deficient in both N and P (Seely & Louw, 1980), however to date, there has been no investigation of the spatial distribution of N, P or Fe along the watersheds of the ephemeral river valleys of Namibia.

CHAPTER 4

4 Methodology

4.1 Introduction

To address the research objectives a combination of fieldwork, laboratory analysis and remote sensing assessment was undertaken. Fieldwork was undertaken between April and September 2013 in three ephemeral river valleys and their upper catchments: the Huab, Kuiseb and Tsauchab. Fieldwork involved the installation of dust and meteorological monitoring equipment and sample collection of both airborne dust and surface sediment samples. Fieldwork and laboratory analysis of collected samples was undertaken to achieve research objectives 1, 2 and 3 remotely sensed data and imagery were utilised to address objectives 3 and 4.

The empirical evidence generated to answer the research question entailed the field-collection of:

- meteorological data using eleven automatic meteorological monitoring stations that collected high frequency (minute) data on erosive forces (wind shear stress and direction), resisting forces (surface soil moisture), and subsequent erosion of dust (airborne dust concentration and surface-grain saltation).
- physical sediment samples of both surface sediments and capture of windblown dust.

- physical sediment samples from Etosha Pan and the Makgadikgadi Pan system provided by the DO4 research project.

To determine the ocean fertilisation potential of sediments from the river valleys and compare these regionally to the dry lake bed (Etosha and Makgadikgadi) sources, the grain size, shape and key nutrients were quantified in the collected samples. As presented in Section 2.3-2.4 the most important externally-supplied nutrients in ocean fertilisation are the macronutrients N and P and the micronutrient Fe. To ensure a holistic assessment of ocean fertilisation potential, regardless of which nutrient may be the limiting factor off the coast of Namibia at the time of deposition, laboratory analysis of collected samples was undertaken to determine:

- Nitrogen (N) content - Total nitrogen (TN), and the bioavailable nitrate (NO_3^-) and ammonia (NH_4^+).
- Phosphorus (P) content - Total phosphorus (TP) and bioavailable P (Mehlich P).
- Bioavailable iron (Fe) - DTPA-extractable Fe^{2+} and Fe^{3+}, or plant-available Fe.
- Grain size of sediment, both the parent grains and in-situ peds and sediment assemblages.

To determine any photosynthetic response to dust deposition, remote sensing data were downloaded and processed to identify over-ocean dust plume extent (aerosol optical depth, AOD) and chlorophyll *a* concentrations in surface waters. To identify spatial and temporal upwelling within the region of interest, and frame it within the annual cycle, sea surface temperature data were similarly downloaded and processed. Remotely sensed data were obtained from the Moderate Resolution Imaging Spectroradiometer (MODIS) instrument aboard the Terra and Aqua NASA satellites, covering the entire earth surface

every 1-2 days. Correlation of ocean chlorophyll levels is then investigated with the in-valley concentrations of windblown dust recorded by field equipment measurements.

4.2 Monitoring stations

Analysis of satellite imagery had recognised that persistent sources of dust emission tended to be located in the lower regions of the river valleys and generally no further than 100 km inland (Vickery & Eckardt, 2013; Eckardt & Kuring, 2005). Informed by the work of Vickery & Eckardt (2013) and site visits in April 2013 confirming the presence of likely emissive sediments, the DO4 project erected eleven monitoring stations in the lower catchment areas of each of the three valley systems identified as frequent dust emitters (Figure 17). The stations operated for 20 weeks between April and September 2013 (the known dust 'season', Vickery & Eckardt (2013)) with equipment set up for the collection of windblown dust samples and data on airborne dust concentration and meteorological conditions (Table 4). Six stations were set up in the Huab, two in the Kuiseb and three in the Tsauchab (Figure 17c, d and e).

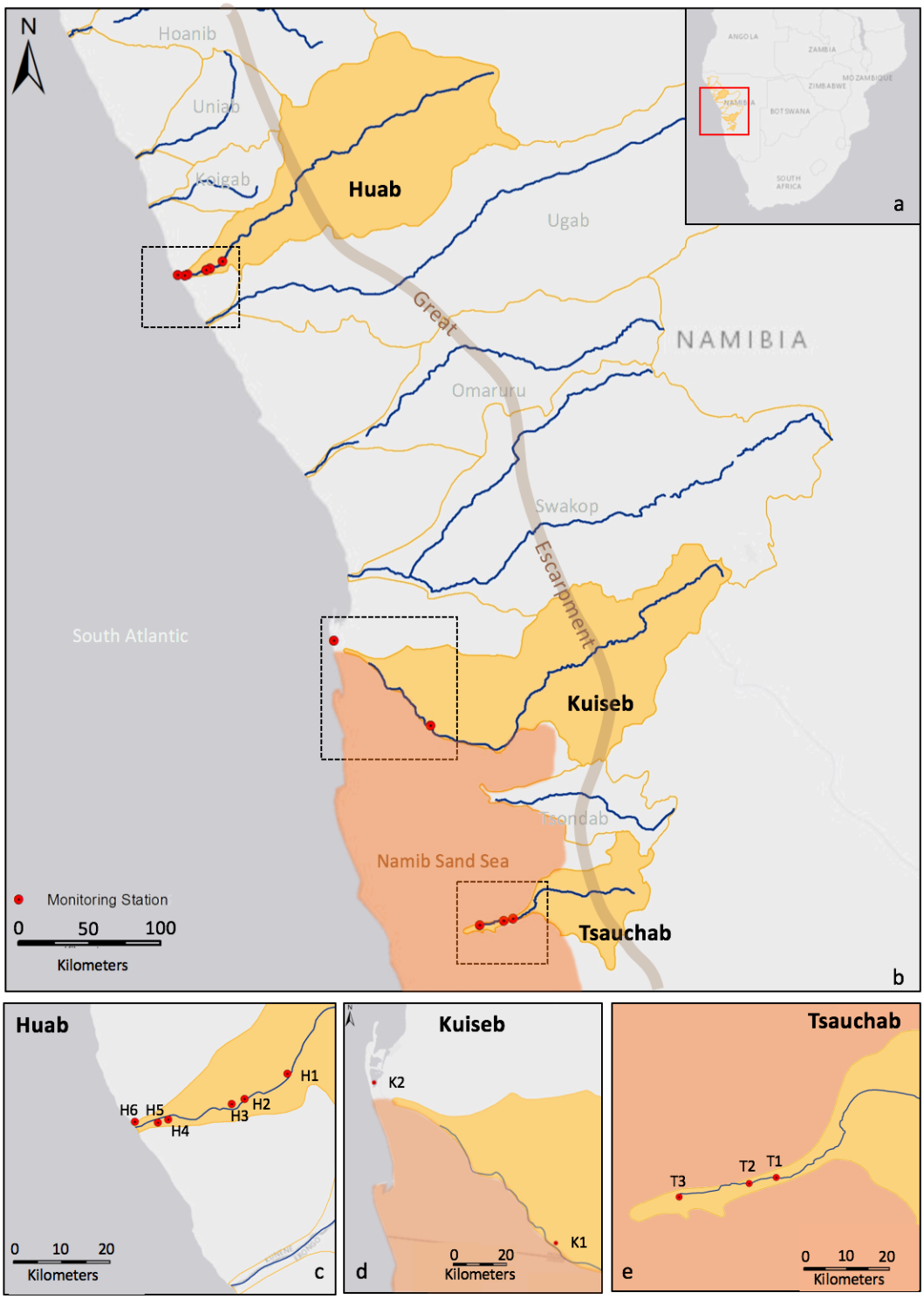


Figure 17 | Monitoring station site locations.

At each automatic weather station (AWS) meteorological monitoring equipment was installed to collect high frequency (minute) data on erosive forces (wind shear stress and

direction), resisting forces (surface soil moisture), and subsequent erosion of dust (airborne dust concentration and surface-grain saltation). The equipment deployed at each station that was relevant to this project is listed in Table 4.

Table 4 Station instrumentation

River Valley	Monitoring Station Name	Distance inland from termini (km)	Airborne dust		Wind strength	Wind direction
			DustTrak	BSNEs	Anemometers (6 heights)	Windvane at 3.18 m
Huab	H1	30.32	X	X	X	X
	H2	21.3	X	X	X	X
	H3	18.70	-	X	X	X
	H4	9.18	X	X	X	X
	H5	4.09	X	X	X	X
	H6	0.2	-	X	X	X
Kuiseb	K1	84.1	X	X	X	X
	K2	1.17	X	-	X	X
Tsauchab	T1	25.09	X	X	X	X
	T2	19.54	X	X	X	X
	T3	4.07	X	X	X	X

The AWS monitoring equipment was attached to a 6m high mast (Figure 18). Cup anemometers were at heights of 0.25 m, 0.47 m, 0.89 m, 1.68 m, 3.18 m and 6 m above the ground surface, and a wind vane at 3.18 m. Wind strength and direction data was recorded on CSI Campbell Data Loggers at one-minute intervals. Stations were visited, at a minimum, monthly and data downloaded from the data loggers.

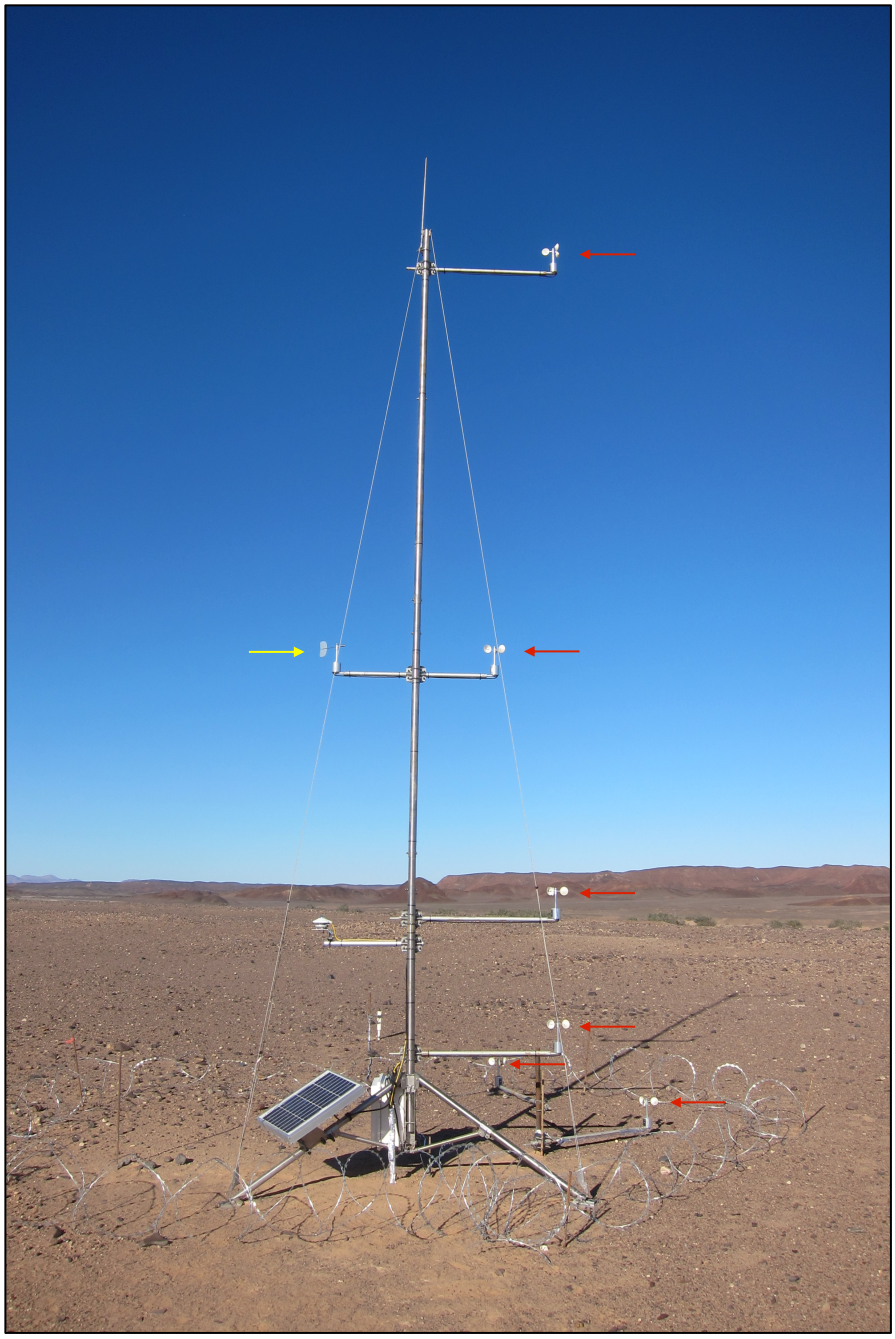


Figure 18 | Meteorological monitoring mast and measurement equipment with cup anemometers at 0.25 m, 0.47 m, 0.89 m, 1.68 m, 3.18 m and 6 m (red arrows) and the wind vane at 3.18 m (yellow arrow), site H1 shown as example. Additional equipment visible in the photos (short and long wave solar radiation sensor on boom below wind vane and Sensit^{TM} saltation monitor in the background behind mast) were deployed by other researchers on the DO4 Models project and not used in this study.

At nine sites (see Table 4) a DustTrak™ DRX aerosol monitor (Wang et al., 2009) (Figure 19) was erected at a height of 3.18 m to measure the airborne dust concentration at two minute intervals. The instruments pump (3.0 $L.min^{-1}$) air and particulates into the optical chamber where it utilizes both photometric measurement of the particle cloud and optical sizing of single particles, Figure 20 (Wang et al., 2009). This enables the determination of the mass fraction concentrations of airborne particles at PM1, PM2.5, PM10 and Total PM (hereafter Total Suspended Particulates (TSP)) at two minute intervals throughout the study period. The suite of deployed instrumentation presented in this section and dust event observed during station erection are shown in Figure 21.

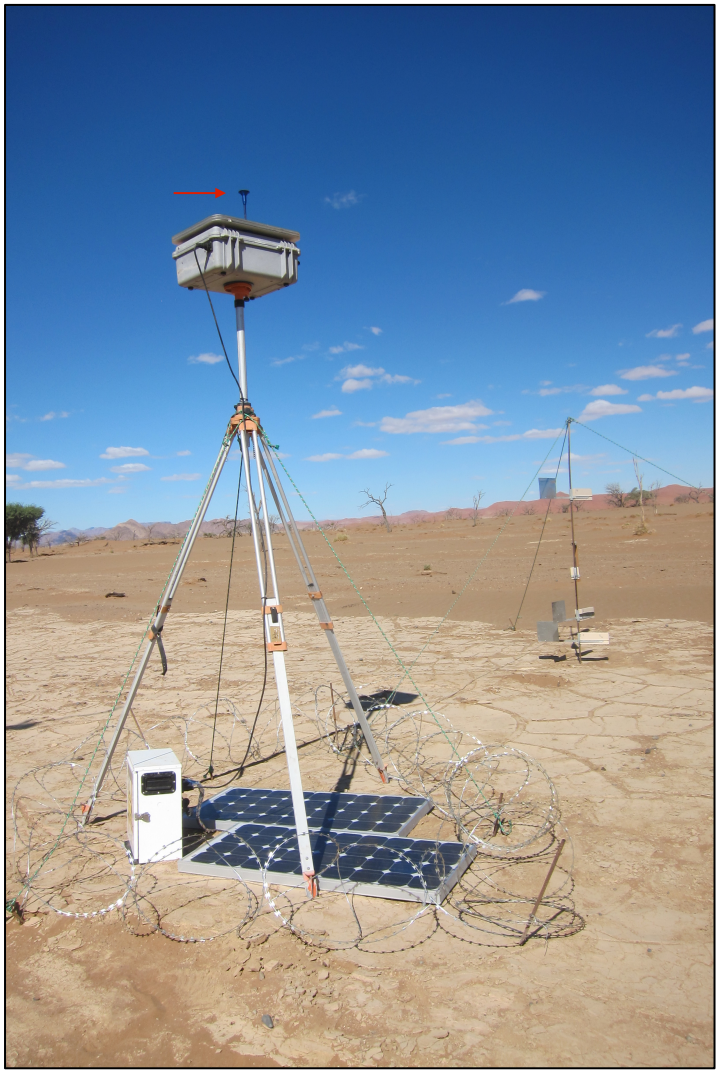


Figure 19 | DustTrak™ DRX Aerosol Monitor deployed in the field with intake at 3.18 m shown by arrow, station T2 shown as example and BSNEs (see Section 4.3.1) visible in background.

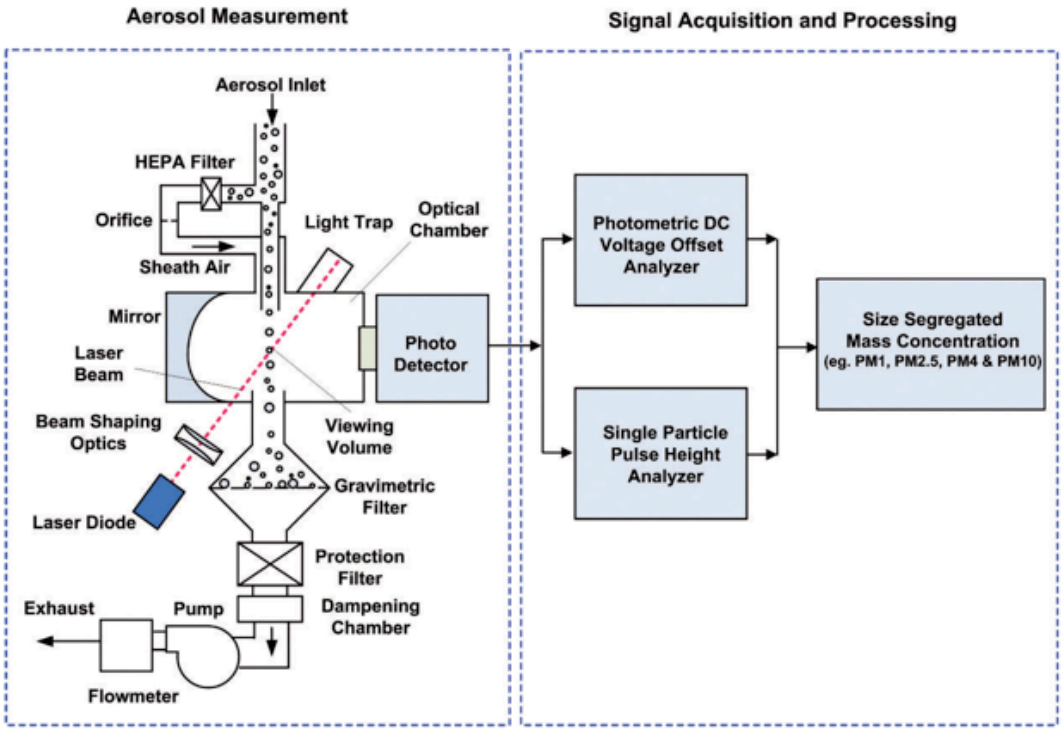


Figure 20 | Schematic diagram of the DRX. The particle beam, laser beam, and the axis of the mirror are orthogonal to each other (Wang et al., 2009).

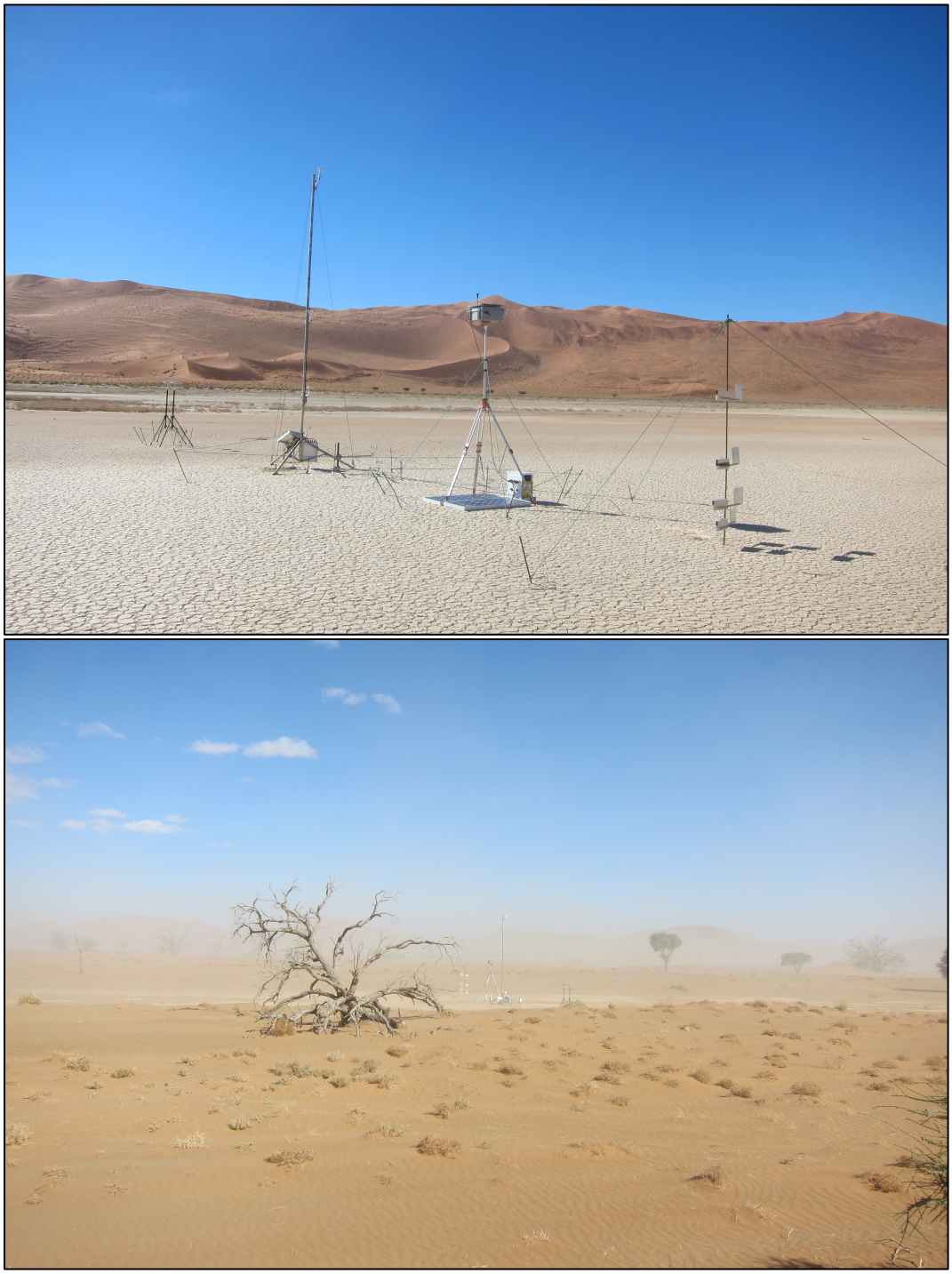


Figure 21 | Example of erected monitoring station instrumentation at (top) T3 showing from right to left; BSNEs, DustTrak™, AWS mast, and vertical flux collectors (not used in this research) and (bottom) windblown dust at T1 on 19 April 2013.

4.3 Sample collections

4.3.1 Windblown Dust

Physical capture of horizontal dust flux was undertaken at ten stations (see Table 4) using Big Spring Number Eight (BSNE) aeolian sediment samplers (Figure 22) erected in a vertical profile at heights of 0.25 m (BSNE 1), 0.47 m (BSNE 2), 0.89 m (BSNE 3) and 1.68 m (BSNE 4) above the ground surface, corresponding to anemometer heights (Mendez et al., 2011; Fryrear, 1986). Dust captured in the BSNE samplers was brushed into pre-weighed ziplock bags (Zobeck et al., 2003) at a minimum frequency of once per month. The collection dates are provided in Appendix 2. Samples were transported back to the UK and dried in the laboratory at 40°C for 48 hrs. Sample weight was calculated gravimetrically on a microbalance (ten-thousandth of a gram accuracy) by subtracting the pre-weighed bag weight. The mass of airborne sediment collected determined the suite of nutrient and grain size analyses possible from each station, with 18 g required for the suite of nutrient analyses and ~4 g for both wet and dry grain size analyses. Only collections that had adequate sample in each BSNE 1, 2, 3 and 4 were analysed, i.e. where enough sample was present in the lower BSNEs but not the higher BSNEs no samples from the collection were analysed. In the Tsauchab sufficient mass for nutrient determination could only be acquired by the addition of BSNE 1-4 samples. The very small amounts of dust collected in the Kuiseb meant only dry grain size analysis was possible. In total 25 dust samples were analysed for nutrient content and wet (disaggregated) and dry (in situ) grain size and 61 samples analysed for grainsize using dry analysis only. The raw data of these results and list of analyses conducted on each sample is provided in Appendix 2.

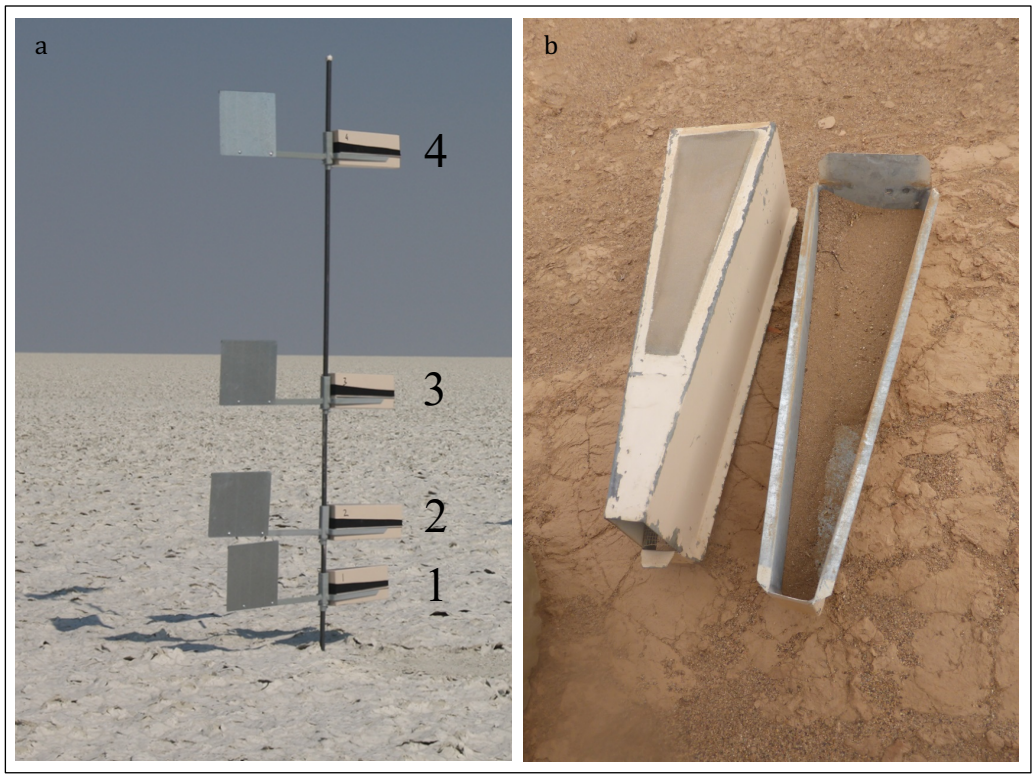


Figure 22 | a) Big Spring Number Eight (BSNE) aeolian sediment samplers erected to collect horizontal sediment flux at 0.25 m (BSNE 1), 0.47 m (BSNE 2), 0.89 m (BSNE 3) and 1.68 m (BSNE 4) in Sua Pan. b) Internal view of sampler containing captured sediment prior to being emptied into a pre-weighed ziplock bag. Photo credits: Dave Thomas.

4.3.2 Surface Sediments

4.3.2.1 River Valley Dust Source Sediments

Ocean fertilisation via mineral aerosol deposition is predetermined, to a large extent, by the grain size and biogeochemical make-up of source sediments (Kanakidou et al., 2012; Mahowald et al., 2008; Jickells et al., 2005). The former determines uplift and transport potential (Alfaro & Gomes, 2001; Arimoto et al., 1997) and the latter the relevance of nutrient input to phytoplankton community needs (Moore et al., 2013). In the time between deflation and deposition, it is understood that the composition and bioavailability of nutrients is altered by atmospheric processing (see Section 2.4.1.3), so that mineral aerosols at the time of deposition could be expected to have a higher fertilisation impact

than source sediments. On-water deposition (vertical flux) collectors were, however, beyond the scope of this research. As the bioavailability of mineral aerosol nutrients only increases during atmospheric transport (Shi et al., 2015; Nenes et al., 2011), the source sediment nutrient load can be safely considered a conservative estimate of fertilisation potential. Both the grain size (determining surface area to volume ratio) (Buck et al., 2010a) and the biogeochemistry (Journet et al., 2008) of mineral aerosols have also been shown to influence atmospheric processing rates and characterisation of source sediments is an essential first step in understanding land-atmosphere-ocean nutrient pathways. Determining source sediment nutrient content addresses an important knowledge gap in ocean aeolian fertilisation (Bhattachan et al., 2015a; Scheuvens et al., 2013) and will improve abilities to model atmospheric processing between source and sink.

In order to determine the aeolian transport and fertilisation potential of the river valleys, samples of surface sediments were collected along transects across the valley floor, including the modern river channel (See Section 5.2.2 and accompanying Figures 32 and 33). The sampling regime targeted changes in sediment geomorphology to determine the grain size of in situ sediment assemblages, the individual grains of the parent material, and the proportion of parent grains that were both bound within assemblages and unconsolidated. Transect sampling was undertaken at monitoring stations that were located within the river valley (i.e. Huab and Tsauchab) and hosted BSNE samplers (Table 4) to allow for comparison of deflated material with adjacent source sediments. Meeting this criteria, transect sampling was undertaken at five Huab stations (H1, H2, H4, H5, H6) and the three Tsauchab stations (Figure 17). See Figure 32 for maps of each cross section location and coordinates of the individual sampling locations are provided in Appendix 4. 68 cross section samples (5-11 samples per cross section) were taken in total. Approximately 200 g of loose sediment sample was collected using a trowel to a

depth of 10 mm. Clay pads and surface crust were extracted to their naturally-occurring depth and the thickness measured. The sampling methodology for the cross section samples is described in detail in Chapter 5/Paper 1 (Figure 32 and 33) and not repeated here.

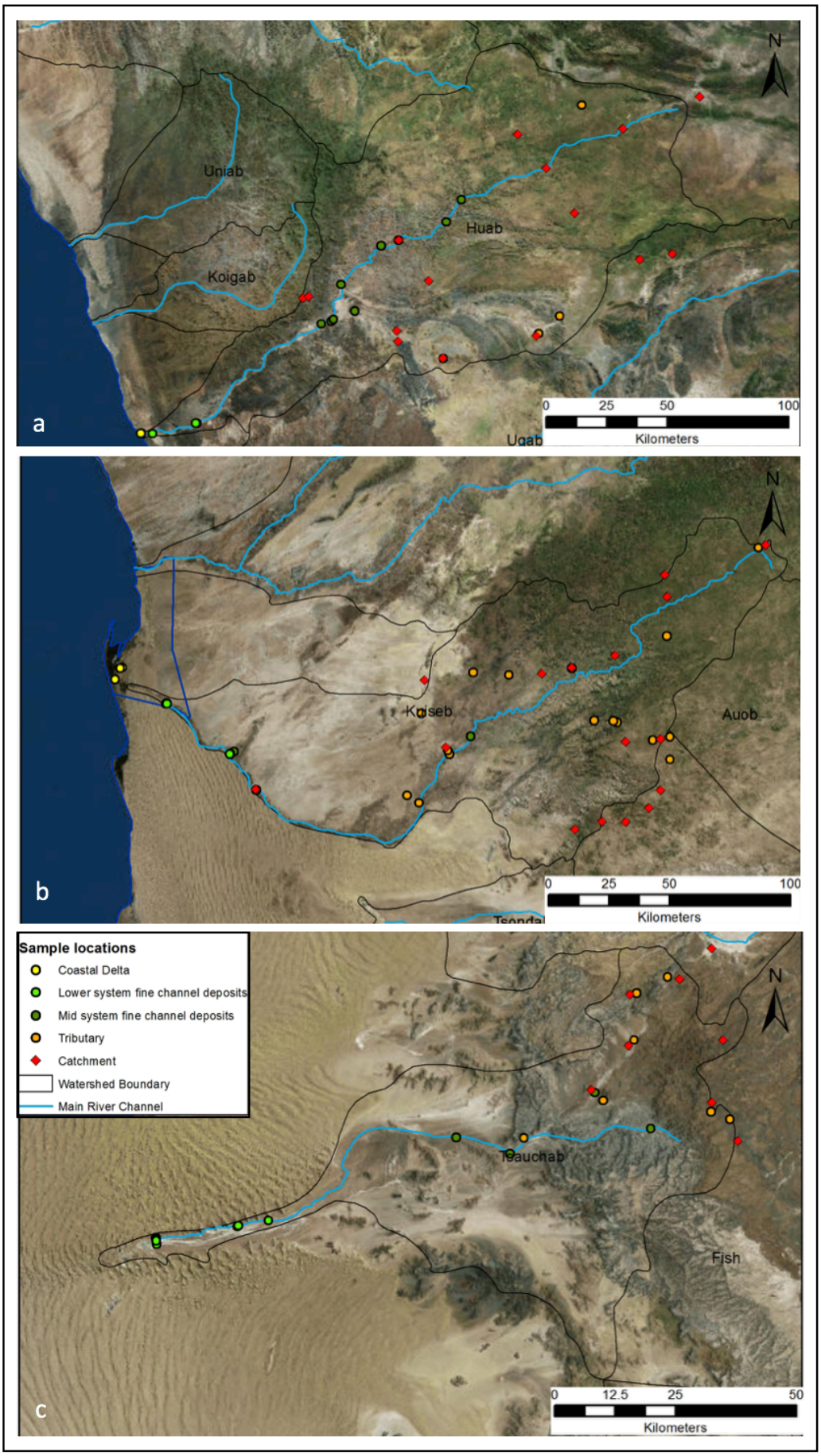
4.3.2.2 Upper Catchment Surface Sediments

The dust emission source sediments in the lower valleys (Vickery et al., 2013) are known to be a result of erosion and transport from pluvial activity above the Great Escarpment, as outlined in Section 3.2.1. Differences in upper catchment rainfall, geology, terrestrial productivity, and land use could therefore be expected to influence the nutrient content of downstream alluvial deposits, similar to the diverging clay mineralogy of alluvial silts that has been reported between valleys (Heine & Völkel, 2010). Correlation of the downstream nutrient composition with upper catchment landscape characteristics would allow both similarities and differences to be extrapolated to the other nine ephemeral river valleys based on their upper catchment characteristics.

Upper catchment samples were collected for the Huab, Kuiseb and Tsauchab according to the E-W precipitation gradient, vegetation, underlying geological sequence and land use classification (as described in Paper 2, Chapter 6 and shown in Figure 40a-d). Spatial classification was made using 1:250000 topographical and geological maps (Directorate of Survey and Mapping, 2002). Sampling was also undertaken to consider the hydrological connections and transport from the upper catchments to the river termini's using the 1:1000000 Hydrogeological Map of Namibia (van Wyk et al., 2001). Samples were collected in tributaries draining the upper catchments to main river channels atop the escarpment then along the main channels through the Namib Desert to the coast and Sand Sea for the Huab/Kuiseb and Tsauchab respectively.

Collection of surface sediment samples in the upper catchments and along the tributaries and main river channels of the Huab, Kuiseb and Tsauchab rivers was undertaken between May and August 2013. Sample collection sites are shown in Figure 23 and their geographical coordinates and sample IDs provided in Appendix 4, the sampling design and methodology is described in detail in Paper 2, Chapter 6 Section 6.3. Approximately 200 g of surface sediment was collected at each sample location using a trowel (to a depth of 10 mm) for laboratory analyses of bioavailable iron, P and N compounds and grain size distribution analysis. A field duplicate was collected for every 20 samples.

Figure 23 (*over page*) **|** Surface sampling locations in the (a) Huab, (b) Kuiseb and (c) Tsauchab catchments (sample IDs and geographical coordinates provided in Appendix 4 table and maps).


N
Uniab
Huab
Koigab
a
0 25 50 100
Kilometers
N
Kuiseb
Auob
b
0 25 50 100
Kilometers
Sample locations
Coastal Delta
Lower system fine channel deposits
Mid system fine channel deposits
Tributary
Catchment
Watershed Boundary
Main River Channel
N
Fish
c
0 12.5 25 50
Kilometers

4.4 Laboratory Analysis

Airborne dust and surface sediment samples were first dry sieved through 2 mm mesh and the <2 mm subset split with a riffle box into subsets for wet and dry grain size analysis and chemical analyses. Solid crust and clay pad/pan material was broken into appropriately weighted pieces for wet grain size and chemical analyses. Field duplicates were collected at a rate of 1:20 and underwent the same splitting and analysis procedures. The results of the duplicates are presented in Section 4.4.2.

4.4.1 Chemical Analyses

A subset of sieved <2 mm samples, including field duplicates, were split and sent to the Kansas State University Soil Testing Laboratory for analysis. Samples were dried overnight in a 50°C oven with the exception of sub-samples for iron analyses which were air-dried. Methods for the following analyses were taken from Brown (1998) unless otherwise stated.

Bioavailable Fe: Bioavailable Fe^{2+} and Fe^{3+} (combined) was extracted using DTPA (diethylenetriaminepentaacetic acid) then quantified using Flame Atomic Absorption spectrometry, following method described by Lindsay and Norvell (1978). Reported bioavailable Fe concentrations are known to be susceptible to changes in extractant pH and chelating agent concentration, shaking time and extraction temperature (Khan, 1979; Khan & Soltanpour, 1978; Soltanpour et al., 1976).

10 g of air-dried sample was added to 20 mL of extracting solution (0.005 M DTPA (diethylenetriaminepentaacetic acid), 0.01 M CaCl2 and 0.1 M triethanolamine (TEA) adjusted to pH 7.3) then shaken on a reciprocating shaker at 180 epm (excursions per minute) for 2 hours. The soil-extraction mixture was filtered through 2 μm pore filter

paper then analysed using a Flame Atomic Absorption spectrometer using standard procedures (Russell et al., 1957).

Bioavailable Phosphorus: Bioavailable P was determined using Mehlich III extraction as it is applicable to a wide range of soil properties and pH (Mehlich, 1984). 2 g of sample was digested in an extraction solution (20 g of ammonium nitrate, 4 mL NH_4^+ F-EDTA stock solution, 11.5 mL acetic acid, 0.82 mL of nitric acid, distilled water to bring total volume to 1 L) and shaken at 200 epm for 5 minutes. The soil-extraction mixture was filtered through 2 µm pore filter paper. After 10 minutes to allow colour development the filtered extract was analysed using a colour spectrophotometer (wavelength 882 nm).

Inorganic Nitrogen, Ammonium and Nitrate: Ammonium (NH_4^+) and nitrate (NO_3^-) extraction was undertaken using 1 M KCl using 2 g of sediment, shaken for 1 hr then filtered through 2 µm filter paper using methods developed by Black et al. (1965). NH_4^+ colorimetric quantification used the Berthelot method (Berthelot, 1859). This involved the addition of a phenol that binds with ammonium ions to form an indophenol dye that absorb light between 630 and 720 nm (Searle, 1984). Nitrate colorimetric quantification was through cadmium reduction as described in Brown (1998). Aliquots of the filtrate were then simultaneously run in a flow analyser to determine ammonium and nitrate concentrations using colorimetric procedures.

Total Nitrogen and Phosphorus: A modified Kjeldahl digestion, derived from Blakemore et al. (1987) was performed on 1 g of ground soil as described by Taylor (2000). The soil was placed in a 50 mL test tube, moistened with a few drops of water and a Kjeldahl catalyst tablet added. 10 mL of 12% v/v Sulfuric Acid (H_2SO_4) and deionized (DI) water solution was added and tubes were heated in an aluminium digestion

block for 2 hrs. Once cool, water was added to bring the total volume to 50 mL, shaken and allowed to settle overnight. Aliquots of the digested sample were prepared for N and P quantification in a flow analyser (N as described by McLeod (1992) and P as described by Taylor (2000)).

Organic Matter – Total Carbon: Total carbon was determined using a LECO CN 2000 combustion analyser at 1200 °C as described by Wright & Bailey (2001) using 0.5 g of sample and calculated on a weight percent basis.

pH: pH was measured directly using a 1:1 slurry of 10 g of prepared soil with DI water with an automated system.

Raw data of the analyses listed above is given in Appendix 3 (BSNE and surface sediment samples), as provided by Kansas State University.

4.4.2 Field and Laboratory Quality Assurance and Quality Control

Field and laboratory duplicates were run to ensure reliability of results and robustness of analyses for interpretation.

4.4.2.1 Field Duplicates

Five surface sediment samples representative of a range of geomorphological contexts from the upper catchment, tributaries and main river channels were sent with five blind duplicates to the laboratory for analyses, Figure 24 and Figure 25. Variation between duplicates was quantified by calculating the standard deviation for each element of analysis, shown as error bars in Figure 24 and Figure 25 and provided in tabular format in Appendix 5. The results of the field duplicates showed good levels of replicability with the duplicate pairs showing similar concentrations of nutrients to each other. Bioavailable Fe showed the greatest similarity between duplicates with averaged standard deviation

being 3.27% of the averaged duplicate concentrations (n = 10). Mehlich P (7.9 %), Total N (10.07 %) and Total P (15.42 %) also showed good degree of similarity with each nutrient having one duplicate produce an outlying larger standard deviation (HUW060, HUW040 and KR40 respectively). The more volatile ammonia and nitrate (Turner & Romero, 2009) showed the greatest variance within duplicate samples, 33.43 and 29.42 % respectively, while pH varied only 1.2 %. Inter-comparison between sample pairs, contrasted to intra-comparison within duplicate pairs, demonstrates a much higher variability between sampling locations than within duplicate pairs. This shows that the sensitivity of analysis allows meaningful investigation and inter-location comparison to be undertaken.

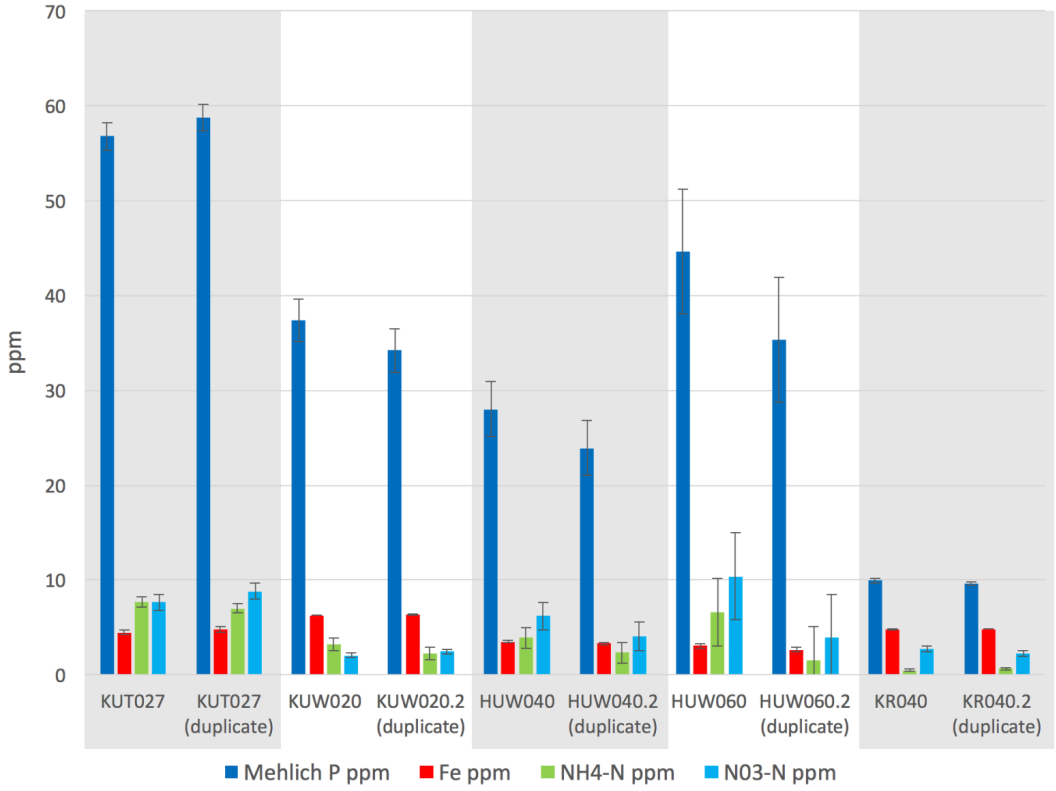


Figure 24 | Field duplicates analyses of bioavailable P (Mehlich P), bioavailable Fe (Fe), ammonium (NH_4^+) and nitrate (NO_3^-).

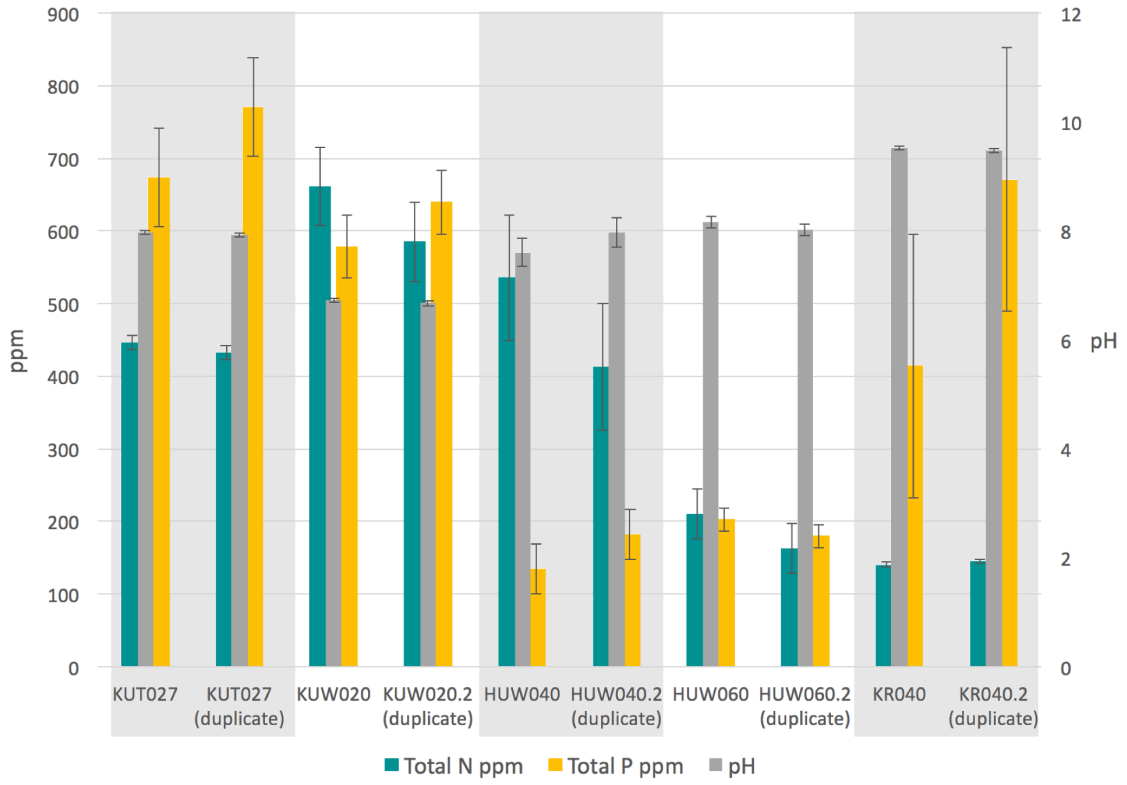


Figure 25 | Field duplicate analyses of Total N, Total P and pH.

4.4.2.2 Laboratory Duplicates

Twelve samples were used by Kansas State University (KSU) for internal quality control as laboratory duplicates for bioavailable P, Fe, ammonium and nitrate and six for TN, TP and pH. Variation between duplicates was quantified by calculating the standard deviation for each element of analysis, shown as error bars in Figure 26a, b and Figure 27 and provided in tabular format in Appendix 5. All elements showed a high degree of reproducibility with standard deviation averaging less than 4% for all elements and within KSU laboratory reproducibility guidelines of 5%, demonstrating the reliability of the results obtained.

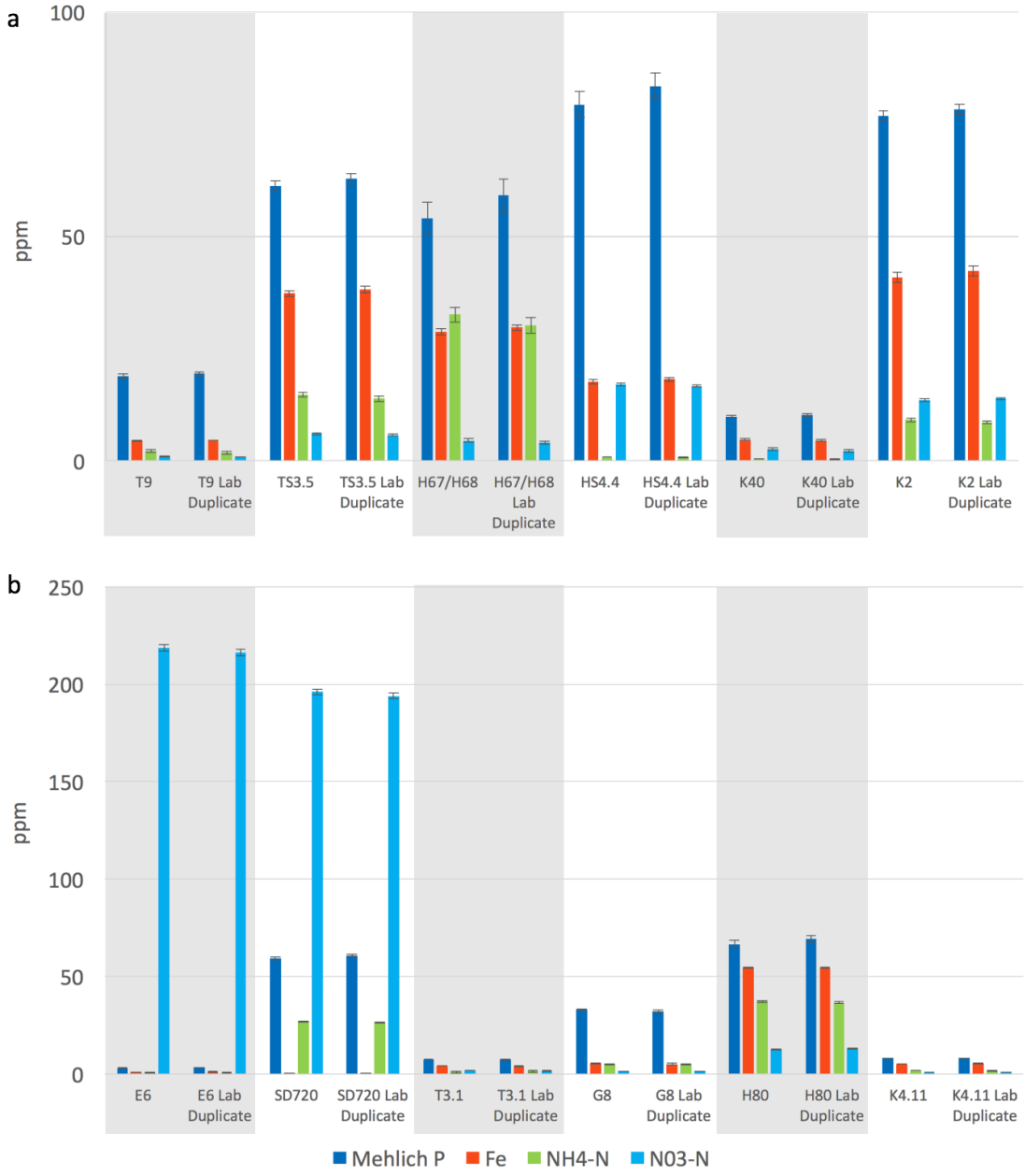


Figure 26 | Laboratory duplicate analyses of bioavailable P (Mehlich P), bioavailable Fe (Fe), ammonium (NH_4^+) and nitrate (NO_3^-).

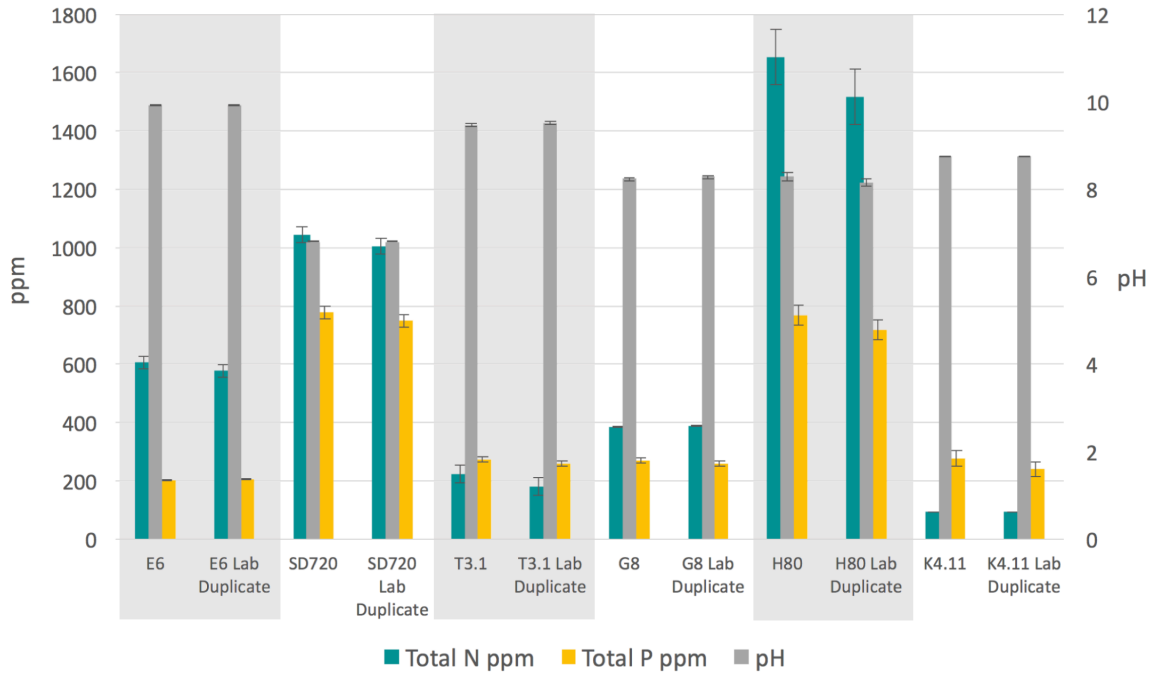


Figure 27 | Laboratory duplicate analyses of Total N, Total P and pH

4.4.3 Grain Size Distribution Analysis

The uplift and aeolian transport potential of sediment grains is largely determined by their size (Arimoto et al., 1997; Tegen & Lacis, 1996). The particle size of mineral aerosols is determined by two factors, the grain size of individual, or parent, grains and the size of secondary structures formed through interparticle cohesion, see Haustein et al. (2015) and Shao & Lu (2000). These secondary structures will be referred to as aggregates from here on to include a range of terminology for bound-groupings of individual grains such as assemblages, peds, and fragments of fluvially-derived crust. The geomorphic connectivity of alluvial-fine deposits and coarse sand grains has also been shown to provide highly productive settings for dust emission (Bullard et al., 2011). The sand grains increase the susceptibility of consolidated-sediment surfaces to deflation through both abrasion of surface crusts and clay deposits (Wiggs, 2011; Shao et al., 1993) as well as bombardment via saltation of unconsolidated sediments, causing the ejection of fines (Gillette, 1981). It

is therefore beneficial to understand the grain size of sediment aggregates, the smaller parent grains that they are made up of, and the relative abundance of larger non-divisible grains in a dust source area. Laser defraction identification of the grain size distribution of sediment samples provides one of the best methods to achieve this (Goossens, 2008). A laser particle size analyser employing wet dispersion methods provides quantification of disaggregated sediments, showing grain size for individual grains and aggregate parent material. Dry dispersion methods allow the quantification of the naturally-occurring, or in situ, grain sizes that includes both sediment aggregates and individual grains. Both individual grains and aggregates can be transported over hundreds, even thousands, of kilometres, e.g. Middleton & Goudie (2001), Prospero et al. (1970) and Schroeder (1985) respectively.

4.4.3.1 Wet Analysis

3-5g of sample was dried at 40°C for 48hrs was placed in 50 mL centrifuge tubes for salt and carbonate removal using methods adapted from Soukup et al. (2008). Salt was removed with 20 mL washes of deionised (DI) water, centrifuging and testing of the supernatant until an electrical conductivity (EC) of under 1000 µS was recorded. Supernatant was discarded and samples were then dried at 40°C for 48 hrs and salt content recorded via gravimetric loss and compared with initial EC values recorded in first 25 mL wash. Carbonate removal was then undertaken following Soukup et al. (2008) methods using 20 mL of 1M Sodium Acetate (CH_3COONa) adjusted to pH 5 with glacial acetic acid and two digestion periods of 20 minutes in an 80°C water bath, ensuring evanescence had stopped before removal. DI water was added and the pH adjusted to 9 to 10 using 1M NaOH solution. The sample was then shaken, centrifuged and the supernatant discarded. The carbonate fraction was then calculated gravimetrically after a minimum 48 hrs oven drying at 40°C.

Oven-dried salt- and carbonate-removed samples were ground using a mortar and pestle and riffled to range of weights from 0.016 g to 3.8 g and suspended in a 1:1 solution of 50 g/L sodiumhexametaphosphate and DI water. Samples were placed on a linear shaker and shaken for four hrs at a rate of 250 rpm then left to stand overnight.

Samples were run using DI water in the Malvern Mastersizer Hydro 2000MU with a pump/stirrer speed of 3000 rpm ensuring laser obscuration measurement was between 10-20%. One-in-ten sample repeats were run to ensure reproducibility of results (presented in Section 4.4.4) and runs using glass microspheres (15-150 μm, part number CRM0014, Whitehouse Scientific) were used for calibration after every ca. 200 measurement cycles. Samples each had three measurements taken (each lasting for 15 seconds and comprising 150000 measurement snaps) and an average of the measurements used for interpretation.

4.4.3.2 Dry Analysis

Unmodified samples were riffled to a weight of 0.1 – 3.5 g and analysed using the Malvern Mastersizer Scirocco 2000 dry unit with a 2 mm sluice opening. The SOP used to analyse the samples was set using standard procedures for soil analysis (Malvern Instruments, 2007) with 70% vibration speed rate and 1 bar of dispersive air pressure. Samples were riffled to appropriate weights to ensure laser obscuration values were always between 1-3.5 %. Repeats were run to ensure the reproducibility of results (Section 4.4.4) with each measurement lasting for 15 seconds and comprising 150000 measurement snaps.

4.4.4 Grain Size Analyses Quality Assurance and Quality Control

Of the 68 cross-section samples and 61 dust samples, 18 laboratory duplicate samples were analysed for wet and dry grain size distribution using identical procedures as described in 4.4.3.1 and 4.4.3.2. Duplicates were representative across the

geomorphological classifications sampled. Both wet (Figure 28) and dry (Figure 29, presented as three graphs for clarity) duplicate pairs showed near-matching grain size distributions demonstrating the high reproducibility and reliability of the analyses.

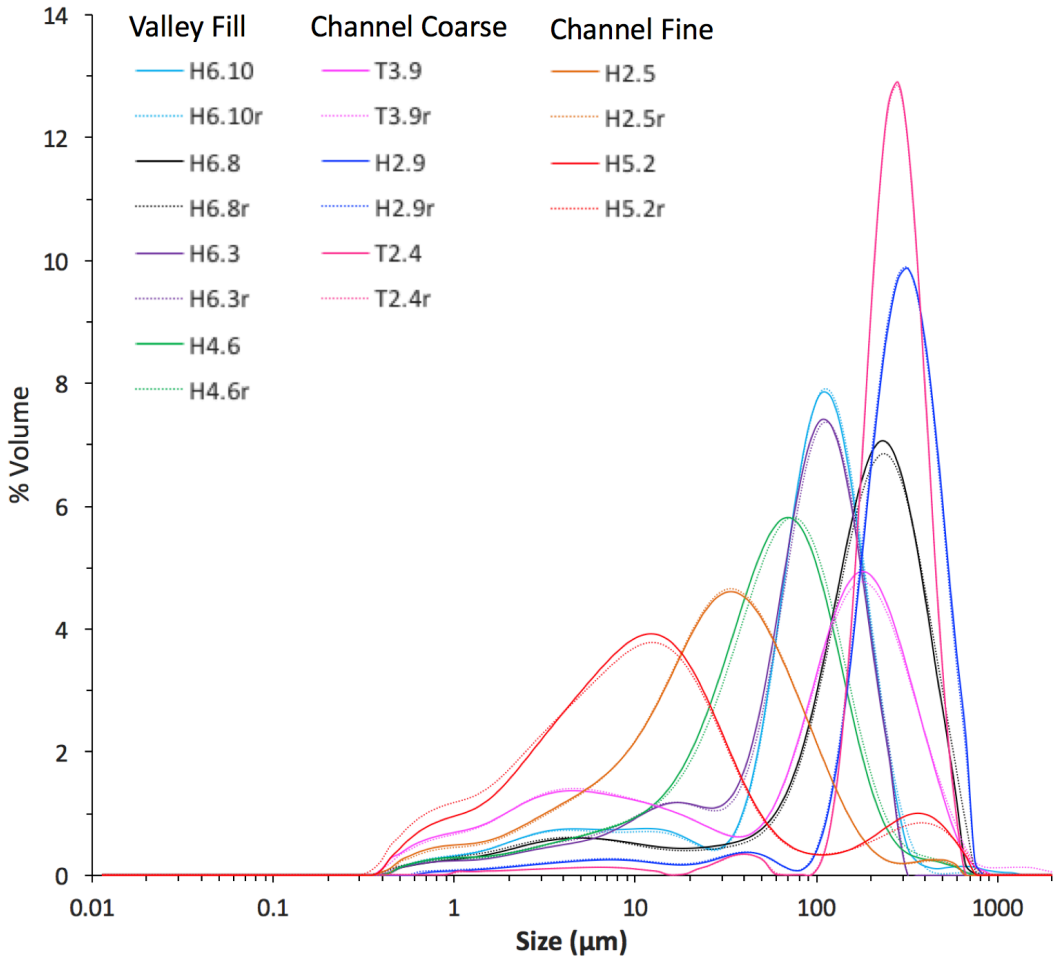


Figure 28 | Wet grain size distribution analysis sample duplicates with replicate (r) samples shown by perforated lines.

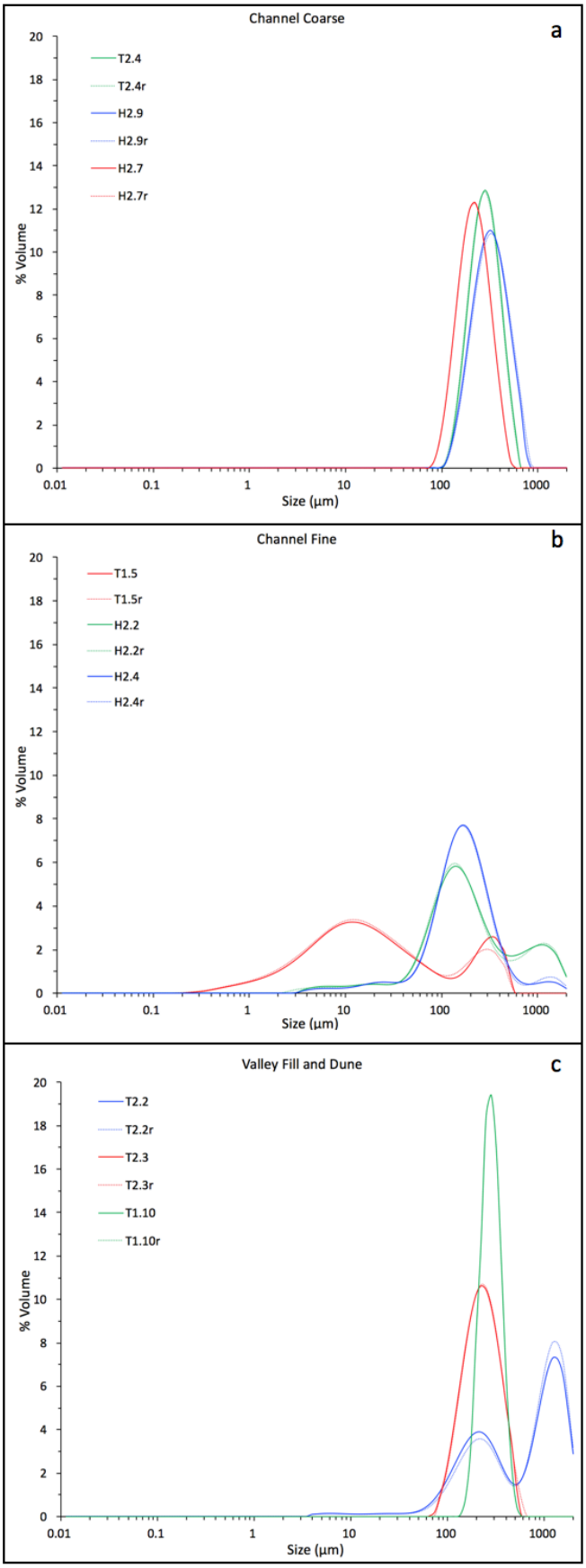


Figure 29 | Dry grain size distribution analysis sample duplicates with replicate (r) samples shown by perforated lines for a) channel coarse, b) channel fine, and c) valley fill and dune geomorphological units.

Further, to assess the reliability of the dry dispersion results reported by laser diffraction, 200 g of oven-dried (40°C) sediment was dry-sieved (on a mechanical shaker for one hour) into nine grain size fractions and analysed (Figure 30). The grain size distributions are shown to fall within expected size ranges (Figure 30). The reported volume weighted means match the expected size range (Table 5) with two minor exceptions. The reported volume weighted means for the 500 – 710 µm size fraction was 3.18 % larger than the largest expected size fraction and the 710 µm – 1 mm was 1.48% larger. This can be explained due to the presence of elongated and plate-like particles that were between 500 µm and 710 µm or 710 µm and 1 mm along one particle axis (allowing the particle to pass through the respectively-sized sieve mesh) but longer along the perpendicular particle axis (Malvern Instruments, 2007). The reported volume weighted means are considered reliable and representative of the sample grain size distributions.

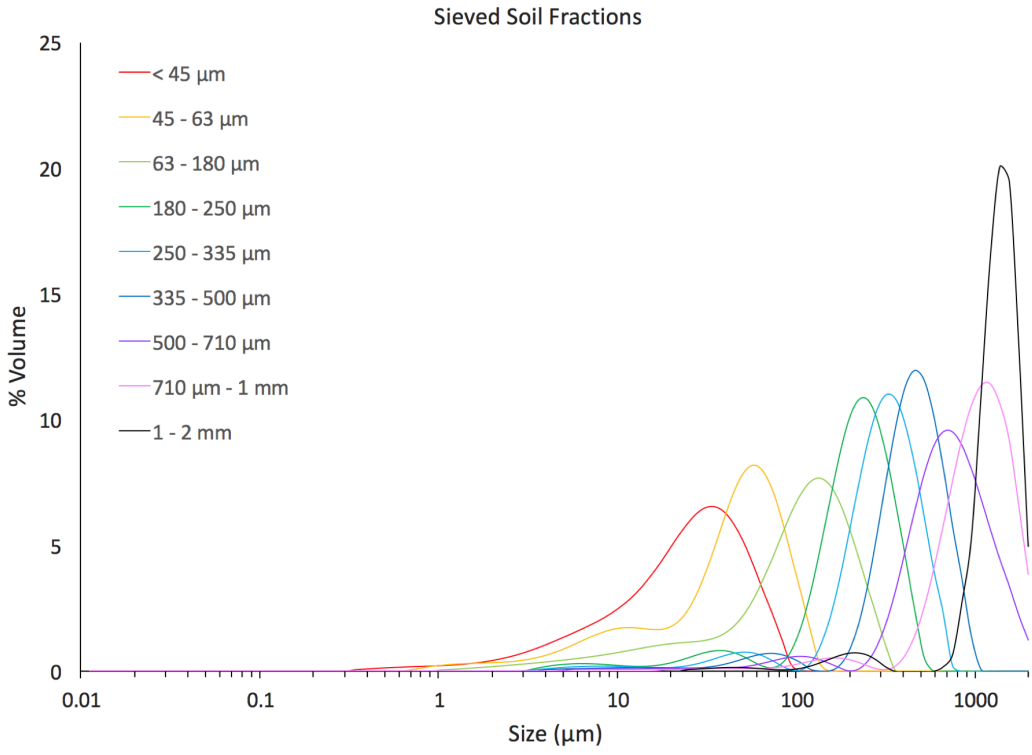


Figure 30 | Dry grain size analysis of dry-sieved sediment into known grain size fractions

Table 5 Volume weighted means of dry-sieved samples as shown in Figure 30

Sieved size fraction	Volume Weighted Mean (µm)
< 45 µm	26.76
45 - 63 µm	44.53
63 - 180 µm	106.82
180 - 250 µm	211.92
250 - 335 µm	301.11
335 - 500 µm	431.71
500 - 710 µm	732.61
710 µm - 1 mm	1014.77
1 - 2 mm	1246.22

4.4.5 Scanning Electron Microscope

Scanning electron microscopy (SEM) analysis as a tool to measure the size, the shape, and the mineral composition of individual particles has seen increasing application to investigation of mineral aerosols collected by aircraft the atmosphere (e.g. Krueger et al. (2004), Laskin et al. (2006), and Chuo et al. (2008)). Most recently, advances in technology and application have seen individual grains analysed down to the nanometer resolution for surface roughness investigation (Woodward et al., 2015). SEM is now also contributing to increased micro- and nano-level understanding on the light scattering and absorption properties, water absorption, ice-nucleation and atmospheric processing characteristics of mineral aerosols (Tang et al., 2016).

For the intents and purposes of this research, investigating a geographically extensive and diverse dust source area, SEM offers the ability to measure the size and shape of deflated dust, providing further insight to the grain size distribution analyses (Section 4.4.3), as well as characterisation of the dust into grain types, e.g. quartz grains, sediment peds, and fluvial crusts.

Dust samples collected from each BSNE height at one station from each the Huab, Kuiseb and Tsauchab were used for SEM investigation (see Section 7.6). SEM dust samples were taken by pressing an adhesive carbon disc (mounted on a standard SEM sample stub) into a small, riffled sub-sample of the oven-dried BSNE samples. The sample collected on the adhesive carbon stub was then sputter coated using a carbon ribbon in a Bio Rad MicroScience Division SEM Coating System. The coated sample was analysed using a JEOL JSM 5910 SEM with a tungsten filament at an accelerating voltage of 15 kv, a probe current of 1 nA and INCA software (Oxford Instruments Analytical, 2006).

4.5 Remote sensing

4.5.1 Data acquisition

Remote sensing analyses is widely applied in dust and oceanic investigations. The MODerate resolution Imaging Spectroradiometers (MODIS) twin sensors aboard the Terra and Aqua satellites are used for contemporary investigations of aerosol optical depth (AOD) and ocean surface water chlorophyll concentrations (e.g. Tan et al. (2016), Naud et al. (2016)). Discussions with experts from the Remote Sensing and Ecosystem Modelling (REMSEM) team at the Royal Belgian Institute of Natural Sciences and the University of Sheffield further confirmed the suitability of MODIS products for application in this research.

The atmospheric investigation of dust plumes emitted from the river valleys was undertaken using the MODIS Aqua and Terra Deep Blue Dark Target AOD[4] Collection 6 data (550 nm) product (‘aod’) that has been optimised algorithmically for AOD

[4] Long name: MODIS Deep Blue AOD version 6 data reprojected from Level-2 tiles and concatenated into gridded daily field.

identification and cloud removal over land (Hsu et al., 2013) and ocean (Sayer et al., 2014). It is noted that the Deep Blue AOD product can be further processed to determine dust optical depth (DOD). DOD values are determined by screening the 550 nm AOD data against the two additional criteria of (i) an Ångstrom exponent between 0 - 0.5 ($\alpha < 0.5$) and (ii) increasing the absorption from red to deep blue wavelengths ($\omega650 - \omega412 > 0$), to target a specific optical property of dust (Hsu et al., 2013; Ginoux et al., 2012). The benefits of using DOD is that finer particles such as sea-salt aerosols or those associated with biomass burning are less likely to be confused with the larger mineral aerosols (Huang et al., 2015). For the purposes of this research the commonly used AOD is deemed suitable with aerosol loading over southern Africa has been shown to be dominated by aeolian dust (Piketh et al., 1999). This counters previous hypotheses of the dominance of particulates from biomass burning (Van Wilgen & Scholes, 1997; Levine, 1996). In contrast to studies that are reliant solely on the remotely sensed identification of mineral aerosols, this study also employs TSP monitoring equipment and horizontal flux traps in tandem with satellite observation. This enables the validation and characterisation of the particles forming the dust plumes as mineral aerosols. The MODIS Aerosol Product (AOD) selected for this study monitors the aerosol optical thickness globally with daily Level-2 data products produced at the spatial resolution of a 10x10 1-km pixel array (at nadir). Data were downloaded from https://ladsweb.nascom.nasa.gov.

The oceanic investigation of chlorophyll and sea surface temperature was undertaken using MODIS Aqua and Terra (4 km spatial resolution) mapped daily Level-3 ‘chlor_a’ data products. Surface water concentration data of chlorophyll a is generated with the Ocean Colour Index (OCI) algorithm as described by Hu et al. (2012), using three bands of blue-to-green wavelength reflectance (between 440 – 570 nm) to estimate chlorophyll *a* concentrations based on empirical relationships defined by in situ measurements. Sea

surface temperature measurement was based on longwave (11-12 μm) thermal radiation (daytime) 'sst' data as described by Minnett et al. (2004). Both data sets were downloaded from http://oceandata.sci.gsfc.nasa.gov.

Remote sensing investigations of ocean fertilisation by dust deposition commonly compare MODIS-derived products for both AOD and chl-a (e.g. Qu et al., 2016; Gabric et al., 2015; Tan & Wang, 2014; Lin et al., 2011), as is undertaken in this study. Robust comparison is possible due to the independence of the datasets, which is due to the development of the AOD and chl-a products using selective reflectances from varying MODIS bands[5]. AOD identification incorporates bands 1, 3 and 8 with respective spectral radiances (W/m^2-μm-sr) / bandwidths (nm) of 21.8 / 620-670, 35.3 / 459-479 and 44.9 / 405-420. Band 1 detects red light wavelength reflectance while bands 3 and 8 detect that of blue light. Chl-a also uses band 8 plus bands 9, 10 and 12 with their spectral radiances (W/m^2-μm-sr) / bandwidths (nm) being 41.9 / 438-448, 32.1 / 483-493 and 21.0 / 546-556 respectively. These bands span blue-to-green light.

Further independent detection of the target variable, i.e. AOD or chl-a measurements, is achieved with algorithmic processing of the band-specific reflectance data. These have been developed to retrieve the specific reflectance readings resulting from either atmospheric dust (as detailed in Hsu et al. (2013) and Sayer et al. (2014)) or surface water chlorophyll *a* content (as detailed in and Hu et al. (2012)). The inclusion of band 8 in both AOD and chl-a identification is to identify dust particle interference, and exclude algorithmically, for chl-a identification.

[5] The band specifications are provided at https://modis.gsfc.nasa.gov/about/specifications.php.

For AOD, aerosol retrieval is defined by:

$$R(\mu, \mu_0, \phi) = \frac{\pi I(\mu, \mu_0, \phi)}{\mu_0 F_0}$$

where, as described in verbatim by Hsu et al. (2013), R is the normalized radiance (or apparent reflectance), F_0 is the extraterrestrial solar flux, I is the radiance at the top of the atmosphere, μ is the cosine of the view zenith angle, μ_0 is the cosine of the solar zenith angle, and ϕ is the relative azimuth angle between the direction of propagation of scattered radiation and the incident solar direction.

Chl-a identification incorporates the fraction of light that enters the ocean then eventually scatters back up through the surface. This light is called the water-leaving radiance ($L_w(\lambda)$), and it can be deduced from space after removal of atmospheric effects. Within this water-leaving radiance, chl-a reflectance is defined by:

$$R_{rs}(\lambda) = \frac{f\ t^2}{Q(\lambda)n^2} \frac{b_b(\lambda)}{[a(\lambda) + b_b(\lambda)]}$$

where f is an empirical factor and function of the solar zenith angle (Morel & Gentili, 1991), t is the transmittance of the air-sea interface, Q(λ) is the upwelling irradiance-to-radiance ratio $E_u(\lambda)/L_u(\lambda)$, and n is the real part of the index of refraction of seawater (Carder et al., 2003). $b_b(\lambda)$ is the total backscattering coefficient, which can be expanded as:

$$b_b(\lambda) = b_{bw}(\lambda) + b_{bp}(\lambda)$$

with bw and bp referring to backscattering of light by water and particles both constant and well-known values (Carder et al., 2003; Smith & Baker, 1981). The incorporation of

these known backscattering coefficient values allows their contribution to reflectance measurements to be accounted for, and removed, to identify chl-a concentrations in the ocean surface waters.

4.5.2 Data analyses

The aod, chlor_a and sst MODIS datasets (hereafter AOD, chl-a and SST) were plotted (10°S, 10°W by 30°S, 20°E) using a Python integrated development environment software application and visually inspected to determine the transport extent of mineral aerosols, chlorophyll distribution and upwelling. The visually-identified extent of dust transport was used to determine the geographical area (Figure 31) for calculation of the AOD, chl-a and SST average values, total pixel count and total-pixel count data (blank pixels due to cloud masking and swath gaps not used for calculation of averages). Multiple rectangular calculation areas were combined to allow for the curvature of the coastline (Figure 31) ranging from 720-1,000 km westwards from the coast covering a total area of 800,000 km^2. Days with <20 % data coverage were excluded from further analyses. The MODIS aqua and terra average values were then averaged together to produce final AOD, chl-a and SST daily values. Only days with ≥20 % data for both AOD, chl-a and SST were used for t-test calculation of correlation significance. Daily value correlation was determined using two-tailed t-tests, calculated using the formula:

$$t_{calc} = r.\sqrt{\frac{n-2}{1-r^2}} \qquad \text{where r is calculated as} \qquad r_{xy} = \frac{(\sum_{i=1}^{n} x_i y_i) - n\bar{x}\bar{y}}{(n-1)s_x s_y}$$

Significance was determined using a two-tailed p value of 0.05 against T_{crit} values according to *n* for each calculation.

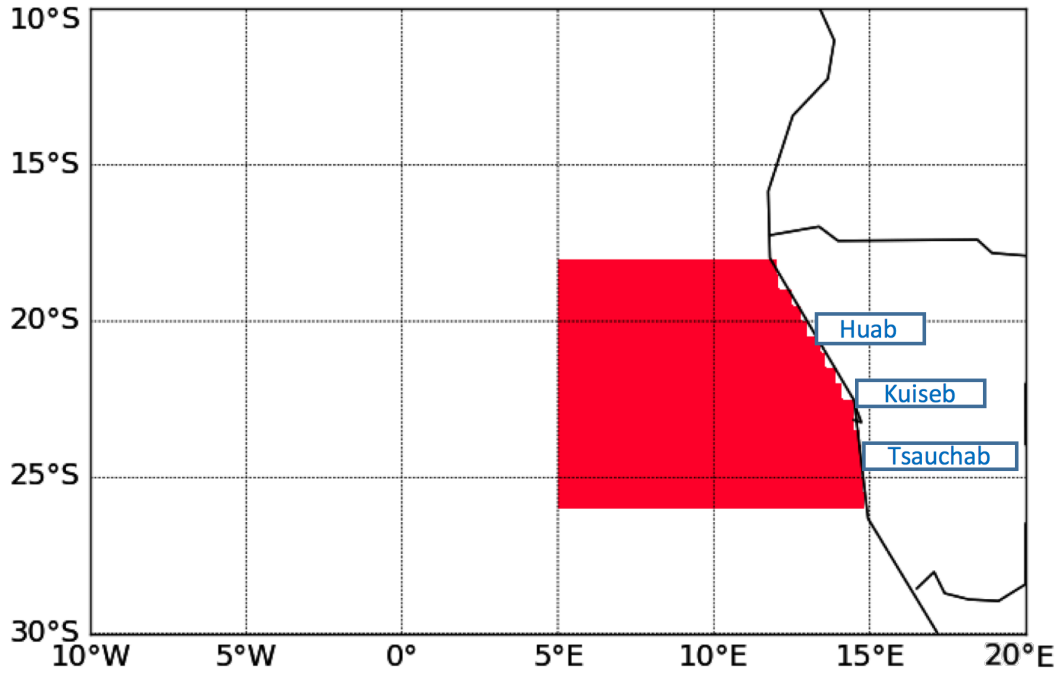


Figure 31 | Area of investigation for calculation of AOD, chl-a and SST average values and total pixel counts

4.5.2.1 Data availability

Analysis of multi-day trends in the region posed difficulties due to the prevalence of atmospheric moisture at both high altitudes (cloud cover) and near-surface fog generated the cold upwelling region itself (Seely & Louw, 1980). During the six months of investigation 37% (67 days) had over 20% coverage, with the longest unobstructed duration being between 29 April to 7 May (as presented in Figure 64). Further, once the short-lived and diurnal dust-delivering easterly winds (Lindesay & Tyson, 1990) subside the dominant regional weather circulation of south to southwesterly trade winds (Lancaster, 1985) resume, which are laden with atmospheric moisture and resultantly causing frequent obstruction of the ocean surface by clouds. August and September were the most data sparse months with 51 days obstructed by clouds and fog and also saw minimal dust activity in the river valleys. July, August and September saw increased AOD values associated with the recirculation of air mass from central Africa bringing

particulates from biomass burning in that region, the recirculation a known-occurrence during these months caused by a semi-permanent continental high pressure cell that provides significant influence on the subtropical atmospheric circulation in the region (Tyson & D'Abreton, 1998). The increase in fire activity during these months in Angola, the Democratic Republic of the Congo, and neighbouring smaller countries is visible using the 'Terra/Aqua Fire and Thermal Anomalies' product of the MODIS satellites with the recirculated biomass haze visible on MODIS true colour imagery (www.worldview.earthdata.nasa.gov) and on plots of daily AOD MODIS data used to calculate daily means in this study. The increases in chl-a on data-available days in July appeared to be the result of upwelling. These months were therefore excluded from further analyses. April, May and June were selected as the optimum months for assessing oceanic response to dust plumes originating from Namibia's coastal valleys.

SECTION 3

- Investigation -

NB: Inter-paper referencing is as follows:

Dansie et al. (2016a) – Paper 1

Dansie et al. (2016b) – Paper 2

Dansie et al. (2016c) – Paper 3

CHAPTER 5

Paper One

IRON AND NUTRIENT CONTENT OF WIND-ERODIBLE SEDIMENT IN THE EPHEMERAL RIVER VALLEYS OF NAMIBIA

A. Dansie[1], G.F.S. Wiggs[1], D.S.G Thomas[1,2,3]

[1] School of Geography and the Environment, University of Oxford, Oxford OX13QY, UK

[2] Geography, Archaeology and Environmental Studies, University of the Witwatersrand, Johannesburg, South Africa

[3] Department of Environmental and Geographical Science, University of Cape Town, Rondebosch, South Africa

Status: Submitted to *Geomorphology* on 06 May 2016, accepted for publication on 14 March 2017.

Abstract

Research concerning the global distribution of aeolian dust sources has principally focussed on salt/clay pan and desiccated lacustrine emission areas. In southern Africa such sources are identified as Etosha Pan in northern Namibia and Makgadikgadi Pans in northern Botswana. Dust emitting from ephemeral river valleys has been largely overlooked. Rivers are known nutrient transport pathways and ephemeral river valleys frequently replenish stores of sediment which, because of its fine texture, can become susceptible to aeolian erosion. Such airborne sediment may be nutrient rich and thus be significant for the fertilisation of marine waters once deposited. This study investigates the potential for airborne fertilisation of the South Atlantic by collecting sediment from three ephemeral river valleys in Namibia and analysing samples for their fertilisation potential in terms of their grain size distribution and their concentrations of bioavailable N, P and Fe. We compare fertilisation potential of these ephemeral river samples to sediments collected from Etosha and Makgadikgadi Pans. Our results show that the ephemeral river valleys contain fine grained sediment similar to Etosha and Makgadikgadi Pans yet have a much higher loading of bioavailable iron and nutrients important for ocean fertilisation. Our findings suggest that the ephemeral river valleys of Namibia may be a significant aeolian dust source of regional importance, and potentially the most important source of ocean fertilising mineral aerosols in Southern Africa. Given this finding a re-assessment of the potential role of ephemeral river valleys in providing nutrient rich sediment into the aeolian and marine systems in other dryland areas is necessary.

5 Iron and nutrient content of wind-erodible sediment in the ephemeral river valleys of Namibia

5.1 Introduction

Land-ocean and land-atmosphere-ocean sediment transport provide pathways of nutrients essential for ocean productivity (Bouwman et al., 2013; Kroeze et al., 2012; Aufdenkampe et al., 2011). Marine phytoplankton provide half of the planet's primary production (Worden et al., 2015; Chavez et al., 2011) and the biological consumption of sediment-associated nutrients plays an important role in photosynthetic marine uptake of CO_2 (Hauck & Völker, 2015; Jickells et al., 2014). Nutrient input is especially important in High Nutrient Low Chlorophyll (HNLC) regions, which includes the Southern Atlantic (Meskhidze et al., 2007), where phytoplankton is limited by the absence of one or more nutrients required for photosynthetic growth (Quéguiner, 2013; Martin et al., 1994). Iron (Fe), phosphorus (P) and nitrogen (N) are known to play a role as a trigger for phytoplankton growth in HNLC zones when these nutrients become available in otherwise nutrient abundant waters (Moore et al., 2013; Quéguiner, 2013; Okin et al., 2011).

Globally, fluvial delivery provides the largest contributions to the oceans of sediment (Syvitski, 2003), Fe (Poulton & Raiswell, 2002), and N and P from both natural processes and human activities (Glibert et al., 2006; Howarth & Marino, 2006). Excluding glacial sediment, considered here a form of fluvial delivery over a longer timescale, the next largest contributor of sediment and bound-nutrients to the ocean is aeolian transport and deposition (Mahowald et al., 2008; Jickells et al., 2005). Aeolian deposition is widely recognised as significant for ocean productivity where sediment and bound nutrients are delivered directly to the ocean surface, an environment abundant in light and oxygen

which are fundamental requirements for photosynthesis (Ryther, 1956; Kroopnick, 1975). Experimental application of desert dust to HNLC ocean surfaces has been shown to trigger phytoplanktonic growth (Giovagnetti et al., 2013). However, ocean fertilisation pathways that encompass both modern fluvial sources and atmospheric transport have yet to be investigated.

At the global scale major sources of aeolian dust in the atmosphere are identified as dry or ephemeral lakes in arid and semi-arid regions, where deep and extensive deposits of alluvial source material have accumulated via fluvial inundation during Pleistocene lake highstand phases (Prospero et al., 2002). This includes the world's largest dust source, the Bodélé Depression formed from the remnants of paleo Lake Chad (Washington et al., 2009; Koren et al., 2006; Washington et al., 2003). Similar sources of windblown sediment are found in southern Africa such as the topographic lows of the Magkadikgadi Pan system in Botswana and Etosha Pan in Namibia (Bryant et al., 2015; Mahowald et al., 2005; Prospero et al., 2002).

Ephemeral rivers, on the other hand, serve as extant and replenishing sources of alluvial fines. Rivers with natural flooding and drying regimes characteristically transport large loads of sediment (Laronne, 1993) and dissolved nutrients (Skoulikidis & Amaxidis, 2009). These are deposited along flats and floodplains (Reid & Laronne, 1995) as flow events dissipate via subterranean transmission and evaporation (Dahan et al., 2008; Seely et al., 2003). This process occurs to such an extent in Namibia's ephemeral valleys that the downstream river profiles have developed a convex shape near the coast due to the magnitude of sediment transport and deposition (Vogel, 1989). Furthermore, ephemeral rivers experience flow and flood pulses on an annual or multi-year frequency (see Tooth (2000)) providing replenishment of sediment. Such sediment has a high percentage of

fines (silt-clay) and is geochemically representative of the watershed through which it has been fluvially transported (Collins et al., 1998; Schumm, 1960).

Ephemeral channel systems provide nutrients that support corridors of biological productivity in otherwise nutrient-poor dryland ecosystems (e.g. Zeglin et al. (2011) and Bunn et al. (2006)) and they have also been identified as notable sources of windblown dust (e.g. Schepanski et al. (2013)). Yet, to date, research focused on the chemistry of airborne sediment emitted from ephemeral river valleys has been limited to respiratory and pollution-related human health impacts (e.g. Fu et al. (2014), Kuo et al. (2010), Nickling & Gillies (1993)). There are no published studies investigating the potential for ephemeral river channels to act as ocean fertilizers. This is despite mineral aerosols making up 82% of atmospheric P (Mahowald et al., 2008) and about 95% of the global averaged Fe budget (Mahowald et al., 2009). Atmospheric processing during aeolian transport increases the bioavailability of mineral aerosol nutrients, most notably Fe (Shi et al., 2015). This processing in the atmosphere and efficient ocean-uptake of bioavailable nutrients is partly determined by particle surface area and dust concentration (Mackie et al., 2005), thus finer grains tend to be larger contributors to ocean fertilisation. However, fertilisation-potential is also constrained by particle-reactivity which is determined by the terrestrial mineralogy and chemistry of the source material (Krueger et al., 2004).

Remote sensing studies have shown that the ephemeral river valleys of Namibia are important contributors to regional dust emissions (e.g. (Vickery et al., 2013; Vickery, 2010; Eckardt & Kuring, 2005; NASA, 2003; NASA, 2002; Eckardt et al., 2001). These analyses of dust plume frequency in southern Africa (2005-2008) noted that 34% of plumes originated from the Namibian ephemeral valleys, with 16% sourced in the Makgadikgadi Pan system and 10% in Etosha Pan. Each year strong seasonal easterly

winds generate dust plumes over the Southern Atlantic. The coastal proximity of the river valley sources would be expected to increase the incidence of deposition over the ocean when compared to Etosha Pan which is approximately 400 km from the west coast, following the E/E-NE winds that would transport dust, and Makgadikgadi Pan which is 1200km from the coast.

Southern African dust has been hypothesised as a potentially important source of minerals for ocean fertilization (Bhattachan et al., 2015; Piketh et al., 2000) but to date there has been only limited analysis of the characteristics of either airborne dust or emission source material from Southern Africa. The long-term accumulated sediment in Makgadikgadi and Etosha Pans have been shown to have an enriched Total P and Total N in the fine fraction (<45µm) compared with the parent sediment (Bhattachan et al., 2015). The same study also showed, conversely, that bioavailable Fe concentrations were higher in the un-sieved parent sediment in the Makgadikgadi Pan and some parts of Etosha Pan. Nutrient levels along the Namibian ephemeral river channels are known to increase downstream as the channels travel through the otherwise nutrient-poor Namib Desert (Jacobson & Jacobson, 2013; Jacobson et al., 2000; Abrams et al., 1997). However, the nutrient content and enrichment of the ephemeral river sediments in the dust emitting regions of the river have not been investigated to date.

Given the combination of factors discussed above, it can be hypothesized that the ephemeral river valley sediments of Namibia might be an important source of nutrients to the ocean through the process of atmospheric mineral dust transport. However, there has been no assessment of the sedimentary characteristics of fluvial fines to aeolian erosion, and no quantification of the potential nutrient content of such sediment. Global remote sensing and modelling assessments of dust have focused on the major single sources of

emission in southern Africa (the Makgadikgadi and Etosha Pan systems), with the active dust emission sites of the ephemeral river valleys being largely overlooked, and excluded completely from any on-the-ground investigation. This paper addresses these issues for Namibian ephemeral river valleys by examining the sedimentary characteristics of valley sediments, particularly the fine fraction (susceptible to wind erosion) and the bioavailable iron and macronutrient content, which are components important for ocean fertilization. Further we compare these properties of the valley sediments with sediments from two other major dust emitting sources in the region, Etosha and Makgadikgadi Pans.

5.2 Research Design and Methods

5.2.1 Regional setting

The Namib Desert runs 2,000 km N-S along the coast, from South Africa to Angola (Heine & Heine, 2002) with the Namib Sand Sea lying between the coastal towns of Luderitz and Walvis Bay. North of the Sand Sea gravel plains occupy the 150-200 km wide coastal strip for 500 km until a smaller, northern sand sea begins near the Huab River mouth (Grünert, 2000). Twelve ephemeral river valleys extend east-west towards the Atlantic coast, although two, the Tsondab and the Tsauchab, presently terminate within the sand sea without reaching the ocean base level (Figure 32a).

The coastal Namib receives almost zero precipitation with the non-river channel biota reliant on frequent ocean fog as a moisture source. The river catchments themselves extend inland for over 300 km, on to the 1000 m high Great Escarpment (Morin et al., 2009) where average annual rainfall reaches 300 mm a year or more (Jacobsen et al., 1995). As the rainfall increases towards the eastern edges of the watersheds native vegetation biomass, agriculture and grazing increases (Jacobsen et al., 1995a). The Great Escarpment runs parallel to the coast, 100-150 km inland and serves as the eastern border

for the Namib Desert and the expansive central plateau of southern Africa (Goudie & Eckardt, 1999). On the plateau and highlands above the escarpment, sufficient precipitation supports vegetation and the development of at least minimal colluvium on hillslopes (Bierman & Caffee, 2001). The ephemeral river catchments occupy the 1000 – 750 million years old geological Damaran Granites and Damara Sequence Swakop Facies and, in the north, the ancient geological features of the Khoabendus and Haib Groups (Jacobson et al., 1995). The catchments display relatively strong slope-channel coupling and moderately abundant sediment supply, promoting a variety of confined bedrock and alluvial braided rivers (Jacobson et al. (1995) in Thomas (2011)). The dust emission sites of interest are concentrated in the lower-reaches of the rivers Figure 32b and c, within the Namib Desert. The modern river channels cut through valley fill comprised of Late Pleistocene deposited silts, the most studied being the Homeb silts of the Kuiseb valley (Smith et al., 1993). Channel width across the valley floor varies along the interchanging stream and braided channel system, ranging from 20-100 m in width until the 1.8 km or 2 km wide terminal braided fan of the Huab and Tsauchab respectively. Within the modern channels are fluvial-aeolian sand deposits and fluvial silt and mud deposits (Svendsen et al., 2003; Jacobson et al., 2000). Larger flow events spread into additional, non-primary, branches and floodplains of the braided system within the low-gradient valleys.

5.2.2 Research Design

Field Sites

Two contrasting dry river valleys were investigated in this study: the Huab, which reaches the ocean during periods of high flood, and the Tsauchab, which terminates in the Namib Sand Sea (Figure 32). Both river valleys had previously been identified as significant emitters of aeolian dust by remote sensing analysis (Vickery et al., 2013;

Vickery, 2010). The 14,800 km^2 Huab watershed extends 300 km inland, the upper watershed receiving 300-350 mm of annual rainfall (Jacobsen et al., 1995a). The shorter Tsauchab watershed is 3,950 km^2 in area with the upper reaches ending between the 150-200 mm isohyets (Jacobsen et al., 1995a).

Surface sediment sampling was undertaken across the lower valleys at 8 cross-sections (5 in the Huab and 3 in the Tsauchab) in April-May 2013. These locations had previously been identified as sources of aeolian dust emission (Vickery, 2010). The cross-sections are shown in Figure 32b) and 1c). In total, 68 samples of surface sediment (5-11 samples per cross section) were collected plus eight field duplicates. Inter-sample distance along each cross section was determined in the field by the specific channel morphology at each site with samples collected within geomorphological units identified visually below (see Figure 33):

- valley fill –above-channel deposits forming valley-floor and river banks
- coarse channel deposits –in-channel sandy deposits
- fine channel deposits – either in-channel fines forming a surface crust on top of coarse channel deposits or in-channel clay material often forming a distinct, smooth depositional pad feature ranging from 10-100 m^2 in size, or the larger clay pan system in the Tsauchab terminus
- dune deposits – sandy aeolian material originating from adjacent dune forms, or samples from the dune face itself (Tsauchab only)

Further surface samples were collected from the Etosha and Makgadikgadi Pans, Figure 32a, as part of a wider study (Haustein et al., 2015) and are used in this paper for comparative purposes. Four samples were collected from NE Sua Pan in Botswana in 2012. These consisted of two surface crust samples (c. 1-2 cm thick) and two sub-

crust samples that consisted of loose, dry powdery sediment. Six samples were collected from W Etosha Pan in 2015. These were similar to the Sua samples and consisted of three crust and three sub-crust samples.

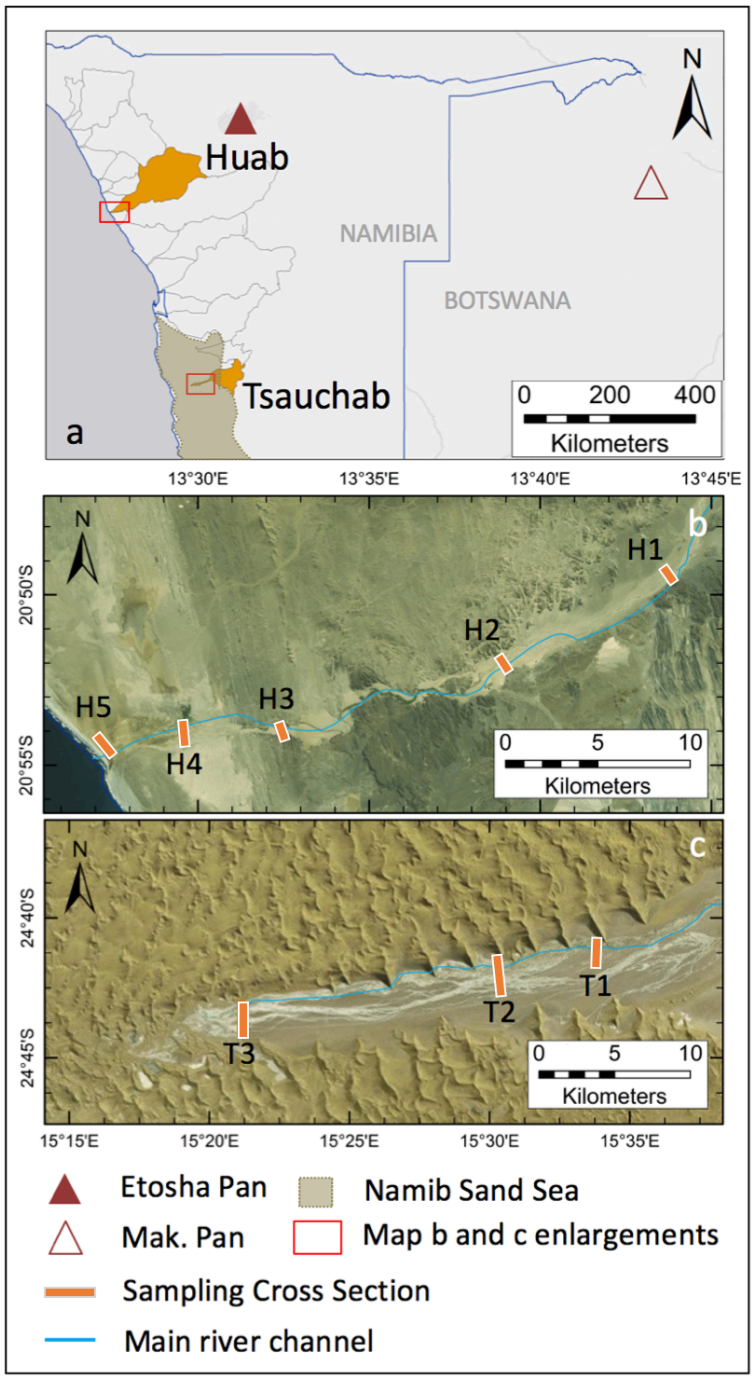


Figure 32 | a) Map of south-western Africa showing the ephemeral watersheds of western Namibia (black outline) with Huab and Tsauchab watersheds highlighted in orange. The location

of Etosha Pan and Makgadikgadi Pans in Namibia and Botswana respectively are also shown. Map enlargements b and c show the 5 cross section sampling locations across the Huab river channel and 3 cross section sampling locations across the Tsauchab river channel respectively.

5.2.3 Methods

5.2.3.1 Sample Collection

Surface samples were collected using a trowel to obtain approximately 200 g of loose sediment to a depth of about 10 mm. The more consolidated crust of fine channel deposits and clay pad/pan deposits were pried up and the natural thickness measured with a tape measure. Samples were stored in ziplock bags and shipped to the UK for preparation for analyses of grain size, bioavailable Fe, and P and N nutrient compounds.

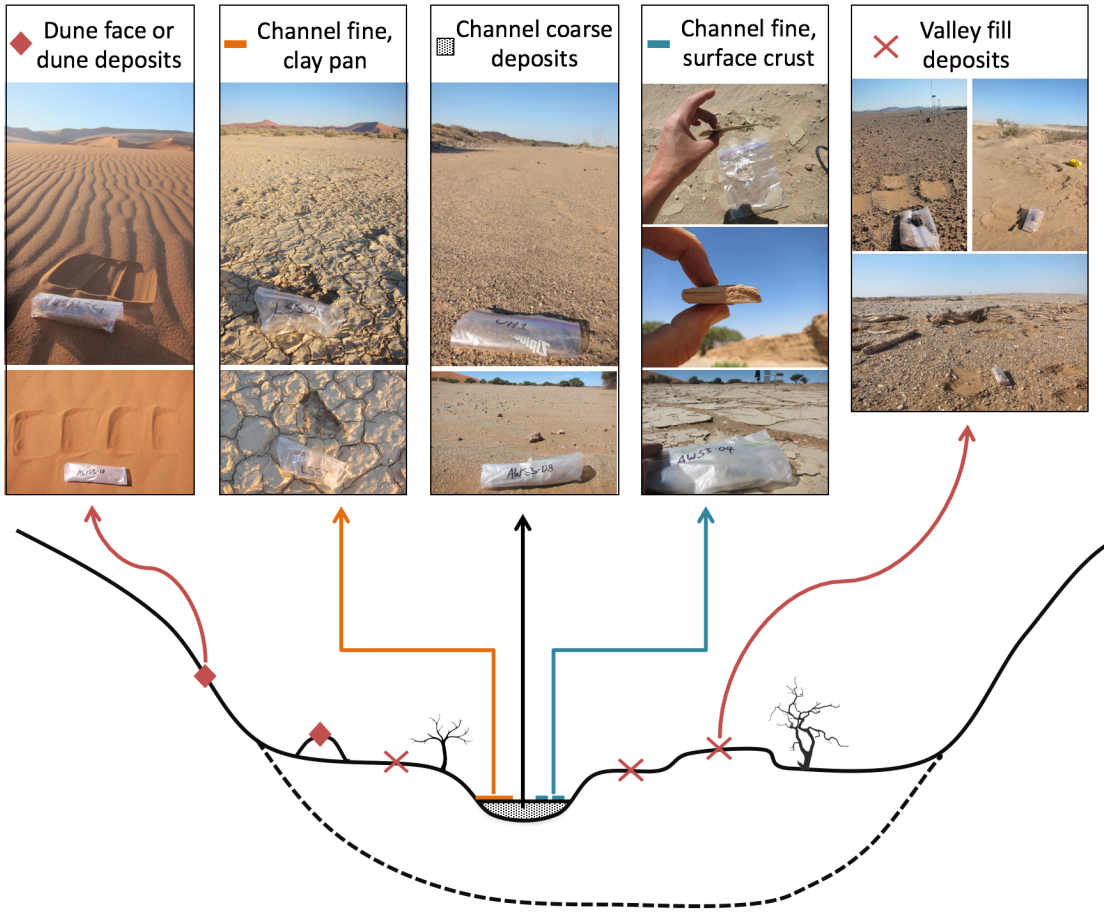


Figure 33 | Sampling points showing geomorphological units targeted along cross sections

Each sample (including field duplicates) was sieved through 2 mm mesh and the <2 mm subset split with a riffle box into subsets for wet grain size analysis and chemical analyses. Solid crust and clay pad/pan material was broken into appropriately 5 g and 40 g and pieces for wet grain size and chemical analyses respectively

5.2.3.2 Chemical Analyses

A subset of sieved <2 mm samples, including field duplicates, were split and sent to the Kansas State University Soil Testing Laboratory where they were dried overnight in a 50°C oven with the exception of sub-samples for iron analyses which were air dried. Samples were analysed for analyses of Mehlich III Phosphorus, DTPA extraction of bio-available Fe^{2+} and Fe^{3+} (combined) followed by analyses with by Flame Atomic Absorption spectrometry (following method described by (Lindsay & Norvell, 1978), inorganic Nitrogen NH_4^+ and NO_3^- extracted with 1M of KCl and analysis in a flow analyser, total nitrogen and total phosphorus using a modified Kjeldahl digestion followed by analyses in separate colorimetric reactions using a flow analyser, and soil pH using a 1:1 mixture of soil and DI water. Methods for analysis were taken from (Brown, 1998) unless otherwise stated.

5.2.3.3 Grain Size

Grain size analyses was undertaken using a Malvern Mastersizer Hydro 2000MU to determine sample particle size ranges and to identify the proportion of fine material that might be susceptible to aeolian erosion. Wet-dispersion grain size analysis was conducted in order to disaggregate peds and pellets to their parent sediment sizes.

3-5 g of sample was processed for salt and carbonate removal as described in Soukup et al. (2008). Oven-dried (40°C) samples were then ground using a mortar and pestle and riffled to range of weights from 0.016g to 3.8g and suspended in a 1:1 solution of 50g/L

sodiumhexametaphosphate and DI water. Samples were placed on a linear shaker and shaken for 4 hrs at a rate of 250 rpm then left to stand overnight. Samples were run in the Malvern Mastersizer using standard procedures, taking 3 measurements per sample and an average calculated that was used for interpretation. Cleaning runs using DI water were undertaken between each sample.

5.3 Results

5.3.1 Grain size characteristics

Figure 34 presents mean grain size data for the main geomorphic units in the study, and the example sediments from Etosha and Makgadikgadi. These data demonstrate the general characteristics of the units. Of note is the concentration of fine material in the channel fluvial deposits, showing similar grain size distribution to the Etosha and Makgadikgadi samples. Valley fill sediments contain a relative larger amount of coarser grains, with a peak at 200 μm. As would be expected, the dune sediments are dominated by sand-size material and contain the highest relatively coarse fraction, but do not contain material >1000 μm. Intra-sample variance is very low within geomorphic units (see Table 6) and laboratory sample repeats for each unit produced matching results.

Division of the grain size distribution into size classifications representative of atmospheric (aeolian transport) and settling (wind deposited) particle size (Ginoux et al., 2004; Arimoto et al., 1997; Tegen & Lacis, 1996) is shown in Table 7. Fine channel deposits show 91.46% of grains <100 μm, a similar content to Etosha Pan (84.86%) and Makgadikgadi Pan (91.04%). Valley fill contains 39% grains <100 μm while the coarse channel sediment assemblage is predominantly 100 μm - 2 mm.

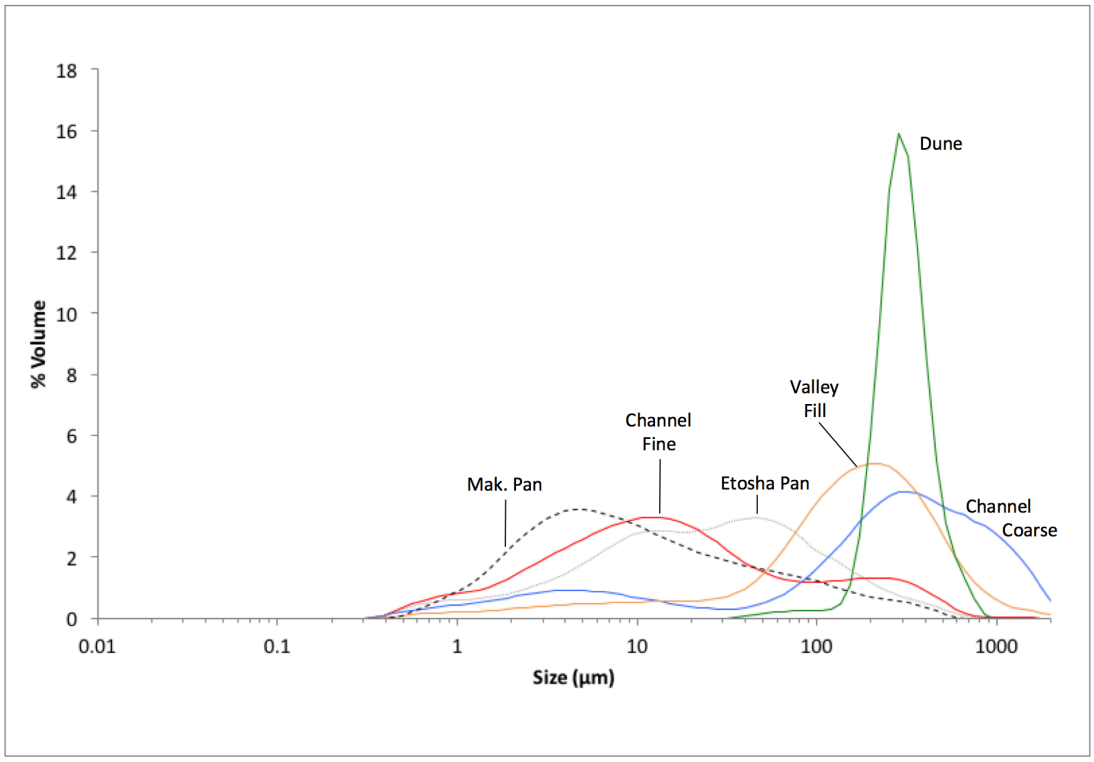


Figure 34 | Mean grain size distributions of river valley geomorphological units with the combined means of Etosha Pan and Makgadikgadi Pan crust and sub-crust samples.

Table 6 Mean grain size variance calculated and averaged according to grouped grain sizes

	Number of samples	0-0.1 (µm)	0.1-1 (µm)	1-10 (µm)	10-100 (µm)	100-1000 (µm)	1000 – 2000 (µm)
Channel Coarse	17	0	0.122	1.487	0.457	8.270	3.586
Channel Fine	23	0	0.012	0.168	0.576	0.398	0
Valley Fill	17	0	0.004	0.097	1.206	4.908	0.220
Dune	3	0	0	0	0.046	8.123	0
Etosha Pan	6	0	0.018	0.764	2.823	1.647	0
Mak. Pan	4	0	0.007	0.112	0.350	0.071	0

Table 7 Mean grain size fraction (%) of ephemeral river geomorphological units, Etosha Pan and Makgadikgadi Pan samples for <1 µm (Atmospheric Dust), 1-100 µm (Settling Dust) and 100 µm-2 mm from wet-dispersion grain size analysis.

	Course Channel Deposit	Fine Channel Deposit	Valley Fill Deposit	Dune	Etosha Pan	Mak. Pan
0 - 1 µm	1.79	3.81	1.08	0.00	3.06	2.51
1-100 µm	21.71	78.90	38.11	1.46	81.80	88.53
100-2000 µm	76.51	17.29	60.81	98.54	15.14	8.96
Total	100	100	100	100	100	100

Figure 35 shows that the channel fines of the river valleys have a similar clay (<2 µm) content to Etosha and Makgadikgadi Pans of slightly below 10%. The Tsauchab channel fines had a higher sand fraction (39%) than the Huab (16%). This is likely explained by windblown transport of sand from the surrounding Namib Sand Sea and flow events eroding slipfaces encroaching into the channel. This sand source hypothesis is supported in Figure 34, the grain size of channel fines shows a bimodal distribution with a second peak between 200-300 µm that aligns with grain size of the dune samples.

River channel coarse deposits contained an average of 16% (Huab) and 41% (Tsauchab) fines between 16-2µm. Over three quarters (77%) of fill deposits in both valleys comprise sediment coarser than 63µm (i.e. sand). The similarity of valley fill composition between the river valleys would suggest a common long-term geomorphological process has formed the valley fill. Grain sizes of samples from pan crust and sub-crust fluff in both Etosha and Makgadikgadi Pans show similar composition, Figure 35.

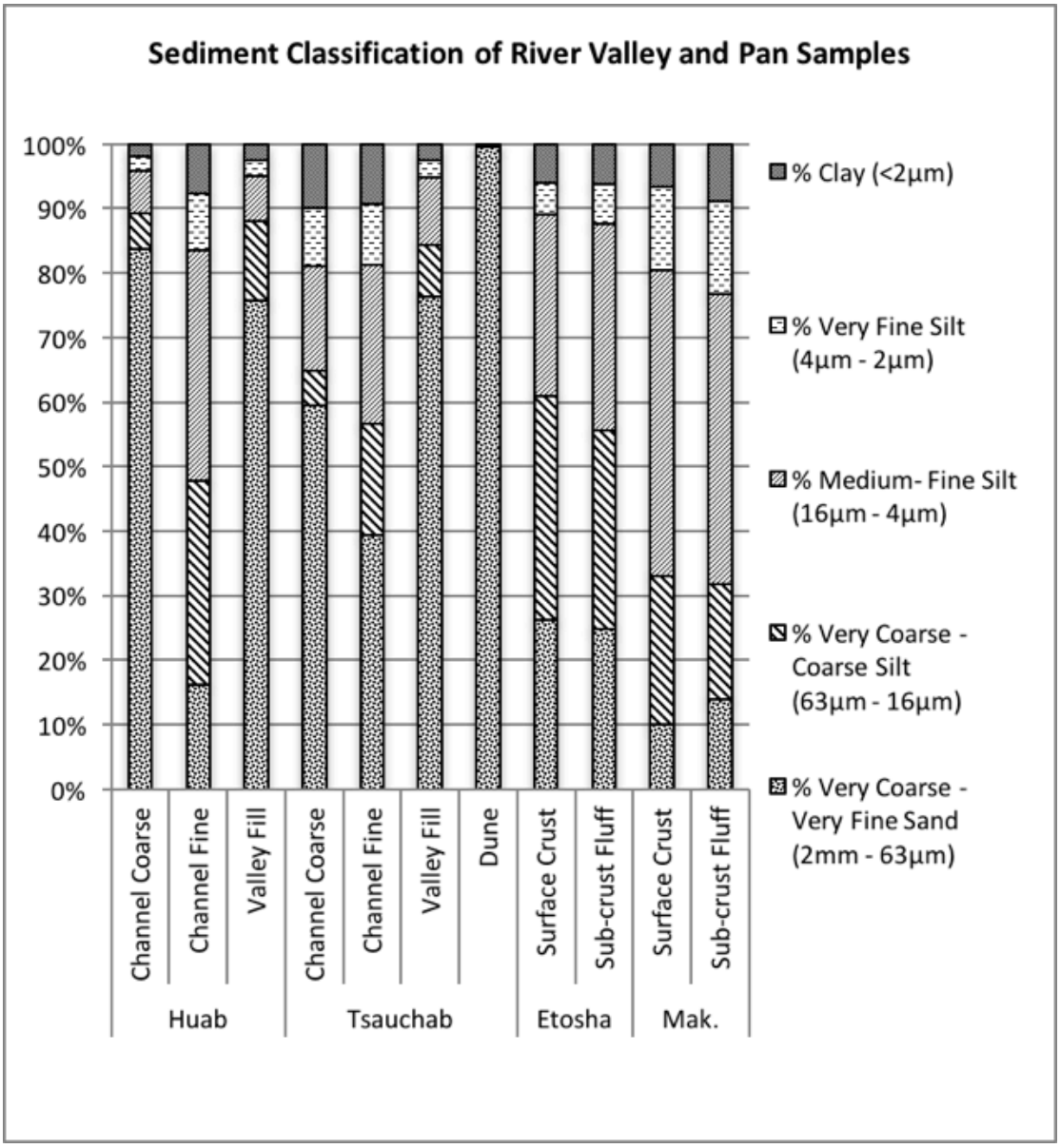


Figure 35 | Mean sediment size fractions of Huab and Tsauchab River geomorphological units compared to Etosha and Makgadikgadi Pan samples

5.3.2 Bioavailable Fe, N and P content

The results of the bioavailable nutrients, Mehlich P, DTPA-extractable Fe (hereafter referred to as bioavailable Fe), ammonium (NH_4^+), nitrate (NO_3^-) as well as total N (TN) and total P (TP) are given in Figure 36. A 1-way ANOVA of chemical analysis results against river valley geomorphological unit classification was performed to assess the significance of the results presented in Figure 36. Further post hoc analyses was

undertaken using Tukey and Bonferroni tests to identify between which geomorphological classifications the significant relationships existed. These p values are provided in the text. An additional 1-way ANOVA and post hoc analysis that included Etosha and Makgadikgadi Pan samples with the river samples was also performed.

The results show that, compared to the other geomorphological units sampled, the fine channel deposits have higher concentrations of all-but-one of the bioavailable nutrients as well as TN and TP. The exception is the nitrate concentrations which did not show an elevated median (16.79 ppm) concentration (post hoc analyses p values between 0.235 and 0.635 against other valley sample units). The presence of a skewed distribution containing some higher sample concentrations (mean 47.35 ppm) are noted in Figure 36d.

The mean concentrations of bioavailable nutrients, TN and TP of in-channel fine deposits (Figure 36) was used to calculate enrichment ratios against other river valley geomorphological units. The enrichment ratio was calculated (after Wan and El-Swaify (1998)) for each nutrient element as:

average ppm of fine channel deposits / average ppm of geomorphological unit

Table 8 shows these enrichment ratios of fine channel deposits compared to other geomorphological units. The nutrient ratios are all greater than 1, showing the fine channel deposits are enriched in nutrient content compared to other geomorphological units.

Table 8 Fine channel deposit enrichment ratio calculation against other geomorphological units

Alluvial vs:	pH	Meh. P	Fe	NH_4^+	$N0_3^-$	TN	TP
Channel Coarse	0.94	4.13	4.33	2.54	10.87	6.62	1.98
Valley Fill	0.93	1.52	2.87	3.83	1.95	4.66	1.18
Dune	0.94	20.90	6.50	2.08	18.93	8.73	3.98

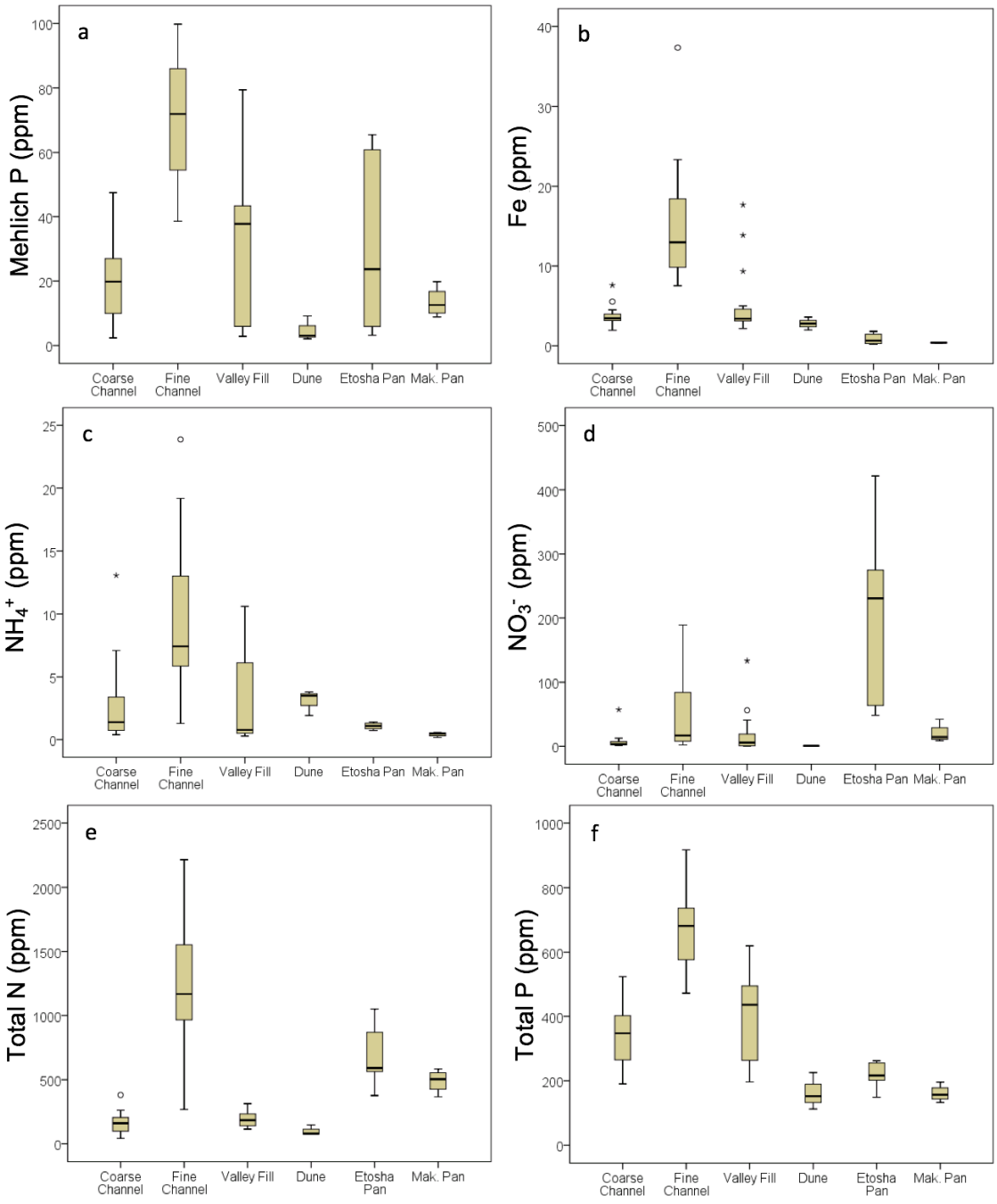


Figure 36 | Nutrient content of the Huab and Tsauchab geomorphological units and averaged crust and sub-crust samples from Etosha and Makgadikgadi Pans for (a) bioavailable P, (b) bioavailable Fe, (c) ammonium, (d) nitrate, (e) TN, and (f) TP.

Comparison of the nutrient content of these river channel fines to Etosha and Makgadikgadi Pan samples (Figure 36) shows important differences. Of particular note is that bioavailable iron concentration (14.82 ppm) is higher in the river fines than either the Etosha (0.85 ppm, p=0) or Makgadikgadi Pans (0.40 ppm, p=0.001) samples (Figure 36b). No statistically significant difference was found between coarse channel deposits, valley fill or dune samples for bioavailable Fe. Further, no statistically significant difference is shown between bioavailable Fe concentrations in coarse channel/valley fill/dune samples with either Etosha or Makgadikgadi Pans[6]. The ephemeral river valley deposits of channel fines are also significantly higher in bioavailable phosphorus, ammonium and total phosphorus than either Pan (p>0.5 for individual comparison of both Huab and Tsauchab with each Etosha and Makgadikgadi in all cases[7]).

Comparison between the ephemeral river valleys

Analyses of the data (Figure 36) shows the Tsauchab river samples have the highest concentrations of both TN[8] and ammonium[9] of all clay pan/pad locations. The Etosha Pan samples have much higher levels of nitrate than any other site[10]. The bioavailable Fe content of Tsauchab in-channel fluvial deposits appears marginally higher than the Huab deposits but this was not significant (p= 0.638 Tukey, 1.0 Bonferroni). Both TP and bioavailable P concentrations are highest in the Huab channel fine deposits (TP mean

[6] Etosha/Makgadikgadi bioavailable Fe p values compared to other geomorphological units samples are p = 0.413/0.489 for valley fill, 0.855/0.864 for coarse channel deposits, 0.998/0.996 for dune deposits and a p value of 1.0 for inter-pan comparison.

[7] p>0 for individual comparison of both Huab and Tsauchab with each Etosha and Makgadikgadi in all cases.

[8] mean 1,624 ppm (p = 0.001 against Huab, 0.000 against each Etosha and Makgadikgadi).

[9] mean 13.27 ppm (p = 0.57 against Huab (not significant), p = 0.000 against each Etosha and Makgadikgadi).

[10] mean 211.61 ppm (p = 0.018, 0.002, 0.010 for Huab, Tsauchab and Makgadikgadi respectively).

874,93ppm, Mehlich P mean 80.33ppm), 150% that of the Tsauchab and 400% compared to the Pans, (Sua Mehlich P 13.44ppm, TP 160.59). pH of the river clay deposits is lower (8.4 Huab, 8.1 Tsauchab average) than that of Etosha (9.6 mean) or Makgadikgadi (9.1 mean).

5.4 Discussion

5.4.1 Sediment size and suitability for aeolian transport

Surface deposits collected from the extant dry river channels in the lower catchments, which are known to emit dust (Vickery et al., 2013), showed a grain size distribution similar to samples collected from Etosha and Makgadikgadi Pans, the major dust emitting sources in southern Africa. In the ephemeral river valleys, over 80% of the channel fines comprised particles under 100 μm (Table 7), the size range commonly found in airborne dust (Mahowald et al., 2009). These fines are derived from both the upper catchments and re-working of valley fill and constitute the suspended sediment load when the rivers are in flood. They are deposited in the lower catchments when the flood events subside and subsequently form surface crusts and clay pads which are susceptible to wind erosive forces.

Valley fill was shown to have a more-varied grain size comprising both larger grains with 75% classified as very fine to very coarse sand (Figure 35) and smaller grains with ~39% under 100 μm, a size susceptible to deflation. Valley fill consists of alluvial material within the valleys that is repeatedly reworked by ephemeral river flow. This process has been well documented, e.g. (Merritt & Wohl, 2003; Tooth, 2000; Patton & Schumm, 1981), and results in an abundance of sediment fines. In all our sampling locations an abundance of quartz sand was observed (see photographs in Figure 33). These sand grains are likely to increase the susceptibility of the surface to deflation through both abrasion of

surface crusts and clay pads (Wiggs, 2011; Shao et al., 1993) and bombardment via saltation of unconsolidated sediments, causing the ejection of fines (Gillette, 1981).

The Tsauchab coarse channel samples displayed a greater proportion of fines than those from the Huab (Figure 35). This is expected to be a result of the Tsauchab terminus location within the Namib Sand Sea. High flood events would see river flow and suspended sediment loads reach the coast in the Huab while the Tsauchab would retain all suspended sediment load within the basin terminus. This may result in a larger long-term net accumulation of deflation material in the Tsauchab and the Tsondab compared to the other river valleys.

5.4.2 Nutrient content of sediments within southern Africa dust emission sites

Higher concentrations of TP, TN, and bioavailable P and N nutrients, excluding nitrate, were observed in fluvial channel fines when compared with other river valley geomorphological units and Etosha or Makgadikgadi Pans. In order to consider geomorphological and biogeochemical influences on nutrient content a regression analysis using mean grain size and source of samples was conducted (Figure 37). Grain size is shown not to correlate with nutrient concentration independently of the sample source. This suggests a role for the geomorphological processes influencing nutrient content and composition within sediments. Beyond this there are also biogeochemical processes that occur due to microbial and biological activities in response to ephemeral river flows (Monger & Bestelmeyer, 2006). The wetting and drying effects on nutrient cycling and nitrification and denitrification processes in dryland ephemeral rivers are diverse and dependant on bacterial community composition (Gómez et al., 2012; Song et al., 2012; Zeglin et al., 2011; Scholz et al., 2002). While the precise biogeochemical processes occurring within the geomorphological units are not known, the silts associated

with hydrological flow in these valleys are known to correlate with higher levels of N and P, resulting in increased productivity and biota abundance (Jacobson et al., 2000).

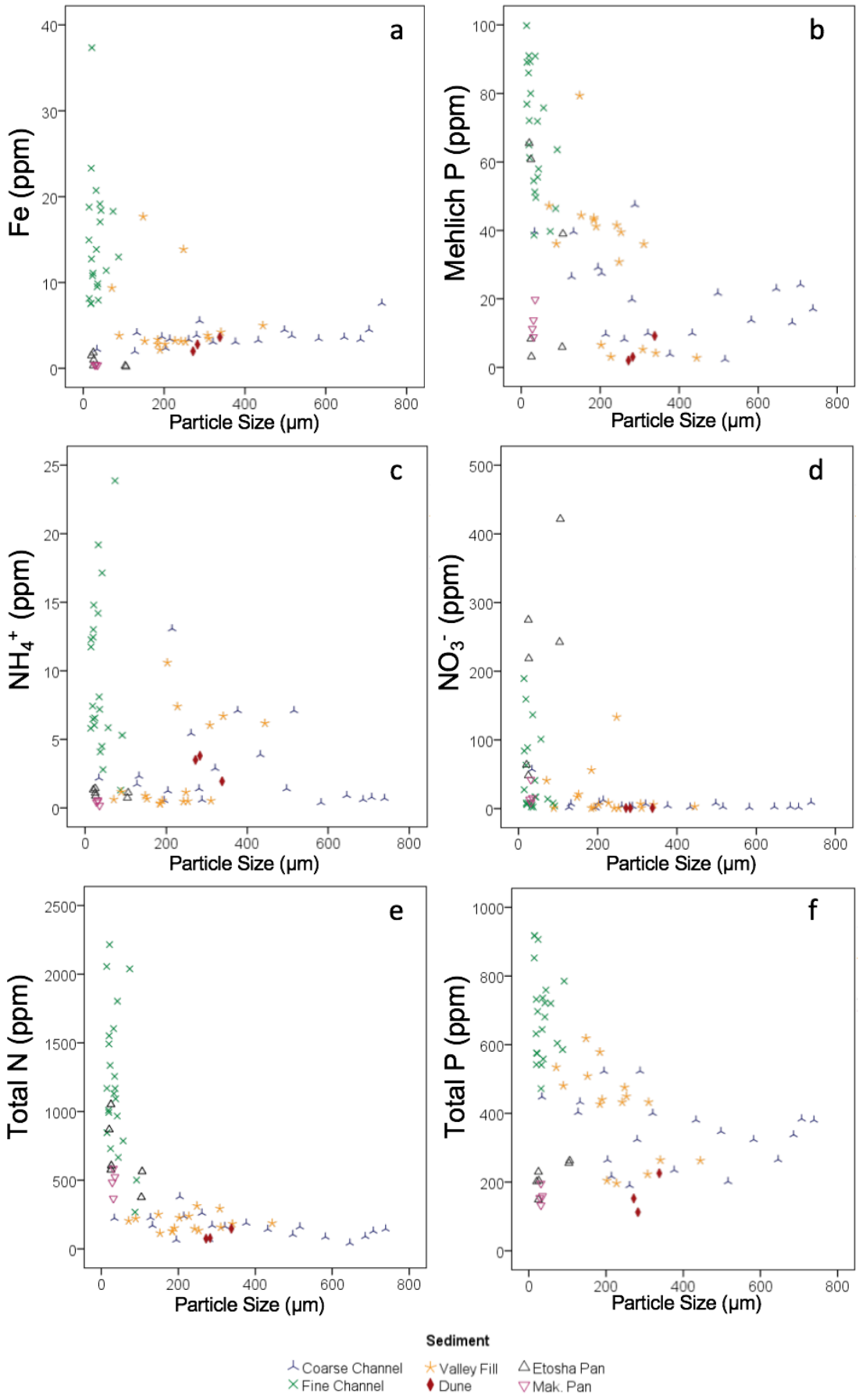

a
Fe (ppm)
Particle Size (µm)
b
Mehlich P (ppm)
Particle Size (µm)
c
NH_4^+ (ppm)
Particle Size (µm)
d
NO_3^- (ppm)
Particle Size (µm)
e
Total N (ppm)
Particle Size (µm)
f
Total P (ppm)
Particle Size (µm)
Sediment
Coarse Channel
Fine Channel
Valley Fill
Dune
Etosha Pan
Mak. Pan

Figure 37 | Grain Size (weighted volume mean) versus nutrients concentration of river valley geomorphological units, Etosha Pan and Makgadikgadi (Sua) Pan samples for (a) bioavailable Fe, (b) bioavailable P, (c) ammonium, (d) nitrate, (e) TN, and (f) TP.

5.4.2.1 Bioavailable iron

The alluvial deposits in both river valleys contained higher levels of bioavailable Fe than in samples of clay pan crust or sub-crust sediment from both Etosha and Makgadikgadi Pans (Figure 36). Bioavailable Fe in the river channel fines were between 15 and 43 times the concentrations found in southern Africa's major dust emitting Pans (Table 9) yet the samples showed a similar grain size distribution (Figure 34). Further, no surface area (grain size):concentration relationship is observed (Figure 37). This suggests that grain size is not the primary determinant of bioavailable Fe availability, see Journet (2008), but that mineralogy and other geomorphological processes or catchment characteristics have a significant influence. As shown in Table 4 the Tsauchab river terminal deposits contained slightly higher levels of bioavailable Fe than the Huab although this was not statistically significant.

Table 9 Mean bioavailable Fe concentrations of ephemeral river channel fine deposits against Etosha and Makgadikgadi Pan deposits

Source (mean ppm)	Etosha (0.85)	Makgadikgadi (0.40)
Huab (12.79)	15	32
Tsauchab (17.57)	20	43

Studies on iron and nutrient content of pre-emission sediment in Etosha and Makgadikgadi Pans are limited. In a previous study ferrous iron (Fe^{2+}) had been found to be higher in the sediment parent material (63µm – 2mm) than fine fraction (<63 µm) (Bhattachan et al., 2015). The same study also showed higher bioavailable Fe in Kalahari dune sediments than either Pans (170-500ppm). The higher bioavailable Fe content of the Kalahari sediments was stated as likely being a result of iron-oxides generated from the weathering of iron rich minerals in the Kalahari sands ((Thomas & Shaw, 1991) in Bhattachan et al. (2015)). This same process would be expected to be occurring in the Namibian river valleys from iron-oxide coated sands (White et al., 1997). Importantly, the bioavailable Fe concentrations are not directly relatable between the two studies. The bioavailable Fe extraction methodology using HCl by Bhattachan et al. (2015) differs from the chelating DTPA extraction used here to extract plant-available Fe. DTPA can chelate Fe^{2+} or Fe^{3+} when it is not physically occluded, this form of Fe makes up a minute fraction of total Fe, approximately 0.02% (Lindsay & Norvell, 1978). Additionally, the parent material was ground using a Pica-Mill Soil grinder for biogeochemical analyses by Bhattachan (2015) which would reduce physical occlusion and expose a larger surface area for chemical digestion.

Noting Fe concentrations cannot be directly compared, insight into importance of the geomorphological processes occurring in the river valleys can be made. The fine channel sediments of the river valleys showed higher levels of bioavailable Fe than the surrounding coarser sediments. This is opposite to what was found by Bhattachan (2015) in the Makgadikgadi, the Kalahari interdunes and two of the four Etosha samples. This suggests that the ephemeral fluvial processes operating on the valley fill and sand deposits play an important role in biological Fe enrichment.

5.4.2.2 Phosphorus

TP and bioavailable P concentrations in valley fill and channel coarse deposits show a linear fit to grain size (Figure 37). Bioavailable P is produced as a result of weathering of geological P sources (Holtan et al., 1988) and shows strong correlation with TP via reduced major axis regression, Figure 38. This suggests that it is weathering of geological material and fluvial transport that is the source of enriched P in the wind-erodible sediments of the river valleys.

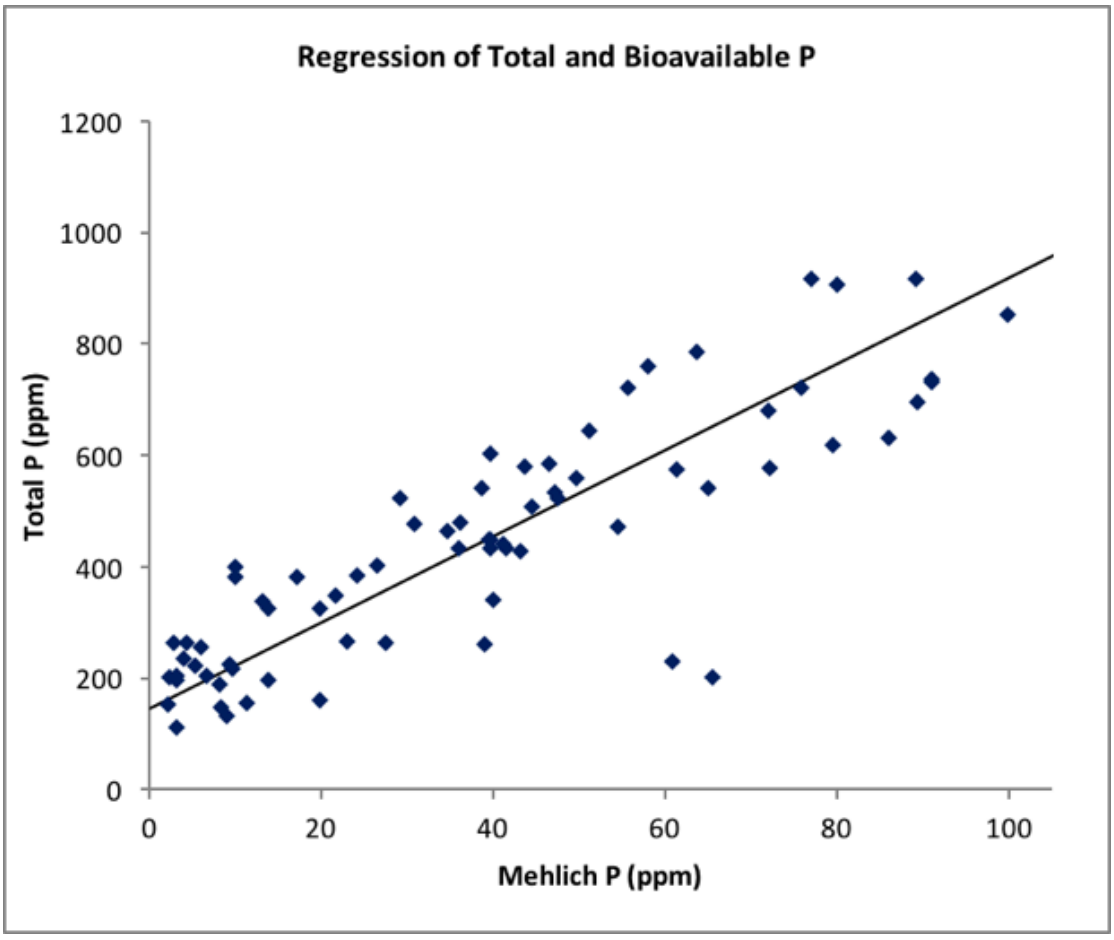


Figure 38 | Reduced Major Axis (RMA) regression analysis of TP and bioavailable P (Mehlich P) for river valley geomorphological unit samples

5.4.2.3 Nitrogen

TN is shown at higher and lower concentrations irrespective of grain size within the geomorphological units of the river valleys (Figure 37). The geomorphological unit appears to be a bigger determinant for nutrient content than the mean particle size. The large biological and ecological component of the nitrogen cycle (Coleman et al., 1983) would suggest that terrestrial and aquatic processes would need to be considered to determine N origins. The smaller watershed, the Tsauchab, has the highest levels of TN and ammonium in fluvial deposits while Etosha Pan had markedly high concentrations of nitrate (Figure 36). Land use for grazing in the smaller Tsauchab and highly dense fauna population of the Etosha National Park that surrounds Etosha Pan could be influencing factors.

River flow does not always reach the river mouths of the Namibian ephemeral rivers (e.g. (Svendsen et al., 2003); (Morin et al., 2009)) which would result in a spatially varied deposition of sediment and nutrient interactions made further complex by large flood events resuspending alluvial deposits. Additionally, there are likely to be biological or environmental limitations of the nitrogen cycle simultaneously occurring in the Namibian Desert (Evans & Belnap, 1999) or being overcome in river channel ecosystems (Johnston et al., 2001).

To understand the complexities of nitrogen fixation, ammonification and nitrification that may be occurring in the different geomorphological units (e.g. Monger & Bestelmeyer (2006)) would require further analysis and collection of upper channel and watershed samples. Here we have shown that fluvial processes in the river valleys play a role in N enrichment of downstream alluvial deposits, although the processes involved appear more complex than the geomorphological accumulation of Fe and P.

5.4.3 Ocean fertilisation

Ocean fertilization is known to be influenced by nutrient inputs delivered by mineral aerosol deposition (Jickells et al., 2014). The bioavailability of these nutrients dictates the amount of nutrients available for phytoplanktonic uptake (Krishnamurthy et al., 2010) and is influenced by the added complexity of atmospheric processing before ocean deposition (Shi et al., 2011). The solubility and bioavailability of Fe in mineral aerosols remains a major uncertainty in the global biogeochemical Fe cycle (Jickells et al., 2005), with concentrations ranging from 2-80% in mineral aerosol studies (Mahowald et al., 2009). Conflicting theories on the relative importance of grain size (Baker et al., 2006) mineralogy of source material (Journet et al., 2008) and iron speciation (Schroth et al., 2009) exist. Irrespective of which plays the most important role, likely a combination of processes, our results show that the Namibian river valleys are a source of bioavailable nutrient-rich sediments, which are of a grain size suitable for wind erosion and atmospheric transport, and are therefore likely to play a role in the fertilisation of the South Atlantic.

5.5 Conclusions

Fluvially deposited sediment in Namibian ephemeral river valleys that emit aeolian dust show significant levels of nutrients considered important for ocean fertilisation, especially bioavailable Fe. These river valleys show a higher fertilization potential than either Etosha or Makgadikgadi Pans which are the other major sources of aeolian dust in the region. The coastal proximity of the aeolian dust source regions in the lower catchments of the ephemeral rivers is also likely to facilitate a high rate of deposition of nutrients into the ocean. Such a proximity would also increase the likelihood of deposition into the oceans of the larger grain size fractions. The findings of this research show the ephemeral

river valleys of Namibia to be a regionally important, perhaps the most important, source of aeolian ocean fertilizing material. Given this finding a re-assessment of the potential role of ephemeral river valleys in providing nutrient rich sediment into the aeolian and marine systems in other dryland areas is necessary.

Acknowledgments

The authors gratefully acknowledge the Clarendon Fund and Oxford University Press for supporting this research and the John Fell Fund for providing partial support of fieldwork activities. We are very thankful to Prof. Kendra McLauchlan at the Department of Geography, Kansas State University and Prof. Kelly Munkittrick at the University of New Brunswick for the provision of funding and resources for laboratory analyses. We thank the Namibian Ministry of Environment and Tourism for all their support and assistance, especially with access to field sites permitted under permit number 1788/2013. This research has been carried out in collaboration with the Natural Environment Research Council grant NE/H021841/1.

CHAPTER 6

Paper Two

SPATIAL VARIABILITY OF OCEAN FERTILISING NUTRIENTS IN THE DUST-EMITTING EPHEMERAL RIVER CATCHMENTS OF NAMIBIA

A. Dansie[1], D.S.G Thomas[1,3,4], G.F.S. Wiggs[1], K.R. Munkittrick[2]

[1] School of Geography and the Environment, University of Oxford, Oxford OX13QY, UK

[2] Canadian Rivers Institute, University of New Brunswick, St. John, New Brunswick, Canada

[3] Geography, Archaeology and Environmental Studies, University of the Witwatersrand, Johannesburg, South Africa

[4] Department of Environmental and Geographical Science, University of Cape Town, Rondebosch, South Africa

Status: Submitted to *Earth Surface Processes and Landforms* on 20 August 2016,

reviewer comments received and currently being addressed.

Abstract

Research into global hot-spots of dust emission has focused on clay pans and exposed paleolacustrine sources of fine, desiccated sediment including Etosha Pan (Namibia) and Makgadikgadi (Botswana). Namibia's western ephemeral river valleys are also known to produce dust but have remained largely overlooked as a regionally significant source. Nutrient enrichment of valley sediments and proximity to the South Atlantic suggests aeolian dust could play an important role in ocean fertilisation. The fertility of valley sediments is dependent on fluvial flow originating in the upper catchments on the Southern African Central Plateau. In this study we investigate climate, geology, vegetation and land use variability and how these may influence the amount of nitrogen, phosphorus and iron in the catchments. We intensely sampled the Huab, Kuiseb and Tsauchab river catchments to map the spatial distribution of nutrients from the upper catchments to the river termini. Results show that the lower valley reaches are sources of aeolian dust enriched in nutrients. Nitrogen levels correlate with precipitation and vegetation levels and phosphorus levels with geology. However, differences in upper catchment sediment nutrient levels were not representative of downstream nutrient differences between valleys. Rather, it is the hydrological and geomorphological processes of the ephemeral river systems that are the key factors producing the enriched sediments in the lower reaches. We propose that the ephemeral river valleys along the coast of Namibia are considered an extensive and enriched source of dust that could play a critical role in marine productivity of the southern Atlantic.

6 Spatial variability of ocean fertilising nutrients in the dust-emitting ephemeral river catchments of Namibia

6.1 Introduction

Terrestrial primary productivity is lowest in the world's deserts and arid lands (Potter et al., 1993; Hadley & Szarek, 1981). This low productivity is principally due to a lack of water (Juhren et al., 1956; Went & Westergaard, 1949), followed by either a nitrogen (N) limitation (Gutierrez & Whitford, 1987; West & Skujins, 1978; Noy-Meir, 1973), phosphorus (P) limitation (Charley & Cowling, 1968), or a combination of both (Vitousek et al., 2010). These same desert regions are, however, the most important sources of mineral aerosols for ocean fertilization (Mahowald et al., 2005; Jickells et al., 2005). Desert dust is known to transport photosynthesis-dependent N and P macronutrients as well as the biologically essential mineral iron (Fe) to phytoplanktonic communities (Okin et al., 2011; Krishnamurthy et al., 2010). Importantly, it is areas of exposed alluvial and lacustrine material within deserts and dryland environments that provide hot spots of dust emission (Jickells et al., 2005; Prospero et al., 2002). Macronutrients and iron concentrated in the wind-erodible sediments of ephemeral river valleys in deserts may therefore provide an important source of fertilising material where aeolian dust is deposited in oceans.

Ephemeral rivers act as conduits of water and fluvially-transported nutrients (Harms & Grimm, 2010; Skoulikidis & Amaxidis, 2009; Laronne, 1993) through deserts and arid landscapes. These support corridors of microbiological activity (Belnap et al., 2005) and increased levels of primary production biomass (Steward et al., 2012). When floodwaters dissipate due to infiltration and evaporation (Dahan et al., 2008; Seely et al., 2003), the sediment and nutrient loads of ephemeral rivers are deposited along valley floodplains

(Reid & Laronne, 1995) and river channels (Abdullatif, 1989; Stear, 1985) and become susceptible to aeolian entrainment and transport. The macronutrients and minerals in these fluvial sediments are representative of the chemical and physical properties of the upstream river and watershed environment (Haddadchi et al., 2013) and sub-catchments (Franz et al., 2013). The biogeochemistry of alluvial sediments can be influenced by: catchment geology (Collins et al., 1998); land use activities including agriculture (Wijdenes et al., 2000) and livestock grazing (Wilkinson et al., 2013); industrial activities (e.g. (Yi et al., 2011; Cheung et al., 2003; Binning & Baird, 2001)), and point-source pollution such as urban sewer or agricultural waste (Ruiz-Fernández et al., 2002). In remote regions, catchment geology and land use are likely to be the primary determinants.

In Namibia, twelve ephemeral river valleys cross the arid to hyperarid Namib Desert east to west (Jacobson et al., 1995), their annual or multi-annual flow events sometimes only lasting a few days (Stanistreet & Stollhofen, 2002). Flow events are a result of precipitation in the upper catchments, located atop the southern African plateau 200-300 km inland (Svendsen et al., 2003). The majority of annual rainfall occurs between January and March (Krapf et al., 2003), though the Namib Desert itself receives virtually zero rainfall due to the cold offshore Benguela Current in the adjacent Southern Atlantic Ocean (Vogel, 1989; Lancaster et al., 1984). As a result, the majority of Namib Desert biota are reliant on fog capture for their water needs (Henschel & Seely, 2008).

The ephemeral river valleys represent rather different environments and habitats compared to the rest of the desert. Infrequent flows provide enough moisture to support corridors of flora and fauna not found elsewhere in the desert (Jacobson et al., 2000; Cowlishaw & Davies, 1997). Flood events are known to deposit nutrient-enriched sediment along the valleys (Morin et al., 2009; Jacobson et al., 2000). Further, the surface

alluvial sediments, which have high N, P and Fe concentrations (Dansie et al., 2016a), have been shown through remote sensing analyses to be major sources of dust plumes over the Southern Atlantic (Vickery et al., 2013; Vickery, 2010).

Dansie et al. (2016a) have shown, that the river valley geomorphological units are neither homogeneous in sediment and nutrient characteristics nor in their susceptibility to deflation. Given that these sediments are a function of channel flows sourced in upper catchments, it is pertinent to suggest that the physical characteristics of the catchments themselves, and the variability within and between them, may play an important role in influencing both the availability of material for subsequent downstream deflation, and the nutrient levels and composition of deflated sediments. Previous studies of nutrient variability in the Namib are limited, but it has been noted that N and P are deficient in Namib Sand Sea sediments (Seely & Louw, 1980), while levels of mineral Fe are highly variable in the same system (White et al., 2007). This can be at least partially explained by location on the region's climatic gradient, due to the role of moisture in mobilizing iron (Walden et al., 2000; White et al., 1997).

The purpose of this paper is to investigate the causes of variability in N, P, and Fe concentrations in the catchments of ephemeral valleys across the regional climatic gradient, and assess how these may influence the fertility of windblown dust that subsequently deposits in the SE Atlantic Ocean. The study was carried out through analysis of the spatial distribution of N, P and Fe from the upper catchments to the termini in three ephemeral river valleys in western Namibia. We further evaluate relationships between N, P and Fe in the sediments of the river catchments that differ in aspects of climate, land use, vegetation and geology.

6.2 Study Sites

6.2.1 Regional Setting

The Namib Desert runs N-S along the western extreme of Namibia, extending for 2,000 km from Angola to South Africa (Heine & Heine, 2002). The ~1000 m high Great Escarpment (Morin et al., 2009) runs parallel to the coast 100-150 km inland, see Figure 39, and serves as the eastern border for the Namib Desert and the beginning of the expansive central plateau of southern Africa (Goudie & Eckardt, 1999). The twelve E-W aligned ephemeral rivers (Table 10) have watersheds ranging in size from 30,100 – 2,200 km^2 with the river channels extending inland for 80 km (Khumib River) to 460 km (Ugab River). Ten of the river systems reach the Atlantic Ocean while the two southern-most channels, the Tsondab and Tsauchab, terminate within the Namib Sand Sea. The W-E precipitation gradient ranges from 0-25 mm average annual rainfall at the coast to over 500 mm at 400 km inland (Jacobsen et al., 1995) (Figure 40a). On the central plateau and highlands above the escarpment, precipitation is sufficient to support the accumulation of thin veneers of colluvium on hillslopes (Bierman & Caffee, 2001) and increased vegetation cover (Okitsu, 2005; Hachfeld et al., 2000), supporting a larger animal grazing density (Ward et al., 2004). This in turn maintains commercial and communal farming areas (Leggett et al., 2003) within upper river catchments (Figure 40b and c. Table 11).

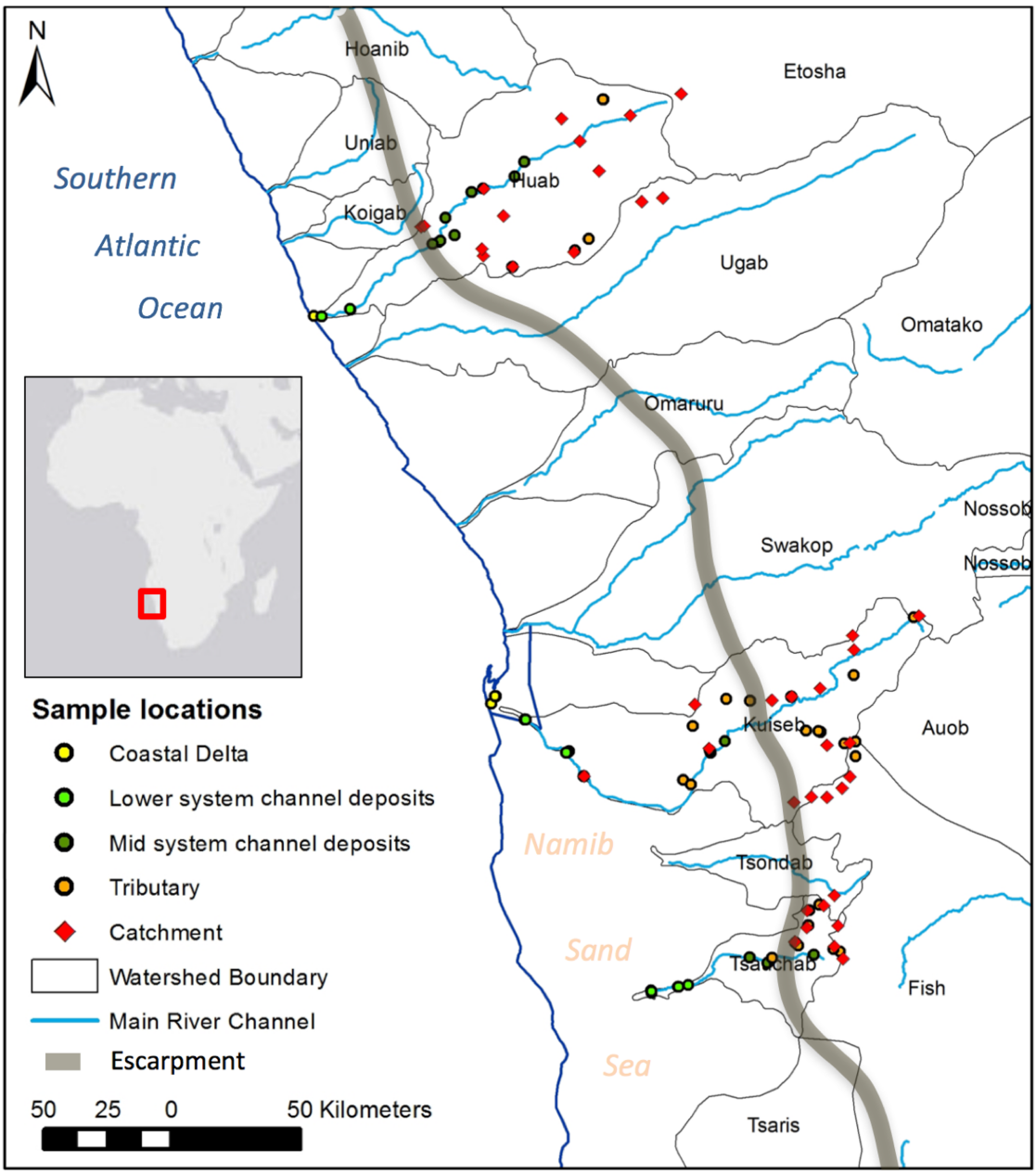


Figure 39 | Ephemeral river watersheds of Namibia and the Great Escarpment with surface sample locations shown in the Huab, Kuiseb and Tsauchab watersheds. Inset map shows location of figure in global context. Map created using GIS data (Project E1 - Atlas of Namibia).

Table 10 Namibia ephemeral river catchment overview (area calculated using Atlas of Namibia (2002) with additional information compiled from Jacobson et al. (1995)).

Watershed	Catchment Area (km^2)	Elevation Range (m)	River Length (km)	Precipitation Range (mm)	Area with rainfall >100mm (%)	Area with Rainfall >300mm (%)	Total Population
Khumib	2,200	0-1542	80	0-25	0	0	<100
Hoarusib	15,100	0-1964	300	0-325	40	8	12,653
Hoanib	17,200	0-1821	270	0-325	72	12	7,866
Uniab	4,500	0-1635	110	0-125	2.3	0	<100
Koigab	2,400	0-1571	130	0-100	2	0	<100
Huab	14,800	0-1597	300	0-345	80	13	14,762
Ugab	28,400	0-1865	450	0-535	85	49	34,460
Omaruru	13,100	0-2082	330	0-375	78	20	11,990
Swakop	30,100	0-2479	460	0-475	80	39	183,120
Kuiseb	15,500	22-2081	420	0-335	52	5	24,935
Tsondab	3,500	640-1927	150	0-205	70	0	411
Tsauchab	4,000	586-1931	150	0-175	60	0	230

Table 11 Catchment land use variability according to land tenure classification (all values given as %; compiled from Jacobson et al. (1995)).

Watershed	Private Farmland	Communal Farmland	Conservation and Tourism Park	Mining
Khumib	0	93	7	
Hoarusib	0	98	2	
Hoanib	3	91	6	
Uniab	0	89	11	
Koigab	0	80	20	
Huab	36	62	2	
Ugab	60	38	2	
Omaruru	46	52	2	
Swakop	89	1	8	2
Kuiseb	63	0	37	
Tsondab	74	0	26	
Tsauchab	78	0	22	

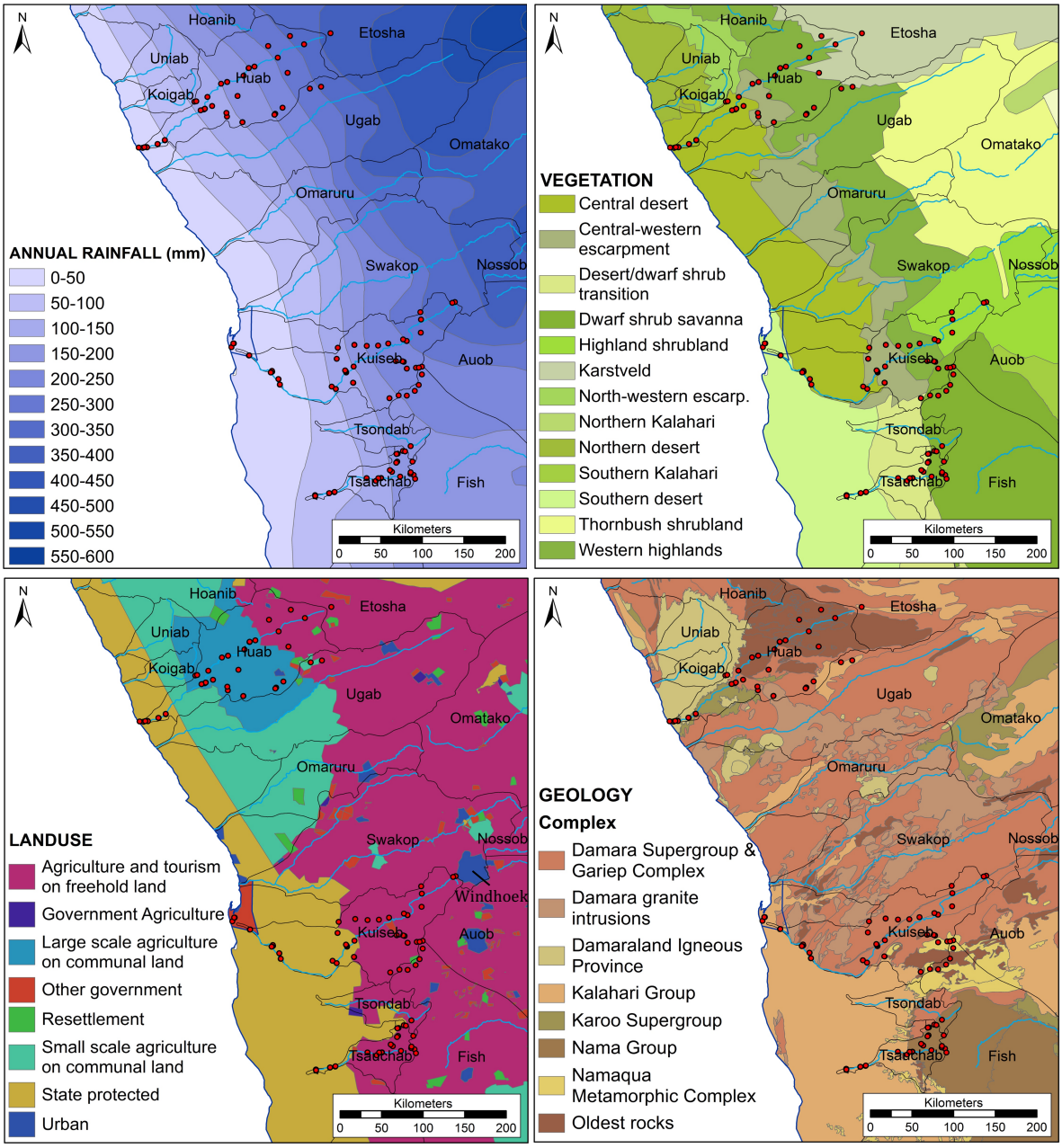


Figure 40 | Sampling locations in the Huab, Kuiseb and Tsauchab catchments in the context of (a) average annual precipitation, (b) vegetation type, (c) land use, and (d) geology. Maps created using GIS data (Project E1 - Atlas of Namibia).

6.3 Research Design

6.3.1 Field Sites

Three valleys that had previously been identified as significant emitters of aeolian dust (Vickery et al., 2013; Vickery, 2010) were investigated. The similarly sized (Table 10) Huab and Kuiseb catchments (14,800 and 15,500 km^2 respectively) and the smaller Tsauchab (4,000 km^2) encapsulate differences in precipitation range, vegetation, geology and land use intensities shown in Figure 40. The Huab and Kuiseb receive similar precipitation along the W-E rainfall gradient, 350 plus mm annually, while the Tsauchab catchment only receives a maximum of into 150-200 mm in the most easterly extent of the catchment (Figure 40a). The Huab and Kuiseb systems both terminate at the Atlantic, while the drier and smaller Tsauchab system terminates in the Namib Sand Sea (Figure 39).

Broadly, the vegetation in the upper catchments above the escarpment comprises sparse woodlands and grasslands associated with arid environments (Burke & Strohbach, 2000; Jacobsen et al., 1995). Although vegetation assemblages in the upper catchments do differ (see Figure 40b) with the drier Tsauchab predominantly supporting dwarf shrub savannah comprised of *Acacia hereroensis*, and *Combretum apiculatum.* The Huab and Kuiseb western highlands (Figure 40b) are dominated by *Acacia reficiens* and *Commiphora* species, before giving way to Mopane-dominated savannah of the Karstveld in the Huab and in the Kuiseb, highland shrubland dominated by the same species as the dwarf shrub savannah of the Tsauchab. Below the escarpment, the southern and central desert vegetation (Figure 40b) are similarly sparse and dominated by lichens outside of the ephemeral river channels that host stands of large trees (Jacobson et al., 1995).

Freehold ownership of agricultural land is common to all three catchments (Figure 40c), with agricultural influences seen in the majority of the Tsauchab and eastern-half of the Kuiseb before reaching the state protected southern and central desert ecosystems. Agriculture in the Huab catchment is undertaken on both freehold and communal land with both forms revolving around livestock husbandry, predominantly cattle (Jacobson et al., 1995). Namibian studies have shown that significant impact on vegetation density and composition can be caused by cattle density in areas surrounding artificial watering points (Katjiua & Ward, 2007). However land use and cattle grazing in the Hoanib catchment was overall found to not influence vegetation abundance, with rainfall being the primary determinant (Leggett et al., 2003b; Leggett et al., 2003). It is not yet known whether any of these factors affect nutrient composition of sediments downstream.

The geology of Namibia contains large, recent deposits of sand and calcretes with the majority of the ephemeral river catchments located atop Damara sequence rocks laid down 850-500 Ma, intermixed with Damara granite intrusions (see Figure 40d) (Jacobsen et al., 1995). The Kuiseb catchment consists almost entirely of such Damaran geology (see Figure 40d). The Huab upper catchment can be seen to prominently consist of granite and gneisses Epupa, Huab and Abbabis Metamorphic Complexes, termed ‘oldest rocks’ (Figure 40d), from 2600-1650 Ma (Atlas of Namibia Project, 2002; Jacobson et al., 1995). In the south, the Tsauchab upper catchment sits over the more recent (570-500 Ma) Cambrian Nama Group (Jacobson et al., 1995) characterised by sandstones, limestones and shales (Atlas of Namibia Project, 2002). Detailed geological descriptions of the catchments can be found in Jerram et al. (1999) and Jacobson et al. (1995).

6.3.2 Sampling strategy

Sampling was undertaken in the three catchments during April - August 2013 to analyse the concentrations of N and P compounds and bioavailable Fe. Surface sediment samples were collected within the modern channels of the lower and mid-catchments and in the minor tributaries and non-riverine terrain of the upper catchments of each river. A description of these lower, mid and upper regions of the hydrological system within the catchments is provided in Table 12. The geomorphological units targeted for sampling within the regions and their classification is further described in Table 12 and shown in Figure 41. The coarse and fine channel deposits targeted in the lower and mid-system were all taken from the modern channel where signs of extant ephemeral flows were noted. Fluvial activity in the main river channels had resulted in a discernible crust of fines being present that was not seen in the tributaries. Sampling targeted this fluvial crust in the lower and mid system where encountered as well as taking an adjacent sample of the underlying sandy river bed. The fine and coarse sample distinctions were retained to allow comparison of the nutrient content between these geomorphological units, both a result of fluvial deposition, but with visibly discernible grain size difference and subsequent relevance for deflation. Lower-system sample locations in the Huab and Tsauchab also included valley fill samples (see Figure 41 inset, see Dansie et al. 2016a for further details) in addition to the coarse and fine channel deposits targeted in all three rivers. Samples of fluvial fines were also taken above the marine high water line in the coastal deltas of the Huab and Kuiseb systems.

Table 12 Sample classifications.

		Description	Geomorphological Sediment Unit Targeted	Sample Classification	
HYDROLOGICAL SYSTEM	Lower	Coastal delta sediment, above tidal zone (Huab and Kuiseb only)	Alluvial fan	Coastal Delta	
		Downstream portion of main river channel extending from channel terminus inland: - Huab: 30 km - Kuiseb: 40km - Tsauchab: 25 km	Coarse channel deposits^	Lower system	coarse channel deposit
			Fine channel deposits+		fine channel deposit
	Mid	Main river channel section at distances from terminus of: - Huab: 90-150 km - Kuiseb: 40-120km - Tsauchab: 60- 90km	Coarse channel deposits^	Mid system	coarse channel deposit
			Fine channel deposits+		fine channel deposit
	Upper	Tributary channels (2-12m channel width) connecting main river channel to river catchment	Fine channel deposits+	Tributary	
		Upper catchment area of non-riverine land	Surface sediment	Upper Catchment	

^ coarse channel deposits comprising unconsolidated and poorly-sorted material.

+ visually-identifiable fine-grained material forming a 2-20 mm crust on top of coarse channel deposits or, in the lower reaches, larger areas (10-100 m^2) of surface clays (hereafter termed clay pads) pads and the terminal clay pans of the Tsauchab.

Upper catchment samples were taken to be representative of the climate gradient, land uses, vegetation and geologies as shown in Figure 40, using spatial data obtained from the Digital Atlas of Namibia (2002), datasets are provided in Table 13.

In total, 167 samples, excluding field duplicates (1 duplicate per 20 samples), were collected. These comprised 41 upper catchment, 36 tributary, 38 mid-system coarse/fine channel deposits, and 44 lower system coarse/fine channel deposits, and 8 coastal delta samples. Data from the analysis of the 44 lower system and 8 coastal delta samples has also been utilized in detail in Dansie et al. (2016a) in conjunction with 16 valley fill samples.

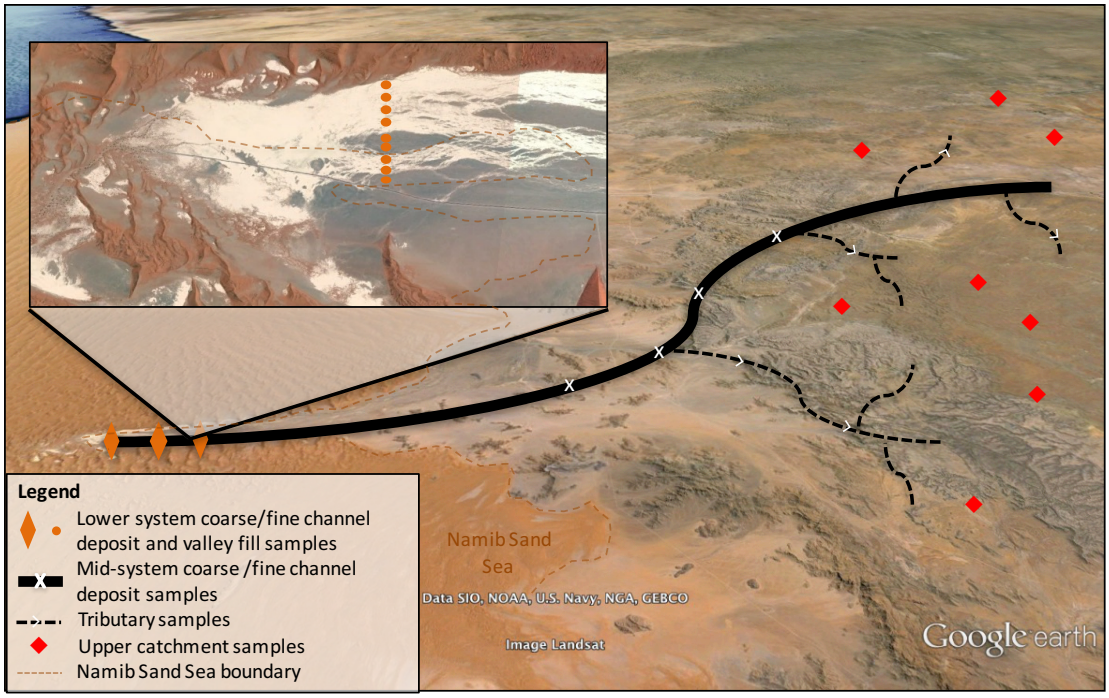


Figure 41 | Overview of hydrological system sampling classification, Tsauchab river valley. Inset shows samples taken through modern channel coarse and fine channel deposits and valley fill.

Table 13 Spatial classifications as defined by the Digital Atlas of Namibia (2002).

Catchment Geographies	Dataset used for spatial classification
East-west climate gradient	Average annual rainfall ($mm.yr^{-1}$)
Land use	Agricultural classifications as defined under 'Land use in Namibia'
	'Densities of Cattle in Namibia', number of animals per km^2
Vegetation	Vegetation assemblage according to 'vegetation type classification
	Average green vegetation biomass (GVB) production
Geology	Geology of Namibia: major geological divisions

6.4 Methods

Samples were collected by trowel to obtain approximately 200 g of loose sediment to a depth of 10 mm. The more consolidated crust of fine channel deposits and clay pad/pan

deposits were removed intact and their thickness measured with a tape measure. Samples were stored in airtight bags and shipped to the UK for analysis.

6.4.1 Chemical Analyses

A 40 g subset of sieved <2 mm samples, including field duplicates[11], were split and sent to the Kansas State University Soil Testing Laboratory where they were dried overnight in a 50°C oven, with the exception of sub-samples for iron analyses which were air-dried. Samples were processed for analyses of Mehlich III Phosphorus; DTPA extraction of bio-available Fe^{2+} and Fe^{3+} (combined) followed by analyses with by Flame Atomic Absorption spectrometry (following method described by Lindsay and Norvell (1978)), inorganic Nitrogen NH_4^+ and NO_3^- extracted with 1M of KCl and analysis in a flow analyser; total nitrogen and total phosphorus using a modified Kjeldahl digestion followed by analyses in separate colorimetric reactions using a flow analyser; and soil pH using a 1:1 mixture of soil and DI water. Methods for analysis were taken from (Brown, 1998) unless otherwise stated.

6.4.2 Grain Size

Grain size analyses was undertaken using a Malvern Mastersizer Hydro 2000MU to determine sample particle size ranges and to identify the proportion of fine material that might be susceptible to aeolian erosion. Wet-dispersion grain size analysis was conducted in order to disaggregate peds and pellets to their parent sediment sizes. 3-5 g of sample was processed for salt and carbonate removal as described in Soukup et al. (2008). Oven-dried (40°C) samples were then ground using a mortar and pestle and riffled to a range of

[11] Chemical analysis of field duplicates showed variation was within standard deviation for all nutrient analyses with the exception of ammonium. All field duplicate samples had very low levels of ammonium (0.5 – 6.6 ppm), producing variations between field duplicates greater than the standard deviation of all samples (7.8). The results are considered suitable for interpretation. Further laboratory duplicate analysis conducted by Kansas State University confirmed reliability of results produced.

weights from 0.011 g to 4.2 g and suspended in a 1:1 solution of 50 g/L sodium hexametaphosphate and DI water. Samples were placed on a linear shaker and shaken for 4 hr at a rate of 250 rpm then left to stand overnight. Samples were analysed using standard Mastersizer procedures, taking three measurements per sample to allow calculation of an average value. Cleaning runs using deionised water were undertaken between each sample.

6.5 Results

6.5.1 Nutrient concentrations along the hydrological system

A general trend of increasing nutrient content in the fine channel deposits occurs from upper to lower parts of all three catchments (Figure 42). TP increases clearly down the hydrological systems, with a minimum doubling of concentrations compared to catchment values. TN shows a similar trend, with concentrations in the channel systems up to five times greater (in the Kuiseb, Figure 42c) than in the catchments.

In the Huab, nutrient concentrations are shown (Figure 42a and b) to increase in mid-system locations more-so than in the lower system for all non-phosphorus based nutrients. In contrast to the other two valleys, the Huab passes through a topographic constriction, 85 km upstream from the mouth. A consequence of this is that fluvially-deposited sediments are extensive upstream of the topographically-controlled constriction; it is hypothesised that this acts as a barrier to flow, causing ponding and sediment deposition during flow events. The lower Mehlich P and TP concentrations seen in the Tsauchab lower system fine channel deposits compared to the Huab and Kuiseb (Figure 42) could be expected in a smaller watershed where the P cycle is dominated by geological weathering rather than land use.

The coastal deltas of the Huab and Kuiseb show lower concentrations of nutrients than the fine channel deposits in the lower and mid-systems. This may be due to a damper environment because of the influence of seawater spray and inundation by storm surges, higher soil moisture contents close to groundwater, and less-frequent flood replenishment from only the largest river flows.

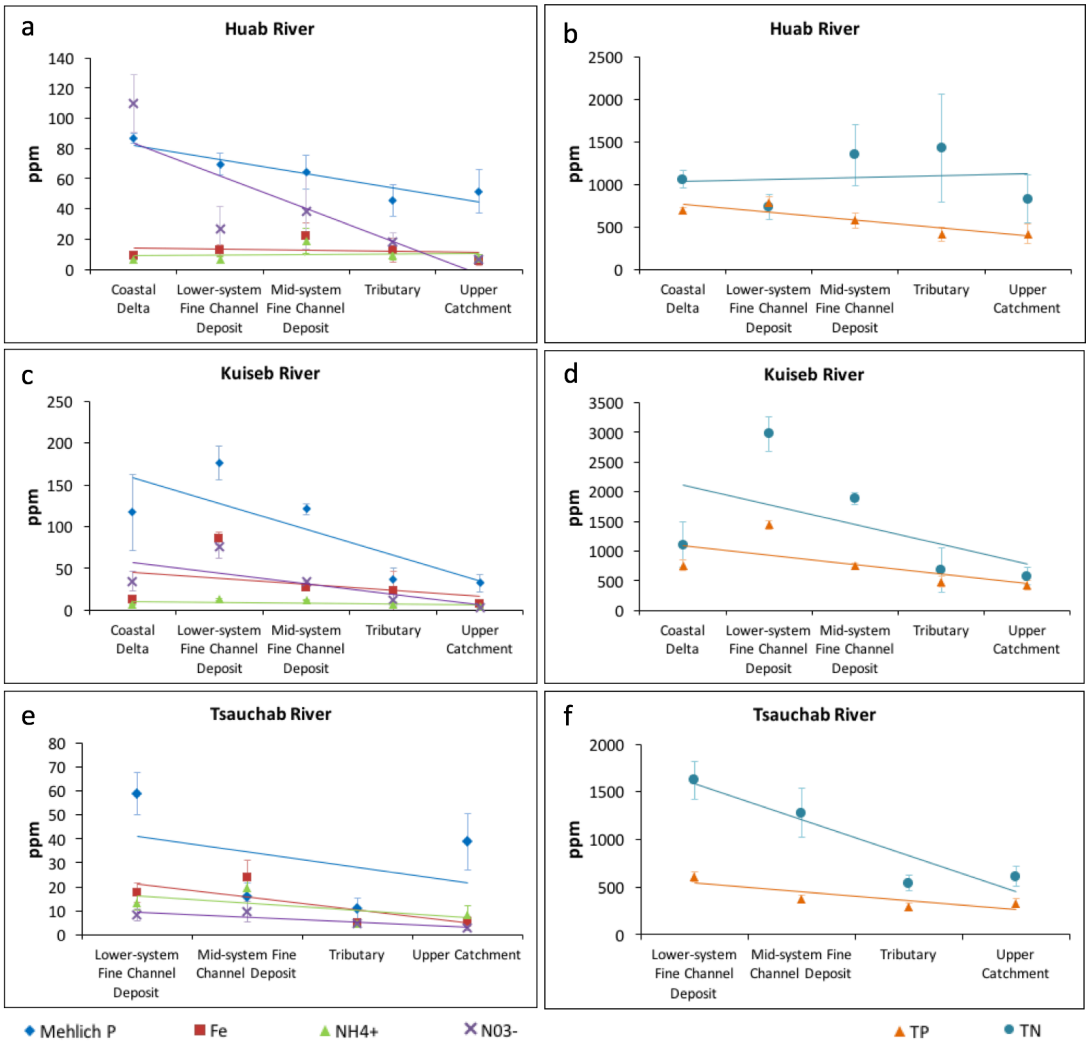


Figure 42 | Mean nutrient content of in-channel deposited fine material along the hydrological sections of the (a, b) Huab, (c, d) Kuiseb and (e, f) Tsauchab rivers, trend line for each nutrient shown with error bars showing standard deviation of calculated means.

Enrichment ratios for the lower-system fine channel deposits against the other sampling classifications (Table 12) were calculated according to Wan and El-Swaify (1998) for

each of the studies river systems (Figure 43). Nutrient enrichment is clearly increasing as the lower-system fine channel deposits are compared further upstream against mid-system fine channel deposits, the tributaries and ultimately the upper catchments. Of particular note is the increasing bioavailable Fe concentration in fluvial sediment down the river channels, being present in concentrations between 3.5 to 7 times the values in the upper catchments of the three rivers. Mehlich P in the Tsauchab (Figure 43c) is the only nutrient not to demonstrate downstream enrichment compared to catchment samples.

Nutrient enrichment is therefore shown to occur in the fine channel deposits down the hydrological system of the river valleys. In comparison, the mean nutrient concentrations of the coarse channel deposits compared to their respective catchments are shown in Figure 44. Bioavailable P (Mehlich P) and TN and concentrations are between 2 to 4 and up to 8 times greater in the upper catchment compared to lower system coarse channel deposits, respectively. The remaining bioavailable nutrients (Figure 44a, c, e) and TP (Figure 44b, d, f) are also shown to be found in higher or similar concentrations to the lower system coarse channel deposits. Data therefore suggest that nutrients are being transported downstream in an enriched fine fraction of fluvial sediments, and not in the coarse sediment load.

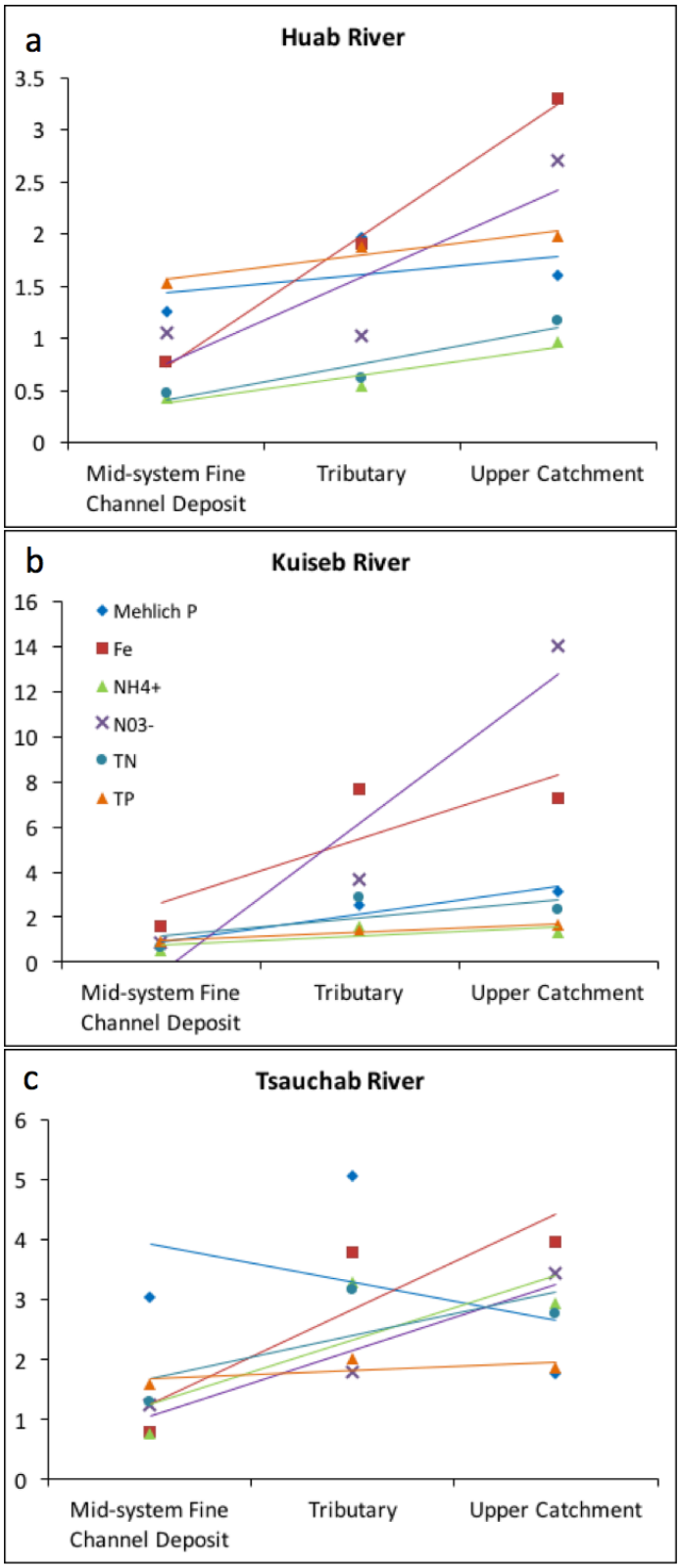


Figure 43 | Nutrient enrichment ratios of median nutrient content in the lower-system fine channel deposits against mid-system fine channel deposits, tributary and upper catchment samples in the (a) Huab, (b) Kuiseb and (c) Tsauchab rivers.

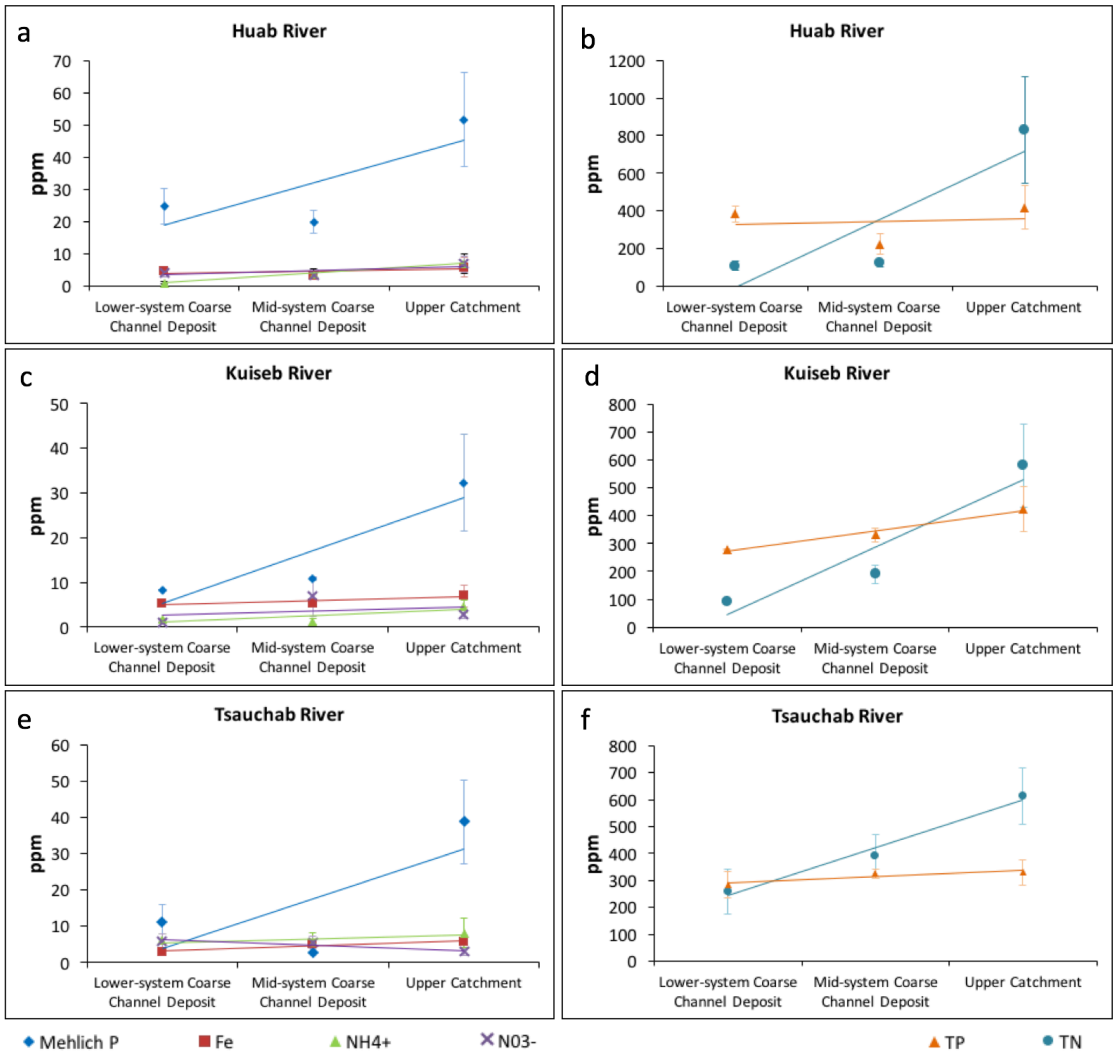


Figure 44 | Nutrient content of in-channel deposited coarse material along the (a, b) Huab, (c, d) Kuiseb and (e, f) Tsauchab rivers and their catchments, trend line for each nutrient shown with error bars showing standard deviation of calculated means.

6.5.2 Spatial distribution of nutrients across the upper catchments

Upper catchment and tributary samples were used to explore potential relationships between nutrient levels in valley sediments and the upper catchment characteristics of rainfall, geology, vegetation and land use (Table 13). Only those that demonstrated a significant relationship or notable trends are presented here. Significance was calculated

using ANOVA for the categorical variables of geology and vegetation type and using median regression analysis for the linearly-increasing rainfall and cattle density data.

Across the W-E climate gradient, the mean TN and ammonium concentrations showed a positive trend of increasing concentrations with precipitation (Figure 45a and c). Regression analysis of median values showed this relationship was only significant for TN (TN $p = 0.001$, ammonium $p = 0.725$). In contrast mean nitrate concentrations show a strong inverse relationship with rainfall (Figure 45d). Where mean precipitation exceeded 100-150 mm, mean nitrate values all fall between 3.8-8.4 ppm. In the driest areas (0-50 mm mean rainfall) the highest nitrate levels occur in the Kuiseb tributaries that drain the gravel plain of the Central Desert (mean = 165 ppm; Figure 40b) and nitrate levels are therefore likely associated with sediment geomorphology of the gravel plains rather than rainfall. TP levels show greater variance within mean precipitation ranges (Figure 45b), with no distinct trend.

As shown in Figure 46, catchment geology also has an influence on nutrient concentrations. The highest levels of bioavailable P and TP are associated with Damara igneous lithologies, with high levels of bioavailable P also associated with older units of Khoabendus and Haib groups of undifferentiated Precambrian metamorphic complexes (termed ‘oldest rocks’, Figure 46). However, only TP shows a significant relationship ($p = 0.018$). While not statistically significant, the elevated bioavailable P ($p = 0.096$), produced from the weathering of mineral phosphorus in rocks, could be explained by increased weathering and accumulation over the older lithologies. This assumes rock is exposed and available for weathering, as is commonplace across western Namibia (see photographs of catchments throughout Jacobson (1995)) in contrast to P-depleted old soils where no replenishing process is available (Walker & Syers, 1976). Bioavailable Fe

shows no lithology-driven trends (p = 0.463) and iron contribution to fluvial sediments is therefore expected to occur ubiquitously from all upper catchment geological regions.

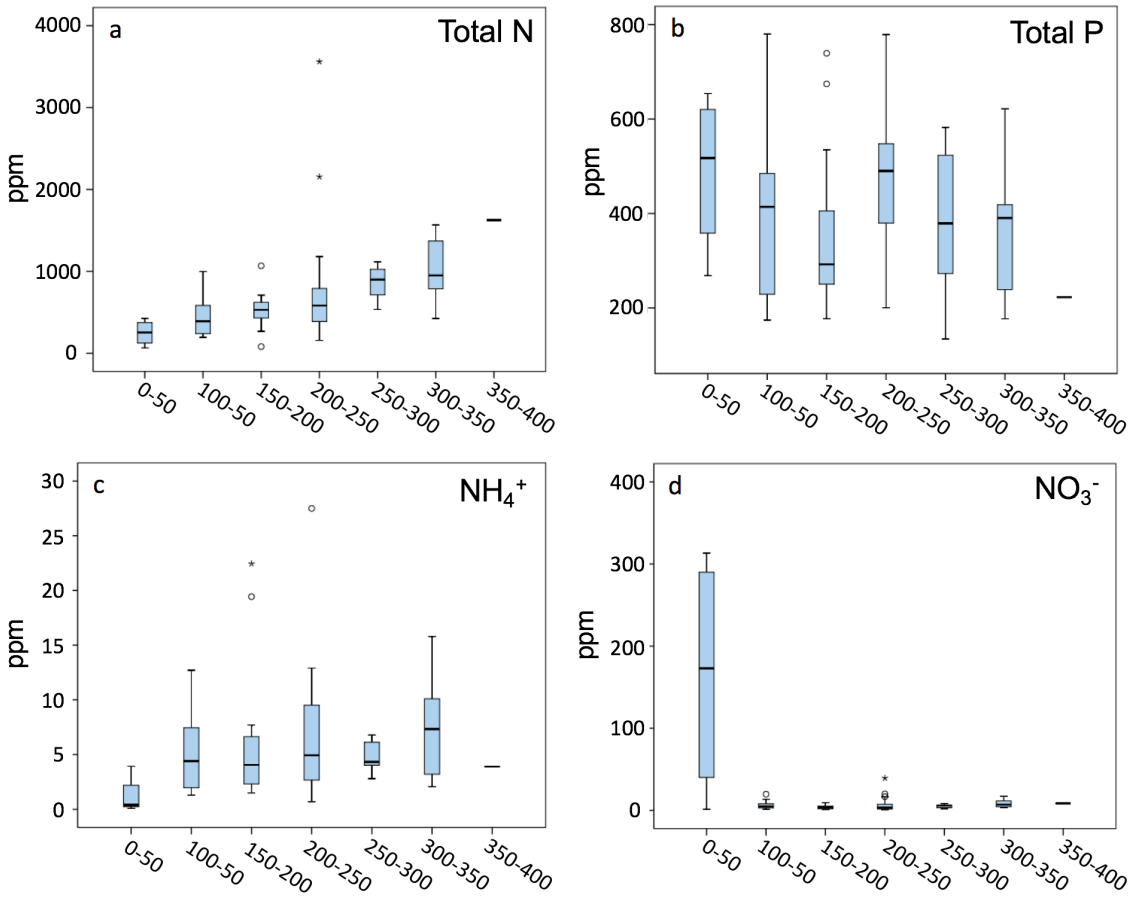


Figure 45 | Average annual rainfall (mm.yr^{-1}) and (a) TN, (b) TP, (c) ammonium and (d) nitrate concentrations in upper catchment and tributary samples across the Huab, Kuiseb and Tsauchab river valleys. Inset (e) shows the total area (km^2) of each river catchment according to rainfall zone.

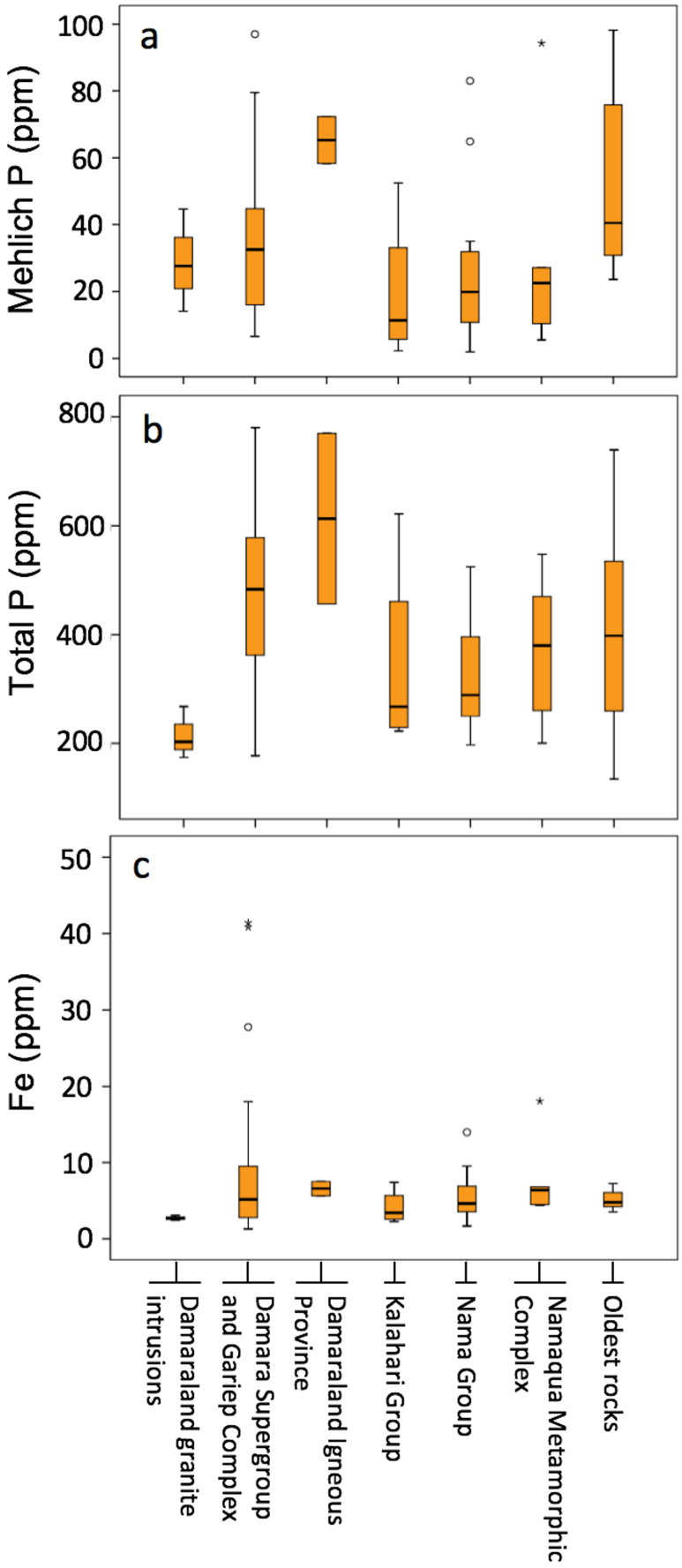


Figure 46 | (a) Bioavailable P, (b) TP, and (c) bioavailable Fe and concentrations in the upper catchment and tributary samples across the Huab, Kuiseb and Tsauchab river valleys according to geological complex.

In terms of vegetation types across the upper catchments, the highest mean levels of TN are associated with the Karstveld, highland shrubland and western highlands ($p = 0.017$) (Figure 47a). These vegetation assemblages are found in the east and north-east regions of the study area (Figure 40b) which also experience the highest annual rainfall (Figure 40a). TP had a strongly significant relationship ($p = 0.001$) with vegetation type classifications and Mehlich P showed a weaker correlation ($p = 0.051$). Phosphorus levels (Figure 47b and c) decrease as vegetation density and complexity increases. The vegetation-bare central desert contains the highest P concentrations which then decrease up and over the increasingly vegetated escarpment. This could suggest that rock-derived P is accumulating in sediments below the escarpment where the aridity prevents full vegetative uptake of P. It is noted that the western highlands sample locations also fall within the oldest rocks lithology (Figure 40b and d) which may explain the increased P levels (Figure 47b and c) compared to other plateau vegetation types. No other nutrient showed any significance against vegetation type.

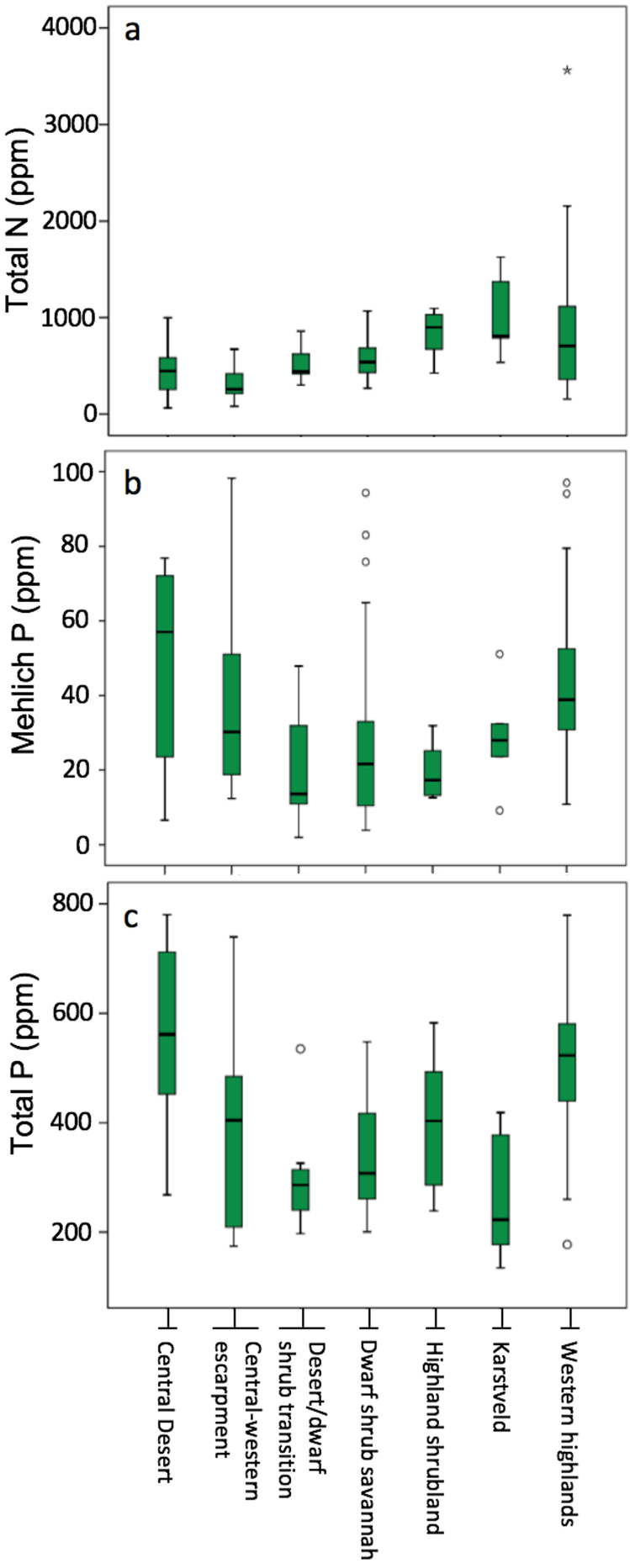


Figure 47 | (a) Total N, (b) bioavailable P (b), and (c) total P concentrations in catchment and tributary samples across the Huab, Kuiseb and Tsauchab river valleys according to vegetation type.

Agricultural and non-agricultural land use classifications (Figure 40c) did not show any clear relationships to nutrient levels. Cattle stocking density data were used as an indicator of land use intensity (Figure 48) and showed increasing TN as animal intensity increased from 1-8 animals per km^2, with a significant correlation (TN $p = 0.031$ versus $p = 0.305$ for NH_4^+), Figure 48a. However, the nitrogen compounds that would increase as direct result of cattle intensity (NH_4^+ and NO_3^- products in animal waste) do not support increasing TN levels as a result of cattle densities. While ammonium concentrations showed a similar trend to TN (Figure 48b), there was no significant relationship ($p = 0.305$). Nitrate can be seen to not alter in association with cattle density (Figure 48c, $p = 0.46$). Levels of phosphorus that would also be expected in association with animal waste showed no relationship with increased animal density (TP $p = 0.571$, Mehlich P $p = 0.145$). The results suggest that the N and P cycles of the upper catchments are not measurably altered by cattle density. The stocking densities themselves are low, a reflection of the aridity of the grazing lands. No major difference in stocking densities exist between communal and freehold agricultural lands (Figure 40c), as both land users sustain their cattle herds over large grazing areas, whether they be fenced or unfenced (Sweet, 1998).

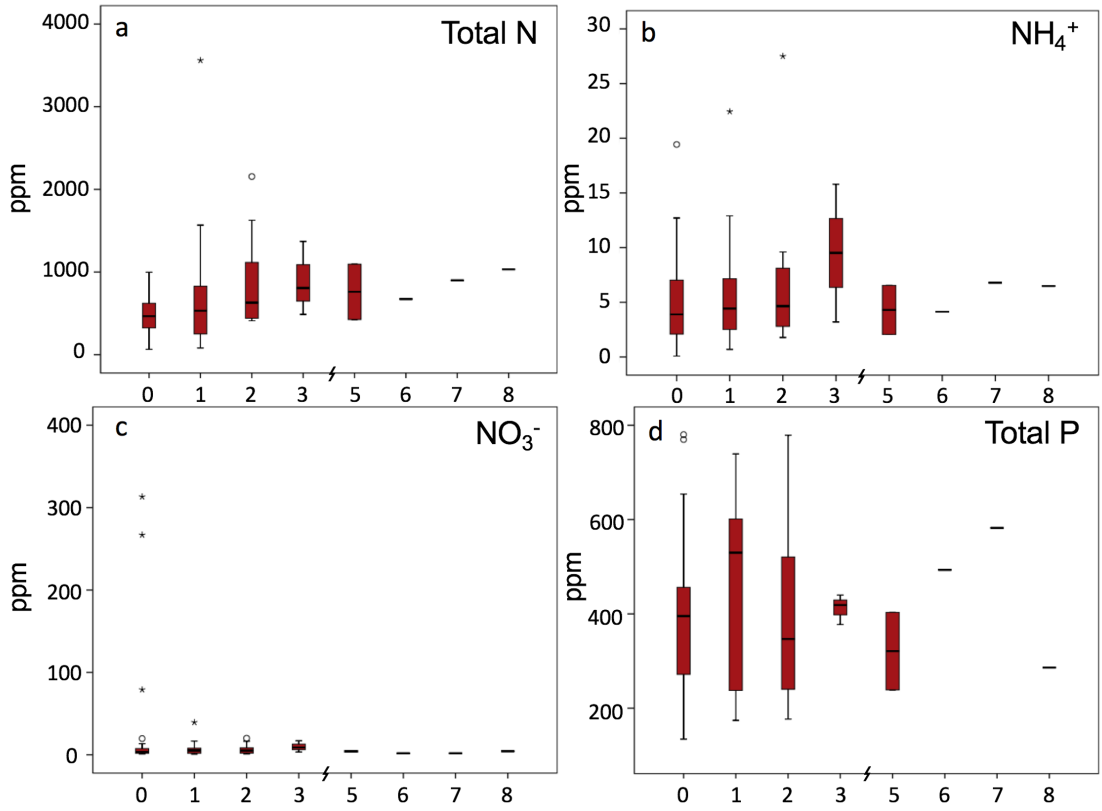


Figure 48 | Cattle density (number of animals per km^2) and (a) total N, (b) ammonium, (c) nitrate and (d) total P concentrations in catchment and tributary samples across the Huab, Kuiseb and Tsauchab river valleys.

6.6 Discussion

6.6.1 Nutrients and sedimentary units

The analysis of samples in the Huab and Tsauchab systems (See also Dansie et al., 2016a) reveals additional relationships between nutrient levels and different sedimentary units within these dryland channel systems (Figures 49 and 50). Compared to coarser valley fill deposits, the highest concentrations of nutrients occur within the finer grained sedimentary units in either lower channel reaches or in surface accumulations in the middle reaches of the Huab. The middle reaches of the Huab comprise distinct channels incised within the valley fill. Ephemeral flow events supply suspended sediment, derived from the upper catchments, as well as material reworked from existing fluvial (valley fill)

deposits. When flow events subside, suspended sediment accumulates in surface locations, concentrating nutrient levels compared to the more-mixed grain size valley fill deposits. It is this fine surface sediment, derived from the upper catchment and from fill-reworking, as well as the unconsolidated fine fraction of the valley fill that are exposed to wind erosion and saltation impacts that cause deflation (Wiggs & Holmes, 2011; Shao et al., 1993), resulting in recorded dust plumes emanating from the river valleys (Vickery et al., 2013; Vickery, 2010).

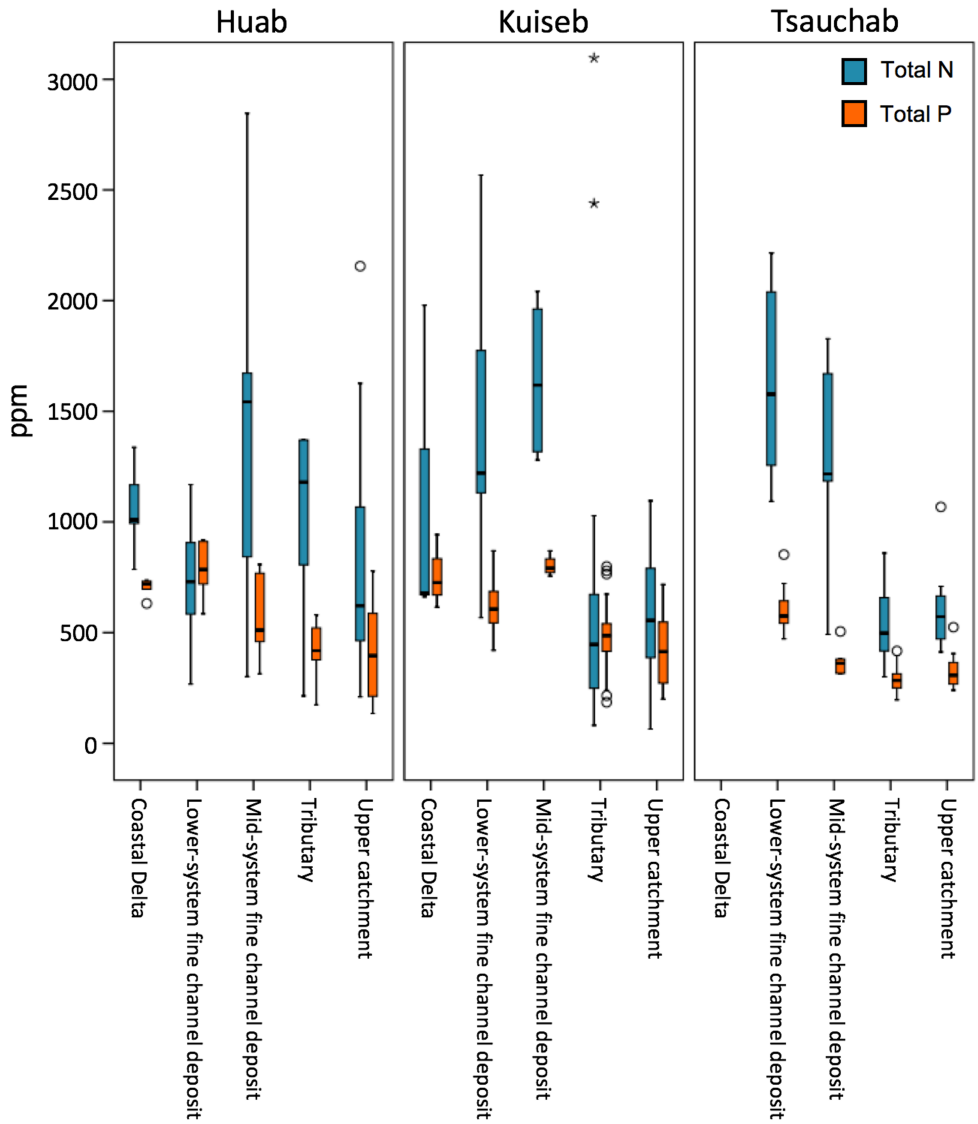


Figure 49 | TN and TP concentrations of sediment along the hydrological sections and including the valley fill geomorphological unit in the lower-systems of the Huab and Tsauchab river valleys.

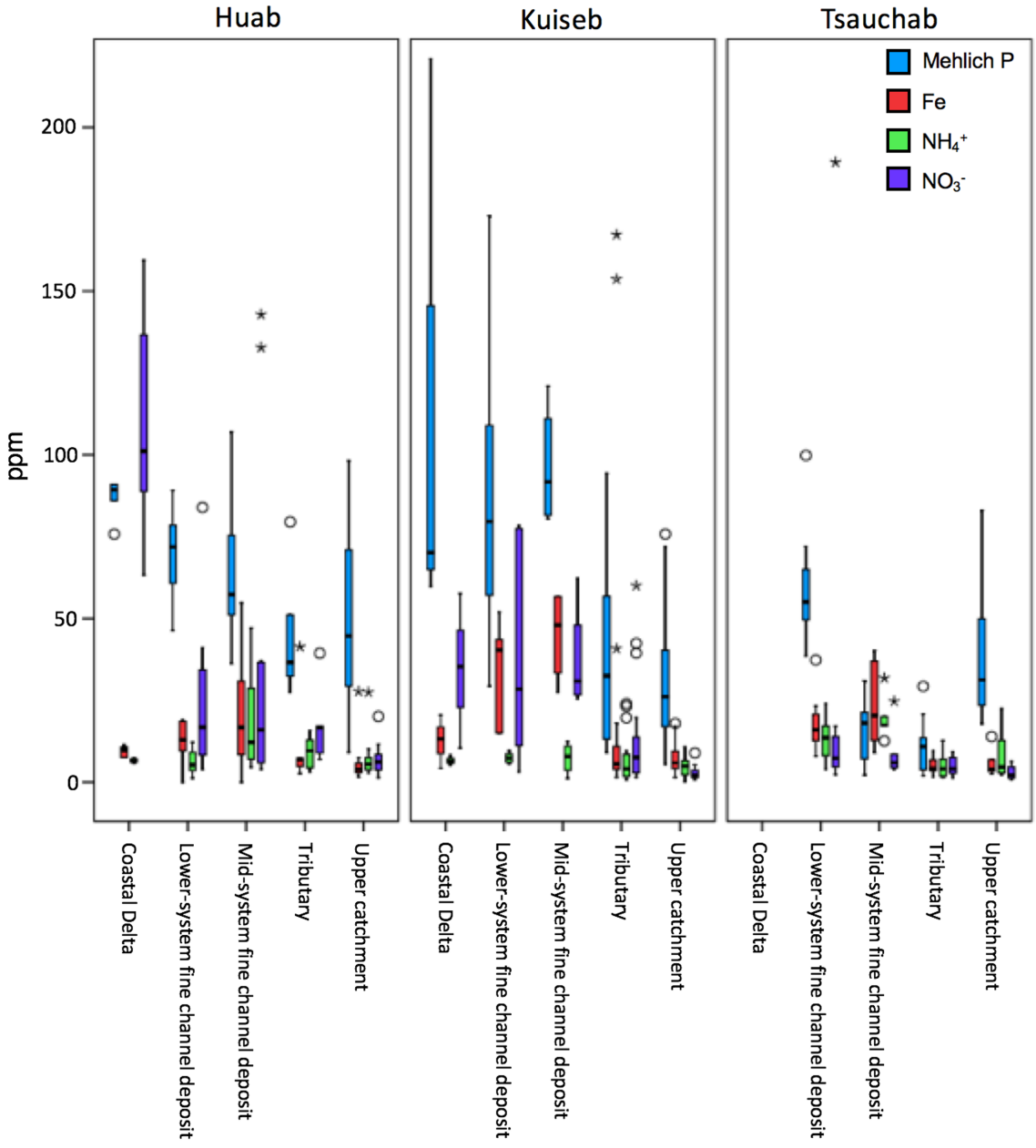


Figure 50 | Bioavailable P, Fe, ammonium and nitrate concentrations of sediment along the hydrological sections and including the valley fill geomorphological unit in the lower-systems of the Huab and Tsauchab river valleys

6.6.2 Catchment-wide controls on nutrient patterns

The mean nutrient levels across the upper catchments of the three systems are summarised in Figures 49 and 50, showing broadly similar TP and TN and bioavailable nutrients. The greatest variability in nutrient concentrations is seen in the largest upper catchment, the Huab, and the least variability in the smallest catchment, the Tsauchab. Our results suggest that the N cycle is dominated by rainfall (Figure 45) and, most likely in association, vegetation (Figure 47). The P cycle appears to be dictated by geology (Figure 46) and supported by extant weathering processes in the upper catchments. Phosphorus levels would therefore seem to be influenced by natural processes and not impacted by anthropogenic activities that can alter the P-cycle (Filippelli, 2008). Land use was not a discernible identifier of any nutrients, with the increased TN levels associated with cattle density explained by higher rainfalls and subsequent increased biomass dictating higher carrying capacities for cattle. This is supported by the first-order vegetation determinant of rainfall seen in the Hoanib (Leggett et al., 2003).

Nutrient enrichment of fine channel deposits is occurring down the hydrological systems of each river (Figure 43). This extends to the lower system sediments of the Kuiseb and Tsauchab, but the highest concentrations in the Huab occur in the middle reaches of the system due to topographical factors affecting channel behaviour. Although the Tsauchab has a particularly small catchment, this clearly does not inhibit the development of zones of higher nutrient concentrations in fluvial sediments (TN, Figure 50). This may indicate that biological production and processes play an important role in the nitrogen cycle in this desert system, as proposed by Jacobson et al. (2000) in the Namibian ephemeral rivers and as has been seen in other desert landscapes (Zhang & Zak, 1998; Gallardo & Schlesinger, 1992). It is noted that many uncertainties remain, as the N cycle in arid environments is complex, down to the N-transforming gene expression in soil microbial

communities that is dependent on a range of environmental conditions (Kidron et al., 2015).

A key finding is that bioavailable Fe content is enriched in the lower-system fine channel deposits, which are known to emit dust (Vickery et al., 2013). Most importantly, this increase in bioavailable Fe was seen across all river valleys and could not be specifically correlated with any geological (Figure 46), or other, catchment characteristic. This would suggest that the extant fluvial processes in the ephemeral river valleys are serving to accumulate bioavailable Fe from iron-containing minerals and iron oxide-coated quartz grains (White et al., 2007), and from rock erosion and sediment production across the catchment (Bierman & Caffee, 2001). The river channels below the escarpment have been shown to contain nutrient-enriched sediments, associated with their hydrological flows (Jacobson & Jacobson, 2013), in comparison to the surrounding desert and that these are essential to primary and secondary production in the terrestrial riverine ecosystems (Jacobson et al., 2000). It is now apparent that the fluvial transport and geomorphological processes of the ephemeral river valleys serve to support and replenish a nutrient-enriched deposit of fine sediments in the dust emitting lower reaches of the river valleys. It is therefore highly feasible that these sediments provide source of nutrient-enriched mineral aerosols that could fertilise the adjacent South Atlantic.

6.7 Conclusions

We have shown that fluvial systems in the dust-emitting regions of the ephemeral river valleys of Namibia contain sediments that are enriched compared to their upper catchments. Most importantly, bioavailable Fe was found at the highest concentrations in these regions. Downstream enrichment occurred irrespective of the upper catchment climate gradient, geology, vegetation and land use investigated. This would suggest that

similar enrichment processes of bioavailable Fe might be found in the remaining nine ephemeral river valleys of Namibia. In the upper catchments nitrogen was seen to correlate with the climatic gradient and terrestrial productivity while phosphorus appears to be predominantly of geological origin, with no land use alterations detected in this study. Crucially, identification of the enrichment in all three river valley fluvial deposits, irrespective of upper catchment climate gradient, vegetation, land use or geology, would suggest a similar finding for the remaining nine ephemeral river valleys. Generation of downstream fluvial fines, enriched in bioavailable Fe and P and N-based macronutrients would evoke consideration of the coastal ephemeral river valleys of Namibia as a significant emission source of nutrient-rich dust important for ocean fertilisation.

Acknowledgments

The authors gratefully acknowledge the support by the Clarendon Fund and Oxford University Press for this research and the John Fell Fund for providing partial support of fieldwork activities. We are very thankful to Prof. Kendra McLauchlan at the Department of Geography, Kansas State University for the assistance in undertaking the laboratory analyses and for feedback on the draft manuscript. We thank the Namibian Ministry of Environment and Tourism for all their support and assistance, especially with access to field sites permitted under permit number 1788/2013. This research has been carried out in collaboration with the Natural Environment Research Council grant NE/H021841/1.

CHAPTER 7

Paper Three

MEASUREMENTS OF WINDBLOWN DUST CHARACTERISTICS AND OCEAN FERTILIZATION POTENTIAL: THE EPHEMERAL RIVER VALLEYS OF NAMIBIA

A. Dansie[1], G.F.S. Wiggs[1], D.S.G Thomas[1,2,3]

[1] School of Geography and the Environment, University of Oxford, Oxford OX13QY, UK

[2] Geography, Archaeology and Environmental Studies, University of the Witwatersrand, Johannesburg, South Africa

[3] Department of Environmental and Geographical Science, University of Cape Town, Rondebosch, South Africa

Status: Submitted to *Aeolian Research* on 07 January 2017, under review at time of thesis submission

Abstract

Delivery of nutrients to the ocean by mineral aerosol deposition involves complex biogeochemical interactions that include atmospheric processing, dissolution and biotic uptake of available nutrients in the surface waters. Research into the fertilization potential of aeolian dust is currently constrained by a lack of understanding of the nutrient composition and bioavailability in dust source areas. Further, research into hot-spots of dust emission has largely focused on paleo-lacustrine sources and pans, to the detriment of other potential sources such as ephemeral river valleys in desert regions. Here, we investigate the sediment characteristics and nutrient content of windblown and surface sediments of a largely overlooked southern African dust source, Namibia's ephemeral river valleys. We deployed monitoring equipment in three river valleys to capture deflated sediments and monitor airborne dust concentration and meteorological conditions throughout an annual dust season. Our results show that the bioavailable nutrient-enriched sediments of the river valleys are an important source of windblown dust transported over the southern Atlantic Ocean. The terrestrial source sediment and windblown dust contain a significantly higher content of bioavailable nutrients than either of southern Africa's major dry lake bed dust sources, Etosha Pan and Makgadikgadi Pan. Further, the source areas in the ephemeral river valleys are adjacent to the southern Atlantic waters, unlike those of the distant dry lake bed sources, and so are likely to input a considerable quantity of nutrients into the ocean. We find that the deflated sediments from the ephemeral river valleys are highly suited to long-range atmospheric transport and so are likely to play an important role in the fertilization of marine waters. This work builds on previous findings demonstrating that the ephemeral river valleys of Namibia are regionally important sources of dust with enhanced ocean fertilisation potential compared to other southern African dust sources.

7 Measurements of windblown dust characteristics and ocean fertilization potential: the ephemeral river valleys of Namibia

7.1 Introduction

Airborne mineral dust, with particles <100 μm diameter (Ginoux et al., 2004; Maring et al., 2003; Tegen & Lacis, 1996), is a critical component of Earth System behaviour affecting atmospheric, oceanic and terrestrial processes. Presently dry or seasonally inundated lacustrine systems in drylands are widely identified as key sources of global dust (Jickells et al., 2005). These sources include both Quaternary lake basins, such as the Bodélé Depression, Chad (Washington et al., 2009; Todd et al., 2007); Makgadikgadi Pans in Botswana (Bryant et al., 2007), Etosha Pan in Namibia (Prospero et al., 2002), and Lake Eyre in Australia (McTainsh & Strong, 2007), and basins desiccated in the twentieth century by human activity such as the Aral Sea (Singer et al., 2003) and Owens Lake (Reid et al., 1994)). Ephemeral dryland valleys in a range of global contexts have also been identified as important dust sources, including in Alaska (Muhs et al., 2016; Brungard et al., 2015), Antarctica (Bhattachan et al., 2015), Iraq, Kuwait, the UAE (Jish Prakash et al., 2015) and Namibia (Vickery et al., 2013).

Once airborne, mineral aerosols can travel considerable distances, with deposition occurring in oceans and over landmasses far from source. These dryland-sourced mineral aerosols have been estimated to account for 95% of atmospheric iron (Fe) (Mahowald et al., 2009) and 82% of atmospheric phosphorus (P) (Mahowald et al., 2008). This flux of nutrients from source to sink can have significant biological and ecological impacts. It has been proposed, for example, that the Amazon rainforest is dependent on phosphorus derived from mineral aerosols emanating from the Sahara (Swap et al., 1992), and that

primary production in nutrient-limited regions of the open oceans derives Fe, P and N from dust inputs (Jickells & Moore, 2015). While uncertainties remain as to the precise biogeochemical roles of Fe, P and N across the global spectrum of marine sinks (Achterberg, 2014), the overall nutrient loading of dust is widely recognised as essential to marine productivity (Bouwman et al., 2013; Zehr & Kudela, 2011; Mahowald et al., 2008), and especially so in high nutrient, low chlorophyll (HNLC) zones (Jickells et al., 2014). The waters of large upwelling systems, biogeochemically-similar to HNLC zones, such as the Benguela upwelling system on Namibia's coast have similarly shown the capacity to be severely Fe-limited for primary production (Capone & Hutchins, 2013).

The ephemeral river valleys of Namibia are a prime example of a seasonal dryland dust emission source, with deflation due to strong easterly winds in the austral winter (Vickery & Eckardt, 2013). Visible on satellite imagery as distinct linear plumes (NASA, 2003), windblown dust frequently falls out over the surface of the South Atlantic (Stuut et al., 2002). The surface sediments in these ephemeral valleys have been shown to contain high levels of ocean-fertilising nutrients, most notably bioavailable Fe, (Dansie et al. 2016a, manuscript submitted for publication), but as yet there are no measured data quantifying the physical characteristics, geochemistry or nutrient content of the windblown dust, and so the potential for fertilisation in the oceanic deposition region is unknown.

To address this data gap we monitored dust emission events in three Namibian river valleys during the austral winter of 2013 and sampled the windblown dust emitted from key emission sites within the lower valley systems. This paper determines for the first time the aerosol concentration, sediment characteristics and nutrient content of windblown dust emitted from Namibia's dry river valleys, and compares the nutrient content of the transported dust with those of the source material. The frequency of dust

plumes observed using remote sensing during the field season is assessed, with a particular focus on identifying those observed to terminate over the South Atlantic. Together, these analyses provide the first evidence for the ocean fertilisation potential of mineral aerosols derived from the ephemeral river valleys of Namibia. It additionally provides a comparison to southern Africa's major dry lacustrine dust source areas of Etosha and the Makgadikgadi Pan system.

7.2 Regional setting

The E-W aligned ephemeral river valleys of Namibia are located between latitudes 18°S and 25°S (Figure 51a). The river valleys are sourced in the 1000 m high Great Escarpment (Morin et al., 2009) and flow through the 100-150 km wide Namib Desert to terminate in either the South Atlantic or Namib Sand Sea (Figure 51b). The river channel width within the valley floor varies between 20-100 m, interchanging between stream and braided channel systems (Jacobsen et al., 1995), with the twelve catchments combined covering an area of 151,800 km^2. On the plateau and highlands above the escarpment the average annual rainfall reaches over 300 mm a year (Jacobsen et al., 1995). This can generate slope wash and colluvium movement in the upper watershed (Bierman & Caffee, 2001) that over time enters the ephemeral fluvial system and is subject to down-valley transport. Below the escarpment the valleys hold several metres of alluvial material that has accumulated in various phases during the Late Quaternary, notably in the last 40 ka (Stone & Thomas, 2013). Reworking and fluvial incision of this valley fill occurs during modern flood events that erode and reshape the channel through the valley floor. These ephemeral flows originate from precipitation in the upper catchment between January and March (Krapf et al., 2003), with pluvial activity having seen a modest increase compared to 8-9 ka ago (Eitel et al., 2001). Rainfall rarely occurs below the escarpment in the west

with the Namib desert experiencing only 0-25 mm of annual precipitation which is mostly in the form of fog (Jacobson et al., 1995).

Regional atmospheric circulation patterns generate predominantly south-to-southwesterly trade winds over the dry river valley regions for most of the year (Lancaster, 1985). The notable exception to this general airflow pattern is the occurrence of strong east-to-northeasterly 'berg' winds during the austral winter months (Fryberger et al., 1979), a result of outflow from the winter position of the quasi-permanent continental high pressure cell over southern Africa (Newell et al., 1972). The seasonal circulation also impacts localised diurnal wind patterns that are produced by a strong thermo-topographic coupling (Lindesay & Tyson, 1990) generating local nocturnal winds in winter that drain towards the coast (Tyson & Seely, 1980). The E-W alignment of the Namibian valleys may additionally funnel the regional easterly and more local winds, enhancing their ability to entrain valley floor sediments, a potential noted by Wiggs et al. (2002).

7.3 Methods

7.3.1 Field stations

Three ephemeral river valleys were investigated in this study: the Huab and Kuiseb, which both terminate in the South Atlantic, and the Tsauchab, which terminates endoreically in the Namib Sand Sea (Figure 51b). All three valleys had previously been identified as significant annual emitters of dust using remote sensing analysis (Vickery et al., 2013; Eckardt & Kuring, 2005). Such analysis of satellite imagery recognised that persistent sources of dust emission tended to be located in the lower regions of the river valleys and generally no further than 100 km inland (Vickery & Eckardt, 2013). Informed by the work of Vickery & Eckardt (2013) we erected eleven monitoring stations in the lower catchment areas of each of the three valley systems identified as frequent dust

emitters (Figure 51). The stations operated for 20 weeks between April and September 2013 (the known dust 'season', Vickery & Eckardt (2013)) with equipment set up for the collection of windblown dust samples and data on airborne dust concentration and meteorological conditions (Table 14 and Figure 52). Six stations were set up in the Huab, two in the Kuiseb and three in the Tsauchab (Figure 51c, d and e). Physical capture of horizontal dust flux was undertaken at ten stations (see Table 14) using Big Spring Number Eight (BSNE) aeolian sediment samplers erected in a vertical profile at heights of 0.25, 0.47, 0.89 and 1.68 m (Mendez et al., 2011; Fryrear, 1986). At nine sites (see Table 14) a DustTrak DRX aerosol monitor (Wang et al., 2009) was also erected at a height of 3.18 m. This instrument recorded PM1, PM2.5, PM5, PM10 and total suspended particulate (TSP) concentrations at two minute intervals throughout the study period. At each site an automatic weather station (AWS) was erected measuring average wind velocity and wind direction at 3.18 m height at an interval of one minute.

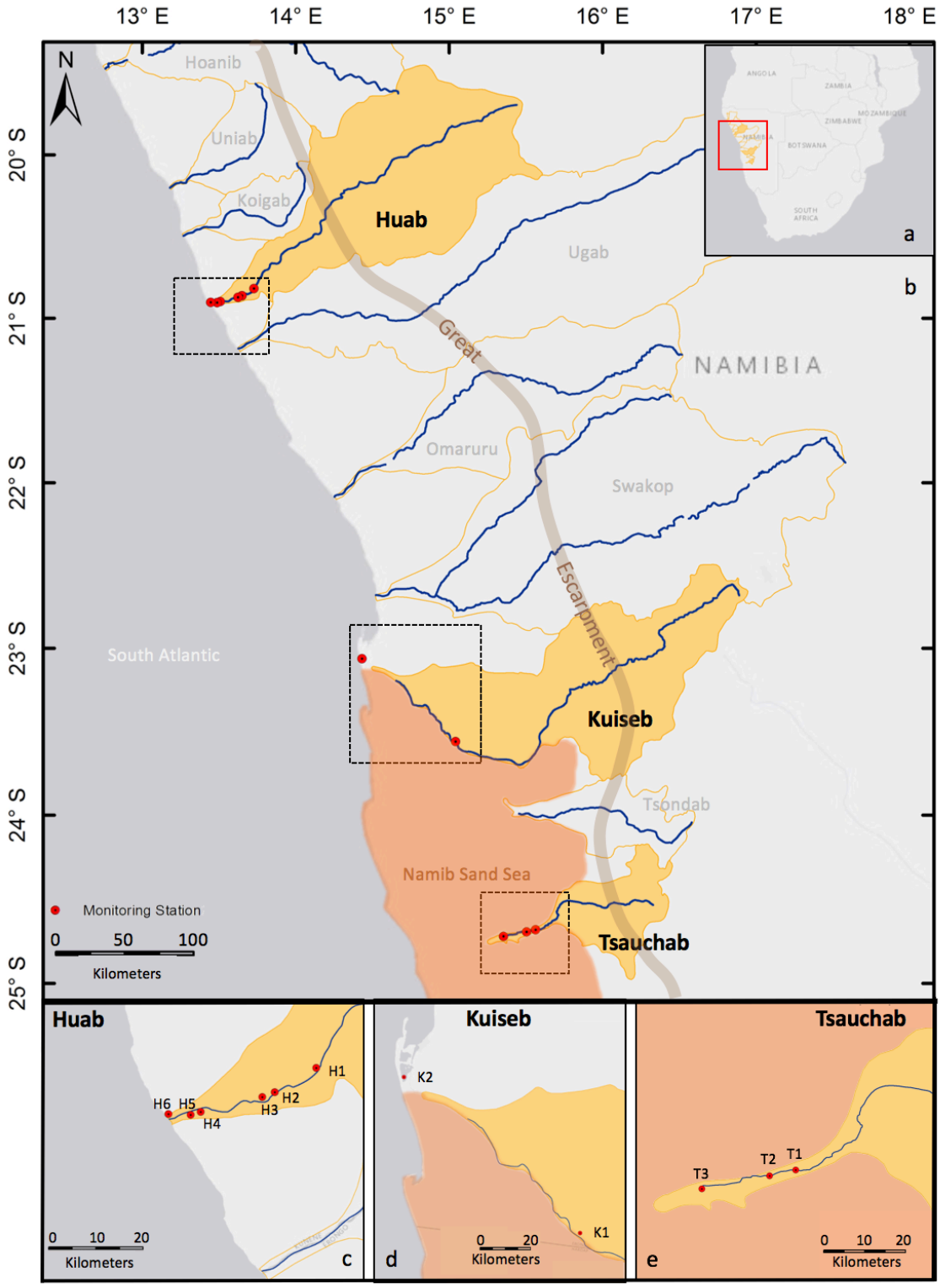


Figure 51 | (a) The ephemeral river valleys of western Namibia with (b) the location of the monitoring stations in the lower Huab, Kuiseb and Tsauchab river valleys. Station names are shown for the (c) Huab, (d) Kuiseb and (e) Tsauchab.

Table 14 Deployed instrumentation

River Valley	Monitoring Station	Distance inland from terminus (km)	Location description (valley width)	DustTrak	BSNEs
Huab	H1	30.32	Valley floor (970m)	X	X
	H2	21.3	Valley floor (1100 m)	X	X
	H3	18.70	Valley floor (230 m)	-	X
	H4	9.18	Valley floor (320 m)	X	X
	H5	4.09	Valley floor, (1360 m)	X	X
	H6	0.2	River mouth delta (2490 m)	-	X
Kuiseb	K1	84.1	Gobabeb research station, northern valley edge 600 m from river channel	X	X
	K2	1.17	River delta on artificial breakwater constructed for salt evaporation ponds	X	-
Tsauchab	T1	25.09	Valley floor (480 m)	X	X
	T2	19.54	Valley floor (430 m)	X	X
	T3	4.07	Terminal clay pan (230)	X	X

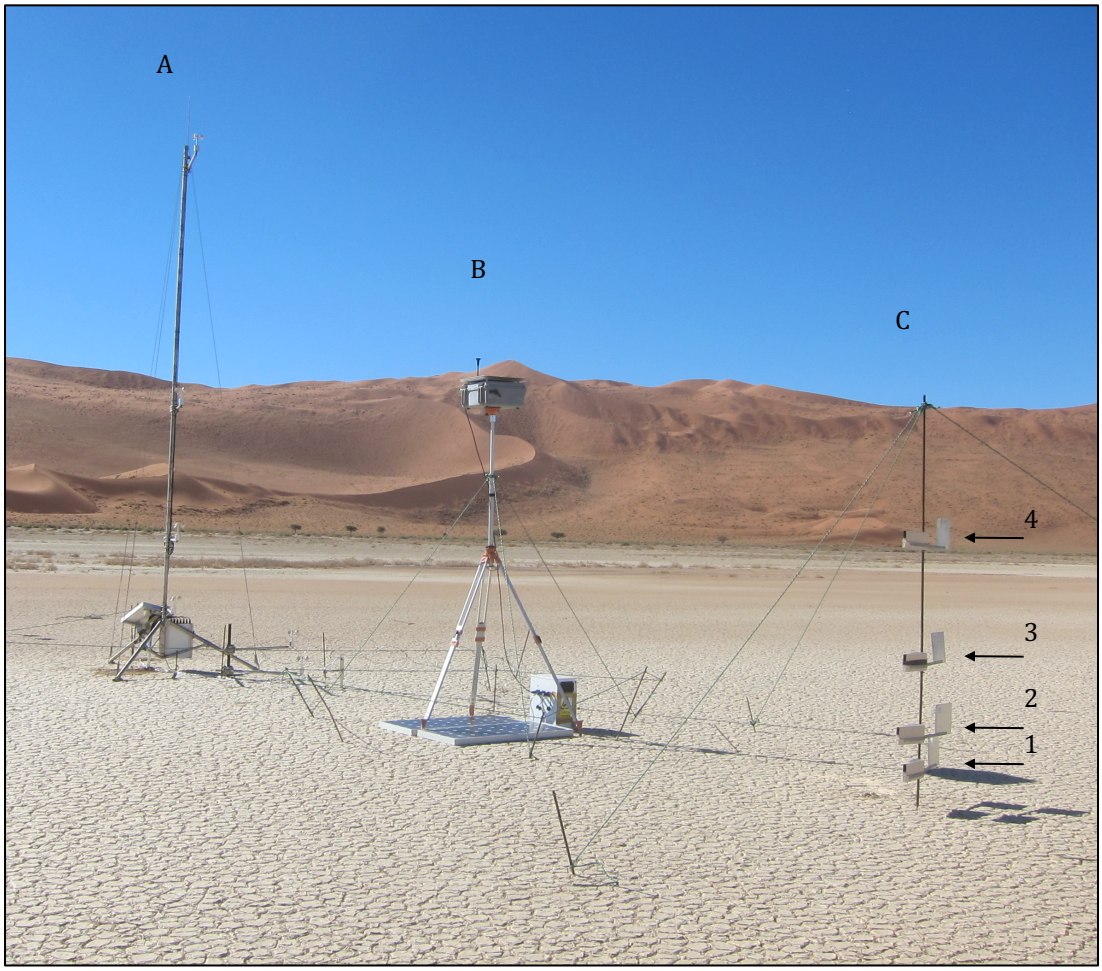


Figure 52 | Typical monitoring station consisting of (A) 6 meter meteorological mast with anemometer and wind vane at 3.18 m, (B) DustTrak with inlet at 3.18m, (C) BSNE horizontal flux collectors 1-4 with samplers set at 0.25, 0.47, 0.89 and 1.68 m collection heights respectively. The photograph shows station T3 as an example, with the transport direction of dust during strong easterly winds from right to left in the photo.

7.3.2 Sample Collection

Samples of windblown dust in transport (collected by the BSNEs), surface sediment in the river valleys, and (for comparison) surface sediment of Etosha and Makgadikgadi pans were collected for particle size and chemical analysis. For collection of windblown dust stations were visited monthly to empty BSNE traps and download meteorological

data. Each BSNE was brushed into a pre-weighed ziplock bag using standard collection procedures (Zobeck et al., 2003; Fryrear, 1986).

Surface sediment samples were collected along transects adjacent to eight of the monitoring stations, as described by Dansie et al. (2016a), and data from their analyses are used here for comparison with the windblown dust samples collected from the BSNE traps. Surface samples were collected in a transect taken N-S perpendicular to the valley strike across the valley floor, modern channel deposits and, where present, any contemporary aeolian deposits.

Additionally, surface samples were collected from the Etosha and Makgadikgadi pans as part of a wider study. These samples are analysed here to allow a comparison of the ocean fertilisation potential of all the key southern African dust sources; the ephemeral river valleys, and Etosha and Makgadikgadi pans.

7.3.3 Sample Analysis

Gravimetric weights were used to determine the scope of chemical (Fe, P, N) and physical (dry and wet grain size distribution) laboratory analyses that were possible on the windblown dust samples trapped in the BSNEs. A minimum of 18 g of sample was required for a full set of nutrient analyses to be undertaken, with a further minimum of 4 g needed for particle size measurements. A sufficient sample weight was not available from each individual BSNE sampler (a total of only 14% of samples met this criteria) so some within-site aggregation of samples was necessary. Samples from sites H2, H3 and H6 were sufficient to allow the sample from each individual collector to have a full set of nutrient and wet and dry grain size analyses. At T2 it was necessary to aggregate all four BSNEs in the vertical profile to generate sufficient mass for both chemical and grain size analysis. Remaining samples that did not reach the 18 g threshold were only analysed for

dry-dispersion grain size (collections from the Huab (H2, H3, H4, H5, H6), Kuiseb (K1) and Tsauchab (T1, T2)). Two stations (H1 and T3) did not collect enough sample for any analyses to be carried out.

7.3.4 Chemical Analyses

Sub-samples were analysed at the Kansas State University Soil Testing Laboratory where they were dried overnight in a 50°C oven with the exception of sub-samples for iron analyses which were air-dried. Chemical extraction and analyses were as described in detail in Dansie et al. (2016a) with all procedures following Brown (1998) unless otherwise stated. Bioavailable (Mehlich III) Phosphorus, and DTPA extraction of bio-available Fe^{2+} and Fe^{3+} (combined) was followed by Flame Atomic Absorption spectrometry (Lindsay & Norvell, 1978). Inorganic Nitrogen NH_4^+ and NO_3^- was extracted with 1M of KCl for measurement in a flow analyser. Total N and total P were determined using a modified Kjeldahl digestion followed by analysis of separate colorimetric reactions using a flow analyser. pH was measured using a 1:1 mixture of soil and DI water.

7.3.5 Grain size analysis

Grain size data were generated using a Malvern Mastersizer Hydro 2000MU, with both dry and wet (disaggregated) methods being applied to splits of the same samples. Dry analysis represents the particle size distributions of samples as found in the field, preserving sediment pellets, peds and other aggregates, while wet analysis requires a breakdown of sediments into their individual-grain constituents. The terms ‘sediment aggregates’ and ‘individual grains’ are used to identify the dry and wet analyses results respectively.

For dry analysis samples were riffled to a weight of 0.1-3.5 g and analysed using a Malvern Mastersizer Scirocco 2000, using standard procedures (Malvern Instruments, 2007). Where required, samples were re-riffled to appropriate weights to ensure laser obscuration values were maintained between 1.0-3.5%. The analysis of one in ten samples was repeated to ensure reproducibility of results.

For wet analysis 3.0-5.0 g of sample was processed to remove salts and carbonates as described by Soukup et al. (2008). Oven-dried (40°C) samples were ground using a mortar and pestle, split into sub-samples and suspended in a 1:1 solution of 50g/L sodiumhexametaphosphate and DI water. The samples were then shaken for 4 hrs at 250 epm and left to stand overnight. Grain size analysis was then performed using soil optimised procedures (Sperazza et al., 2004) with acceptable obscuration of 10-20%. Three measurements per sample were taken and the average calculated. Similar to the dry analyses, one in ten samples were repeated to ensure reproducibility of results.

7.3.6 Identification of dust plumes over the ocean

Visual inspection of satellite imagery was used to identify dust plumes emitted from the river valleys during the 20 weeks duration of the field deployment. Visual inspection of 15-minute interval SEVIRI true colour and dust detection imagery (provided at http://www.fennec.imperial.ac.uk) and daily MODIS Aqua and Terra Corrective Reflectance (True Colour) accessed in the Earth Observing System Data and Information System (EOSDIS) (available at https://worldview.earthdata.nasa.gov) was undertaken for the period April to September 2013 inclusive.

7.4 Results and Discussion

7.4.1 Dust emission events

During the course of field data collection a total of 18 dust events occurred that produced dust plumes extending over the ocean, as observed using EOSDIS and SEVIRI imagery. Airborne dust concentration data from the river valleys are shown in Figure 53 with observed plumes over the ocean highlighted by date. Four of these major plumes emanated from the Huab, nine from the Kuiseb and five from the Tsauchab.

The Huab was the dustiest river valley, with average two-minute TSP concentrations reaching up to 9.87 $mg.m^{-3}$ during emission events (see Table 15), compared to the highest averages reached in the Kuiseb of 0.5 $mg.m^{-3}$ and Tsauchab of 5.34 $mg.m^{-3}$. Whilst the Kuiseb produced the greatest number of ocean-bound plumes, measured dust concentrations for each event in the Kuiseb were approximately an order of magnitude lower than values from the other valleys (Figure 53). The relatively low dust concentrations recorded in the Kuiseb are likely to result partly from the locations of the two monitoring stations in this valley (see Figure 51). For practical reasons, both stations in the Kuiseb were located on the edge of the river valley, rather than on the floor of the river valley. These stations therefore recorded dust already in transport, rather than dust concentrations at the site of actual emission on the valley floor. However, visible identification of dust plumes using satellite imagery showed that the Kuiseb site at the distal end of the valley (K2) was located within the transport pathway of all emitted plumes and so we have confidence that the measured data reflect true dust concentrations. Similarly, analysis of remote sensing imagery revealed that measurement sites in the Tsauchab and Huab were also within the transport pathway of emitted plumes in their respective valleys.

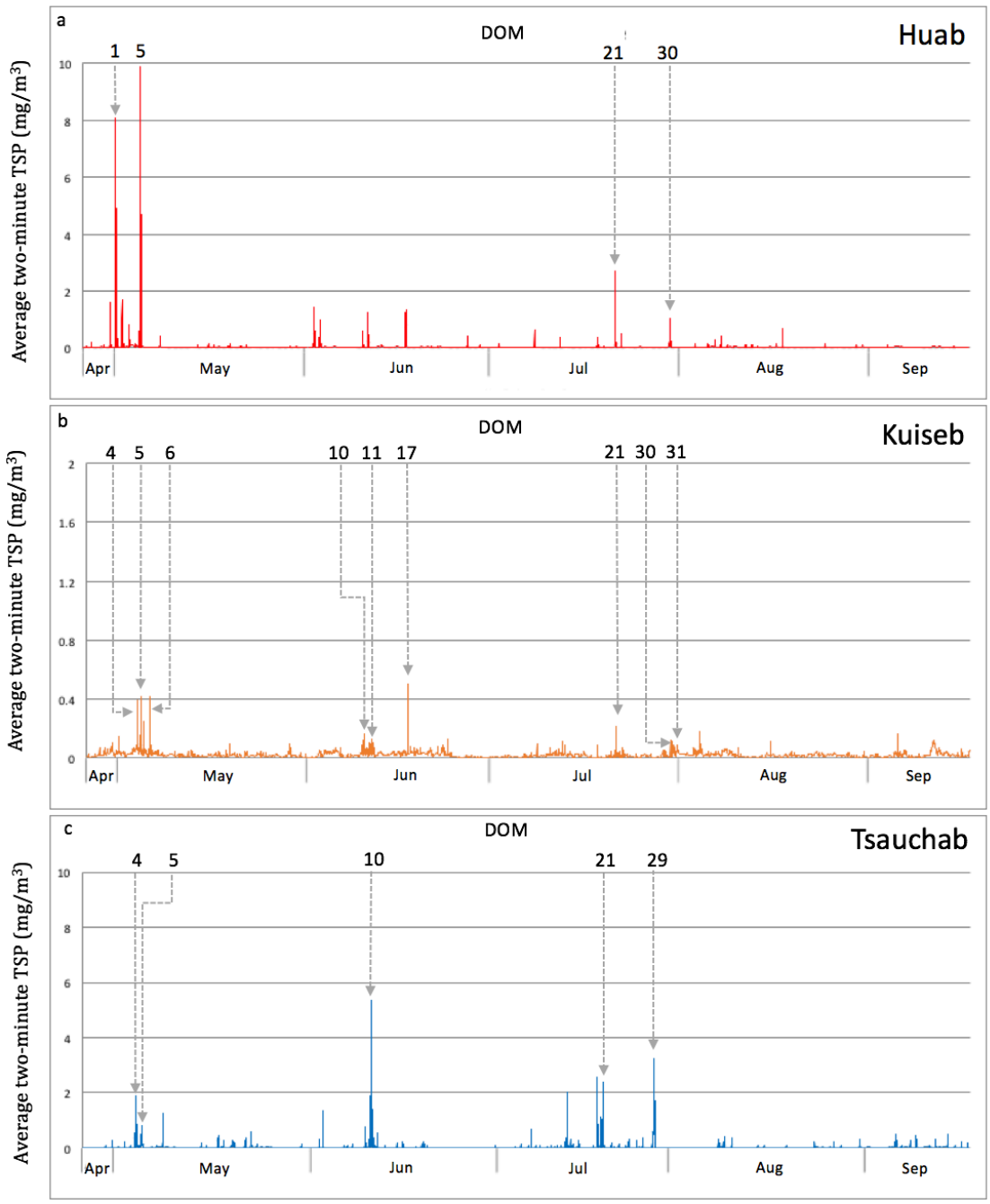


Figure 53 | Average two-minute TSP concentrations in the (a) Huab, (b) Kuiseb and (c) Tsauchab between April to September 2013 (recorded two-minute TSP concentrations at each station averaged within each river valley). Note differing y-axis scales. Dates that produced visible plumes off the coast identified with DOM (date of month).

Table 15 River valley airborne TSP concentrations ($mg.m^{-3}$) on dates of observed ocean-bound dust plumes (highlighted events as denoted in Figure 53) with valley-averaged wind speed (ms^{-1}) recorded during the event and calculated daily wind speed average within each valley.

		Huab	Kuiseb	Tsauchab
May	1	**8.10**[a] (9.06[b], 4.94[c])	- (9.53, 4.48)	- (3.31, 3.05)
	4	- (5.24, 3.87)	**0.41** (11.64, 7.80)	**1.88** (9.88, 6.98)
	5	**9.87** (10.52, 5.49)	**0.25** (8.18, 5.90)	**0.83** (8.39, 5.90)
	6	- (5.63, 4.25)	**0.42** (9.73, 6.15)	- (4.68, 3.78)
June	10	- (3.99, 3.10)	**0.16** (8.55, 7.47)	**5.34** (9.72, 7.73)
	11	- (5.63, 3.82)	**0.13** (3.95, 4.06)	- (5.55, 4.42)
	17	- (4.75, 3.33)	**0.51** (11.57, 6.61)	- (3.82, 3.54)
July	21	**2.72** (10.31, 5.81)	**0.22** (9.90, 7.07)	**2.38** (9.67, 6.71)
	29	- (5.79, 4.94)	- (7.97, 6.78)	**3.25** (10.25, 8.66)
	30	**1.04** (10.55, 6.69)	**0.12** (8.67, 6.62)	**~** (10.73, 8.07)
	31	- (5.00, 4.37)	**0.95** (8.04, 5.86)	- (4.91, 3.83)

[a] Average two-minute TSP concentrations ($mg.m^{-3}$) in the river valleys (two-minute TSP concentration measurements at each station averaged within each valley) during dust events on dates of ocean-bound plume emission.

[b] Average wind speed (ms^{-1}) during recorded dust events in emitting valleys (cells highlighted) and for the matching period of time in non-emitting valley(s) (cells not highlighted).

[c] Daily average wind speed (ms^{-1}) within each river valley calculated from two-minute measurements.

The most extensive dust events, where all three valleys produced dust plumes extending over the ocean, were on the 5 May, 21 July and 30 July 2013. Wind speed was between 8.18-10.73 ms^{-1} in all valleys during these emission events (Table 15). Differences in key

emission dates between the river valleys were also observed (Figure 53 and Table 15). The reason for this was variations in easterly wind strengths through the region on dust-emitting days. Daily averages were calculated (Table 15) and show the non-emitting valleys all recording below 5 ms^{-1} daily averages compared to 90% of dust-emitting valleys reporting a daily average >5 ms^{-1}. Note that no TSP data in the Tsauchab is shown for this latter event in Figure 53c and Table 15 due to field equipment failure.

The observed variance in dust emission days between river valleys is most prominent on 1 May when only the Huab produced a distinct dust plume. The average wind strength during the dust-event, across all monitoring stations in the Huab, was 9.06 ms^{-1} compared to a lower maximum of 3.31 ms^{-1} in the non-emitting Tsauchab and 9.53 ms^{-1} in the minimally-emitting Kuiseb (Figure 53b, Table 15). In spatial contrast, June saw emissions from the Kuiseb and Tsauchab on the 10th and the Kuiseb only on the 11th and 17th (Figure 53) with none from the Huab. Wind speed measurements during these dust events and calculated daily average wind speeds both show elevated wind strength in the southern two valleys (event averages up to 9.72 ms^{-1} and 11.57 ms^{-1}) compared to the Huab during the same period (3.99 – 5.63 ms^{-1}). Over 100 % increases in recorded wind speed between emitting and non-emitting valleys are shown on 10 and 17 June (Table 15).

Wind conditions clearly show localised differences between the river valleys (Table 15) and these play a definitive role in the dust emission potential of each valley (Figure 53). A composite image of dust emission events (accounting for cloud coverage) for 5 May and 29 July is shown in Figure 54. This clearly demonstrates that these large events enable the transport of significant amounts of valley-derived dust over the ocean. All dust events with plumes observed to reach the ocean occurred before midday during strong

(11-12 ms^{-1}) easterly winds, (Preston-Whyte et al., 1994; Lindesay & Tyson, 1990), Over-ocean dust events were observed to peak at 10:30 UTC on each emission date with plumes first reaching the coast at dawn (05:45 UTC) and becoming separated from the mainland at around 10:15 UTC, matching the temporal characteristics (Lancaster, 1985; Fryberger et al., 1979)of the thermo-topographic induced (Lindesay & Tyson, 1990) berg winds.

No dust plumes were seen to reach the ocean in August or September, with only small events evident in Figure 53 and wind speed daily averages only exceeding 5 ms^{-1} once in each of the Kuiseb (5.09 ms^{-1} on 15 September) and Tsauchab (5.94 ms^{-1} on 5 Sep). The Huab, however, recorded daily averages exceeding 5 ms^{-1} on 15 days in August and September but this was not matched with either notable increases in TSP concentrations (Figure 53a) or observed dust plumes. The absence of dust plumes at this time was confirmed by visual inspection of 15-minute interval SEVIRI true colour and dust detection imagery (provided at http://www.fennec.imperial.ac.uk) and daily true colour MODIS Aqua and Terra EOSDIS images (https://worldview.earthdata.nasa.gov) which showed the coast dominated by cloud and fog during these months (34 fog/cloud total obscuration days out of the 46 monitored days from 1 August to 16 September). Easterly winds were less prevalent in these months and regionally recirculated air movements carrying biomass haze were identifiable (EOSDIS), traversing the ephemeral river region from the NW to E direction. This recirculation is a known-occurrence during these months caused by the

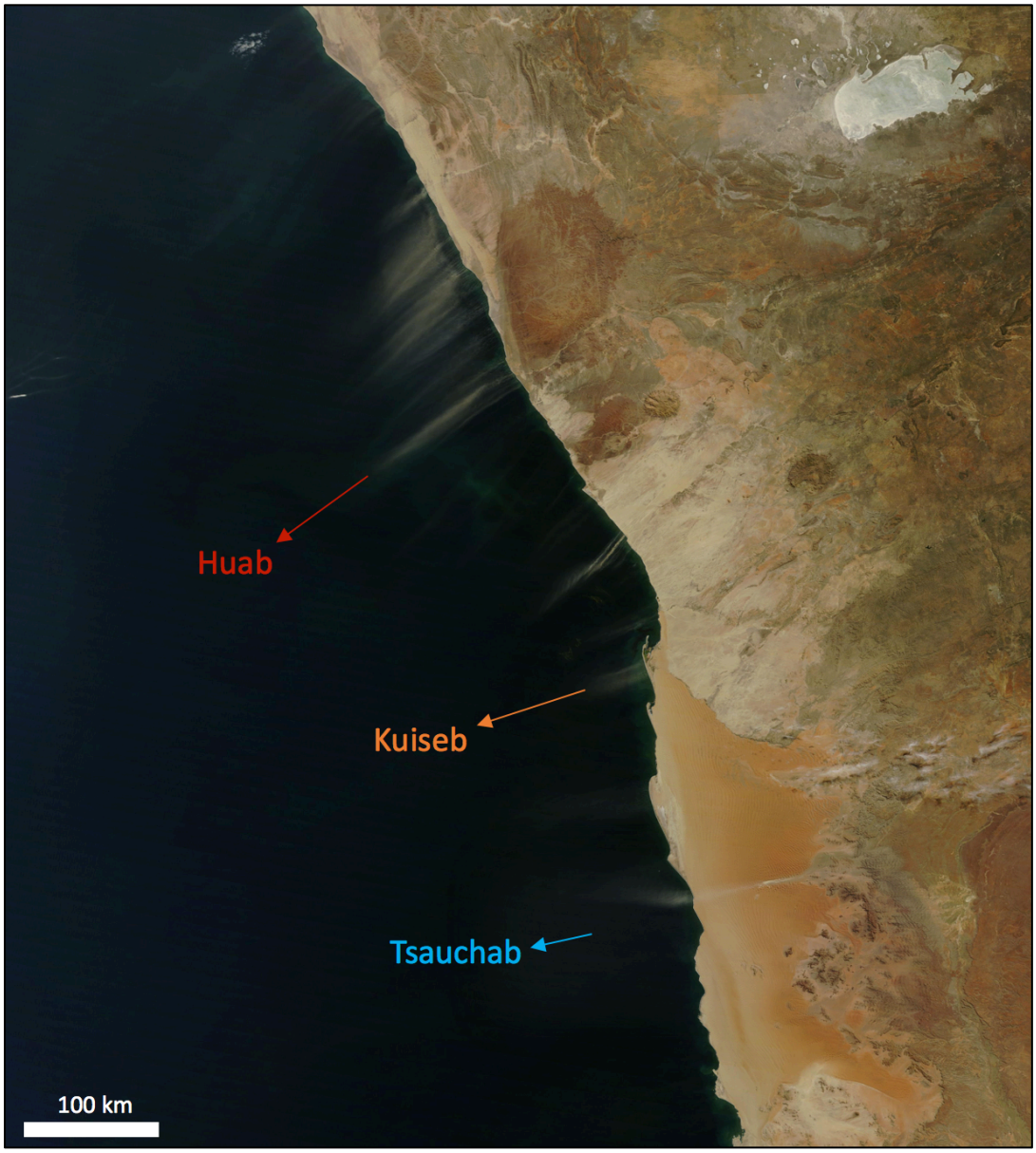


Figure 54 | Composite image of dust plumes emitted off the coast from the Huab and Kuiseb (5th May) and Tsauchab (29th July) taken from MODIS Terra Corrected Reflectance (True Colour) obtained from the Earth Observing System Data and Information System (EOSDIS) available at NASA Worldview (www.worldview.earthdata.nasa.gov).

semi-permanent continental high pressure cell that provides significant influence on the subtropical atmospheric circulation in the region (Tyson & D'Abreton, 1998) and is not conducive to dust emission over the South Atlantic from the ephemeral valleys.

Our analysis of both field data and satellite imagery confirms that windblown dust derived from the ephemeral river valleys is transported offshore during large easterly wind events. During the course of our field experiment each valley emitted between 4 and 9 of such over-ocean plumes This seasonal frequency of large events is similar to that found by the remote sensing analyses of Eckardt & Kuring (2005) who investigated 150 plumes emitted from the river valleys and coastal sabkhas between 1998-2001 and also the higher resolution study of Vickery et al. (2013) which identified 111 river valley plumes between 2005-2008. This was more than the combined emission frequency from southern Africa's major paleolacustrine sources which, in the same high-resolution study, saw 32 plume emissions from Etosha and 53 from Makgadikgadi pans (Vickery et al., 2013). Our results provide the first TSP concentration measurements of dust-plumes from the river valleys that have only previously been defined in terms of emission frequency from remote sensing observations. This is an important first step towards characterising the magnitude of aeolian sediment flux from the river valleys to the ocean each year.

7.4.2 Grain size of windblown dust

Results from the dry and wet grain size analyses for the Huab (Figure 55) show that the windblown dust is comprised of both individual grains and sediment aggregates formed through the cohesion of finer sediments. Large (up to 340 μm) aggregates such as crust pieces captured in the lowest BSNE (BSNE 1) are seen to be lifted up to 0.25 m height and aggregates up to 170 μm to 0.47 m (BNSE 2, Figure 55). Once in motion, these large aggregates are subject to in-air collisions and impacts with the surrounding terrain, resulting in aggregate disintegration that forms both smaller fragments and causes the release of individual parent grains (Shao, 2004) that are able to be transported at greater heights, with the higher placed BSNE traps collecting greater proportions of finer dust particles (Table 16) (Dong et al., 2003; Greeley et al., 1983). Both individual grains and

sediment aggregates show a volume weighted mean size of 100 µm or less in the upper BSNEs (BSNE 4 in Figure 55), a size range common to

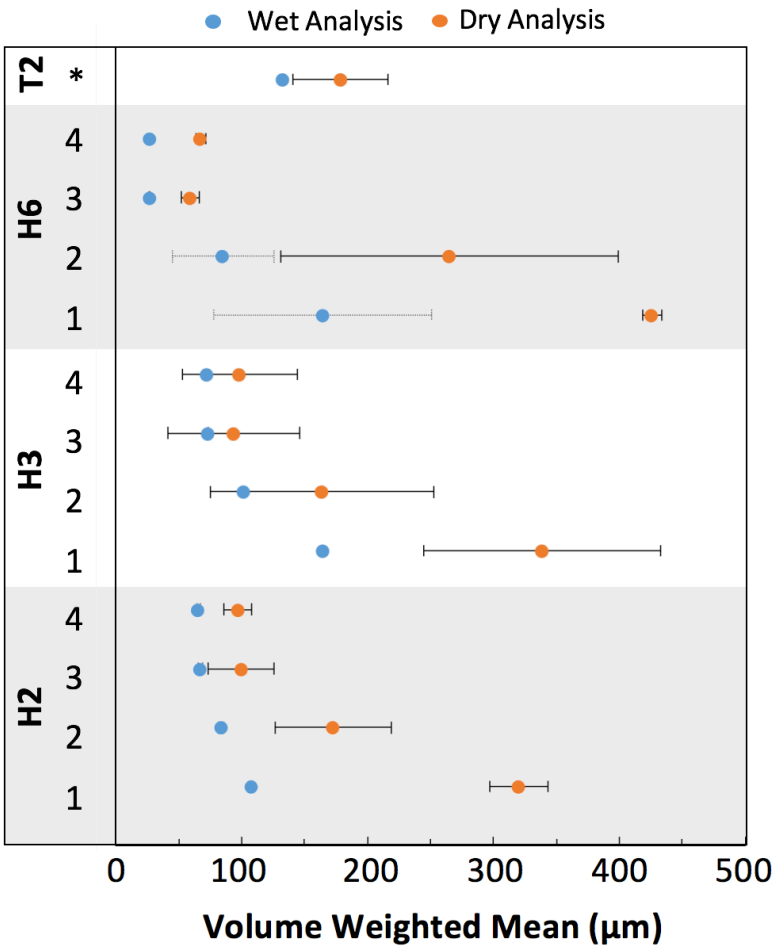


Figure 55 | Volume weighted mean grain size of wet and dry grain size distribution analyses from BSNE samplers in the Huab and Tsauchab (* T2 is combined BSNE 1, 2, 3 and 4 samplers) river valleys (averages calculated across multiple collections for H2 and H6. Horizontal bars show standard deviation where multiple collection dates were analysed (all dry analyses and only H2 and H6 for wet analyses). Standard deviation bars are too small to be observed for H2 (BSNE 1 = 2.32 µm, BSNE 2 = 2.31 µm, BSNE 3 = 1.62 µm, BSNE 4 = 1.24 µm) and BSNE 3 and 4 at H6 (0.33 and 0.06 µm respectively).

mineral aerosols (Ginoux et al., 2004; Arimoto et al., 1997; Tegen & Lacis, 1996). This demonstrates that the observed dust plumes (Figure 54) would contain both individual grains and sediment aggregates, with a greater proportion of the former. The surface sediments of accumulated alluvium that form the valley floors comprise 40% individual grains <100 µm (Dansie et al., 2016a), providing an abundant source of fine unconsolidated sediment for wind erosion.

The finer particles (<100 µm) transported higher in the profile, as shown in Figure 55, are capable of being transported long distances during dust emission events (Table 16). Examples of these include particles up to 20 µm that have been shown to travel more than 4000 km (Prospero et al., 1970) and Saharan dust particles of 62.5 µm have been recorded in fallout over the United Kingdom, travelling over 3000 km (Middleton & Goudie, 2001). Similarly-sized fines up to 20 µm and 65 µm are found in the windblown sediments collected by the BSNEs from all river valleys (Figure 55, without laboratory disaggregation) but are most prevalent in the Huab (Table 16) with 44% of deflated material in the top-two BSNEs being < 65 µm (ca. 14-16 % in the Kuiseb and 28-33 % in the Tsauchab). These are considered to thereby have the potential for similar long-range transport under favourable atmospheric conditions. The BSNE samples from the Kuiseb showed the least variation in grain size with collection height and this is a result of the location of K1 capturing dust in transport rather than at the point of deflation.

Table 16 Average grain size class distribution (%, dry analysis) for aggregated BSNE samples and potential transport distances as observed in the literature.

		Grain size fraction (µm)						
River Valley	**BSNE**	**0-20**	**20-65**	**65-100^**	**100-150**	**150-350**	**350-1000**	**1000-2000**
Huab	4	11.60	32.10	28.41	15.05	7.83	1.34	3.67
	3	13.30	30.78	28.89	15.73	8.46	1.35	1.49
	2	8.79	20.11	22.18	14.01	16.85	14.13	3.94
	1	5.12	10.55	11.69	9.40	31.64	27.21	4.39
Kuiseb	4	0.85	15.40	25.60	21.73	29.90	6.52	0.00
	3	0.49	13.07	27.73	24.49	29.27	4.94	0.00
	2	0.54	9.52	17.68	16.35	22.60	10.70	22.61
	1	0.67	9.50	20.25	20.89	33.64	9.07	5.97
Tsauchab	4	4.51	29.21	29.03	16.15	7.77	1.19	12.14
	3	4.14	23.87	27.80	17.10	9.35	2.09	15.64
	2	4.95	21.09	27.86	19.66	20.12	6.32	0.00
	1	1.41	7.72	11.94	12.87	43.46	21.57	1.04
		>4000	**3000**	**650**				
		Transport potential (km)*						

* Empirical evidence for >4000 km, 3000 km and 650 km as provided by Prospero et al. (1970), Middleton & Goudie (2001), and Glaccum & Prospero (1980) respectively.

The historical aeolian contribution to seafloor sediments off the coast of Namibia have been reported as 7-13 µm (Stuut et al., 2002) and 50-60 µm (Pichevin et al., 2005). These grain size fractions, determined by statistical modelling, are smaller than the in situ grain size reported for the majority of in situ windblown sediment grain sizes (ca. 30% up to 65 µm and ca. 4-12% up to 20 µm in the channel-located Huab and Tsauchab upper BSNEs 3 and 4 (Table 16)). Windblown dust in the river-adjacent Kuiseb station was noted for the presence of larger particles and comprised ca. 80% of particle size between 65-350 µm (BSNE 3 and 4, Table 16). Larger sediment aggregate aerosols would disaggregate upon deposition on the ocean surface with the disaggregated individual grains (Figure 55,

wet analysis) better matching the estimated grain size of aeolian fractions to the sea floor. Delivery of nutrients however, could be enhanced in aggregated particles where internal nutrients, having not being exposed to weathering and therefore more bioavailable (Shi et al., 2011), are also released. The aggregated particles up to 350 μm, as found in BSNE 4 collections, are considered suitable for aeolian transport to the ocean. Grain size up to 350 μm has been reported for sediment aggregates and individual particles off the coast of North Africa (Schroeder, 1985; Glaccum & Prospero, 1980).

7.4.3 Nutrient content of windblown dust

The geochemistry of windblown dust is shown in Figure 56. Our results show that entrained sediment collected at all BSNE heights between 0.25-1.68 m contain bioavailable Fe and P and N-based macronutrients and could therefore contribute to the nutrient-loading of observed dust plumes. It is difficult to compare these data with other studies of airborne nutrient concentration measurements, especially the bioavailable fractions, because of the varying analytical extraction methods that produce varying results (López-García et al., 2017; Anderson et al., 2010) with differing detection limits and analytical errors (Formenti et al., 2011). Bioavailable fractions of mineral aerosol Fe, the ocean fertilising nutrient that has seen the most research attention, vary widely in the literature from 0.01-80% (Mahowald et al., 2009). Measurements are highly influenced by the laboratory techniques used, namely both the acidity of the leaching solution and digestion time increases the Fe dissolution (e.g. (Boyd et al., 2010a; Gaspari et al., 2006; Guieu & Thomas, 1996), preventing their meaningful comparison. Call for the standardisation of the methodologies has been made previously to improve the data sets available to biogeochemical models (Boyd et al., 2010b), which would also greatly improve the inter-comparison of dust source nutrient content.

Noting this, some trends of nutrient content varying according to height are observed (Figure 56). Concentrations of bioavailable Fe are seen to increase (33%) between the near-surface (0.25 m) and top (1.68 m) BSNE, although it is noted this is within the standard deviation, which itself increases with collection height. TN concentrations are uniform across collection heights (Figure 56) with variations observed in the bioavailable N fractions. Ammonium (NH_4^+) concentrations are seen to increase (53 %) between BSNE 1 and 4 similar to Fe. Nitrate (NO_3^-) shows an inverse relationship with 15 ppm reported in BSNE 1 compared to 11 ppm in BSNE 4. Both NH_4^+ and NO_3^- are highly accessible for phytoplankton uptake (Moore et al., 2013; Boyd et al., 2010a; Michaels et al., 1996), with NH_4^+ also having the potential for conversion into NO_3^- following oceanic deposition by ammonia-oxidising bacteria (Kowalchuk & Stephen, 2001). TP concentration is similarly shown to modestly increase with collection height (Figure 56). An average TP content of 720 ppm is assumed in global dust models (Myriokefalitakis et al., 2016; Wang et al., 2015; Brahney et al., 2015), which is higher than reported here (maximum of 622 ppm in BSNE 3, Figure 56) but significant geographical variation of this value is known to exist globally (Mahowald et al., 2008) and, more recently, demonstrated across key emission areas previously considered homogenous in modelling assessments of nutrient flux (i.e. the Sahara (Gross et al., 2016)).

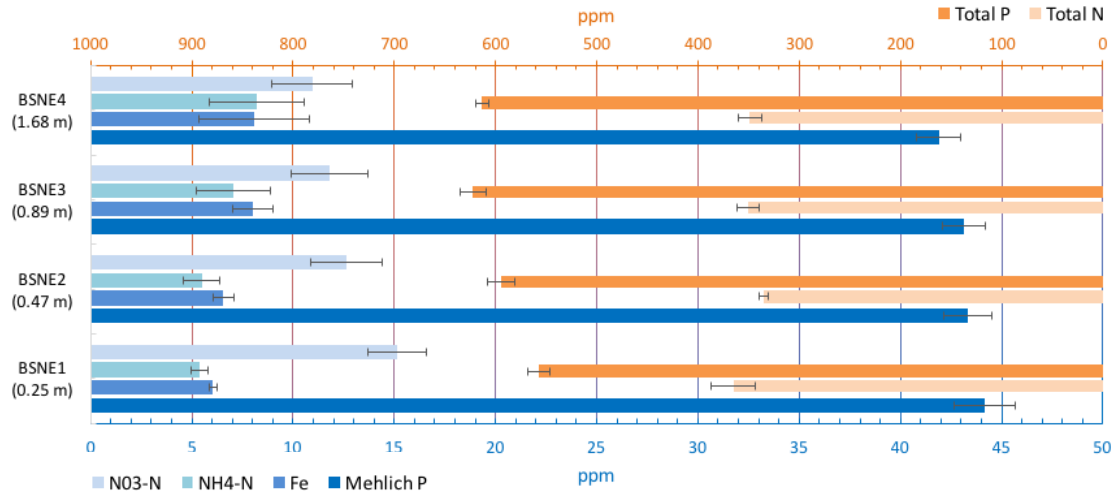


Figure 56 | Mean bioavailable Fe, N and P concentrations according to BSNE height for Huab 2 (three collections) and Huab 3 (one collection). Bars indicate standard deviation. Huab 6 was excluded due to the potential influence of ocean spray.

Our data show that the windblown dust we collected from the ephemeral river valleys of Namibia contain Fe, P and N nutrients, all of which are known to facilitate phytoplanktonic growth in ocean waters (Moore et al., 2013; Jickells et al., 2005; Boyd et al., 2000). The relative importance of each nutrient for ocean fertilisation depends on the biogeochemical conditions and phytoplankton community species composition of the depositional waters (Hecky & Kilham, 1988; Tilman et al., 1982), which varies geographically and seasonally (Cetinić et al., 2015; Edwards et al., 2013). It is known that Fe limitation affects productivity in upwelling systems (Hutchins et al., 2002; Bruland et al., 2001), such as the Benguela Upwelling System located along Namibia's coast, where the vertical transport of macronutrient-rich waters can create near-shore Fe-limited conditions as are found in the HNLC waters of the open ocean (Capone & Hutchins, 2013). Farther offshore from Namibia (-13.3 °N, 0.0 °E), ocean waters have been shown to be co-limited by Fe and N (Moore et al., 2013). N limitation can both be alleviated through the direct input of bioavailable N compounds, or through P and Fe where these

nutrients are limiting microbial nitrogen fixation (Mills et al., 2004). Therefore, in the case of phytoplanktonic growth off Namibia's coast being either Fe-limited, P + N limited (e.g. Tyrell (1999)), or a combination of both (e.g. Bracken et al. (2015)), then these conditions could be mediated by aeolian deposition of mineral aerosols from Namibia's river valleys.

Finally, the fertilisation potential of the windblown dust can be compared to previous reporting of source sediments (Dansie et al., 2016a) and the importance of these river valleys as a source of aeolian fertilisation considered in a southern African context; the comparison possible due to identical laboratory analyses of surface sediment samples from the river valley source sediments and Etosha and Makgadikgadi pans, as described in Dansie et al. (2016a).

7.4.4 The regional fertilisation potential of windblown dust from the ephemeral river valleys

Results in Figure 57 show that bioavailable Fe concentrations of windblown dust in the river valleys are similar to those previously reported for the in-situ sampled surface sediments (Dansie et al., 2016a). The average bioavailable Fe content of deflated dust was 5.5 ppm in both the Huab and Tsauchab, compared to slightly higher levels of 7.1 ppm and 7.5 ppm in the Huab and Tsauchab surface sediments respectively (Figure 57). The dust-emitting lower reaches of the Huab and Tsauchab river valleys are separated N-S by five other river valleys over a distance of ~460 km (Figure 51b). It may therefore be inferred that windblown dust in the other Namibian river valleys might contain similar bioavailable Fe concentrations. This is further supported by Dansie et al. (2016b), who showed that sediment in the dust-emitting lower river valley reaches contained enriched levels of bioavailable Fe irrespective of watershed geology or land use (see Dansie et al. (2016b)). This suggests that Namibia's ephemeral river valleys, combined stretching for

~800 km along the coast (Figure 51a), may be considered an extensive and regionally significant dust source for the Fe-limited waters of the South Atlantic and Benguela upwelling system in comparison to southern Africa's major paleolacustrine dust sources (Figure 57).

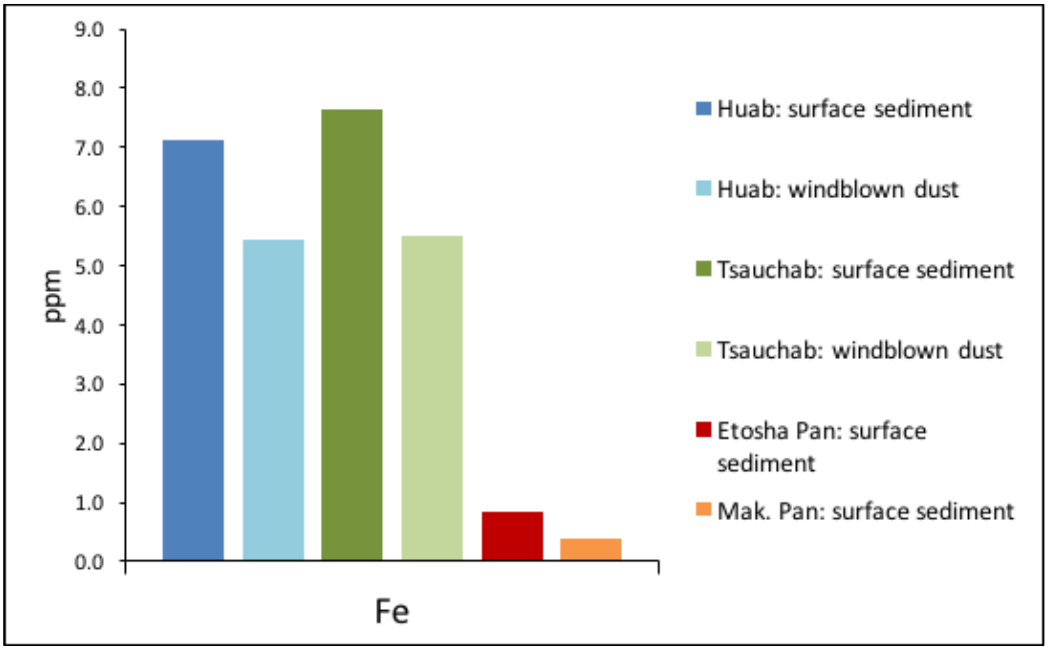


Figure 57 | Mean bioavailable Fe content of surface and windblown dust from the Huab and Tsauchab monitoring stations. Comparison with the regionally significant Etosha and Makgadikgadi pan dust sources is provided, see Dansie et al. (2016a). The mean values in the river valley surface sediment shown in Figure 57 and Figure 58 are calculated using all surface sediment samples of valley fill, channel fines and channel coarse material presented in Dansie et al. (2016a). Mean results of the BSNE samples are calculated using collected samples from H2, H3, and H6 and S2. The mean concentrations include all samples collected from the four BSNE collection heights, representing all material entrained between 0.25 and 1.68 m high during deflation events.

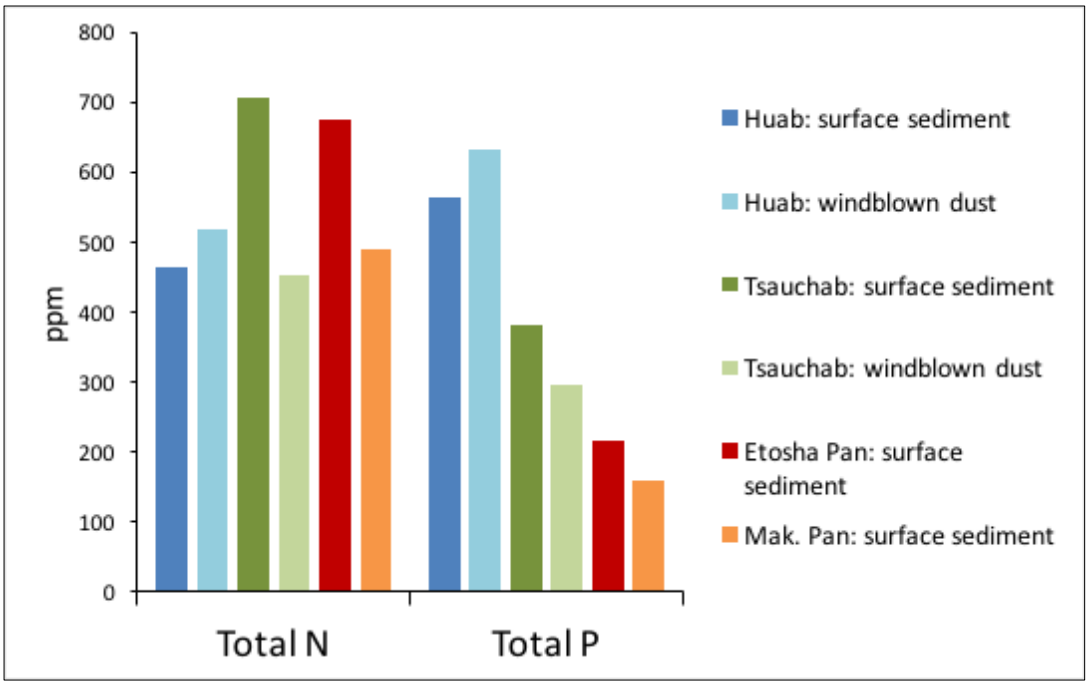


Figure 58 | Mean Total N and Total P content of surface sediment and BSNE samples from the Huab and Tsauchab river valley stations as well as surface sediment from Etosha and Makgadikgadi pans. Mean concentrations calculated as described for Figure 57.

Figure 58 shows the total concentration of N and P macronutrients in windblown dust compared to in-situ sampled surface sediment. Total P concentrations are shown to be comparable between surface sediment and windblown dust samples within each river valley. A similar relationship is seen for Total N in the Huab but not in the Tsauchab. Dansie et al. (2016b) showed that Total N concentrations in the fluvial deposits in the Tsauchab were the highest of all three river valleys. The endoreic terminus of the Tsauchab enhances water accumulation following channel flow, influencing infiltration rates and subsequently microbiological processes that are heavily dependant on soil moisture and environmental conditions (Kidron et al., 2015). Increased N levels have previously been correlated with hydrological flows in these Namibian rivers (e.g. Jacobson et al. (2000)). The macronutrient loading of river valley dust shows that P is found in higher concentrations than in Etosha and Makgadikgadi pan sources, having a

regional significance but not to the extent as shown for bioavailable Fe. River valley N concentrations are not considered regionally significant compared to the pans.

7.5 Conclusion

We have shown that the dust emitted from the ephemeral river valleys of Namibia is influenced by localised differences in wind strength within valleys and can be considered a potentially important source of nutrients for fertilisation in the South Atlantic. Ocean-bound dust collected in the river valleys carries regionally significant levels of nutrients similar to the in-valley source sediment, of overall greater primary production potential than either of southern Africa's major pan sources. As previously identified in the source sediment, bioavailable Fe concentrations were also the most important constituent of the aeolian nutrient flux for ocean fertilisation. The abundant source material in the river valleys and the extant replenishing mechanism of ephemeral flows support consideration of the ephemeral river valleys as a significant dust source of nutrient rich, fine grained sediment suited for long-range aeolian transport. Extrapolation of our results across the twelve Namibian ephemeral river valleys would see an 800 km N-S coastal source of mineral aerosols with elevated bioavailable nutrients: we hypothesise that these play an important mechanism in ocean nutrient cycles. The annual cycle of dust emission and seasonal nutrient upwelling cycle of the Benguela Current, would influence primary production and is proposed to play an important role in nutrient cycling and the marine productivity off the coast of Namibia.

Acknowledgements

The authors gratefully acknowledge the support by the Clarendon Fund and Oxford University Press for this research and the John Fell Fund for providing partial support of fieldwork activities. Prof. Richard Washington, Dr. James King and Dr. Sebastian Engelstäder are thanked for their major contributions in the form of preparation, equipment deployment and assistance in the field. We are very thankful to the Gobabeb Research and Training Centre for their support and for hosting one of the monitoring stations. We thank the Namibian Ministry of Environment and Tourism for all their support and assistance, especially with access to field sites permitted under permit number 1788/2013. This research has been carried out in collaboration with the Natural Environment Research Council grant NE/H021841/1.

7.6 SEM investigation of windblown dust samples

This section is provided in addendum to Paper 3 as an expansion of what was covered in Section 7.4.2 but beyond the scope of the submitted paper.

Fluvial activity in dryland environments are prerequisite conditions for productive dust emission sources globally due to the abundance of desiccated alluvial fines (Prospero et al., 2002). The results presented in Chapter 7.4 show that the ephemeral river valleys provide a source of individual grain fines as well as sediment aggregates, both of which contribute to the observed dust plumes over the South Atlantic (Figures 1, 12 and 54). These aggregates reflect the cohesion of clay, silt and fines and formation of surface crusts that are characteristic of ephemeral river geomorphology, e.g. Dunkerley (2008).

Aeolian sediments have been identified off the Namibian coast in seabed sediment cores by Stuut et al. (2002) and used as a signature of terrestrial aridity in south western Africa over the last 300 kyr. Grain size analysis (undertaken in the range of 0.5 – 100 μm only) followed by end member modelling of results was used to distinguish fractions of fine and coarse aeolian sediments (modal grain size of 7 μm and 13 μm respectively) from the hemipelagic sediment. Airborne dust collection was also undertaken during the core sampling expedition, over an ~800 km ocean transect using a pump filter (dust sampler model GMWL 2000) and showed mean airborne particle size of ca. 20 μm. During the collection period a 20-28 $km.h^{-1}$ SSW wind was present (Stuut et al., 2002) with no active dust emission occurring from the coast. Pichevin et al. (2005) identified an aeolian component of coarser grains, between 50-60 μm, in the sediment cores using statistical modeling, which were considered to be transported by low-altitude winds.

In contrast to the offshore sediment estimates of aeolian material, the dust captured in this study is associated with recorded emission events (Figure 53 and Table 15). The modal grain size of in-situ deflated material and parent grains are larger (> 60 μm) than that reported in sediment cores. The grain size distribution analysis (Table 16) was using dry grain size dispersion, compared to the wet dispersion analysis undertaken by Stutt et al. (2002). Disaggregation of the in-valley collected windblown dust samples (Figure 55, wet analysis) demonstrates that the assemblages are comprised of finer individual grains that better match those calculated by Stuut et al. (2002) and Pichevin et al. (2005), most notably in the upper BSNEs at H6 (26.83-27.13 μm at BSNE 3 and 4 respectively). However, the delivery of sediment in aggregated form is shown to occur at all entrainment heights sampled. The assemblages would be expected to disintegrate under aquatic conditions, resulting in disaggregated parent material grains, matching the disaggregated size fractions given in Figure 55, settling on the sea floor.

SEM analysis offers the ability to further classify grain types and characterise the assemblage particles presented in Figure 55 and Table 15. It also allows the determination of grain shape, which affects the potential for aeolian transport. Figure 59 shows SEM imagery of the dust particles collected in the BSNEs from each valley. Four distinct particle classifications are made; angular quartz grains, thin clay platelets, consolidated assemblages, and small fines. The small fines are likely assemblages of silt and clay particles too small to identify individually here (>16 μm), see examples highlighted in Figure 59. Particle size can be seen to decrease with increasing BSNE height in each valley, matching the results shown in Figure 55. The Kuiseb samples show a higher proportion of larger particles and platelets which is due to the location of K1 outside of the main river channel (Table 14 and Figure 51d). Not being located within a main deflation pathway, as were H2 and T2, would see a less condensed entrainment of fines

passing the sediment samplers. Within the river valleys the ephemeral fluvial mixing, settling and cohesion of fines would produce both the thin platelets and assemblages observed (Figure 59), which are characteristic of desiccated alluvium (Tooth, 2000). The thin platelets are formed by horizontal lamination and mud drapes due to intermittent flows and cohesion of varied sediment grains into assemblages, or intraclasts, and are typical of sediments in dry ephemeral systems (Reid & Frostick, 1997). Once airborne, flat particles have decreased sedimentation velocities compared to spherical particles (Cheng et al., 1988), meaning flatter particles can be transported over longer distances (Formenti et al., 2011).

The non-spherical platelets (Figure 59) in the deflated dust would therefore augment the transport potential of the dust plumes from the river valleys and see enhanced transport potential of larger aggregates. The prevalence of flat aggregates within the captured aeolian sediment, even at K2 outside of the topographical river channel, demonstrates that the river valley dust is of a larger, aggregated grain size than previously reported estimates reliant on seafloor sediment cores. As discussed in Section 7.4.2, aggregates and larger particles up to 350 μm are transportable by wind for hundreds of kilometres, easily surpassing the inland distances (maximum of 80 km) from the collection stations to the ocean (Table 14). These are clearly identifiable in Figure 59 as fluvial-derived plate-like particles.

Characterisation of the grain shape using SEM demonstrates the influence that geomorphology has on grain shape of windblown dust with the fertilisation potential also able to be considered from the aggregate type. Individual particles convey

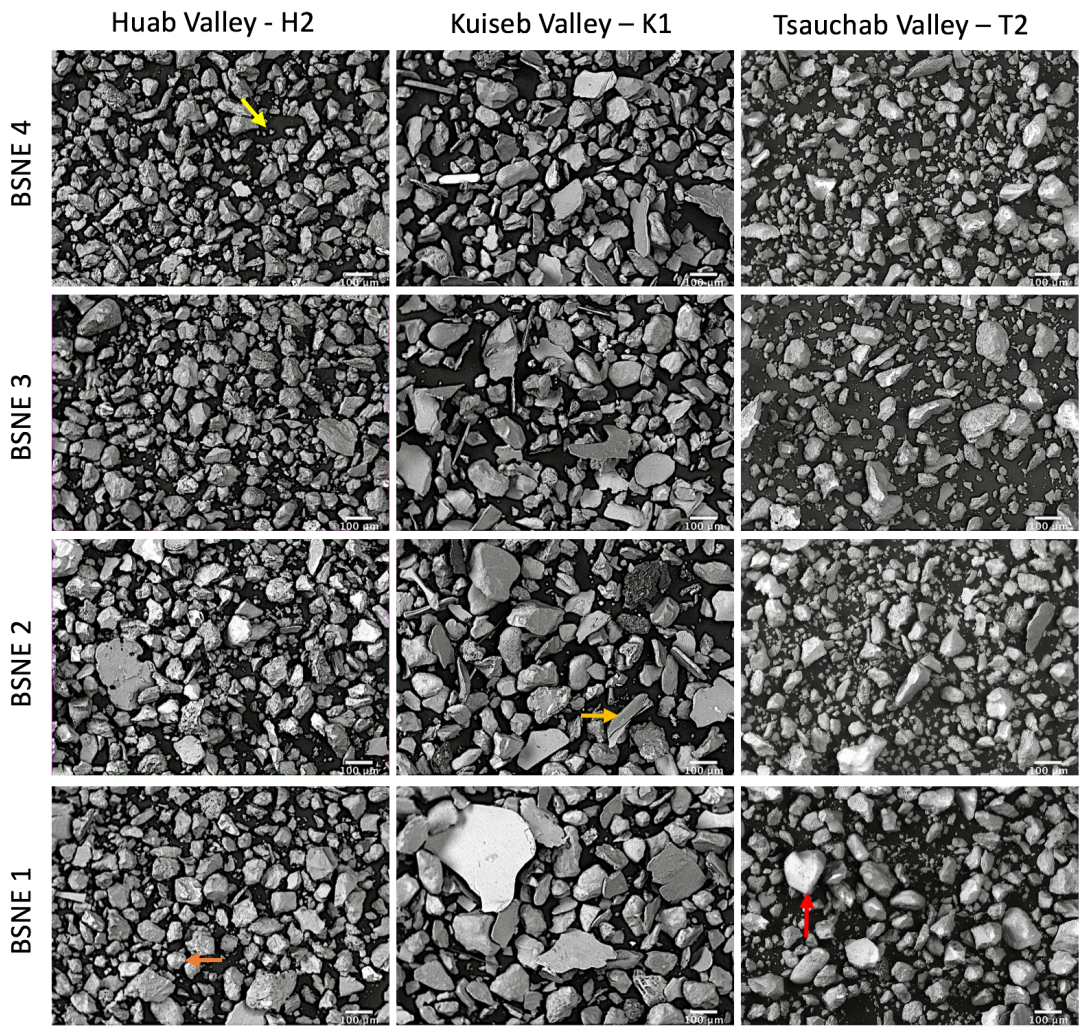


Figure 59 | Scanning electron micrographs (300x magnification, scale bar 100 µm) of dust collected at each BSNE height in the Huab (H2), Kuiseb (K1) and Tsauchab (T2) river valleys. Examples highlighted of angular quartz grains (vertical arrow), thin clay platelets (arrow pointing right), consolidated aggregates (arrow pointing left), and small fines (diagonal arrow).

nutrients attached to the surface of the particle with nutrient loading therefore being a determinant of surface-area to volume ratio (Zhang et al., 2003; Buseck & Posfai, 1999). Aggregates offer increased fertilisation potential due to their dissolution upon deposition and subsequent release of additional nutrients contained within the complex itself (Raiswell et al., 2006). Alluvium in arid environments, such as the valley fill of Namibia's river valleys, has been shown to have higher soluble Fe content than exposed,

non-fluvial surface soils due to the weathering and aging of Fe oxides reducing the bioavailable fraction of Fe (Shi et al., 2011). The collection of sediment aggregates at each BSNE height in each of the three river valleys (Figure 59), and newly-individual grains released during momentum (Shao, 2004), would provide an explanation for the increased levels of bioavailable Fe associated with the ephemeral river valley sediments (Dansie et al., 2016a). Protected from exposure and weathering as crustal fragments and aggregates, the aeolian transport and ocean-delivery shown in this research, followed by the subsequent deposition and dissolving of assemblages in the ocean would then release this instantaneously dissolvable fraction of bioavailable Fe. Ephemeral river geomorphology therefore provides processes responsible for enriched bioavailable Fe sediment that is highly suitable for ocean delivery by wind.

It is lastly therefore useful to consider the hydrological influences of riverine dust sources. The most intensely monitored river valley, the Huab (Figure 51), distinctly shows that the delta-collected windblown dust hosts the smallest median diameter individual grains, 26.83-27.13 μm at BSNE 3 and 4 respectively compared to upstream collections (H2 and H3) (Figure 55, wet analysis)[12]. This can be explained by a combination of fluvial and aeolian processes. Dust plume material that was emitted upstream would progressively contain a larger fraction of fines as the plume travels down the valley due to the removal of larger grains by gravitational forces (Durán et al., 2011; Tegen & Fung, 1994). Depositional events associated with fluvial activity would also transport an increasing fraction of fines in ephemeral flows as they travel downstream (Tooth & Nanson, 2000; Dunkerley, 1992), ultimately depositing a significant source of

[12] It should be noted that the larger aggregates at H6 (425 μm; see Figure 55), cannot be considered representative of in-situ dust due to their collection while saturated and with subsequent laboratory drying determining sediment cohesion and assemblage size.

fine material in the delta. Both fluvial and aeolian processes would therefore see the increased abundance of fines in the lower reaches of the river valleys, providing an abundance of highly deflatable material in close proximity to the ocean. Further, these near-terminal sediments are known to contain the highest nutrient concentrations also due to hydrological processes (Figure 42 and 43). The increasing fraction of fines and higher nutrient content associated with a hydrologically downstream location provides evidence of the importance of riverine geomorphological processes as sources of dust for ocean fertilisation.

In summary, the geomorphology of Namibia's ephemeral rivers produces both large, plate-like assemblages with increased transport potential and enriched nutrient loading as well as the hydrological accumulation of finer individual particles and higher nutrient content in downstream alluvium. Both of these characterisations of the ephemeral river valley dust and source sediments convey a marked potential for ocean fertilisation upon deposition. These characteristics would be expected to be relevant for river dust sources globally with the vast majority of terrestrial drainage systems terminating in the ocean and offshore winds ubiquitous in coastal environments, resulting from temperature differences between the land and sea (Savijärvi, 2004). Riverine dust sources are therefore considered to provide nutrient loads significant to their local and regional environment, which in the majority of cases would be the adjacent marine environment.

CHAPTER 8

Paper Four

PLUMES AND BLOOMS – AEOLIAN DUST FERTILISES PHYTOPLANKTON IN THE BENGUELA UPWELLING SYSTEM

A. Dansie[1], D.S.G Thomas[1,4,5], G.F.S. Wiggs[1], I. Ashpole[2], M.C. Baddock[3]

[1] School of Geography and the Environment, University of Oxford, Oxford

[2] Climate Research Laboratory, Oxford University Centre for the Environment, Oxford.

[3] Department of Geography, Loughborough University, Loughborough, Leicestershire, UK.

[4] Geography, Archaeology and Environmental Studies, University of the Witwatersrand, Johannesburg, South Africa.

[5] Department of Environmental and Geographical Science, University of Cape Town, Rondebosch, South Africa.

Status: Submitted to *Nature* on 10 January 2017.

8 Plumes and Blooms – Aeolian dust fertilises phytoplankton in the Benguela Upwelling System

Oceanic photosynthetic organisms contribute ca. 50% of global primary biological production (Field et al., 1998), with the greatest marine productivity rates occurring in the world's four eastern boundary upwelling systems (EBUS) (Toggweiler & Carson, 1995) (Figure 60a). These are characterised by wind-driven Ekman spirals initiating ocean surface upwelling (Rossi et al., 2009) of nutrient-rich deep water inclusive of nitrates (Gutknecht et al., 2013), phosphates (Neumann et al., 2016), and metals (Noble et al., 2012). Elsewhere, ocean delivery of essential nutrients via deposition of desert-derived mineral dust aerosols has been correlated with phytoplankton blooms in low-nutrient waters (Tan et al., 2017; Calil et al., 2011) and high nutrient low chlorophyll (HNLC) regions (Moore et al., 2013), the latter better resembling the nutrient status of the EBUS waters, (Figure 60a). To date, model-based assessments and marine-only nutrient investigations of EBUS have inadequately captured the significance of the aeolian contribution, resulting in an inadequate understanding of terrestrial, atmosphere, and marine system feedback processes. Here we show that dust plumes from Namibian ephemeral river valleys play a substantial, direct, and under-reported, role in primary production within the complex upwelling Benguela ecosystem. For the first time, real time monitoring of airborne dust concentrations along river valley sources has been undertaken, allowing direct correlation of recorded dust plume intensity and duration with remotely sensed marine chlorophyll levels. We found that oceanic deposition of valley-sourced dust generates immediate biological provision of Fe fractions (i.e. the 'instantaneously soluble fraction' (Buck et al., 2006)) which are accessible for rapid uptake by phytoplankton communities (Shaw et al., 2008; Wieters et al., 2003). We

provide direct evidence of the contribution of these mineral aerosols to ocean fertilisation within the highly productive Benguela upwelling system (BUS). In turn, this provides important insight into the significantly varied chlorophyllic production across EBUS globally. The BUS has the highest nitrate levels of all EBUS but intra-seasonal variations do not correspond well with the timing of marine chlorophyll levels. This suggests alternative factors must also drive chlorophyll flux, with oceanic eddies (Gruber et al., 2011), temporal variations in Ekman forces (Desbiolles et al., 2016) and atmospheric dust inputs of micronutrients (Ohde & Siegel, 2010) postulated.

In-field meteorological and in-valley airborne dust concentration data were collected during the austral winter of 2013 using automated monitoring equipment (see Methods) at sites in three Namibian west-coast valleys (Figure 60b) known to be key mineral aerosol sources (Vickery et al., 2013). In 2013 MODIS Aqua and Terra (see Methods) AOD-defined (hereafter AOD) dust plumes occurred within an 800,000 km^2 area of the eastern Atlantic (Figure 60b). Monthly chlorophyll a (hereafter chl-a, representing primary phytoplankton production), sea surface temperature (SST) (principally driven by ocean upwelling) for this area of the eastern South Atlantic, and dust emission data from key emitting valleys are shown in Figure 60c.

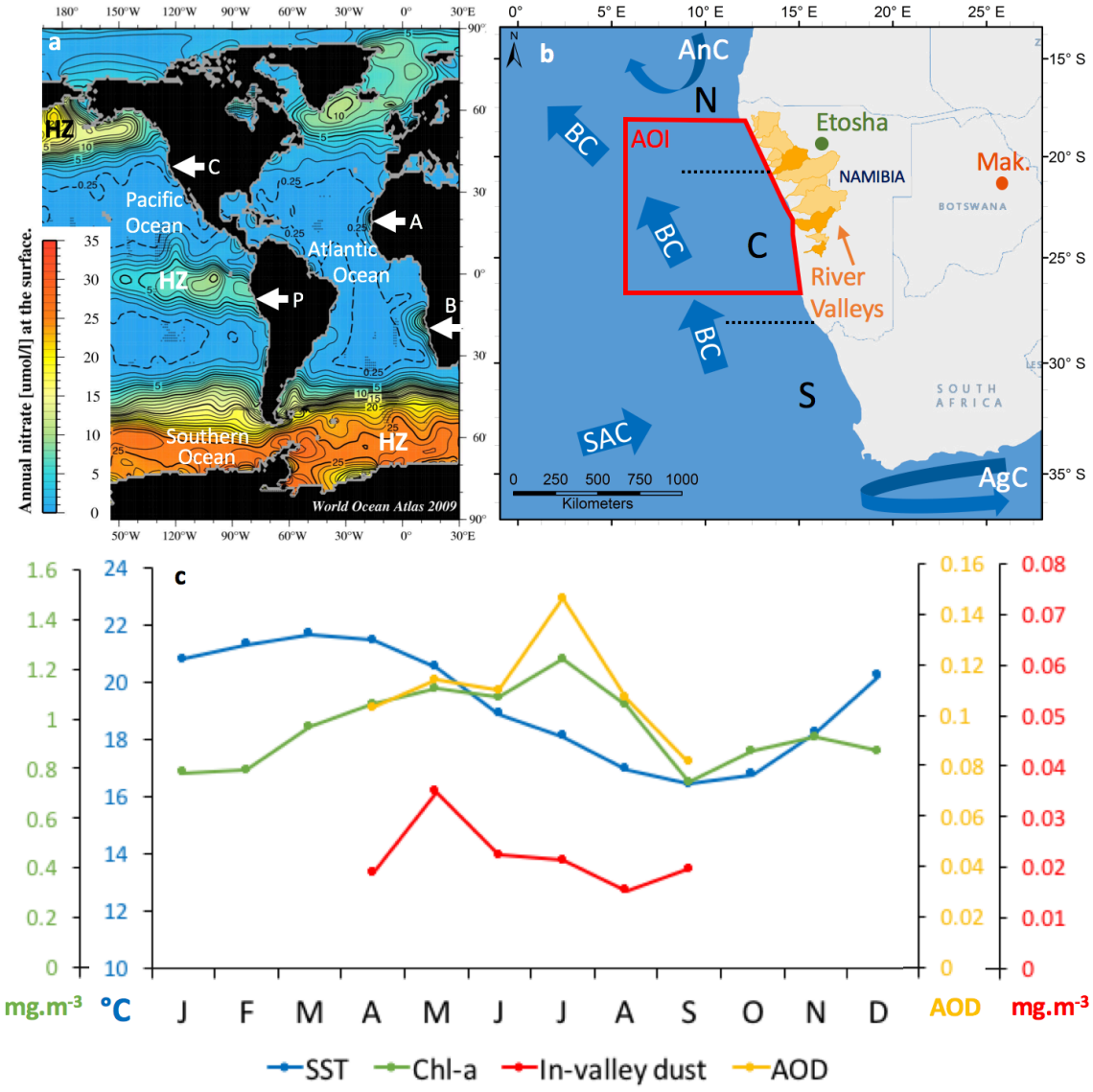


Figure 60 | a) Arrows show location of global EBUS ((C)alifornia, (P)eru, northwestern (A)frica and (B)enguela) with the annual average nitrate (µmol/L) of ocean surface waters shown. The three major global HNLC zones (HZ) are identified with the annual elevated BUS nitrate levels also shown. b) Location of the twelve Namibian ephemeral river catchments, highlighting the Huab, Kuiseb and Tsauchab systems from north to south, and southern Africa's major paleolacustrine pan dust sources, Etosha Pan and Makgadikgadi Pan (Mak.). Major oceanic currents are highlighted; Benguela Current (BC), Angola Current (AnC), Agulhas Current (AgC) and South Atlantic Current (SAC), and the (N)orthern, (C)entral and (S)outhern upwelling zones of the BUS. The area of investigation (AOI) used for AOD chl-a and SST MODIS analyses is

shown (red box). c) 2013 monthly average concentrations of chl-a and AOD, and SST temperature from the AOI (see Methods) and in-valley airborne dust concentrations from the Huab, Kuiseb and Tsauchab monitoring stations (see Methods).

SST and chl-a monthly values parallel the annual trend shown in a previous multi-year analysis (Chavez & Messié, 2009), where concentrations of chl-a do not correlate with trends in SST, i.e. plankton growth cannot be explained simply in terms of nutrients supplied by oceanic upwelling. In this investigation the relationship between SST and chlorophyll is similarly shown to be insignificant during the 2013 April-September dust season (T_{calc} 0.993 against Tcrit value of 2.447, see Figure 63a in Extended Data). Importantly however, AOD and chl-a are significantly correlated (T_{calc} 4.531 against T_{crit} value of 2.447) indicative of aeolian fertilisation of the ocean (see Figure 63b in Extended Data). These 2013 data (Figure 60c) show chl-a levels lower in June compared to May and July, departing from the long term trend of June having the highest chl-a levels through this three month period (see (Chavez & Messié, 2009)). AOD is also low in June, (Figure 60c), further suggesting that inter-annual temporal variability in dust emission may influence chl-a levels via oceanic fertilisation.

Monthly averages of in-valley dust concentration are not significantly correlated with chl-a (T_{calc} of 0.554 against T_{crit} value of 2.447, (Figure 63d)). This likely indicates that monthly data are too coarse to pick up chl-a responses to individual dust events where nutrient uptake and depletion is temporally rapid. Depletion within 1-4 days has been observed in upwelling fertilisation in EBUS (Wieters et al., 2003; Brown & Hutchings, 1987), detectable only as daily changes in chl-a concentrations (Shaw et al., 2008; Wieters et al., 2003).

Daily averages of in-valley dust concentration, AOD, chl-a and SST during the April-September 2013 dust season demonstrate this temporal averaging effect with the AOD-chlorophyll relationship positively correlated at the daily scale (Figure 61a) (T_{calc} of 5.243 against T_{crit} value of 2.0). The response in Chl-a to the AOD peaks (Figure 64) persists for one day after each dust event (+1 day chl-a lag shows significant T_{calc} value 3.781 against T_{crit} value of 2.0), becoming insignificant 2 to10 days following the event (see Extended Data Table 17 for T_{calc} values). Changes in daily SST do not show a significant relationship with chl-a levels during the same period (T_{calc} value -1.089) (Figure 61b) showing that oceanic upwelling is not a key driver of primary productivity at this temporal scale. Further, daily in-valley measurements of dust concentration show a significant correlation with AOD (T_{calc} of 2.344 against T_{crit} value of 2.0) (Figure 61c), demonstrating that the terrestrial aeolian dust emissions from the ephemeral river valleys are likely to be making a significant contribution to aerosols over the South Atlantic at a daily scale. Crucially, our measurements of in-valley airborne dust concentration are significantly correlated with chl-a at this scale of investigation (T_{calc} of 2.105 against T_{crit} value of 2.0) (Figure 61d). The strong and rapid dust-chlorophyll relationship indicates an immediate phytoplanktonic response to deposited mineral aerosols. The rapid growth and dispersal of phytoplankton patches in response to the influx of aeolian dust indicates that the ocean surface biochemical environment is otherwise limited in critical nutrients. Fine sediments in the Namibian ephemeral valleys are rich in bioavailable Fe, N and P (Dansie et al., 2016a), and these nutrients are readily scavenged when they become available (Mélançon et al., 2016).

Spatial variability in the diurnal winds responsible for dust emissions from the ephemeral river valleys (Table 18 in Extended Data and Dansie et al. (2016c)) allows the temporal and spatial comparison of chlorophyllic response to valley-specific events (see Methods

for data selection criteria). Major dust emission events limited to only the Huab and Tsauchab occurred on 1 May and 10 June 2013 respectively, and on both these dates we can demonstrate a corresponding chlorophyllic response in oceanic waters downwind from the emitting valley (Figure 62a and b). The daily ocean chlorophyll response aligns directly and significantly with individual

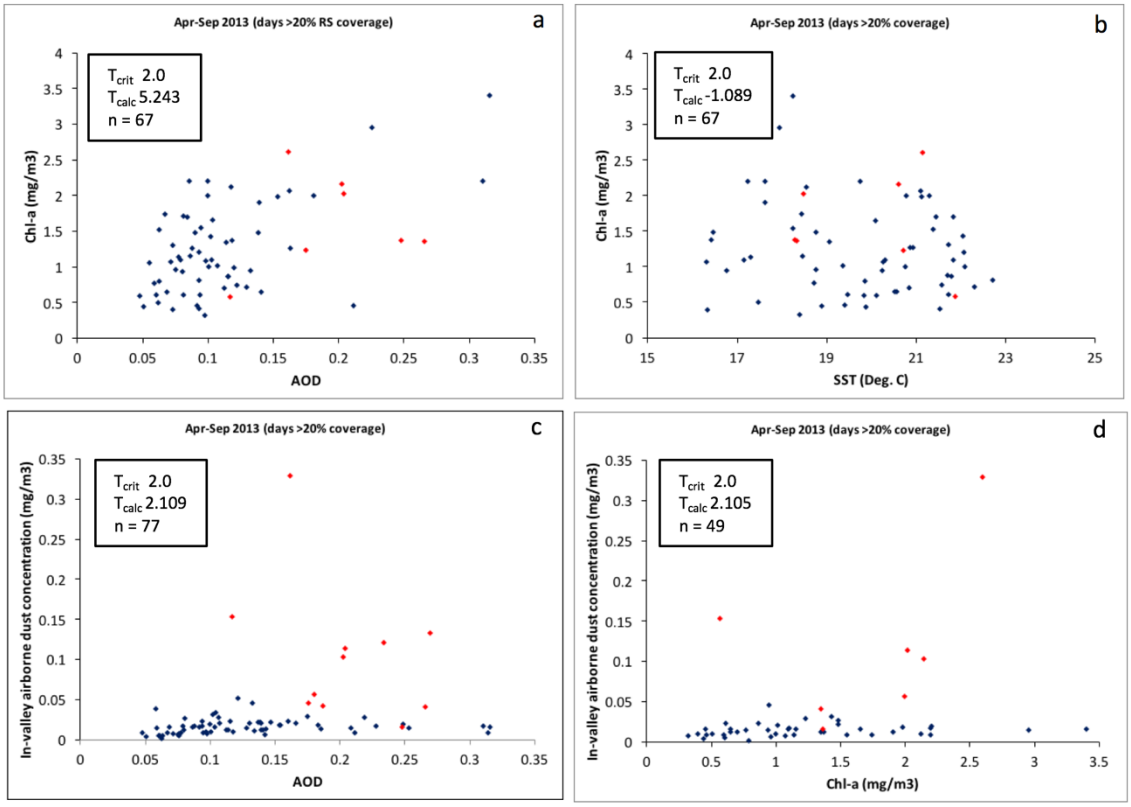


Figure 61 | Scatter plots and T_{crit} and T_{calc} values of daily averages showing the significant relationship between a) chl-a and AOD, b) no significant relationship between chl-a and SST, and the significant relationship between c) in-valley dust concentrations with AOD and d) in-valley dust concentrations with chl-a. Days of observed dust plume emission over the ocean[21] shown in red. Note that figure subsets a and b cover the period from 01 Apr – 30 Sep inclusive while c and d cover 26 Apr – 15 Sep inclusive when dust-monitoring equipment was in operation.

plumes emitted from specific valleys (Figure 62a and b and Extended Data Figures 65a-f). This has a greater significance than correlations using data over the entire depositional

area (Figure 61), clearly demonstrating the direct fertilisation of phytoplankton communities by dust deposition. Further demonstrating this direct dust fertilisation, the chlorophyllic growth was specifically observed around the margin of the AOD dust plumes (see Figure 66 in Extended Data). Non AOD-obstructed chlorophyll streaks were also observed at the beginning of the plume emission on the 17th June from the Kuiseb valley and coastal sabkha sources (Figure 67 in Extended Data). The spatial association of the chlorophyllic growth with the extent of the dust plumes further confirms that fertilisation is occurring as a direct response to deposition and the delivery of essential nutrients.

Iron deficiency has been offered as a possible explanation for primary production limitation in EBUS (Friederich et al., 2008; Hutchins et al., 2002). The upwelling of dissolved Fe is spatially constrained by the width of the underlying continental shelf (Noble et al., 2012) where Fe is produced from metal oxide-rich benthic sediments under suboxic conditions (Lohan & Bruland, 2008). Our results demonstrate aeolian fertilisation in the BUS occurs independently of upwelling over the broad continental shelf region of the central upwelling cell with the chlorophyllic bloom extent associated with that of the dust plume.

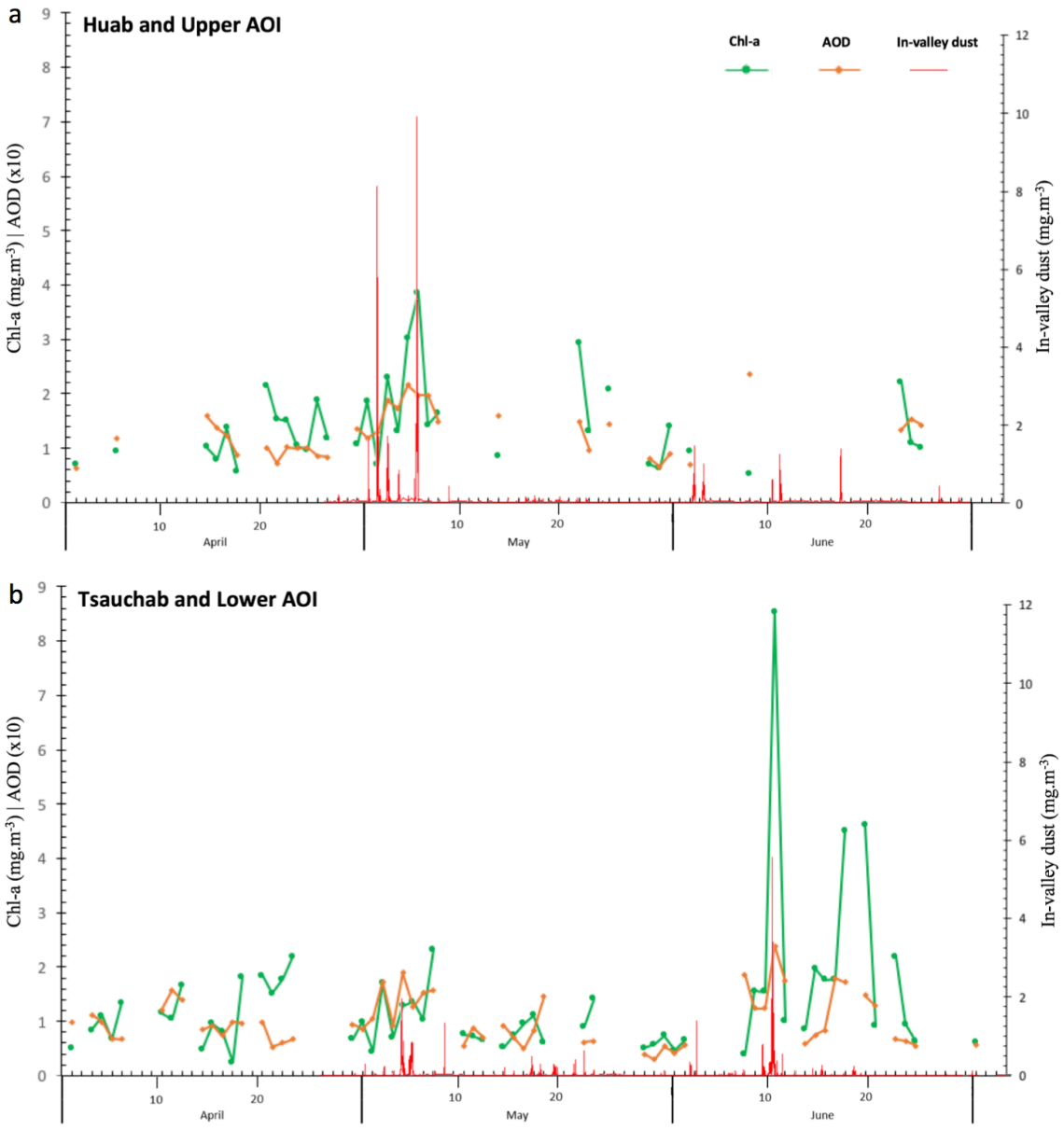


Figure 62 | Averaged two-minute in-valley dust measurements in the a) Huab, with daily AOD and chl-a concentrations in the upper AOI waters of the central Benguela upwelling cell, and b) the Tsauchab with daily AOD and chl-a concentrations in the lower AOI waters of the central Benguela upwelling cell (details provided in Methods). Upper AOI waters are shown to respond to the major Huab emission of 1 May but not in the lower AOI waters adjacent to the non-emitting Tsauchab. 10 June shows the major chl-a response to the Tsauchab emission when the Huab waters obstructed by cloud (and see Figure 64 in Extended Data regarding remote sensing data availability) and not emitting on the 10 June (Table 18 in Extended Data).

The role of aeolian dust-sourced Fe has previously been downplayed as minor compared to dissolved Fe delivery via oceanic upwelling (Noble et al., 2012), yet contributions to EBUS have relied on modeled atmospheric soluble iron deposition as proxies (Messié & Chavez, 2015). Further, of the four EBUS (Figure 60a), both African upwelling systems have the highest chlorophyllic levels and both are downwind of aeolian dust emitting desert regions (Eckardt & Kuring, 2005; Stuut et al., 2002). It is evident from our data that dust plumes from the ephemeral river valleys of Namibia play a previously un-recognised role in primary production within the complex upwelling Benguela ecosystem, providing high concentrations of Fe in which the marine system is otherwise deficient. Aeolian dust emitted from the coastal river valleys contains up to 40 times more instantaneously available bioavailable Fe than other southern African aeolian dust sources (Dansie et al., 2016a), providing an essential external source of Fe into the oceanic system, and, we propose, the most important aeolian source of nutrients for marine primary production. To date, models used to estimate aeolian input to the BUS (e.g. Messié & Chavez (2015), Noble et al. (2012) and the terrestrial sources of emission described therein) have not included the significant dust-emitting Namibian valley sources. Dust emission models traditionally use TOMS-sourced identification of mineral aerosol concentrations occurring >1 km above ground level (e.g. Prospero et al. (2002)), which due to low resolution data fails to identify spatially smaller dust source areas such as Namibia's river valleys. The increasing spatial resolution of global dust emission assessments (most notably Ginoux et al. (2012)) are showing that many small-scale geomorphological features are significant sources of aeolian dust and, as we have demonstrated in the case of ephemeral river valley systems, these can have a critical impact on oceanic primary production.

8.1 Methods

In-valley airborne dust (Total Suspended Particulates) monitoring

Nine DustTrak™ DRX aerosol monitoring stations (Wang et al., 2009) were erected in the Huab (4 stations), Kuiseb (2 stations) and Tsauchab (3 stations) river valleys as described in Dansie et al. (2016c). This instrument recorded PM1, PM2.5, PM5 and PM10 and total suspended particulate (TSP) in-valley airborne dust concentrations at a height of 3.18 m at two-minute intervals throughout the study period (26 April – 15 September 2013). The TSP measurements were used for this study with daily averages of the two-minute TSP calculated for statistical analyses (see below). At each site an automatic weather station was erected measuring average wind velocity at 3.18 m, and wind direction (3.18 m height) at an interval of one minute (as described in Dansie et al. (2016c)). Site location was informed by the work of Vickery et al. (2013) that had identified areas of significant dust emission in the lower valleys using remote sensing analyses.

8.1.1 Remote sensing

The atmospheric investigation of dust plumes emitted from the river valleys was undertaken using the Moderate Resolution Imaging Spectroradiometer (MODIS) Terra and Aqua Deep Blue Dark Target AOD[13] Collection 6 data (550 nm) product ('aod') that has been optimised algorithmically for AOD identification and cloud removal over land (Hsu et al., 2013) and ocean (Sayer et al., 2014). The MODIS Aerosol Product (AOD) monitors the aerosol optical thickness globally with daily Level-2 data products produced at the spatial resolution of a 10x10 1-km pixel array (at nadir). Data were downloaded

[13] Long name: MODIS Deep Blue AOD version 6 data reprojected from Level-2 tiles and concatenated into gridded daily field.

from https://ladsweb.nascom.nasa.gov and described in detail here: http://modis-atmos.gsfc.nasa.gov/Webinar2014/MODIS_Collection6_week4_DTDBmerge.pdf.

The oceanic investigation of chlorophyll and sea surface temperature was undertaken using MODIS Terra and Aqua (4 km spatial resolution) mapped daily Level-3 'chlor_a' and 'sst' data products. Surface water concentration data of chl-a is generated with the Ocean Colour Index (OCI) algorithm as described by Hu et al. (2012), using three bands of blue-to-green wavelength reflectance (between 440 – 570 nm) to estimate chl-a concentrations based on empirical relationships defined by in situ measurements. Sea surface temperature measurement was based on longwave (11-12 μm) thermal radiation (daytime) data as described by Minnett et al. (2004). Both data sets were downloaded from http://oceandata.sci.gsfc.nasa.gov.

The 'aod', 'chlor_a' and 'sst' datasets were plotted (10°S, 10°W by 30°S, 20°E) and visually inspected to determine the transport extent of mineral aerosols, chlorophyll distribution and upwelling. This then informed the area used for calculation of the 'aod', 'chlor_a' and 'sst' average values. A total pixel count for each dataset was calculated, including pixels containing no data due to cloud/fog masking or gaps in satellite data collection swaths. At the daily scale a pixel count of data-only pixels was calculated and % coverage of the area of investigation determined for each day. The western boundary of this was N-S from 18°S, 5°E to 26°S, 5°E and extending eastwards to the Namibian coast. This total area comprised 16 subsets that were combined to allow for the curvature of the coastline. Any days with <20 % data coverage, as calculated by pixel count, were excluded from further analyses. The average MODIS Terra and Aqua average values were then combined (average of both satellite measurements) to produce final 'aod', 'chlor_a' and 'sst' daily values. Only days with ≥20 % data coverage of each 'aod',

'chlor_a' and 'sst' were used for t-test calculation of correlation significance. Daily value correlation was determined using two-tailed t-tests, calculated using the formula:

$$t_{calc} = r.\sqrt{\frac{n-2}{1-r^2}}$$

where r is calculated as:

$$r_{xy} = \frac{(\Sigma_{i=1}^{n} x_i y_i) - n\bar{x}\bar{y}}{(n-1)s_x s_y}$$

Significance was determined using a two-tailed p value of 0.05 against T_{crit} values according to *n* for each calculation. For the spatial consideration presented in Figures 62 and 65 the same approach as above was undertaken but extending N-S; upper AOI waters (18°S, 5°E to 22°S, 5°E) and lower AOI waters (22°S, 5°E to 26°S, 5°E) and the eastern extent following Namibia's coastline.

8.2 Extended Data

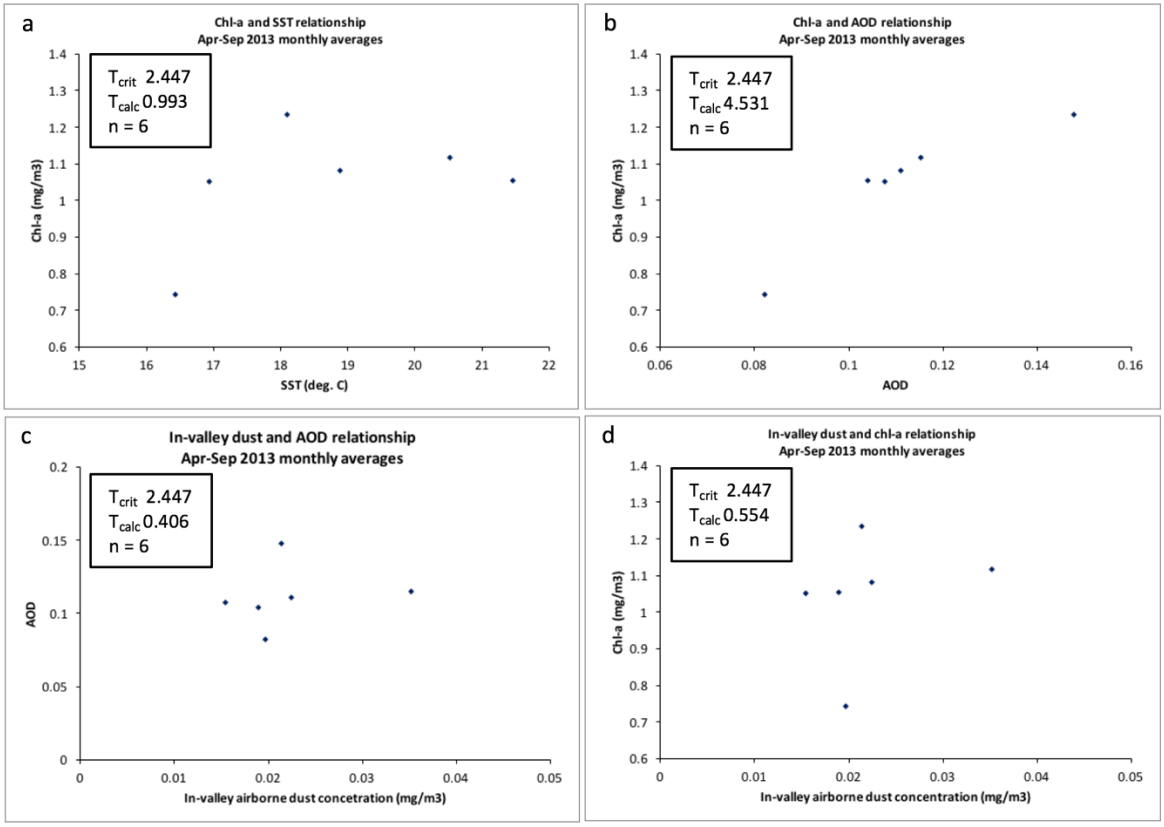


Figure 63 | Scatter plots, T_{crit} and T_{calc} values of monthly averages showing no significant relationship between a) chl-a and SST, b) the significant relationship between in-valley dust and AOD, and no significant relationship between c) chl-a and AOD or d) chl-a and in-valley dust.

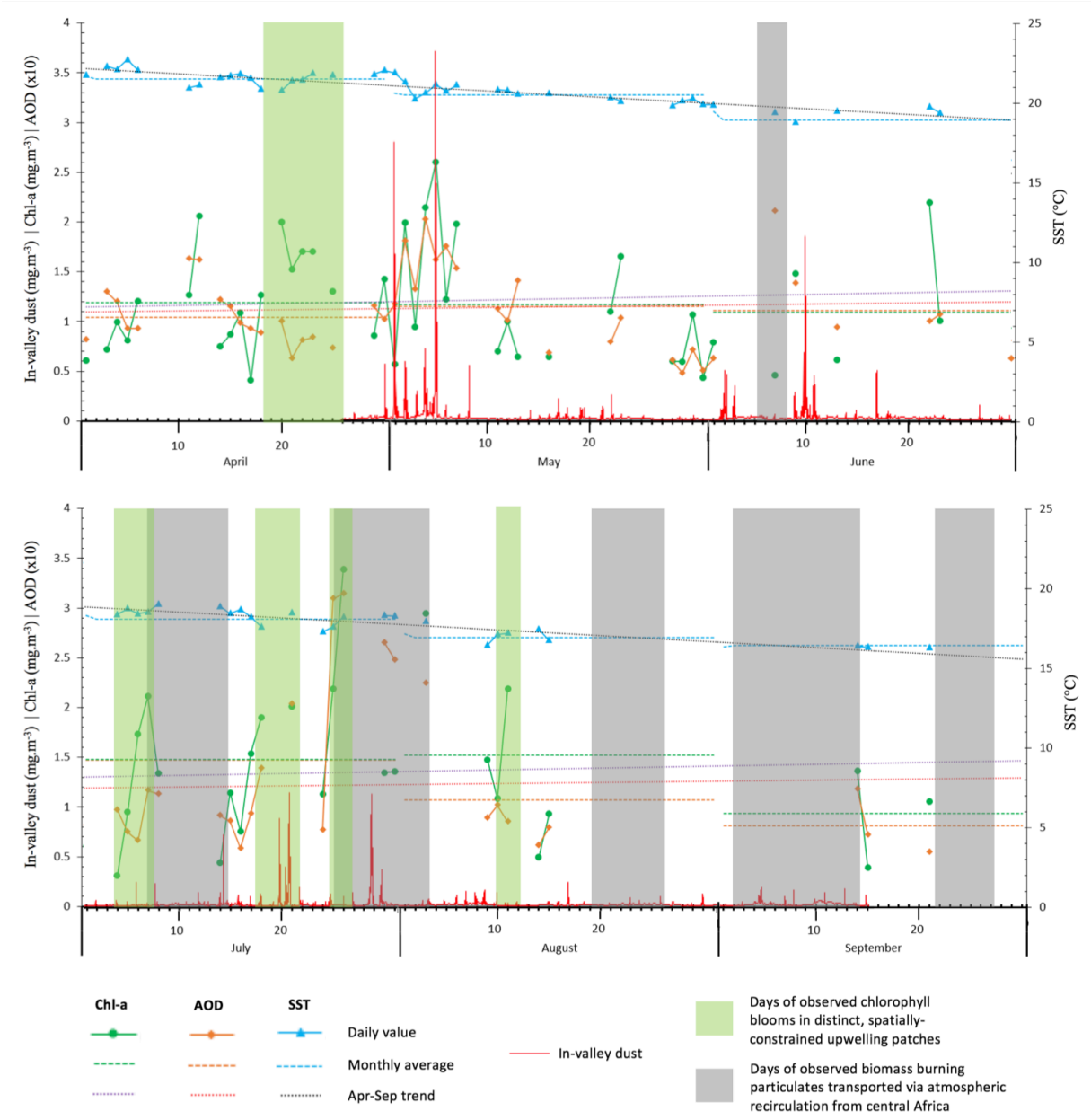


Figure 64 | April-September 2013 two-minute in-valley dust concentration measurements (averaged across all stations in the Huab, Kuiseb and Tsauchab), daily MODIS Terra and Aqua averages chl-a, AOD (multiplied by 10 for scaling purposes) and SST levels (≥20 % coverage, see Methods) with monthly averages and April-September six-month trend lines shown. Analysis of multi-day trends in the region posed difficulties due to the prevalence of atmospheric moisture at both high altitudes (cloud cover) and near-surface fog generated the cold upwelling region itself (Eckardt et al, 2013). During the six months of investigation 37% (67 days) had over 20% coverage, with the longest unobstructed duration being between 29 April to 7 May. Further, once

the short-lived and diurnal dust-delivering easterly winds (Lindesay & Tyson, 1990) subside the dominant regional weather circulation of south to southwesterly trade winds (Lancaster, 1985) resume, which are laden with atmospheric moisture and resultantly causing frequent obstruction of the ocean surface by clouds. August and September were the most data-sparse months with 51 days obstructed by clouds and fog and also saw minimal dust activity in the river valleys. July, August and September saw increased AOD values associated with the recirculation of air mass from central Africa bringing particulates from biomass burning in that region, the recirculation a known-occurrence during these months caused by a semi-permanent continental high pressure cell that provides significant influence on the subtropical atmospheric circulation in the region (Tyson & D'Abreton, 1998). The increase in fire activity during these months in Angola, the Democratic Republic of the Congo, and neighbouring smaller countries is visible using the 'Terra/Aqua Fire and Thermal Anomalies' product of the MODIS satellites with the recirculated biomass haze visible on MODIS true colour imagery (www.worldview.earthdata.nasa.gov) and on plots of daily AOD MODIS data used to calculate daily means in this study. The increases in chl-a on data-available days in July appeared to be the result of upwelling. These months were therefore excluded from further analyses. April, May and June were selected as the optimum months for assessing oceanic response to dust plumes originating from Namibia's coastal valleys.

Table 17 T_{calc} and T_{crit} values showing decreasing correlation between AOD and chl-a from the day of dust plume emission (0) until 10 days following the event.

Day	T calc value	T crit value	*n*
0	5.243	2	67
+1	3.781	2	53
+2	0.154	2.021	41
+3	0.870	2.042	38
+4	0.682	2.042	43
+5	0.132	2.042	43
+6	0.820	2.042	46
+7	0.132	2.042	43
+8	0.834	2.021	46
+9	-0.434	2.021	46
+10	-0.452	2.021	49

Table 18 Average dust concentration along river valleys (averaged two-minute 'total dust' measurements of all stations in each valley) during dust events on dates of ocean-bound plume emission ($mg.m^{-3}$) (from Dansie et al. (2016c)).

		Huab	Kuiseb	Tsauchab
May	1	8.10		
	4		0.41	1.88
	5	**9.87**	**0.25**	**0.83**
	6		0.42	
June	10		0.16	5.34
	11		0.13	
	17		0.51	
July	**21**	**2.72**	**0.22**	**2.38**
	29			3.25
	30	**1.04**	**0.12**	**-**
	31		0.95	

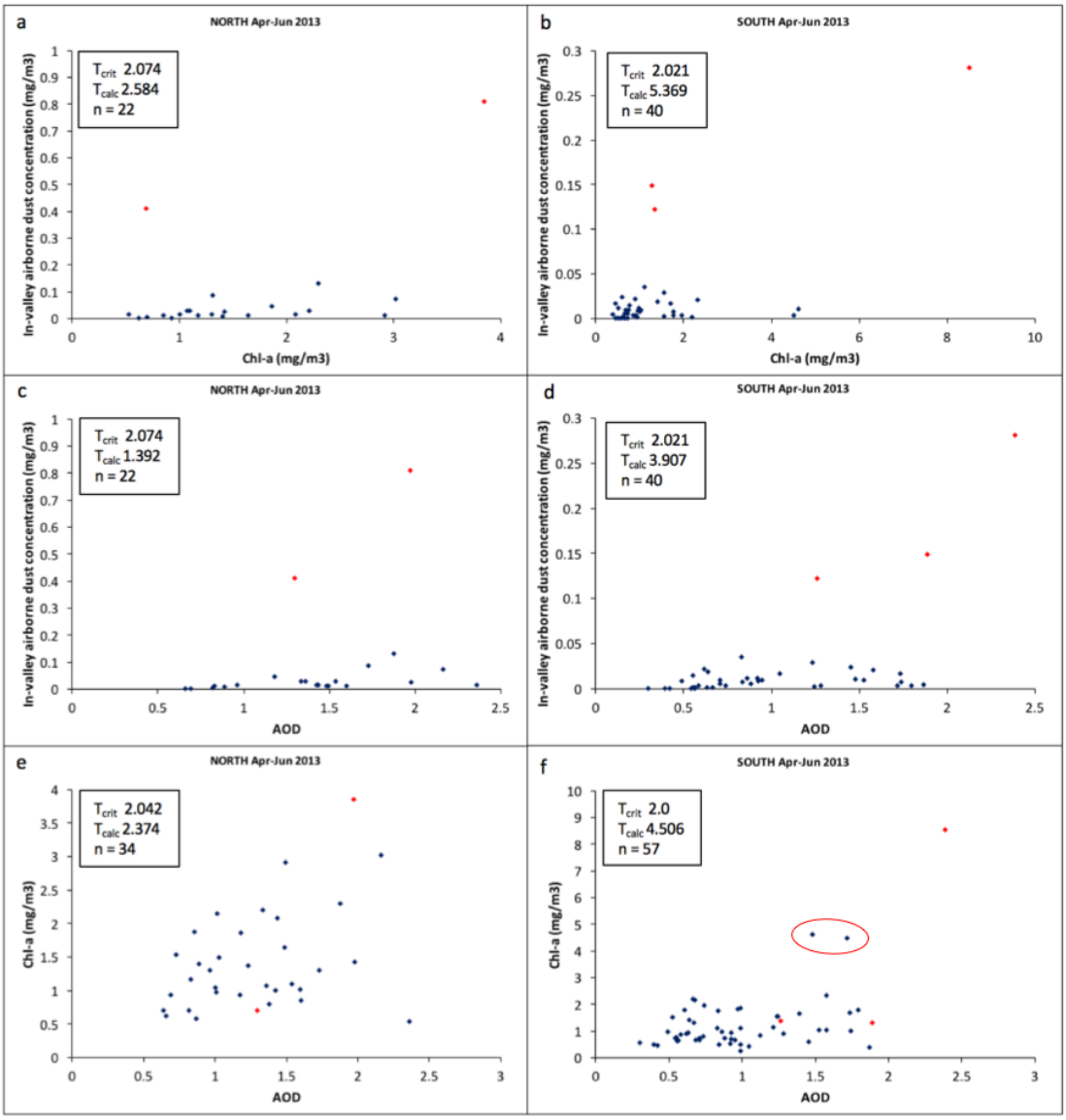


Figure 65 | Scatter plots of daily averages and T_{crit} and T_{calc} values for the Huab and upper AOI waters (a, c, e) and Tsauchab and lower AOI waters (c, d, f) of the BUS central upwelling cell. Significance is demonstrated for all correlations with the exception of (c) AOD and in-valley dust in the Huab. Days of observed dust plume emission over the ocean (as described in Dansie et al. (2016c)) shown in red. Circled points in (f) are the 17 and 19 June where coastal emissions were observed on MODIS true colour imagery (www.worldview.earthdata.nasa.gov) rather than in-valley locations and were not recorded by the in-valley dust.

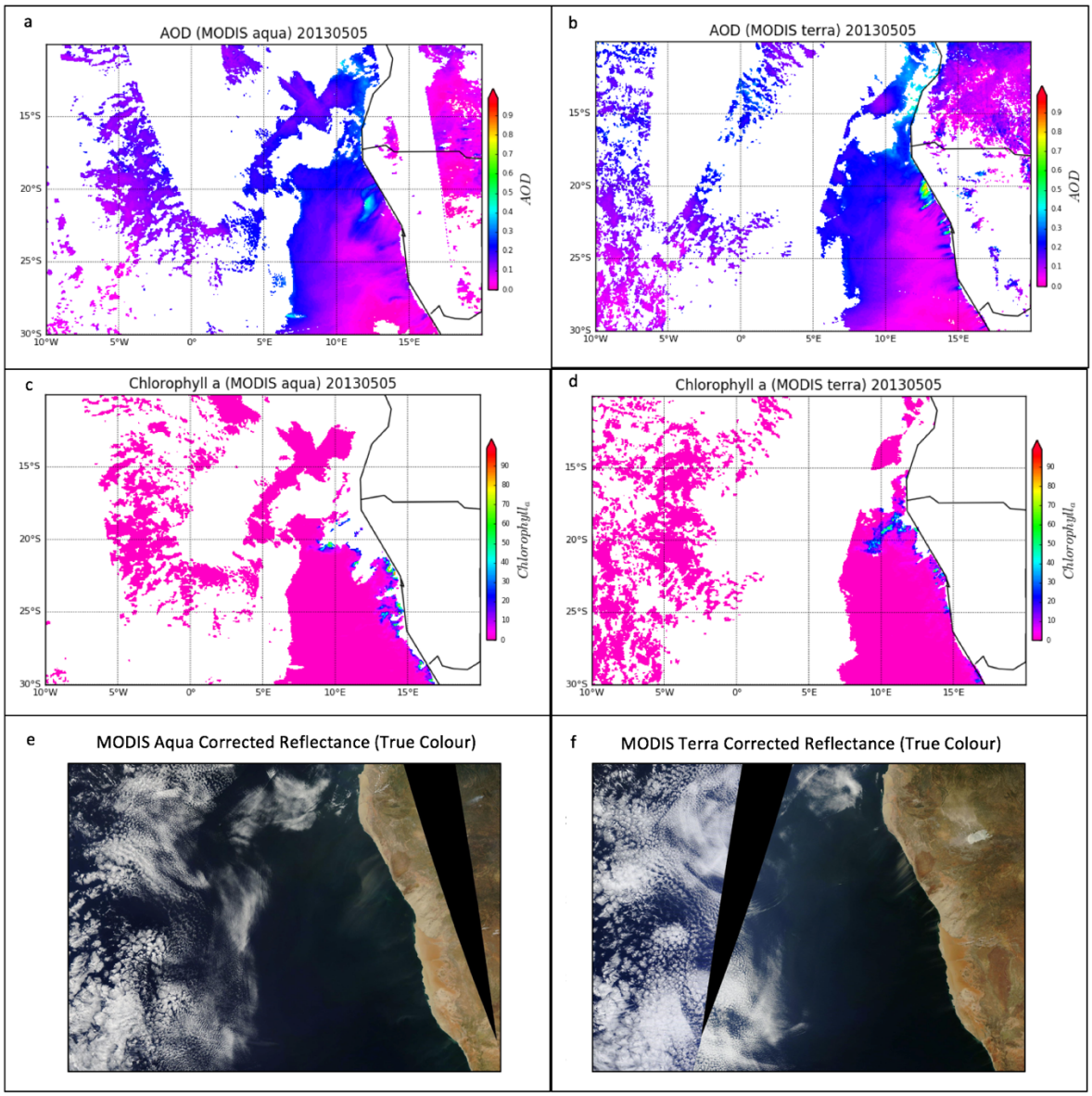


Figure 66 | AOD plots showing dust plumes emitted on 5 May 2013 captured with MODIS Aqua (a, c, e) and Terra (b, d, f) with chlorophyllic response recorded around the proximity of the dust plume shown in MODIS c) Aqua and d) Terra 'chlor-a' measurements. True-colour imagery provided in e and f, noting that distinct upwelling phytoplankton filaments are not occurring as clearly visible in the example provided in Figure 68.

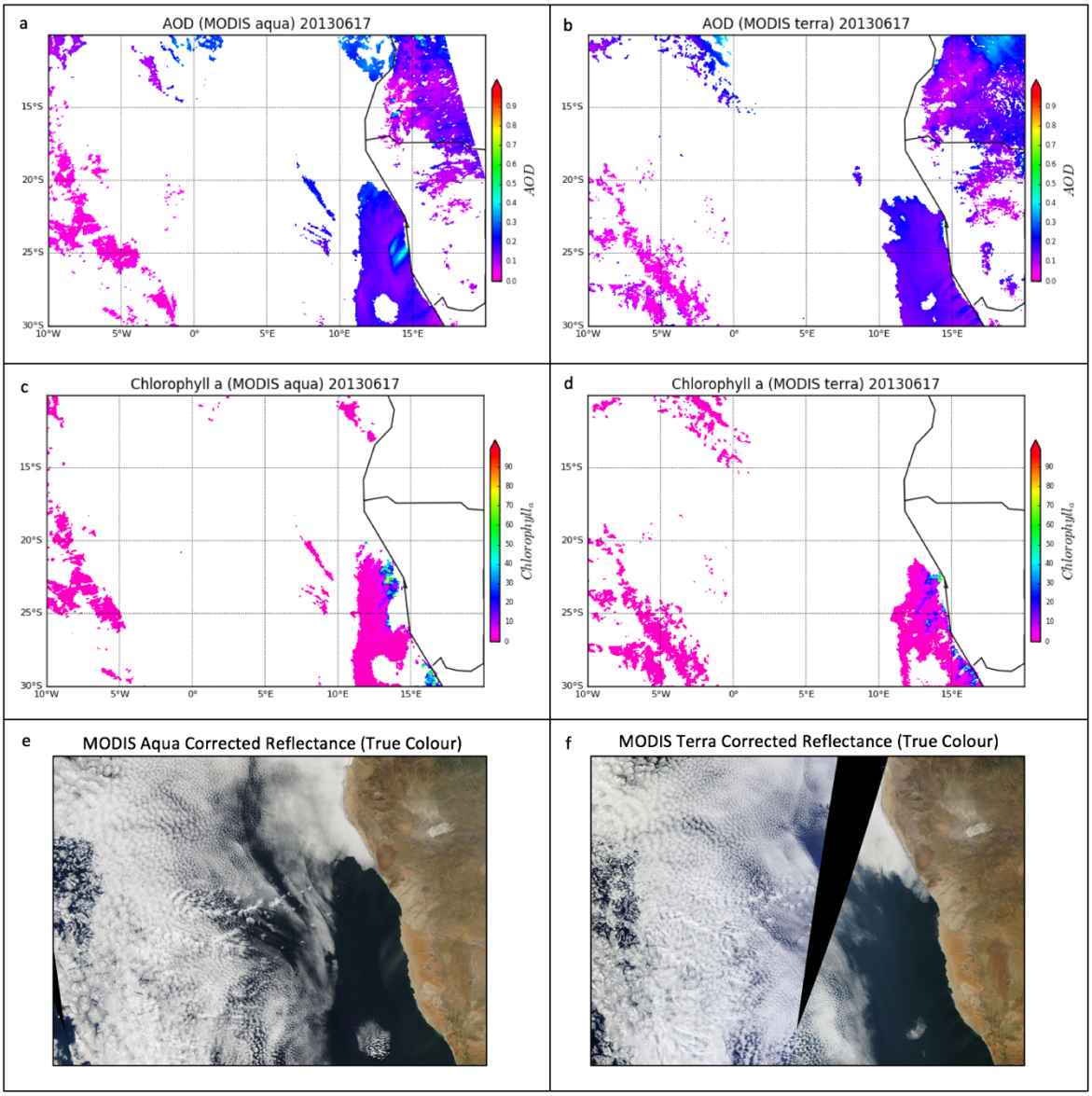


Figure 67 | AOD plots showing dust plumes emitted on 17 June 2013 captured with MODIS Aqua (a, c, e) and Terra (b, d, f) with chlorophyllic response recorded around the proximity of the dust plume shown in MODIS c) Aqua and d) Terra 'chlor-a' measurements. True-colour imagery provided in e and f, noting that distinct upwelling phytoplankton filaments are not occurring as clearly visible in the example provided in Figure 68.

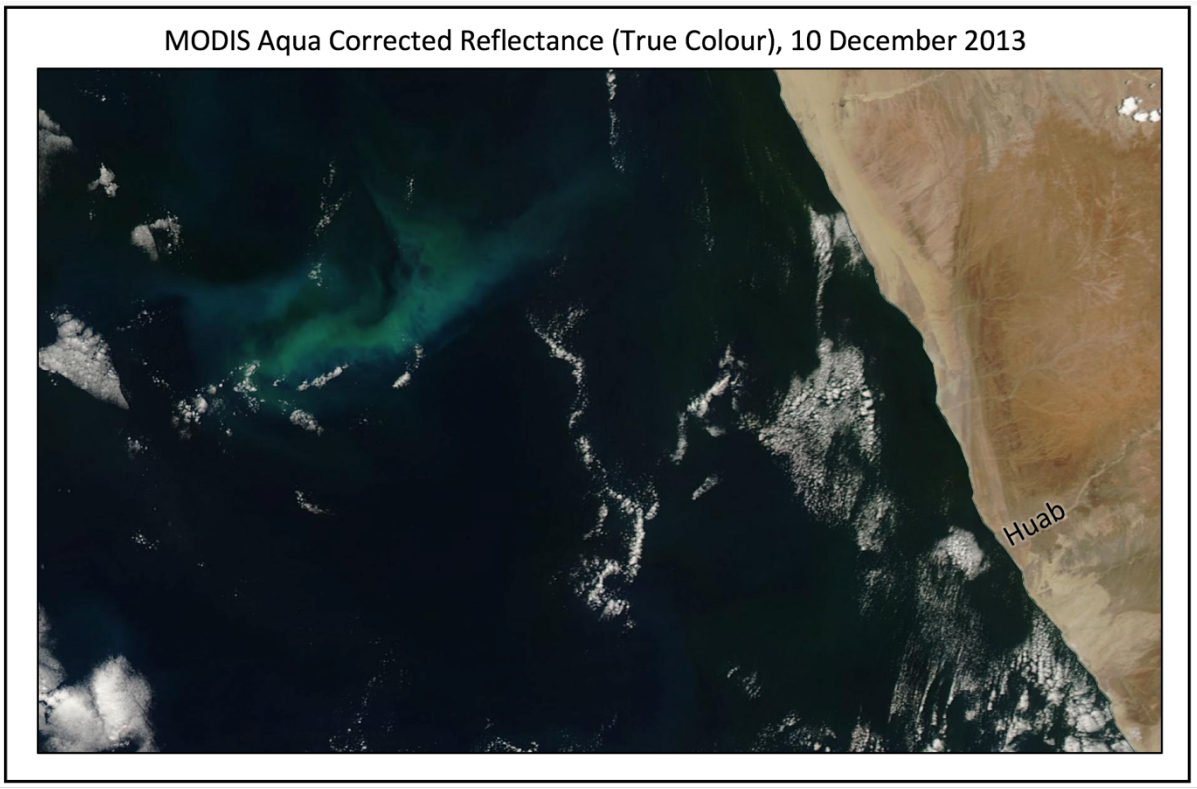


Figure 68 | Distinct upwelling-induced phytoplankton bloom on 10 December 2013 (intense upwelling-induced primary production events of such a scale did not occur during the investigation period but smaller, similarly localised patches were identified as shown in Figure 64).

Acknowledgements: We thank R. Bryant and M. Fettweis for discussion and advice on remote sensing instrumentation; J. Mayaud for statistical analysis guidance; the Namibian Ministry of Environment and Tourism for their support and assistance, especially with access to field sites permitted under permit number 1788/2013, and; the staff of the Gobabeb Research and Training Centre for their support in the field. This research has been carried out in collaboration with the Natural Environment Research Council (UK) grant NE/H021841/1 with additional funding from the Clarendon Fund of the Oxford University Press (researcher stipend and support) and the John Fell Fund (partial support of fieldwork activities).

CHAPTER 9

9 Conclusion

9.1 Research Aim and Objectives

The overarching aims of this study, to determine the sediment characteristics, nutrient content and deflation dynamics of dust plumes from the ephemeral river valleys of Namibia, and to investigate whether chlorophyll concentrations in the southern Atlantic respond to observed dust events, have been addressed through the four research papers presented in Chapters 5-8 and the additional associated text. Each of the four papers chronologically addressed one of the four research objectives, to:

1. determine the physical characteristics and nutrient content of surficial sediment in the dust-emitting dry river valleys along the coast of Namibia.
2. investigate the spatial distribution of surficial sediment nutrient content along the river channels and upper catchments and identify any relationships with climate, geology, and land use.
3. determine the physical characteristics and nutrient load of near-surface windblown sediment associated with large dust events derived from the ephemeral valleys.
4. investigate the potential response of phytoplankton in the Southern Atlantic Ocean to observed dust emission events.

Addressing objectives one and two through laboratory analyses, Chapters 5 and 6 investigate the nutrient load of surface sediments, respectively determining nutrient

concentrations of sediment in the dust emitting lower-reaches of the river valleys and along the river systems onto their upper catchments on the Great Escarpment. This research has shown that the dust-emitting regions of the ephemeral river valleys of Namibia contain sediments that are enriched in nutrients compared to their upper catchments. While some association was found within upper catchments between climate and vegetation with nitrogen, and geology with phosphorus, the enrichment of N, P and Fe nutrients occurs along the hydrological descent irrespective of upper catchment climate gradient, vegetation, land use or geology. In the lower, dust-emitting regions of the river valleys, investigation of the geomorphological sediment types demonstrated that the enriched sediments also contained an abundance of aeolian-transportable fines (<100 μm), making them highly viable source areas for ocean fertilisation. Most importantly, the bioavailable iron content of the river valleys was found to be regionally significant with levels up to 40 times that of Etosha and Makgadikgadi Pans. The nutrient content and grain size distribution of the dust source area sediments were similar between the three river valleys investigated. The thorough comparison of nutrients within and between the river valleys and their catchments allows us to propose that the other nine ephemeral river valleys (Figure 16) could be expected to possess similarly enriched sediments in their known dust-producing regions (as identified by Vickery et al. (2013)) in Figure 13.

To address the third objective, Chapter 7 presents the sediment and nutrient characteristics of deflated dust in the river valleys within the context of the dust events observed for the 2013 dust season. As previously identified in the source sediment, bioavailable Fe concentrations were also the most important constituent of the aeolian nutrient flux for ocean fertilisation. We have shown that ocean-bound dust collected in the river valleys carries regionally significant levels of nutrients, similar to the in-valley source sediment, that are of greater primary production fecundity than either of southern

Africa's major Pan sources. The 18 observed events support previous work that the river valleys are regular and productive emitters of dust, due to diurnal forces, and deflated sediments in the river valleys are transported to the ocean.

A study adjunct to the thesis was undertaken on the replenishment cycles of the dust-source sediments, by looking at the deposition age of river valley alluvium in the Huab river valley, and this work is presented as an appendix to the main thesis (Appendix 1). The findings demonstrate a strong relationship between productive dust source sediments and the Holocene alluvium that now forms the modern valley floor. Age determination using optically stimulated luminescence (OSL) dating of sediment units from the incised-bank of the modern channel adjacent to site H2 show the most recent major flooding and depositional event preserved in the system was ca. 600 years ago (Figure 69).

Younger floods may have occurred, but sediments have either been removed by subsequent deflation or are not present at this particular location. Multiple flood events are recorded in the valley fill, up to 10k years old in the exposed channel cuts and likely older in the deeper valley fill deposits. Historical fluvial deposits in arid environments have been characterised to have higher soluble Fe content than exposed, non-fluvial surface soils due to the weathering and aging of Fe oxides reducing the bioavailable fraction of Fe (Shi et al., 2011). This is supported by the Namibian river valley data where the alluvium, and dust deflated from it, are enriched in bioavailable Fe compared to the sediments of other geomorphological units in the catchment. Therefore, even with infrequent replenishment by major flooding and depositional events, dust emission from the ephemeral river valleys is not considered to be sediment supply-limited. This would also suggest that the biogeochemistry of the deflated dust from the river valleys would be

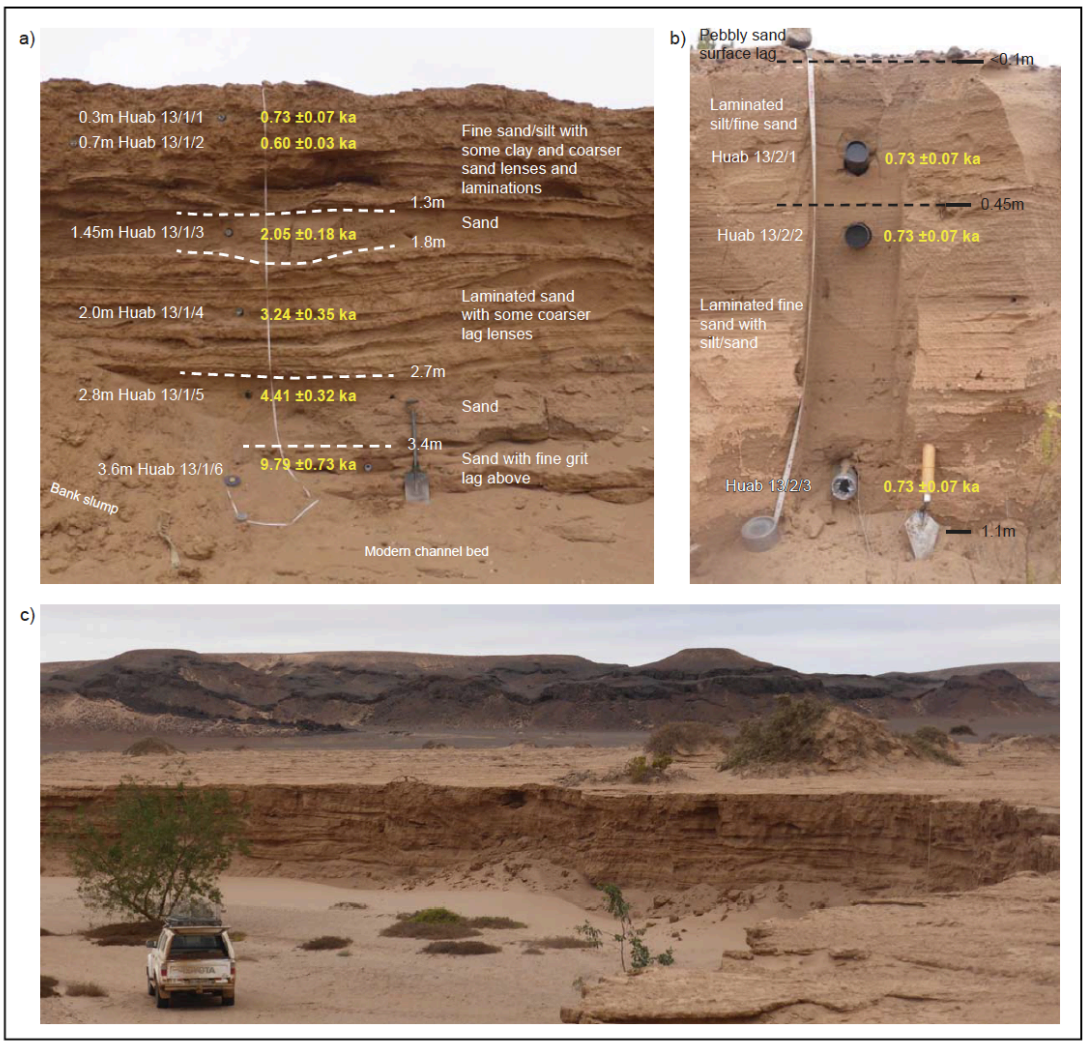


Figure 69 | a-b) Valley fill sampling sites for age determination taken near H2 monitoring station site. c) shows the main channel incision and exposure of valley fill sediments, (figure as presented in the fifth paper provided in Appendix 1.

reliably enriched in bioavailable Fe and macronutrients, as reported in Chapters 5, 6 and 7, independent of recent flooding events. It is known that the variability and endoreic tendency of ephemeral flooding events in the twelve catchments produces a patchwork of depositional sediment along the valleys, with recent flood deposits reported from other Namibian valleys that act as dust sources. For example, large flood events leading to the deposition of datable sediments occurred in the Kuiseb every 30-40 years during the last

millennium (Grodek et al., 2013) and 66 floods have been recorded between 1963-2010 in the Swakop (Greenbaum et al., 2014). Flood events would rework the highly-erodible existing valley fill and sediment replenishment would occur from the upper catchment with these processes providing an abundance of surface fines (Tooth, 2000; Reid & Frostick, 1987) that upon desiccation in the arid landscape would easily be eroded by winds in the river valleys (Von Holdt, 2013). Years subsequent to major flooding events may also be expected to see increased dust emission and higher N and P enrichment associated with hydrological biological productivity (Steward et al., 2012; Belnap et al., 2005) and may have already been eroded in the Huab sampling site. A subsequent stage of research building on the findings presented in this thesis would be to investigate dust emission between river valleys before and after major flooding years and to also attempt sediment biogeochemistry and dust monitoring field studies following the cessation of flood events.

The fourth research objective is investigated in Chapter 8 by the investigation of the spatial and temporal concentration of oceanic phytoplankton correlated with observed dust events. The results demonstrate that a rapid chlorophyllic response to aeolian fertilisation is occurring within the Benguela Upwelling System. Until now the role of depositional fertilisation in this complex system had not been identified or appreciated yet aeolian dust is shown to provide a crucial nutrient delivery mechanism to the highly productive BUS waters. Importantly, the research provides correlation between in-valley windblown dust measurements in Namibia's river valleys and chlorophyll concentrations at the daily scale. The findings presented in Chapters 5-7 gives evidence of the nutrient-enriched river valley dust, most importantly bioavailable Fe, that provides an instantaneously available nutrient input to the highly productive waters supporting the response observed at the daily scale. Positive correlation between in-valley dust and AOD

at the daily scale, and AOD and chl-a at daily and monthly scale further support the finding that dust fertilisation from the ephemeral valleys is occurring in the upwelling region of the South Atlantic.

9.2 Implication of findings within the context of the highly productive Benguela Upwelling System

The Atlantic Benguela upwelling region supports one of the highest primary production rates in the world's oceans (Toggweiler & Carson, 1995; Chavez & Barber, 1987). The role of dust-sourced Fe has previously been downplayed as minor compared to upwelled sources (Noble et al., 2012), yet there are good reasons to question this. The significance of this aeolian nutrient pathway has been overlooked due to two reasons. The first being the unintended exclusion of the Namibian river valleys as contributing dust sources in model-based analyses. The models used to estimate aeolian input into annual productivity cycles in the BUS have relied on flux estimates using Makgadikgadi and Etosha Pans as the main sources. Dust emissivity inputs used in models that have been applied to the research area rely on source emission data that either exclude non-pan sources (Luo et al. (2003), Ginoux et al. (2004), Prospero et al. (2002)) or in the case of Tegen et al. (2004) focus only on agricultural sources. Dust from the ephemeral river valleys is therefore not included in these assessments and a major aeolian contribution to the region is lacking. Such dust emission models align with the identification of global 'hot-spots' of dust emission that has traditionally relied on TOMS identification which identifies dust at 1 km above ground level (e.g. Prospero et al. (2002)). Models that look at dust emission, transport and deposition therefore need to be improved to take account of the expanding identification of dust source emission (i.e. Ginoux et al. (2012)). Sub-basin scale dust source identification in southern Africa had been undertaken by Vickery et al. (2013),

using a combination of remote sensing and visual identification not feasible at a global scale, that demonstrated that the ephemeral valleys of Namibia are more frequent emitters of dust than Etosha and Makgadikgadi Pans combined (Vickery et al., 2013). This non model-based approach then allowed field-based investigation of the dust sources to be feasibly designed and implemented which could then be used to investigate chlorophyllic response to monitored and sampled events.

The second reason is the short but intense response to dust deposition observed which has required identification using high temporal and spatial resolution assisted by the land-based monitoring. The combination of HNLC-equivalent waters of upwelling systems (Capone & Hutchins, 2013) and deposition of highly bioavailable Fe enriched aerosols allows immediate phytoplanktonic uptake and a swift growth response (Shaw et al., 2008; Furnas et al., 2005), as demonstrated in this research. This is in agreement with the chlorophyllic traits of the BUS, which is notable in comparison to the other EBUS in having greatly reduced seasonal fluctuation and instead being dominated by higher-frequency intraseasonal variations in chlorophyll (Chavez & Messié, 2009).

It is noted that aeolian fertilisation is one factor in the complex and highly fertile BUS but a factor that has been underrepresented in the annual productivity cycle of the system. Deep water upwelling on the continental margin is the prime contributing mechanism, by far, for the high ocean productivity found in all the four global EBUS. The transport of nutrient-rich deep waters (i.e. nitrates (Chavez & Messié, 2009), phosphates (Neumann et al., 2016), metals (Noble et al., 2012)) to the photosynthetic ocean surface remain the main driver behind the profound levels of primary production occurring in these systems. Yet the four systems show significant variation in chlorophyllic production between the systems (Carr & Kearns, 2003) that cannot be explained by the upwelling of water and

nutrients alone, suggesting that other factors, such as dust fertilisation, play a role in productivity between the systems.

Of the four EBUS the Benguela hosts the highest surface chlorophyll levels but this does not correspond with the highest nitrate levels, rejecting the hierarchical agreement of nitrate and chlorophyll relationships seen between the other three systems (highest to lowest chlorophyll levels: Benguela, Northwest Africa, Peru then California) (Chavez & Messié, 2009). Notably, the two highest chlorophyllic systems both share major dust emission hot-spots downwind, to their east; in the north the Saharan dust emitting sites (Gross et al., 2015; Washington & Todd, 2005), and in the south the paleolacustrine Etosha and Makgadikgadi Pans as well as the Namibian ephemeral river valleys (Eckardt & Kuring, 2005; Stuut et al., 2002). It has previously been shown that the Saharan dust provides essential nutrients that trigger phytoplankton growth in the waters of the upwelling region of the eastern North Atlantic (Mills et al., 2004). Our research has demonstrated that the waters of the BUS similarly respond to the addition of growth-limiting nutrients from external aerosol deposition. This contributes to the consensus of growth-triggering fertilisation by aeolian deposition in HNLC regions globally (Guieu et al., 2014a) with the overall fertilisation effect of desert-derived aerosols being widely agreed on (Jickells et al., 2014; Mahowald et al., 2005; Ridgwell, 2002).

9.3 Global relevance and application

The global dust cycle is one of the biggest uncertainties in modelling future climate scenarios (Schulz et al., 2012) despite its prevalence in atmospheric and oceanic cycles (Choobari et al., 2014). The significant impacts that dust deposition has on N, P and Fe ocean biogeochemistry (Mahowald et al., 2010) are a major factor in constraining global models to generate empirically-based scenarios that account for both contemporary and

future dust sources under a changing climate (Jickells & Moore, 2015). A crucial, yet under-developed, empirical component of the models are the heterogeneous nutrient characteristics of dust source areas (Zhang et al., 2015). This research has demonstrated the regional significance of a dust source that has been until recently excluded from global source identification efforts and not yet incorporated into global models. Accordingly, the findings of this research also have global relevance and application. The relevance is to consider the combined effect on the global ocean of numerous, non 'global hot-spot' categorised dust sources that may also be 'highly-fertilising' compared to the traditional research foci on paleolacustrine sources, especially for riverine dust sources in anthropogenic-impacted systems. The application is the incorporation of the findings into global dust and ocean fertilisation models and to inform field-based sampling priorities.

Global Relevance

The combined effect on the productivity of the global ocean of numerous, non 'global hot-spot' categorised dust sources may be profound. Advances in the resolution of dust source mapping using remote sensing identification, e.g. MODIS Deep Blue detection by Ginoux et al. (2012), is demonstrating an abundance of 'small-scale' dust emission features not yet incorporated into regional or global dust assessments. Further, sub-basin assessments, e.g. the work by Vickery et al. (2013) and Bullard et al. (2008), are demonstrating that dust emissions from topographic regions are not homogeneous but are influenced by fluvial activity and surface sediment geomorphology. The DO4 Models project in Botswana demonstrated a temporal and spatial variation of erodibility within a 12 km^2 section of the Makgadikgadi Pan system (Sua Pan) much higher than is currently used in the 12x12 km grids of global climate models (Haustein et al., 2015). The results far exceeded expectation with the majority of deflated material coming from a fraction of the surface area. The heterogeneity was the result of a combination of surface moisture,

surface roughness altered by salt crystal formation (described in Nield et al. (2015)), pluvial activity in the preceding wet season and flooding history. Therefore, even within large topographical features that were once considered major dust emitters, the productivity of dust emission from smaller areas is becoming increasingly apparent. Outside of the 'global' dust emission areas (Figures 3 and 5) previously unidentified dust emission areas have been documented on every continent (Ginoux et al., 2012). The combined flux of sediment from many, multiple sources would be expected to have a significant impact on downwind marine waters and large net impact on the productivity of the global ocean. As the identification of high-dust emission areas expands beyond paleolacustrine sediments the geochemistry and nutrient-loading of mineral aerosols must be investigated. Ephemeral and riverine sediments would be expected to have a higher ocean fertilisation potential, as has been demonstrated in this research where the fecundity of the less-intensely studied Namibian river valleys dust is higher than that of the two major pans and therefore of regionally-impacting significance.

Global Application

Coupled dust emission-atmospheric circulation models (e.g., Mahowald et al. (2008; 2005), Tanaka & Chiba (2006) and the 15-model review by Huneeus et al. (2011)) provide an essential tool to investigate the contribution of mineral aerosols and nutrients to depositional environments (Okin et al., 2011; Baker & Croot, 2010; Zhu et al., 1997). The nutrient composition and bioavailability of dust is known to change during atmospheric transport (Shi et al., 2011; Mackie et al., 2005), with the nutrient loading of source areas an essential component of constraining models to more accurately reflect the impact of mineral aerosols within the Earth System. Better understanding of dust nutrient loading at the point of deflation will allow comparison with depositional samples, facilitating a more precise understanding of the complex processing that occurs between

source and sink and the connectivity between the terrestrial, atmospheric and oceanic spheres. As with the focus of this research, fertilisation of the world's oceans is a major contribution of desert-derived mineral aerosols and differences in source sediment nutrient assemblage would be highly informative to include in dust deposition and ocean productivity models (Jickells & Moore, 2015). The mineralogy of dust is also relevant to other aspects of global climate models with mineral composition influencing ice nucleation (Tang et al., 2016) and therefore rainfall, and the absorption and scattering of solar radiation (Liao & Seinfeld, 1998; Tegen & Lacis, 1996), which affects mean global temperature (Hansen et al., 1997).

The biogeochemical analyses of Southern African dust sources by Bhattachan et al. (2015a) provided the first assessment of the fertilization potential of Etosha and Makgadikgadi Pans and the Southern Kalahari. Our research has shown that the ephemeral river valleys of Namibia surpass these dust emission sites in ocean fertilisation potential following the detailed assessment of their deflation productivity (Vickery et al., 2013). Delineating the fecundity of southern Africa's dust source areas is especially important as there are remarkable few sites with measurements of dust deposition, let alone nutrient content, downwind of the source areas (Moore et al., 2013; Huneeus et al., 2011).

Expanding research interest in the effects of dust in the Earth System and the deployment of higher-resolution remote sensing instruments is opening up the global dust source map beyond the major global dust emission areas (Figure 3), i.e. those which are readily detected using TOMS AAI identification approaches that detect dust > 1 km in the atmosphere (e.g. Prospero et al. (2002)). As discussed, these major sources are dominantly paleolacustrine deposits, the now-exposed sediments from historic pluvial

and alluvial regimes located in modern-day dryland environments. The most active dust sources, however, were noted to include present-day fluvial processes that interacted with Quaternary alluvium (Prospero et al., 2002). This is the case for Namibia's ephemeral river valleys that host a nexus of extant fluvial and geomorphological processes with Holocene alluvium. The geomorphology processes and extant fluvial activity have been shown to produce an enriched source of dust with a higher ocean fertilising fecundity than the less dynamic pan systems. Analogous ephemeral and fluvial processes in other systems around the world could be expected to produce similarly enriched dust-sized sediments that are common to ephemeral river geomorphology (e.g. Tooth (2000)). Therefore, investigation of similar ephemeral river systems around the world is highlighted as an important research focus of future dust needs. Central to these investigations would be characterisation of the ocean-fertilising nutrient load of these dynamic dust sources.

9.4 Prioritising future dust source research

Globally, hydrological and ephemeral systems account for an estimated 31% of global dust emissions, with 15% considered natural and 85% anthropogenic (Ginoux et al., 2012). This research has shown that ephemeral river valleys in non-densely human populated areas (Jacobson et al., 1995) produce Fe, N and P-enriched alluvium along the hydrological system. Namibia, as one of the world's least densely populated countries (United Nations Department of Economic and Social Affairs, 2016), could be reasonably considered to provide a baseline study for ephemeral or drying river dust fertilisation potential in a system with minimal anthropogenic impact.

Nutrient-enrichment of riverine systems and sediments are widely documented to rise with increased anthropogenic activities in the catchment (Crossman & Whitehead

editorial and special issue papers therein (2016)). Agricultural pressures are well-understood to increase macronutrients in run-off and fluvial systems and can also result in increased erosion rates and sediment load of the rivers, potentially providing resources for increased dust activity downstream or after floods depending on hydrological flows. Since the industrial revolution there have been massive changes to the terrestrial environment and the secondary impacts these may have on atmospheric and oceanic systems, via aeolian dust, have not yet been considered.

Firstly, the global N cycle has seen major alteration due to industrial N fixation for fertiliser production and plantation of N-fixing leguminous crops, which has more than doubled the rate of biologically available N entering the biosphere (Galloway et al., 2004; Vitousek & Matson, 1993). This is also contributed to by the burning of fossil fuels, which produce bioavailable N fractions (Krishnamurthy et al., 2010; Hameed & Dignon, 1988). Similarly, the mining of P and application in agricultural fertilisers has also seen a greater than two-fold increase in P inputs to the environment over the natural background weathering rate (Fixen & West, 2002; Mackenzie et al., 1998), with three times the pre-industrial flow of P to the ocean occurring (Carpenter & Bennett, 2011). The migration of agricultural N and P into terrestrial drainage systems is well-understood (Sims et al., 1998; Hessen et al., 1997; Ryden et al., 1974) as are the resulting effects of elevated macronutrient concentrations causing hundreds of eutrophic marine ‘dead zones’ globally (Williams et al., 2011; Diaz & Rosenberg, 2008).

The global Fe cycle would see the largest alterations caused by combustion engines that are known to produce Fe that is highly bioavailable (Mahowald et al., 2009) with Fe otherwise being one of the most abundant elements in the earth’s crust (Taylor, 1964). Anthropogenic perturbations to the Fe cycle are likely therefore to be downwind and/or

down stream of urbanised centres. In the natural component of the Fe cycle, our research has identified the importance of dust source geomorphology and that processes in the ephemeral valleys are producing sediments with high levels of bioavailable iron.

The sediment loading of rivers has also increased globally due to amplified erosion rates caused by agricultural practices, deforestation and land-use change (Foley et al., 2005). Further, the hydrological systems themselves have also been greatly altered, with the global mean time for the passage of water being tripled (Vörösmarty et al., 2003). The combined effect of these terrestrial anthropogenic pressures is a global increase in nutrient-rich and eutrophic riverine waters with higher sediment loadings in slower-moving systems. It is pertinent to consider the impact these factors may have on global dust and ocean fertilisation in the coming decades and century. Globally many rivers are also seeing reductions in flow due to changes in pluvial activity as a result of climate change, itself an anthropogenic force, as well as direct reduction via extraction for agricultural, industrial and densely-populated urban uses that will only increase in the future (Alcamo et al., 2007). Decreases in the water flowing through river systems, especially when flow is further severed by man-made barriers such as dams, increases the exposure of previously inundated river-bed sediments to the atmosphere. Upon desiccation these exposed bodies of riverine sediment would then serve as a globally pervasive reserve of fine sediments hosting anthropogenically-enriched macronutrient as well as micronutrient concentrations. The latter associated with industrial activities and, where storm water enters from urbanised catchments, internal combustion engines (Albanese & Breward, 2011; Makepeace et al., 1995).

To conclude on the matter of global importance, the combined global effect of multiple small-scale dust sources on the global ocean is expected to have a significant global

impact. Further, northern Africa is predicted to see a reduction in dust emission and transport in the coming centuries based on projected wind patterns in a warming world (Evan et al., 2016). A reduction in the world's major dust emission area and major contributor to ocean deposition would further the importance of numerous small sources. As the planet adapts to a new climate regime in the 21st century riverine dust sources are proposed to increase in number and supply highly-enriched aeolian sediments into the Earth System.

CHAPTER 10

10 Bibliography

ABDULLATIF, O.M., 1989. Channel-fill and sheet-flood facies sequences in the ephemeral terminal River Gash, Kassala, Sudan. Sedimentary Geology, 63(1), pp. 171-184.

ABRAMS, M., JACOBSON, P., JACOBSON, K. and SEELY, M., 1997. Survey of soil chemical properties across a landscape in the Namib Desert. Journal of Arid Environments, 35(1), pp. 29-38.

ACHTERBERG, E.P., 2014. Grand challenges in marine biogeochemistry. Frontiers in Marine Science, 1, pp. 7.

ALBANESE, S. and BREWARD, N., 2011. Sources of anthropogenic contaminants in the urban environment. Mapping the chemical environment of urban areas.Wiley-Blackwell, Oxford, , pp. 116-127.

ALCAMO, J., FLÖRKE, M. and MÄRKER, M., 2007. Future long-term changes in global water resources driven by socio-economic and climatic changes. Hydrological Sciences Journal, 52(2), pp. 247-275.

ALFARO, S.C. and GOMES, L., 2001. Modeling mineral aerosol production by wind erosion: Emission intensities and aerosol size distributions in source areas. Journal of Geophysical Research: Atmospheres, 106(D16), pp. 18075-18084.

ANDERSON, L., FAUL, K. and PAYTAN, A., 2010. Phosphorus associations in aerosols: What can they tell us about P bioavailability? Marine Chemistry, 120(1), pp. 44-56.

ANDREWS, W. and HUTCHINGS, L., 1980. Upwelling in the southern Benguela Current. Progress in Oceanography, 9(1), pp. 1-81.

ARCHER, D. and JOHNSON, K., 2000. A model of the iron cycle in the ocean. Global Biogeochemical Cycles, 14(1), pp. 269-279.

ARIMOTO, R., RAY, B., LEWIS, N., TOMZA, U. and DUCE, R., 1997. Mass‐particle size distributions of atmospheric dust and the dry deposition of dust to the remote ocean. Journal of Geophysical Research: Atmospheres (1984‐2012), 102(D13), pp. 15867-15874.

ARIMOTO, R., ZHANG, X., HUEBERT, B., KANG, C., SAVOIE, D., PROSPERO, J., SAGE, S., SCHLOESSLIN, C., KHAING, H. and OH, S., 2004. Chemical composition of atmospheric aerosols from Zhenbeitai, China, and Gosan, South Korea, during ACE‐Asia. Journal of Geophysical Research: Atmospheres, 109(D19).

ARNALDS, O., DAGSSON-WALDHAUSEROVA, P. and OLAFSSON, H., 2016. The Icelandic volcanic aeolian environment: Processes and impacts—A review. Aeolian Research, 20, pp. 176-195.

ARNON, D.I., 1956. Phosphorus metabolism and photosynthesis. Annual Review of Plant Physiology, 7(1), pp. 325-356.

ATLAS OF NAMIBIA PROJECT, 2002-last update, Digital Atlas of Namibia. Available: http://www.uni-koeln.de/sfb389/e/e1/download/atlas_namibia/main_namibia_atlas.html [1/28/2016, 2016].

AUFDENKAMPE, A.K., MAYORGA, E., RAYMOND, P.A., MELACK, J.M., DONEY, S.C., ALIN, S.R., AALTO, R.E. and YOO, K., 2011. Riverine coupling of biogeochemical cycles between land, oceans, and atmosphere. Frontiers in Ecology and the Environment, 9(1), pp. 53-60.

AUMONT, O. and BOPP, L., 2006. Globalizing results from ocean in situ iron fertilization studies. Global Biogeochemical Cycles, 20(2).

AUMONT, O., BOPP, L. and SCHULZ, M., 2008. What does temporal variability in aeolian dust deposition contribute to sea‐surface iron and chlorophyll distributions? Geophysical Research Letters, 35(7).

BADDOCK, M.C., ZOBECK, T.M., VAN PELT, R.S. and FREDRICKSON, E.L., 2011. Dust emissions from undisturbed and disturbed, crusted playa surfaces: Cattle trampling effects. Aeolian Research, 3(1), pp. 31-41.

BAKER, A. and CROOT, P., 2010. Atmospheric and marine controls on aerosol iron solubility in seawater. Marine Chemistry, 120(1), pp. 4-13.

BAKER, A., JICKELLS, T., WITT, M. and LINGE, K., 2006. Trends in the solubility of iron, aluminium, manganese and phosphorus in aerosol collected over the Atlantic Ocean. Marine Chemistry, 98(1), pp. 43-58.

BAKER, A., WESTON, K., KELLY, S., VOSS, M., STREU, P. and CAPE, J., 2007. Dry and wet deposition of nutrients from the tropical Atlantic atmosphere: Links to primary productivity and nitrogen fixation. Deep Sea Research Part I: Oceanographic Research Papers, 54(10), pp. 1704-1720.

BANERJEE, P. and PRASANNA KUMAR, S., 2014. Dust‐induced episodic phytoplankton blooms in the Arabian Sea during winter monsoon. Journal of Geophysical Research: Oceans, 119(10), pp. 7123-7138.

BARBEAU, K., 2006. Photochemistry of organic iron (III) complexing ligands in oceanic systems. Photochemistry and photobiology, 82(6), pp. 1505-1516.

BARROW, N., 1980. Evaluation and utilization of residual phosphorus in soils. The role of phosphorus in agriculture, (theroleofphosph), pp. 333-359.

BEHRENFELD, M.J., RANDERSON, J.T., MCCLAIN, C.R., FELDMAN, G.C., LOS, S.O., TUCKER, C.J., FALKOWSKI, P.G., FIELD, C.B., FROUIN, R., ESAIAS, W.E., KOLBER, D.D. and POLLACK, N.H., 2001. Biospheric primary production during an ENSO transition. Science (New York, N.Y.), 291(5513), pp. 2594-2597.

BELNAP, J., WELTER, J.R., GRIMM, N.B., BARGER, N. and LUDWIG, J.A., 2005. Linkages between microbial and hydrologic processes in arid and semiarid watersheds. Ecology, 86(2), pp. 298-307.

BEMAN, J.M., ARRIGO, K.R. and MATSON, P.A., 2005. Agricultural runoff fuels large phytoplankton blooms in vulnerable areas of the ocean. Nature, 434(7030), pp. 211-214.

BERMAN-FRANK, I., QUIGG, A., FINKEL, Z.V., IRWIN, A.J. and HARAMATY, L., 2007. Nitrogen‐fixation strategies and Fe requirements in cyanobacteria. Limnology and Oceanography, 52(5), pp. 2260-2269.

BERTHELOT, M., 1859. Berthelot's reaction mechanism. Report Chim Appl, 2884.

BHATTACHAN, A., D'ODORICO, P. and OKIN, G., 2015a. Biogeochemistry of dust sources in Southern Africa. Journal of Arid Environments, 117, pp. 18-27.

BHATTACHAN, A., D'ODORICO, P., BADDOCK, M.C., ZOBECK, T.M., OKIN, G.S. and CASSAR, N., 2012. The Southern Kalahari: a potential new dust source in the Southern Hemisphere? Environmental Research Letters, 7(2), pp. 024001.

BHATTACHAN, A., WANG, L., MILLER, M.F., LICHT, K.J. and D'ODORICO, P., 2015b. Antarctica's Dry Valleys: A potential source of soluble iron to the Southern Ocean? Geophysical Research Letters, 42(6), pp. 1912-1918.

BIERMAN, P.R. and CAFFEE, M., 2001. Slow rates of rock surface erosion and sediment production across the Namib Desert and escarpment, southern Africa. American Journal of Science, 301(4-5), pp. 326-358.

BINNING, K. and BAIRD, D., 2001. Survey of heavy metals in the sediments of the Swartkops River Estuary, Port Elizabeth South Africa. Water Sa, 27(4), pp. 461-466.

BISHOP, J.K., DAVIS, R.E. and SHERMAN, J.T., 2002. Robotic observations of dust storm enhancement of carbon biomass in the North Pacific. Science (New York, N.Y.), 298(5594), pp. 817-821.

BLACK, C.A., EVANS, D. and DINAUER, R., 1965. Methods of soil analysis. American Society of Agronomy Madison, WI.

BLAKEMORE, L., SEARLE, P. and DALY, B., 1987. Methods for chemical analysis of soils-science report, vol. 80. Wellington, NZ: NZ Soil Bureau, DSIR, .

BONNET, S., GUIEU, C., BRUYANT, F., PRÁŠIL, O., VAN WAMBEKE, F., RAIMBAULT, P., MOUTIN, T., GROB, C., GORBUNOV, M. and ZEHR, J., 2008.

Nutrient limitation of primary productivity in the Southeast Pacific (BIOSOPE cruise). Biogeosciences, 5(1), pp. 215-225.

BOUWMAN, A., BIERKENS, M., GRIFFIOEN, J., HEFTING, M., MIDDELBURG, J., MIDDELKOOP, H. and SLOMP, C., 2013. Nutrient dynamics, transfer and retention along the aquatic continuum from land to ocean: towards integration of ecological and biogeochemical models. Biogeosciences, 10(1), pp. 1-22.

BOYD, P.W., LAW, C.S., WONG, C., NOJIRI, Y., TSUDA, A., LEVASSEUR, M., TAKEDA, S., RIVKIN, R., HARRISON, P.J. and STRZEPEK, R., 2004a. The decline and fate of an iron-induced subarctic phytoplankton bloom. Nature, 428(6982), pp. 549-553.

BOYD, P.W., STRZEPEK, R., FU, F. and HUTCHINS, D.A., 2010a. Environmental control of open-ocean phytoplankton groups: Now and in the future. Limnology and Oceanography, 55(3), pp. 1353.

BOYD, P.W., WATSON, A.J., LAW, C.S., ABRAHAM, E.R., TRULL, T., MURDOCH, R., BAKKER, D.C., BOWIE, A.R., BUESSELER, K. and CHANG, H., 2000. A mesoscale phytoplankton bloom in the polar Southern Ocean stimulated by iron fertilization. Nature, 407(6805), pp. 695-702.

BOYD, P. and ELLWOOD, M., 2010. The biogeochemical cycle of iron in the ocean. Nature Geoscience, 3(10), pp. 675-682.

BOYD, P., MACKIE, D. and HUNTER, K., 2010b. Aerosol iron deposition to the surface ocean—modes of iron supply and biological responses. Marine Chemistry, 120(1), pp. 128-143.

BOYD, P., MCTAINSH, G., SHERLOCK, V., RICHARDSON, K., NICHOL, S., ELLWOOD, M. and FREW, R., 2004b. Episodic enhancement of phytoplankton stocks in New Zealand subantarctic waters: Contribution of atmospheric and oceanic iron supply. Global Biogeochemical Cycles, 18(1).

BOYD, P.W., WONG, C.S., MERRILL, J., WHITNEY, F., SNOW, J., HARRISON, P.J. and GOWER, J., 1998. Atmospheric iron supply and enhanced vertical carbon flux in the NE subarctic Pacific: Is there a connection? Global Biogeochemical Cycles, 12(3), pp. 429-441.

BRACKEN, M.E., HILLEBRAND, H., BORER, E.T., SEABLOOM, E.W., CEBRIAN, J., CLELAND, E.E., ELSER, J.J., GRUNER, D.S., HARPOLE, W.S. and NGAI, J.T., 2015. Signatures of nutrient limitation and co‐limitation: responses of autotroph internal nutrient concentrations to nitrogen and phosphorus additions. Oikos, 124(2), pp. 113-121.

BRAHNEY, J., MAHOWALD, N., WARD, D.S., BALLANTYNE, A.P. and NEFF, J.C., 2015. Is atmospheric phosphorus pollution altering global alpine Lake stoichiometry? Global Biogeochemical Cycles, 29(9), pp. 1369-1383.

BRESHEARS, D.D., WHICKER, J.J., JOHANSEN, M.P. and PINDER, J.E., 2003. Wind and water erosion and transport in semi‐arid shrubland, grassland and forest

ecosystems: Quantifying dominance of horizontal wind‐driven transport. Earth Surface Processes and Landforms, 28(11), pp. 1189-1209.

BRÉVIÈRE, E., METZL, N., POISSON, A. and TILBROOK, B., 2006. Changes of the oceanic CO2 sink in the Eastern Indian sector of the Southern Ocean. Tellus B, 58(5), pp. 438-446.

BRISTOW, C.S., HUDSON‐EDWARDS, K.A. and CHAPPELL, A., 2010. Fertilizing the Amazon and equatorial Atlantic with West African dust. Geophysical Research Letters, 37(14).

BROOK, G.A., MARAIS, E., SRIVASTAVA, P. and JORDAN, T., 2007. Timing of lake-level changes in Etosha Pan, Namibia, since the middle Holocene from OSL ages of relict shorelines in the Okondeka region. Quaternary International, 175(1), pp. 29-40.

BROWN, J.R., 1998. Recommended chemical soil test procedures for the North Central Region. Missouri Agricultural Experiment Station, University of Missouri--Columbia.

BROWN, P. and HUTCHINGS, L., 1987. The development and decline of phytoplankton blooms in the southern Benguela upwelling system. 2. Nutrient relationships. South African Journal of Marine Science, 5(1), pp. 393-409.

BRULAND, K.W., RUE, E.L. and SMITH, G.J., 2001. Iron and macronutrients in California coastal upwelling regimes: Implications for diatom blooms. Limnology and Oceanography, 46(7), pp. 1661-1674.

BRULAND, K.W., RUE, E.L., SMITH, G.J. and DITULLIO, G.R., 2005. Iron, macronutrients and diatom blooms in the Peru upwelling regime: brown and blue waters of Peru. Marine Chemistry, 93(2), pp. 81-103.

BRUNGARD, C.W., BOETTINGER, J.L. and HIPPS, L.E., 2015. Wind erosion potential of lacustrine and alluvial soils before and after disturbance in the eastern Great Basin, USA: Estimating threshold friction velocity using easier-to-measure soil properties. Aeolian Research, 18, pp. 185-203.

BRYANT, R.G., 2003. Monitoring hydrological controls on dust emissions: preliminary observations from Etosha Pan, Namibia. The Geographical Journal, 169(2), pp. 131-141.

BRYANT, R., ECKARDT, F., VICKERY, K., WIGGS, G., HIPONDOKA, M., MURRAY, J., BRINDLEY, H., KING, J., NIELD, J. and THOMAS, D., 2015. Remote sensing of dust source characteristics and emission controls on a large playa.

BRYANT, R.G., BIGG, G.R., MAHOWALD, N.M., ECKARDT, F.D. and ROSS, S.G., 2007. Dust emission response to climate in southern Africa. Journal of Geophysical Research: Atmospheres, 112(D9), pp. n/a-n/a.

BUCK, C.S., LANDING, W.M. and RESING, J.A., 2010a. Particle size and aerosol iron solubility: A high-resolution analysis of Atlantic aerosols. Marine Chemistry, 120(1), pp. 14-24.

BUCK, C.S., LANDING, W.M., RESING, J.A. and MEASURES, C.I., 2010b. The solubility and deposition of aerosol Fe and other trace elements in the North Atlantic

Ocean: Observations from the A16N CLIVAR/CO 2 repeat hydrography section. Marine Chemistry, 120(1), pp. 57-70.

BUCK, C.S., LANDING, W.M., RESING, J.A. and LEBON, G.T., 2006. Aerosol iron and aluminum solubility in the northwest Pacific Ocean: Results from the 2002 IOC cruise. Geochemistry, Geophysics, Geosystems, 7(4), pp. - Q04M07.

BULLARD, J.E., BADDOCK, M., BRADWELL, T., CRUSIUS, J., DARLINGTON, E., GAIERO, D., GASSÓ, S., GISLADOTTIR, G., HODGKINS, R. and MCCULLOCH, R., 2016. High ‐ latitude dust in the Earth system. Reviews of Geophysics, .

BULLARD, J.E., HARRISON, S.P., BADDOCK, M.C., DRAKE, N., GILL, T.E., MCTAINSH, G. and SUN, Y., 2011. Preferential dust sources: A geomorphological classification designed for use in global dust ‐ cycle models. Journal of Geophysical Research: Earth Surface, 116(F4).

BULLARD, J., BADDOCK, M., MCTAINSH, G. and LEYS, J., 2008. Sub ‐ basin scale dust source geomorphology detected using MODIS. Geophysical Research Letters, 35(15).

BUNN, S.E., BALCOMBE, S.R., DAVIES, P.M., FELLOWS, C.S. and MCKENZIE-SMITH, F.J., 2006. Aquatic productivity and food webs of desert river ecosystems. Ecology of desert rivers, , pp. 76-99.

BURKE, A. and STROHBACH, B.J., 2000. Review: vegetation studies in Namibia. Dinteria, 26, pp. 1-24.

BURNS, R.C. and HARDY, R.W., 2012. Nitrogen fixation in bacteria and higher plants. Springer Science & Business Media.

BURROUGH, S.L., THOMAS, D.S. and BAILEY, R.M., 2009. Mega-Lake in the Kalahari: a Late Pleistocene record of the Palaeolake Makgadikgadi system. Quaternary Science Reviews, 28(15), pp. 1392-1411.

BUSECK, P.R. and POSFAI, M., 1999. Airborne minerals and related aerosol particles: effects on climate and the environment. Proceedings of the National Academy of Sciences of the United States of America, 96(7), pp. 3372-3379.

CALIL, P.H., DONEY, S.C., YUMIMOTO, K., EGUCHI, K. and TAKEMURA, T., 2011. Episodic upwelling and dust deposition as bloom triggers in low ‐ nutrient, low ‐ chlorophyll regions. Journal of Geophysical Research: Oceans, 116(C6).

CAPONE, D.G. and CARPENTER, E.J., 1982. Nitrogen fixation in the marine environment. Science, 217(4565), pp. 1140-1142.

CAPONE, D.G. and HUTCHINS, D.A., 2013. Microbial biogeochemistry of coastal upwelling regimes in a changing ocean. Nature geoscience, 6(9), pp. 711-717.

CARBO, P., KROM, M.D., HOMOKY, W.B., BENNING, L.G. and HERUT, B., 2005. Impact of atmospheric deposition on N and P geochemistry in the southeastern Levantine

basin. Deep Sea Research Part II: Topical Studies in Oceanography, 52(22), pp. 3041-3053.

CARDER, K.L., CHEN, F.R., LEE, Z., HAWES, S.K. and CANNIZZARO, J.P., 2003. MODIS ocean science team algorithm theoretical basis document. ATBD, 19(Version 7), pp. 7-18.

CARPENTER, S.R. and BENNETT, E.M., 2011. Reconsideration of the planetary boundary for phosphorus. Environmental Research Letters, 6(1), pp. 014009.

CARR, M. and KEARNS, E.J., 2003. Production regimes in four Eastern Boundary Current systems. Deep Sea Research Part II: Topical Studies in Oceanography, 50(22), pp. 3199-3221.

CASSAR, N., BENDER, M.L., BARNETT, B.A., FAN, S., MOXIM, W.J., LEVY, H.,2nd and TILBROOK, B., 2007. The Southern Ocean biological response to aeolian iron deposition. Science (New York, N.Y.), 317(5841), pp. 1067-1070.

CETINIĆ, I., PERRY, M., D'ASARO, E., BRIGGS, N., POULTON, N., SIERACKI, M. and LEE, C., 2015. A simple optical index shows spatial and temporal heterogeneity in phytoplankton community composition during the 2008 North Atlantic Bloom Experiment. Biogeosciences, 12(7), pp. 2179-2194.

CHARLEY, J. and COWLING, S., 1968. Changes in soil nutrient status resulting from overgrazing and their consequences in plant communities of semi-arid areas.

CHASE, Z., STRUTTON, P.G. and HALES, B., 2007. Iron links river runoff and shelf width to phytoplankton biomass along the US West Coast. Geophysical Research Letters, 34(4).

CHAVEZ, F.P. and BARBER, R.T., 1987. An estimate of new production in the equatorial Pacific. Deep Sea Research Part A. Oceanographic Research Papers, 34(7), pp. 1229-1243.

CHAVEZ, F.P. and MESSIÉ, M., 2009. A comparison of eastern boundary upwelling ecosystems. Progress in Oceanography, 83(1), pp. 80-96.

CHAVEZ, F.P., MESSIÉ, M. and PENNINGTON, J.T., 2011. Marine primary production in relation to climate variability and change. Annual Review of Marine Science, 3, pp. 227-260.

CHEN, Z., YAN, X., JO, Y., JIANG, L. and JIANG, Y., 2012. A study of Benguela upwelling system using different upwelling indices derived from remotely sensed data. Continental Shelf Research, 45, pp. 27-33.

CHENG, Y., YEH, H. and ALLEN, M.D., 1988. Dynamic shape factor of a plate-like particle. Aerosol science and technology, 8(2), pp. 109-123.

CHEUNG, K., POON, B., LAN, C. and WONG, M., 2003. Assessment of metal and nutrient concentrations in river water and sediment collected from the cities in the Pearl River Delta, South China. Chemosphere, 52(9), pp. 1431-1440.

CHOOBARI, O.A., ZAWAR-REZA, P. and STURMAN, A., 2014. The global distribution of mineral dust and its impacts on the climate system: A review. Atmospheric Research, 138, pp. 152-165.

CHOU, C., FORMENTI, P., MAILLE, M., AUSSET, P., HELAS, G., HARRISON, M. and OSBORNE, S., 2008. Size distribution, shape, and composition of mineral dust aerosols collected during the African Monsoon Multidisciplinary Analysis Special Observation Period 0: Dust and Biomass‐Burning Experiment field campaign in Niger, January 2006. Journal of Geophysical Research: Atmospheres, 113(D23).

CHUNG, C., CHANG, J., GONG, G., HSU, S., CHIANG, K. and LIAO, C., 2011. Effects of Asian dust storms on Synechococcus populations in the subtropical Kuroshio Current. Marine biotechnology, 13(4), pp. 751-763.

CLAQUIN, T., SCHULZ, M. and BALKANSKI, Y., 1999. Modeling the mineralogy of atmospheric dust sources. Journal of Geophysical Research: Atmospheres, 104(D18), pp. 22243-22256.

COALE, K.H., 1991. Effects of iron, manganese, copper, and zinc enrichments on productivity and biomass in the subarctic Pacific. Limnology and Oceanography, 36(8), pp. 1851-1864.

COALE, K.H., FITZWATER, S.E., GORDON, R.M., JOHNSON, K.S. and BARBER, R.T., 1996a. Control of community growth and export production by upwelled iron in the equatorial Pacific Ocean. Nature, 379(6566), pp. 621-624.

COALE, K.H., JOHNSON, K.S., FITZWATER, S.E., GORDON, R.M., TANNER, S., CHAVEZ, F.P., FERIOLI, L., SAKAMOTO, C., ROGERS, P., MILLERO, F., STEINBERG, P., NIGHTINGALE, P., COOPER, D., COCHLAN, W.P., LANDRY, M.R., CONSTANTINOU, J., ROLLWAGEN, G., TRASVINA, A. and KUDELA, R., 1996b. A massive phytoplankton bloom induced by an ecosystem-scale iron fertilization experiment in the equatorial Pacific Ocean. Nature, 383(6600), pp. 495.

CODISPOTI, L., 1989. Phosphorus vs. nitrogen limitation of new and export production. Productivity of the ocean: Present and past, 44, pp. 377-394.

COETZEE, C., 1970. The distribution of mammals in the Namib Desert and adjoining inland escarpment. Scientific Papers of the Namib Desert Research Station, 1970(40), pp. 23-36.

COLEMAN, D.C., REID, C. and COLE, C., 1983. Biological strategies of nutrient cycling in soil systems. Advances in Ecological Research, 13, pp. 1-55.

COLLINS, A., WALLING, D. and LEEKS, G., 1998. Use of composite fingerprints to determine the provenance of the contemporary suspended sediment load transported by rivers. Earth Surface Processes and Landforms, 23(1), pp. 31-52.

COSMIC, P., 1987. Wind-driven ocean currents and Ekman transport.

COWLISHAW, G. and DAVIES, J.G., 1997. Flora of the Pro-Namib Desert Swakop River catchment, Namibia: community classification and implications for desert vegetation sampling. Journal of Arid Environments, 36(2), pp. 271-290.

CREAMEAN, J.M., SUSKI, K.J., ROSENFELD, D., CAZORLA, A., DEMOTT, P.J., SULLIVAN, R.C., WHITE, A.B., RALPH, F.M., MINNIS, P., COMSTOCK, J.M., TOMLINSON, J.M. and PRATHER, K.A., 2013. Dust and biological aerosols from the Sahara and Asia influence precipitation in the western U.S. Science (New York, N.Y.), 339(6127), pp. 1572-1578.

CRISPO, S.M., PETERSON, T. and LOHAN, M.C., 2005. Implications of an Asian dust storm on the Gulf of Alaska. Sea Technology, 46(9), pp. 29-35.

CROPP, R.A., GABRIC, A.J., MCTAINSH, G.H., BRADDOCK, R.D. and TINDALE, N., 2005. Coupling between ocean biota and atmospheric aerosols: Dust, dimethylsulphide, or artifact? Global Biogeochemical Cycles, 19(4).

CROSSMAN, J. and WHITEHEAD, P.G., 2016. Bridging gaps across macronutrient cycles. Science of The Total Environment, 572, pp. 1447-1448.

CRUSIUS, J., SCHROTH, A.W., GASSO, S., MOY, C.M., LEVY, R.C. and GATICA, M., 2011. Glacial flour dust storms in the Gulf of Alaska: Hydrologic and meteorological controls and their importance as a source of bioavailable iron. Geophysical Research Letters, 38(6).

CWIERTNY, D.M., BALTRUSAITIS, J., HUNTER, G.J., LASKIN, A., SCHERER, M.M. and GRASSIAN, V.H., 2008. Characterization and acid ‐ mobilization study of iron ‐ containing mineral dust source materials. Journal of Geophysical Research: Atmospheres, 113(D5).

DAHAN, O., TATARSKY, B., ENZEL, Y., KULLS, C., SEELY, M. and BENITO, G., 2008. Dynamics of flood water infiltration and ground water recharge in hyperarid desert. Groundwater, 46(3), pp. 450-461.

DARWIN, C., 1846. An account of the Fine Dust which often falls on Vessels in the Atlantic Ocean. Quarterly Journal of the Geological Society, 2(1-2), pp. 26-30.

DE BAAR, H. and BOYD, P., 2000. The role of iron in plankton ecology and carbon dioxide transfer of the global oceans. The dynamic ocean carbon cycle: a midterm synthesis of the Joint Global Ocean Flux Study, 5, pp. 61-140.

DEMOTT, P.J., SASSEN, K., POELLOT, M.R., BAUMGARDNER, D., ROGERS, D.C., BROOKS, S.D., PRENNI, A.J. and KREIDENWEIS, S.M., 2003. African dust aerosols as atmospheric ice nuclei. Geophysical Research Letters, 30(14).

DESBIOLLES, F., BLANKE, B., BENTAMY, A. and ROY, C., 2016. Response of the Southern Benguela upwelling system to fine-scale modifications of the coastal wind. Journal of Marine Systems, 156, pp. 46-55.

DESBOEUFS, K., SOFIKITIS, A., LOSNO, R., COLIN, J. and AUSSET, P., 2005. Dissolution and solubility of trace metals from natural and anthropogenic aerosol particulate matter. Chemosphere, 58(2), pp. 195-203.

DIAZ, R.J. and ROSENBERG, R., 2008. Spreading dead zones and consequences for marine ecosystems. Science (New York, N.Y.), 321(5891), pp. 926-929.

DIRECTORATE OF SURVEY AND MAPPING, 2002. Namibia 1:250000 Topographical Map Third Edition. Windhoek, Namibia: Directorate of Survey and Mapping of Namibia.

DITULLIO, G.R. and LAWS, E.A., 1991. Impact of an atmospheric-oceanic disturbance on phytoplankton community dynamics in the North Pacific Central Gyre. Deep Sea Research Part A.Oceanographic Research Papers, 38(10), pp. 1305-1329.

DONG, Z., LIU, X., WANG, H., ZHAO, A. and WANG, X., 2003. The flux profile of a blowing sand cloud: a wind tunnel investigation. Geomorphology, 49(3), pp. 219-230.

DOUGLAS, L.A., 1971. Degradation of clay minerals by H2O2 treatments to oxidize organic matter*. Clays and Clay Minerals, 19, pp. 67-68.

DOWNING, J.A. and MCCAULEY, E., 1992. The nitrogen: phosphorus relationship in lakes. Limnology and Oceanography, 37(5), pp. 936-945.

DOWNING, J.A., OSENBERG, C.W. and SARNELLE, O., 1999. Meta‐analysis of marine nutrient‐enrichment experiments: variation in the magnitude of nutrient limitation. Ecology, 80(4), pp. 1157-1167.

DUCE, R.A. and TINDALE, N.W., 1991. Atmospheric transport of iron and its deposition in the ocean. Limnology and Oceanography, 36(8), pp. 1715-1726.

DUCE, R.A., LAROCHE, J., ALTIERI, K., ARRIGO, K.R., BAKER, A.R., CAPONE, D.G., CORNELL, S., DENTENER, F., GALLOWAY, J., GANESHRAM, R.S., GEIDER, R.J., JICKELLS, T., KUYPERS, M.M., LANGLOIS, R., LISS, P.S., LIU, S.M., MIDDELBURG, J.J., MOORE, C.M., NICKOVIC, S., OSCHLIES, A., PEDERSEN, T., PROSPERO, J., SCHLITZER, R., SEITZINGER, S., SORENSEN, L.L., UEMATSU, M., ULLOA, O., VOSS, M., WARD, B. and ZAMORA, L., 2008. Impacts of atmospheric anthropogenic nitrogen on the open ocean. Science (New York, N.Y.), 320(5878), pp. 893-897.

DUNKERLEY, D.L., 2008. Bank permeability in an Australian ephemeral dry‐land stream: variation with stage resulting from mud deposition and sediment clogging. Earth Surface Processes and Landforms, 33(2), pp. 226-243.

DUNKERLEY, D., 1992. Channel geometry, bed material, and inferred flow conditions in ephemeral stream systems, Barrier Range, western NSW Australia. Hydrological Processes, 6(4), pp. 417-433.

DURÁN, O., CLAUDIN, P. and ANDREOTTI, B., 2011. On aeolian transport: Grain-scale interactions, dynamical mechanisms and scaling laws. Aeolian Research, 3(3), pp. 243-270.

ECKARDT, F. and KURING, N., 2005. SeaWiFS identifies dust sources in the Namib Desert. International Journal of Remote Sensing, 26(19), pp. 4159-4167.

ECKARDT, F., SODERBERG, K., COOP, L., MULLER, A., VICKERY, K., GRANDIN, R., JACK, C., KAPALANGA, T. and HENSCHEL, J., 2013. The nature of moisture at Gobabeb, in the central Namib Desert. Journal of Arid Environments,

ECKARDT, F.D., WASHINGTON, R. and WILKINSON, J., 2001. Palaeoecology of Africa, 27, pp. 207.

EDWARDS, K.F., LITCHMAN, E. and KLAUSMEIER, C.A., 2013. Functional traits explain phytoplankton community structure and seasonal dynamics in a marine ecosystem. Ecology Letters, 16(1), pp. 56-63.

EGGE, J. and AKSNES, D., 1992. Silicate as regulating nutrient in phytoplankton competition. Marine ecology progress series.Oldendorf, 83(2), pp. 281-289.

EITEL, B., DIETER BLÜMEL, W., HÜSER, K. and MAUZ, B., 2001. Dust and loessic alluvial deposits in Northwestern Namibia (Damaraland, Kaokoveld): sedimentology and palaeoclimatic evidence based on luminescence data. Quaternary International, 76, pp. 57-65.

EITEL, B., KADEREIT, A., BLÜMEL, W., HÜSER, K., LOMAX, J. and HILGERS, A., 2006. Environmental changes at the eastern Namib Desert margin before and after the Last Glacial Maximum: new evidence from fluvial deposits in the upper Hoanib River catchment, northwestern Namibia. Palaeogeography, Palaeoclimatology, Palaeoecology, 234(2), pp. 201-222.

ELSER, J.J., BRACKEN, M.E., CLELAND, E.E., GRUNER, D.S., HARPOLE, W.S., HILLEBRAND, H., NGAI, J.T., SEABLOOM, E.W., SHURIN, J.B. and SMITH, J.E., 2007. Global analysis of nitrogen and phosphorus limitation of primary producers in freshwater, marine and terrestrial ecosystems. Ecology Letters, 10(12), pp. 1135-1142.

ELTAYEB, M.A., XHOFFER, C.F., VAN ESPEN, P.J., VAN GRIEKEN, R. and MAENHAUT, W., 1993. Sources and composition of aerosol from Khartoum, Sudan. Atmospheric Environment.Part B.Urban Atmosphere, 27(1), pp. 67-76.

ENGELBRECHT, J.P. and DERBYSHIRE, E., 2010. Airborne mineral dust. Elements, 6(4), pp. 241-246.

ENGELSTAEDTER, S. and WASHINGTON, R., 2007. Temporal controls on global dust emissions: The role of surface gustiness. Geophysical Research Letters, 34(15).

ERICKSON, D.J., HERNANDEZ, J.L., GINOUX, P., GREGG, W., MCCLAIN, C. and CHRISTIAN, J., 2003. Atmospheric iron delivery and surface ocean biological activity in the Southern Ocean and Patagonian region. Geophysical Research Letters, 30(12).

EVAN, A.T., FLAMANT, C., GAETANI, M. and GUICHARD, F., 2016. The past, present and future of African dust. Nature, 531(7595), pp. 493-495.

EVANS, R. and BELNAP, J., 1999. Long-term consequences of disturbance on nitrogen dynamics in an arid ecosystem. Ecology, 80(1), pp. 150-160.

FALKOWSKI, P.G., 1997. Evolution of the nitrogen cycle and its influence on the biological sequestration of CO 2 in the ocean. Nature, 387(6630), pp. 272-275.

FALKOWSKI, P.G., BARBER, R.T. and SMETACEK, V.V., 1998. Biogeochemical Controls and Feedbacks on Ocean Primary Production. Science (New York, N.Y.), 281(5374), pp. 200-207.

FAN, S., MOXIM, W.J. and LEVY, H., 2006. Aeolian input of bioavailable iron to the ocean. Geophysical Research Letters, 33(7).

FIELD, J.P., BRESHEARS, D.D. and WHICKER, J.J., 2009. Toward a more holistic perspective of soil erosion: why aeolian research needs to explicitly consider fluvial processes and interactions. Aeolian Research, 1(1), pp. 9-17.

FIELD, C.B., BEHRENFELD, M.J., RANDERSON, J.T. and FALKOWSKI, P., 1998. Primary production of the biosphere: integrating terrestrial and oceanic components. Science (New York, N.Y.), 281(5374), pp. 237-240.

FILIPPELLI, G.M., 2008. The global phosphorus cycle: past, present, and future. Elements, 4(2), pp. 89-95.

FIXEN, P.E. and WEST, F.B., 2002. Nitrogen fertilizers: meeting contemporary challenges. Ambio: a journal of the human environment, 31(2), pp. 169-176.

FLATO, G., MAROTZKE, J., ABIODUN, B., BRACONNOT, P., CHOU, S.C., COLLINS, W.J., COX, P., DRIOUECH, F., EMORI, S. and EYRING, V., 2013. Evaluation of Climate Models. In: Climate Change 2013: The Physical Science Basis. Contribution of Working Group I to the Fifth Assessment Report of the Intergovernmental Panel on Climate Change. Climate Change 2013, 5, pp. 741-866.

FLOHR, A., VAN DER PLAS, A., EMEIS, K., MOHRHOLZ, V. and RIXEN, T., 2014. Spatio-temporal patterns of C: N: P ratios in the northern Benguela upwelling system. Biogeosciences, 11(3), pp. 885-897.

FOLEY, J.A., DEFRIES, R., ASNER, G.P., BARFORD, C., BONAN, G., CARPENTER, S.R., CHAPIN, F.S., COE, M.T., DAILY, G.C., GIBBS, H.K., HELKOWSKI, J.H., HOLLOWAY, T., HOWARD, E.A., KUCHARIK, C.J., MONFREDA, C., PATZ, J.A., PRENTICE, I.C., RAMANKUTTY, N. and SNYDER, P.K., 2005. Global consequences of land use. Science (New York, N.Y.), 309(5734), pp. 570-574.

FORMENTI, P., ELBERT, W., MAENHAUT, W., HAYWOOD, J. and ANDREAE, M., 2003. Chemical composition of mineral dust aerosol during the Saharan Dust Experiment (SHADE) airborne campaign in the Cape Verde region, September 2000. Journal of Geophysical Research: Atmospheres, 108(D18).

FORMENTI, P., SCHÜTZ, L., BALKANSKI, Y., DESBOEUFS, K., EBERT, M., KANDLER, K., PETZOLD, A., SCHEUVENS, D., WEINBRUCH, S. and ZHANG, D., 2011. Recent progress in understanding physical and chemical properties of African and Asian mineral dust. Atmospheric Chemistry and Physics, 11(16), pp. 8231-8256.

FRANCHY, G., OJEDA, A., LÓPEZ-CANCIO, J. and HERNÁNDEZ-LEÓN, S., 2013. Plankton community response to Saharan dust fertilization in subtropical waters off the Canary Islands. Biogeosciences Discussions, 10(11), pp. 17275-17307.

FRANZ, C., MAKESCHIN, F., WEISS, H. and LORZ, C., 2013. Geochemical signature and properties of sediment sources and alluvial sediments within the Lago Paranoá catchment, Brasília DF: a study on anthropogenic introduced chemical elements in an urban river basin. Science of the Total Environment, 452, pp. 411-420.

FRÉON, P., BARANGE, M. and ARISTEGUI, J., 2009. Eastern boundary upwelling ecosystems: integrative and comparative approaches. Progress in Oceanography, 83(1), pp. 1-14.

FREW, R.D., HUTCHINS, D.A., NODDER, S., SANUDO‐WILHELMY, S., TOVAR‐SANCHEZ, A., LEBLANC, K., HARE, C.E. and BOYD, P.W., 2006. Particulate iron dynamics during FeCycle in subantarctic waters southeast of New Zealand. Global Biogeochemical Cycles, 20(1).

FRIEDERICH, G.E., LEDESMA, J., ULLOA, O. and CHAVEZ, F.P., 2008. Air–sea carbon dioxide fluxes in the coastal southeastern tropical Pacific. Progress in Oceanography, 79(2), pp. 156-166.

FRYBERGER, S.G., AHLBRANDT, T.S. and ANDREWS, S., 1979. Origin, Sedimentary Features, and Significance of Low-Angle Eolian. Journal of Sedimentary Research, 49(3).

FRYBERGER, S.G., AL-SARI, A.M. and CLISHAM, T.J., 1983. Eolian dune, interdune, sand sheet, and siliciclastic sabkha sediments of an offshore prograding sand sea, Dhahran area, Saudi Arabia. AAPG Bulletin, 67(2), pp. 280-312.

FRYREAR, D., 1986. A field dust sampler. Journal of Soil and Water Conservation, 41(2), pp. 117-120.

FU, X., WANG, S., CHENG, Z., XING, J., ZHAO, B., WANG, J. and HAO, J., 2014. Source, transport and impacts of a heavy dust event in the Yangtze River Delta, China, in 2011. Atmospheric Chemistry and Physics, 14(3), pp. 1239-1254.

FURNAS, M., MITCHELL, A., SKUZA, M. and BRODIE, J., 2005. In the other 90%: phytoplankton responses to enhanced nutrient availability in the Great Barrier Reef Lagoon. Marine pollution bulletin, 51(1), pp. 253-265.

GABRIC, A.J., CROPP, R., AYERS, G.P., MCTAINSH, G. and BRADDOCK, R., 2002. Coupling between cycles of phytoplankton biomass and aerosol optical depth as derived from SeaWiFS time series in the Subantarctic Southern Ocean. Geophysical Research Letters, 29(7).

GABRIC, A., CROPP, R., MCTAINSH, G., BUTLER, H., JOHNSTON, B., O'LOINGSIGH, T. and VAN TRAN, D., 2016. Tasman Sea biological response to dust storm events during the austral spring of 2009. Marine and Freshwater Research, 67(8), pp. 1090-1102.

GABRIC, A.J., CROPP, R.A., MCTAINSH, G.H., JOHNSTON, B.M., BUTLER, H., TILBROOK, B. and KEYWOOD, M., 2010. Australian dust storms in 2002–2003 and their impact on Southern Ocean biogeochemistry. Global Biogeochemical Cycles, 24(2).

GAIERO, D.M., BRUNET, F., PROBST, J. and DEPETRIS, P.J., 2007. A uniform isotopic and chemical signature of dust exported from Patagonia: Rock sources and occurrence in southern environments. Chemical Geology, 238(1), pp. 107-120.

GALLARDO, A. and SCHLESINGER, W.H., 1992. Carbon and nitrogen limitations of soil microbial biomass in desert ecosystems. Biogeochemistry, 18(1), pp. 1-17.

GALLISAI, R., PETERS, F., VOLPE, G., BASART, S. and BALDASANO, J.M., 2014. Saharan dust deposition may affect phytoplankton growth in the Mediterranean Sea at ecological time scales. PloS one, 9(10), pp. e110762.

GALLOWAY, J.N., DENTENER, F.J., CAPONE, D.G., BOYER, E.W., HOWARTH, R.W., SEITZINGER, S.P., ASNER, G.P., CLEVELAND, C., GREEN, P. and HOLLAND, E., 2004. Nitrogen cycles: past, present, and future. Biogeochemistry, 70(2), pp. 153-226.

GAMMELSRØD, T., BARTHOLOMAE, C., BOYER, D., FILIPE, V. and O'TOOLE, M., 1998. Intrusion of warm surface water along the Angolan-Namibian coast in February–March 1995: the 1995 Benguela Niño. South African Journal of Marine Science, 19(1), pp. 41-56.

GAO, Y., KAUFMAN, Y., TANRE, D., KOLBER, D. and FALKOWSKI, P., 2001. Seasonal distributions of aeolian iron fluxes to the global ocean. Geophysical Research Letters, 28(1), pp. 29-32.

GARCIA, H., LOCARNINI, R., BOYER, T., ANTONOV, J., ZWENG, M., BARANOVA, O. and JOHNSON, D., 2009. World Ocean Atlas 2009, Volume 4: Nutrients (Phosphate, Nitrate, Silicate), NOAA Atlas NESDIS 71, .

GASPARI, V., BARBANTE, C., COZZI, G., CESCON, P., BOUTRON, C.F., GABRIELLI, P., CAPODAGLIO, G., FERRARI, C., PETIT, J.R. and DELMONTE, B., 2006. Atmospheric iron fluxes over the last deglaciation: Climatic implications. Geophysical Research Letters, 33(3).

GELENCSÉR, A., KOVÁTS, N., TURÓCZI, B., ROSTÁSI, A., HOFFER, A., IMRE, K., NYIRŐ-KÓSA, I., CSÁKBERÉNYI-MALASICS, D., TÓTH, A. and CZITROVSZKY, A., 2011. The red mud accident in Ajka (Hungary): characterization and potential health effects of fugitive dust. Environmental science & technology, 45(4), pp. 1608-1615.

GILLETTE, D.A., 1981. Production of dust that may be carried great distances. Geological Society of America Special Papers, 186, pp. 11-26.

GILLETTE, D.A., ADAMS, J., ENDO, A., SMITH, D. and KIHL, R., 1980. Threshold velocities for input of soil particles into the air by desert soils. Journal of Geophysical Research: Oceans, 85(C10), pp. 5621-5630.

GILLETTE, D.A., FRYREAR, D., GILL, T.E., LEY, T., CAHILL, T.A. and GEARHART, E.A., 1997. Relation of vertical flux of particles smaller than 10 μm to total aeolian horizontal mass flux at Owens Lake. Journal of Geophysical Research: Atmospheres, 102(D22), pp. 26009-26015.

GILLIES, J., NICKLING, W. and MCTAINSH, G., 1996. Dust concentrations and particle-size characteristics of an intense dust haze event: inland delta region, Mali, West Africa. Atmospheric Environment, 30(7), pp. 1081-1090.

GINOUX, P., PROSPERO, J.M., GILL, T.E., HSU, N.C. and ZHAO, M., 2012. Global‐scale attribution of anthropogenic and natural dust sources and their emission rates based on MODIS Deep Blue aerosol products. Reviews of Geophysics, 50(3).

GINOUX, P., CHIN, M., TEGEN, I., PROSPERO, J.M., HOLBEN, B., DUBOVIK, O. and LIN, S.J., 2001. Journal of Geophysical Research, 106, pp. 20255.

GINOUX, P., PROSPERO, J.M., TORRES, O. and CHIN, M., 2004. Long-term simulation of global dust distribution with the GOCART model: correlation with North Atlantic Oscillation. Environmental Modelling & Software, 19(2), pp. 113-128.

GIOVAGNETTI, V., BRUNET, C., CONVERSANO, F., TRAMONTANO, F., OBERNOSTERER, I., RIDAME, C. and GUIEU, C., 2013. Assessing the role of dust deposition on phytoplankton ecophysiology and succession in a low-nutrient low-chlorophyll ecosystem: a mesocosm experiment in the Mediterranean Sea. Biogeosciences, 10(5), pp. 2973-2991.

GLACCUM, R.A. and PROSPERO, J.M., 1980. Saharan aerosols over the tropical North Atlantic—Mineralogy. Marine Geology, 37(3), pp. 295-321.

GLIBERT, P.M., HARRISON, J., HEIL, C. and SEITZINGER, S., 2006. Escalating worldwide use of urea–a global change contributing to coastal eutrophication. Biogeochemistry, 77(3), pp. 441-463.

GÓMEZ, R., ARCE, M.I., SÁNCHEZ, J.J. and DEL MAR SÁNCHEZ-MONTOYA, M., 2012. The effects of drying on sediment nitrogen content in a Mediterranean intermittent stream: a microcosms study. Hydrobiologia, 679(1), pp. 43-59.

GOOSSENS, D., 2008. Techniques to measure grain‐size distributions of loamy sediments: a comparative study of ten instruments for wet analysis. Sedimentology, 55(1), pp. 65-96.

GOUBANOVA, K., ILLIG, S., MACHU, E., GARÇON, V. and DEWITTE, B., 2013. SST subseasonal variability in the central Benguela upwelling system as inferred from satellite observations (1999–2009). Journal of Geophysical Research: Oceans, 118(9), pp. 4092-4110.

GOUDIE, A., 2009. Namib sand sea: large Dunes in an ancient desert. Geomorphological Landscapes of the World. Springer, pp. 163-169.

GOUDIE, A. and ECKARDT, F., 1999. The evolution of the morphological framework of the central Namib Desert, Namibia, since the early Cretaceous. Geografiska Annaler: Series A, Physical Geography, 81(3), pp. 443-458.

GRAHAM, P. and VANCE, C., 2000. Nitrogen fixation in perspective: an overview of research and extension needs. Field Crops Research, 65(2), pp. 93-106.

GRAHAM, W.F. and DUCE, R.A., 1982. The atmospheric transport of phosphorus to the western North Atlantic. Atmospheric Environment (1967), 16(5), pp. 1089-1097.

GREELEY, R., WILLIAMS, S.H. and MARSHALL, J.R., 1983. Velocities of Windblown Particles in Saltation: Preliminary Laboratory and Field Measurements. Developments in Sedimentology, 38, pp. 133-148.

GREENBAUM, N., SCHWARTZ, U., BENITO, G., PORAT, N., CLOETE, G.C. and ENZEL, Y., 2014. Paleohydrology of extraordinary floods along the Swakop River at the margin of the Namib Desert and their paleoclimate implications. Quaternary Science Reviews, 103, pp. 153-169.

GRODEK, T., BENITO, G., BOTERO, B., JACOBY, Y., PORAT, N., HAVIV, I., CLOETE, G. and ENZEL, Y., 2013. The last millennium largest floods in the hyperarid Kuiseb River basin, Namib Desert. Journal of Quaternary Science, 28(3), pp. 258-270.

GROSS, A., GOREN, T., PIO, C., CARDOSO, J., TIROSH, O., TODD, M., ROSENFELD, D., WEINER, T., CUSTÓDIO, D. and ANGERT, A., 2015. Variability in sources and concentrations of Saharan dust phosphorus over the Atlantic ocean. Environmental Science & Technology Letters, 2(2), pp. 31-37.

GROSS, A., PALCHAN, D., KROM, M. and ANGERT, A., 2016. Elemental and isotopic composition of surface soils from key Saharan dust sources. Chemical Geology, 442, pp. 54-61.

GRUBER, N., LACHKAR, Z., FRENZEL, H., MARCHESIELLO, P., MÜNNICH, M., MCWILLIAMS, J.C., NAGAI, T. and PLATTNER, G., 2011. Eddy-induced reduction of biological production in eastern boundary upwelling systems. Nature geoscience, 4(11), pp. 787-792.

GRÜNERT, N., 2000. Namibia--fascination of Geology: A Travel Handbook. Klaus Hess Publishers.

GUIEU, C., AUMONT, O., PAYTAN, A., BOPP, L., LAW, C., MAHOWALD, N., ACHTERBERG, E.P., MARAÑÓN, E., SALIHOGLU, B. and CRISE, A., 2014a. The significance of the episodic nature of atmospheric deposition to Low Nutrient Low Chlorophyll regions. Global Biogeochemical Cycles, 28(11), pp. 1179-1198.

GUIEU, C. and THOMAS, A., 1996. Saharan aerosols: From the soil to the ocean. The impact of desert dust across the Mediterranean. Springer, pp. 207-216.

GUIEU, C., DULAC, F., RIDAME, C. and PONDAVEN, P., 2014b. Introduction to project DUNE, a DUst experiment in a low Nutrient, low chlorophyll Ecosystem. Biogeosciences, 11, pp. 425-442.

GUTIERREZ, J.R. and WHITFORD, W.G., 1987. Chihuahuan desert annuals: importance of water and nitrogen. Ecology, , pp. 2032-2045.

GUTKNECHT, E., DADOU, I., LE VU, B., CAMBON, G., SUDRE, J., GARÇON, V., MACHU, E., RIXEN, T., KOCK, A. and FLOHR, A., 2013. Coupled physical/biogeochemical modeling including O-2-dependent processes in the Eastern Boundary Upwelling Systems: application in the Benguela. Biogeosciences, 10(6), pp. 3559-3591.

HACHFELD, B., JÜRGENS, N., DEIL, U. and LOIDI, J., 2000. Climate patterns and their impact on the vegetation in a fog driven desert: the Central Namib Desert in Namibia. Vegetation and climate. A selection of contributions presented at the 42nd Symposium of the International Association of Vegetation Science, Bilbao, Spain, 26-30 July 1999. 2000, Gebrüder Borntraeger Verlagsbuchhandlung, pp. 567-589.

HADDADCHI, A., RYDER, D.S., EVRARD, O. and OLLEY, J., 2013. Sediment fingerprinting in fluvial systems: review of tracers, sediment sources and mixing models. International Journal of Sediment Research, 28(4), pp. 560-578.

HADLEY, N.F. and SZAREK, S.R., 1981. Productivity of desert ecosystems. Bioscience, 31(10), pp. 747-753.

HAGEN, E., FEISTEL, R., AGENBAG, J.J. and OHDE, T., 2001. Seasonal and interannual changes in intense Benguela upwelling (1982–1999). Oceanologica Acta, 24(6), pp. 557-568.

HAGSTROM, G.I., LEVIN, S.A. and MARTINY, A., 2016. Resource ratios determine nutrient limitation of primary productivity in the ocean. bioRxiv, , pp. 064543.

HAMEED, S. and DIGNON, J., 1988. Changes in the geographical distributions of global emissions of NOx and SOx from fossil-fuel combustion between 1966 and 1980. Atmospheric Environment (1967), 22(3), pp. 441-449.

HAND, J., MAHOWALD, N., CHEN, Y., SIEFERT, R., LUO, C., SUBRAMANIAM, A. and FUNG, I., 2004. Estimates of atmospheric ‐ processed soluble iron from observations and a global mineral aerosol model: Biogeochemical implications. Journal of Geophysical Research: Atmospheres, 109(D17).

HANSEN, J., SATO, M. and RUEDY, R., 1997. Radiative forcing and climate response. Journal of Geophysical Research: Atmospheres, 102(D6), pp. 6831-6864.

HARMS, T.K. and GRIMM, N.B., 2010. Influence of the hydrologic regime on resource availability in a semi ‐ arid stream ‐ riparian corridor. Ecohydrology, 3(3), pp. 349-359.

HAUCK, J. and VÖLKER, C., 2015. Rising atmospheric CO2 leads to large impact of biology on Southern Ocean CO2 uptake via changes of the Revelle factor. Geophysical Research Letters, 42(5), pp. 1459-1464.

HAUSTEIN, K., WASHINGTON, R., KING, J., WIGGS, G., THOMAS, D., ECKARDT, F., BRYANT, R. and MENUT, L., 2015. Testing the performance of state-of-the-art dust emission schemes using DO4Models field data. Geoscientific Model Development, 8, pp. 341-362.

HAY, W.W. and BROCK, J.C., 1992. Temporal variation in intensity of upwelling off southwest Africa. Geological Society, London, Special Publications, 64(1), pp. 463-497.

HAYWOOD, J., FRANCIS, P., DUBOVIK, O., GLEW, M. and HOLBEN, B., 2003. Comparison of aerosol size distributions, radiative properties, and optical depths determined by aircraft observations and Sun photometers during SAFARI 2000. Journal of Geophysical Research: Atmospheres, 108(D13).

HECKY, R. and KILHAM, P., 1988. Nutrient limitation of phytoplankton in freshwater and marine environments: a review of recent evidence on the effects of enrichment. Limnology and Oceanography, 33(4), pp. 796-822.

HEINE, K. and HEINE, J.T., 2002. A paleohydrologic reinterpretation of the Homeb Silts, Kuiseb River, central Namib Desert (Namibia) and paleoclimatic implications. Catena, 48(1), pp. 107-130.

HEINE, K. and VÖLKEL, J., 2010. Soil clay minerals in Namibia and their significance for the terrestrial and marine past global change research.

HENSCHEL, J.R. and SEELY, M.K., 2008. Ecophysiology of atmospheric moisture in the Namib Desert. Atmospheric Research, 87(3), pp. 362-368.

HERUT, B., COLLIER, R. and KROM, M.D., 2002. The role of dust in supplying nitrogen and phosphorus to the Southeast Mediterranean. Limnology and Oceanography, 47(3), pp. 870-878.

HERUT, B., KROM, M.D., PAN, G. and MORTIMER, R., 1999. Atmospheric input of nitrogen and phosphorus to the Southeast Mediterranean: Sources, fluxes, and possible impact. Limnology and Oceanography, 44(7), pp. 1683-1692.

HERUT, B., ZOHARY, T., KROM, M., MANTOURA, R.F.C., PITTA, P., PSARRA, S., RASSOULZADEGAN, F., TANAKA, T. and THINGSTAD, T.F., 2005. Response of East Mediterranean surface water to Saharan dust: On-board microcosm experiment and field observations. Deep Sea Research Part II: Topical Studies in Oceanography, 52(22), pp. 3024-3040.

HESSE, P.P. and MCTAINSH, G.H., 2003. Australian dust deposits: modern processes and the Quaternary record. Quaternary Science Reviews, 22(18), pp. 2007-2035.

HESSEN, D.O., HINDAR, A. and HOLTAN, G., 1997. The significance of nitrogen runoff for eutrophication of freshwater and marine recipients. Ambio, , pp. 312-320.

HOLTAN, H., KAMP-NIELSEN, L. and STUANES, A., 1988. Phosphorus in soil, water and sediment: an overview. Phosphorus in Freshwater Ecosystems. Springer, pp. 19-34.

HOOD, R.R., COLES, V.J. and CAPONE, D.G., 2004. Modeling the distribution of Trichodesmium and nitrogen fixation in the Atlantic Ocean. Journal of Geophysical Research: Oceans, 109(C6).

HOWARD, A.D., DIETRICH, W.E. and SEIDL, M.A., 1994. Modeling fluvial erosion on regional to continental scales. Journal of Geophysical Research: Solid Earth, 99(B7), pp. 13971-13986.

HOWARTH, R.W., 1988. Nutrient limitation of net primary production in marine ecosystems. Annual Review of Ecology and Systematics, , pp. 89-110.

HOWARTH, R.W. and MARINO, R., 2006. Nitrogen as the limiting nutrient for eutrophication in coastal marine ecosystems: evolving views over three decades. Limnology and Oceanography, 51(1part2), pp. 364-376.

HSU, N., JEONG, M., BETTENHAUSEN, C., SAYER, A., HANSELL, R., SEFTOR, C., HUANG, J. and TSAY, S., 2013. Enhanced Deep Blue aerosol retrieval algorithm: The second generation. Journal of Geophysical Research: Atmospheres, 118(16), pp. 9296-9315.

HU, C., LEE, Z. and FRANZ, B., 2012. Chlorophyll a algorithms for oligotrophic oceans: A novel approach based on three‐band reflectance difference. Journal of Geophysical Research: Oceans, 117(C1).

HUANG, M., TONG, D., LEE, P., PAN, L., TANG, Y., STAJNER, I., PIERCE, R., MCQUEEN, J. and WANG, J., 2015. Toward enhanced capability for detecting and predicting dust events in the western United States: the Arizona case study. Atmospheric Chemistry and Physics, 15(21), pp. 12595-12610.

HUNEEUS, N., SCHULZ, M., BALKANSKI, Y., GRIESFELLER, J., PROSPERO, J., KINNE, S., BAUER, S., BOUCHER, O., CHIN, M. and DENTENER, F., 2011. Global dust model intercomparison in AeroCom phase I. Atmospheric Chemistry and Physics, 11(15).

HUTCHINGS, L., VAN DER LINGEN, C., SHANNON, L., CRAWFORD, R., VERHEYE, H., BARTHOLOMAE, C., VAN DER PLAS, A., LOUW, D., KREINER, A. and OSTROWSKI, M., 2009. The Benguela Current: An ecosystem of four components. Progress in Oceanography, 83(1), pp. 15-32.

HUTCHINS, D., DITULLIO, G., ZHANG, Y. and BRULAND, K., 1998. An iron limitation mosaic in the California upwelling regime. Limnology and Oceanography, 43(6), pp. 1037-1054.

HUTCHINS, D., HARE, C., WEAVER, R., ZHANG, Y., FIRME, G., DITULLIO, G., ALM, M., RISEMAN, S., MAUCHER, J. and GEESEY, M., 2002. Phytoplankton iron limitation in the Humboldt Current and Peru Upwelling. Limnology and Oceanography, 47(4), pp. 997-1011.

HUTCHINS, D.A., WITTER, A.E., BUTLER, A. and LUTHER, G.W., 1999. Competition among marine phytoplankton for different chelated iron species. Nature, 400(6747), pp. 858-861.

JACOBSON, P.J., JACOBSON, K.N. and SEELY, M.K., 1995. Ephemeral rivers and their catchments: sustaining people and development in western Namibia. Desert Research Foundation of Namibia.

JACOBSON, P. and JACOBSON, K., 2013. Hydrologic controls of physical and ecological processes in Namib Desert ephemeral rivers: implications for conservation and management. Journal of Arid Environments, 93, pp. 80-93.

JACOBSON, P., JACOBSON, K., ANGERMEIER, P. and CHERRY, D., 2000. Hydrologic influences on soil properties along ephemeral rivers in the Namib Desert. Journal of Arid Environments, 45(1), pp. 21-34.

JERRAM, D., MOUNTNEY, N., HOLZFÖRSTER, F. and STOLLHOFEN, H., 1999. Internal stratigraphic relationships in the Etendeka Group in the Huab Basin, NW

Namibia: understanding the onset of flood volcanism. Journal of Geodynamics, 28(4), pp. 393-418.

JICKELLS, T., AN, Z., ANDERSEN, K.K., BAKER, A., BERGAMETTI, G., BROOKS, N., CAO, J., BOYD, P., DUCE, R. and HUNTER, K., 2005. Global iron connections between desert dust, ocean biogeochemistry, and climate. Science, 308(5718), pp. 67-71.

JICKELLS, T., BOYD, P. and HUNTER, K.A., 2014. Biogeochemical Impacts of Dust on the Global Carbon Cycle. Mineral Dust. Springer, pp. 359-384.

JICKELLS, T. and MOORE, C.M., 2015. The Importance of Atmospheric Deposition for Ocean Productivity. Annual Review of Ecology, Evolution, and Systematics, 46, pp. 481-501.

JICKELLS, T.D. and SPOKES, L.J., 2001. Atmospheric iron inputs to the oceans. IUPAC series on analytical and physical chemistry of environmental systems, 7, pp. 85-122.

JISH PRAKASH, P., STENCHIKOV, G., KALENDERSKI, S., OSIPOV, S. and BANGALATH, H., 2015. The impact of dust storms on the Arabian Peninsula and the Red Sea. Atmospheric Chemistry and Physics, 15(1), pp. 199-222.

JO, C.O., LEE, J., PARK, K., KIM, Y.H. and KIM, K., 2007. Asian dust initiated early spring bloom in the northern East/Japan Sea. Geophysical Research Letters, 34(5).

JOHNSON, K.S., ELROD, V.A., FITZWATER, S.E., PLANT, J.N., CHAVEZ, F.P., TANNER, S.J., GORDON, R.M., WESTPHAL, D.L., PERRY, K.D. and WU, J., 2003. Surface ocean‐lower atmosphere interactions in the northeast Pacific Ocean gyre: Aerosols, iron, and the ecosystem response. Global Biogeochemical Cycles, 17(2).

JOHNSTON, C.A., BRIDGHAM, S.D. and SCHUBAUER-BERIGAN, J.P., 2001. Nutrient dynamics in relation to geomorphology of riverine wetlands. Soil Science Society of America Journal, 65(2), pp. 557-577.

JOURNET, E., DESBOEUFS, K.V., CAQUINEAU, S. and COLIN, J., 2008. Mineralogy as a critical factor of dust iron solubility. Geophysical Research Letters, 35(7).

JUHREN, M., WENT, F. and PHILLIPS, E., 1956. Ecology of desert plants. IV. Combined field and laboratory work on germination of annuals in the Joshua Tree National Monument, California. Ecology, , pp. 318-330.

JURY, M.R., 2012. Physical oceanographic influences on Central Benguela fish catch. Earth Interactions, 16(6), pp. 1-15.

KANAKIDOU, M., DUCE, R.A., PROSPERO, J.M., BAKER, A.R., BENITEZ-NELSON, C., DENTENER, F.J., HUNTER, K.A., LISS, P.S., MAHOWALD, N., OKIN, G.S., SARIN, M., TSIGARIDIS, K., UEMATSU, M., ZAMORA, L.M. and ZHU, T., 2012. Atmospheric fluxes of organic N and P to the global ocean. Global Biogeochemical Cycles, 26(3), pp. n/a-n/a.

KARL, D., MICHAELS, A., BERGMAN, B., CAPONE, D., CARPENTER, E., LETELIER, R., LIPSCHULTZ, F., PAERL, H., SIGMAN, D. and STAL, L., 2002.

Dinitrogen fixation in the world's oceans. The Nitrogen Cycle at Regional to Global Scales. Springer, pp. 47-98.

KATJIUA, M. and WARD, D., 2007. Pastoralists' perceptions and realities of vegetation change and browse consumption in the northern Kalahari, Namibia. Journal of Arid Environments, 69(4), pp. 716-730.

KHAN, A., 1979. Distribution of DTPA‐extractable Fe, Zn, and cu in soil particle‐size fractions 1. Communications in Soil Science & Plant Analysis, 10(9), pp. 1211-1218.

KHAN, A. and SOLTANPOUR, P., 1978. Effect of wetting and drying on DTPA‐extractable Fe, Zn, Mn, and Cu in soils 1. Communications in Soil Science & Plant Analysis, 9(3), pp. 193-202.

KIDRON, G.J., POSMANIK, R., BRUNNER, T. and NEJIDAT, A., 2015. Spatial abundance of microbial nitrogen-transforming genes and inorganic nitrogen in biocrusts along a transect of an arid sand dune in the Negev Desert. Soil Biology and Biochemistry, 83, pp. 150-159.

KIENAST, S.S., HENDY, I.L., CRUSIUS, J., PEDERSEN, T.F. and CALVERT, S.E., 2004. Export production in the subarctic North Pacific over the last 800 kyrs: No evidence for iron fertilization? Journal of Oceanography, 60(1), pp. 189-203.

KOREN, I., KAUFMAN, Y.J., WASHINGTON, R., TODD, M.C., RUDICH, Y., MARTINS, J.V. and ROSENFELD, D., 2006. The Bodélé depression: a single spot in the Sahara that provides most of the mineral dust to the Amazon forest. Environmental Research Letters, 1(1), pp. 014005.

KOWALCHUK, G.A. and STEPHEN, J.R., 2001. Ammonia-oxidizing bacteria: a model for molecular microbial ecology. Annual Reviews in Microbiology, 55(1), pp. 485-529.

KRAEMER, S.M., BUTLER, A., BORER, P. and CERVINI-SILVA, J., 2005. Siderophores and the dissolution of iron-bearing minerals in marine systems. Reviews in mineralogy and geochemistry, 59(1), pp. 53-84.

KRAPF, C.B., STOLLHOFEN, H. and STANISTREET, I.G., 2003. Contrasting styles of ephemeral river systems and their interaction with dunes of the Skeleton Coast erg (Namibia). Quaternary International, 104(1), pp. 41-52.

KRISHNAMURTHY, A., MOORE, J.K., MAHOWALD, N., LUO, C., DONEY, S.C., LINDSAY, K. and ZENDER, C.S., 2009. Impacts of increasing anthropogenic soluble iron and nitrogen deposition on ocean biogeochemistry. Global Biogeochemical Cycles, 23(3).

KRISHNAMURTHY, A., MOORE, J.K., MAHOWALD, N., LUO, C. and ZENDER, C.S., 2010. Impacts of atmospheric nutrient inputs on marine biogeochemistry. Journal of Geophysical Research: Biogeosciences, 115(G1), pp. - G01006.

KROEZE, C., BOUWMAN, L. and SEITZINGER, S., 2012. Modeling global nutrient export from watersheds. Current opinion in environmental sustainability, 4(2), pp. 195-202.

KROOPNICK, P.M., 1975. Respiration, photosynthesis, and oxygen isotope fractionation in oceanic surface water1. Limnology and Oceanography, 20(6), pp. 988-992.

KRUEGER, B.J., GRASSIAN, V.H., COWIN, J.P. and LASKIN, A., 2004. Heterogeneous chemistry of individual mineral dust particles from different dust source regions: the importance of particle mineralogy. Atmospheric Environment, 38(36), pp. 6253-6261.

KUMA, K. and MATSUNAGA, K., 1995. Availability of colloidal ferric oxides to coastal marine phytoplankton. Marine Biology, 122(1), pp. 1-11.

KUO, C., LIN, C., HUANG, L., WANG, S., SHIEH, P., LIN, Y. and WANG, J., 2010. Spatial variations of the aerosols in river-dust episodes in central Taiwan. Journal of hazardous materials, 179(1), pp. 1022-1030.

LAFON, S., RAJOT, J., ALFARO, S.C. and GAUDICHET, A., 2004. Quantification of iron oxides in desert aerosol. Atmospheric Environment, 38(8), pp. 1211-1218.

LAIR, G.J., ZEHETNER, F., KHAN, Z.H. and GERZABEK, M.H., 2009. Phosphorus sorption–desorption in alluvial soils of a young weathering sequence at the Danube River. Geoderma, 149(1), pp. 39-44.

LAM, P.J. and BISHOP, J.K., 2008. The continental margin is a key source of iron to the HNLC North Pacific Ocean. Geophysical Research Letters, 35(7).

LAMBERT, F., TAGLIABUE, A., SHAFFER, G., LAMY, F., WINCKLER, G., FARIAS, L., GALLARDO, L. and POL ‐ HOLZ, D., 2015. Dust fluxes and iron fertilization in Holocene and Last Glacial Maximum climates. Geophysical Research Letters, 42(14), pp. 6014-6023.

LAMY, F., GERSONDE, R., WINCKLER, G., ESPER, O., JAESCHKE, A., KUHN, G., ULLERMANN, J., MARTINEZ-GARCIA, A., LAMBERT, F. and KILIAN, R., 2014. Increased dust deposition in the Pacific Southern Ocean during glacial periods. Science (New York, N.Y.), 343(6169), pp. 403-407.

LANCASTER, N., 1989. The namib sand sea. Balkema, Rotterdam, , pp. 180.

LANCASTER, N., 1985. Winds and sand movements in the Namib sand sea. Earth Surface Processes and Landforms, 10(6), pp. 607-619.

LANCASTER, J., LANCASTER, N. and SEELY, M.K., 1984. Madoqua, 14, pp. 5.

LANGBEIN, W.B. and SCHUMM, S.A., 1958. Yield of sediment in relation to mean annual precipitation. Eos, Transactions American Geophysical Union, 39(6), pp. 1076-1084.

LARONNE, J.B., 1993. Very high rates of bedload sediment transport by ephemeral desert rivers. Nature, 366(6451), pp. 148-150.

LASKIN, A., COWIN, J.P. and IEDEMA, M.J., 2006. Analysis of individual environmental particles using modern methods of electron microscopy and X-ray

microanalysis. Journal of Electron Spectroscopy and Related Phenomena, 150(2), pp. 260-274.

LEE, J.A., GILL, T.E., MULLIGAN, K.R., ACOSTA, M.D. and PEREZ, A.E., 2009. Land use/land cover and point sources of the 15 December 2003 dust storm in southwestern North America. Geomorphology, 105(1), pp. 18-27.

LEGGETT, K.E., 2006. Home range and seasonal movement of elephants in the Kunene Region, northwestern Namibia. African Zoology, 41(1), pp. 17-36.

LEGGETT, K., FENNESSY, J. and SCHNEIDER, S., 2003. Does land use matter in an arid environment? A case study from the Hoanib River catchment, north-western Namibia. Journal of Arid Environments, 53(4), pp. 529-543.

LEGGETT, K., FENNESSY, J. and SCHNEIDER, S., 2003b. Seasonal vegetation changes in the Hoanib River catchment, north-western Namibia: a study of a non-equilibrium system. Journal of Arid Environments, 53(1), pp. 99-113.

LENES, J.M., DARROW, B.P., CATTRALL, C., HEIL, C.A., CALLAHAN, M., VARGO, G.A., BYRNE, R.H., PROSPERO, J.M., BATES, D.E. and FANNING, K.A., 2001. Iron fertilization and the Trichodesmiumresponse on the West Florida shelf. Limnology and Oceanography, 46(6), pp. 1261-1277.

LEVINE, J.S., 1996. Biomass Burning and Global Change: Remote sensing, modeling and inventory development, and biomass burning in Africa. MIT Press.

LI, F., GINOUX, P. and RAMASWAMY, V., 2008. Distribution, transport, and deposition of mineral dust in the Southern Ocean and Antarctica: Contribution of major sources. Journal of Geophysical Research: Atmospheres, 113(D10).

LIAO, H. and SEINFELD, J., 1998. Radiative forcing by mineral dust aerosols: sensitivity to key variables. Journal of Geophysical Research, 103(D24), pp. 31637-31645.

LIGHT, M., MASLANYJ, M. and BANKS, N., 1992. New geophysical evidence for extensional tectonics on the divergent margin offshore Namibia. Geological Society, London, Special Publications, 68(1), pp. 257-270.

LIN, I., HU, C., LI, Y., HO, T., FISCHER, T.P., WONG, G.T., WU, J., HUANG, C., CHU, D.A. and KO, D.S., 2011. Fertilization potential of volcanic dust in the low‐nutrient low‐chlorophyll western North Pacific subtropical gyre: Satellite evidence and laboratory study. Global Biogeochemical Cycles, 25(1).

LINDESAY, J. and TYSON, P., 1990. Climate and near-surface airflow over the central Namib. Namib ecology, 25, pp. 27-37.

LINDSAY, W.L. and NORVELL, W.A., 1978. Development of a DTPA soil test for zinc, iron, manganese, and copper. Soil Science Society of America Journal, 42(3), pp. 421-428.

LOHAN, M.C. and BRULAND, K.W., 2008. Elevated Fe (II) and dissolved Fe in hypoxic shelf waters off Oregon and Washington: an enhanced source of iron to coastal upwelling regimes. Environmental science & technology, 42(17), pp. 6462-6468.

LONG, J.A., LARGE, R.R., LEE, M.S., BENTON, M.J., DANYUSHEVSKY, L.V., CHIAPPE, L.M., HALPIN, J.A., CANTRILL, D. and LOTTERMOSER, B., 2015. Severe selenium depletion in the Phanerozoic oceans as a factor in three global mass extinction events. Gondwana Research, .

LONGHURST, A., SATHYENDRANATH, S., PLATT, T. and CAVERHILL, C., 1995. An estimate of global primary production in the ocean from satellite radiometer data. Journal of Plankton Research, 17(6), pp. 1245-1271.

LÓPEZ-GARCÍA, P., GELADO-CABALLERO, M.D., COLLADO-SÁNCHEZ, C. and HERNÁNDEZ-BRITO, J.J., 2017. Solubility of aerosol trace elements: Sources and deposition fluxes in the Canary Region. Atmospheric Environment, 148, pp. 167-174.

LOUIS, J., BRESSAC, M., PEDROTTI, M.L. and GUIEU, C., 2015. Dissolved inorganic nitrogen and phosphorus dynamics in seawater following an artificial Saharan dust deposition event. Frontiers in Marine Science, 2, pp. 27.

LUO, C., MAHOWALD, N.M. and DEL CORRAL, J., 2003. Sensitivity study of meteorological parameters on mineral aerosol mobilization, transport, and distribution. Journal of Geophysical Research: Atmospheres, 108(D15).

MACKENZIE, F., VER, L. and LERMAN, A., 1998. Coupled biogeochemical cycles of carbon, nitrogen, phosphorous and sulfur in the land-oceanatmosphere system. Asian Change in the Context of Global Climate Change, , pp. 42-100.

MACKIE, D.S., BOYD, P.W., MCTAINSH, G.H., TINDALE, N.W., WESTBERRY, T.K. and HUNTER, K.A., 2008. Biogeochemistry of iron in Australian dust: From eolian uplift to marine uptake. Geochemistry, Geophysics, Geosystems, 9(3).

MACKIE, D., BOYD, P., HUNTER, K. and MCTAINSH, G.H., 2005. Simulating the cloud processing of iron in Australian dust: pH and dust concentration. Geophysical Research Letters, 32(6).

MACKIE, D., PEAT, J., MCTAINSH, G.H., BOYD, P. and HUNTER, K., 2006. Soil abrasion and eolian dust production: Implications for iron partitioning and solubility. Geochemistry, Geophysics, Geosystems, 7(12).

MAHER, B.A., PROSPERO, J.M., MACKIE, D., GAIERO, D., HESSE, P.P. and BALKANSKI, Y., 2010. Global connections between aeolian dust, climate and ocean biogeochemistry at the present day and at the last glacial maximum. Earth-Science Reviews, 99(1–2), pp. 61-97.

MAHOWALD, N.M., BAKER, A.R., BERGAMETTI, G., BROOKS, N., DUCE, R.A., JICKELLS, T.D., KUBILAY, N., PROSPERO, J.M. and TEGEN, I., 2005. Atmospheric global dust cycle and iron inputs to the ocean. Global Biogeochemical Cycles, 19(4).

MAHOWALD, N.M., BRYANT, R.G., DEL CORRAL, J. and STEINBERGER, L., 2003. Ephemeral lakes and desert dust sources. Geophysical Research Letters, 30(2).

MAHOWALD, N.M., ENGELSTAEDTER, S., LUO, C., SEALY, A., ARTAXO, P., BENITEZ-NELSON, C., BONNET, S., CHEN, Y., CHUANG, P.Y. and COHEN, D.D., 2009. Atmospheric Iron Deposition: Global Distribution, Variability, and Human Perturbations*. Annual Review of Marine Science, 1, pp. 245-278.

MAHOWALD, N.M., KLOSTER, S., ENGELSTAEDTER, S., MOORE, J.K., MUKHOPADHYAY, S., MCCONNELL, J.R., ALBANI, S., DONEY, S.C., BHATTACHARYA, A. and CURRAN, M., 2010. Observed 20th century desert dust variability: impact on climate and biogeochemistry. Atmospheric Chemistry and Physics, 10(22), pp. 10875-10893.

MAHOWALD, N., JICKELLS, T.D., BAKER, A.R., ARTAXO, P., BENITEZ-NELSON, C.R., BERGAMETTI, G., BOND, T.C., CHEN, Y., COHEN, D.D. and HERUT, B., 2008. Global distribution of atmospheric phosphorus sources, concentrations and deposition rates, and anthropogenic impacts. Global Biogeochem.Cy, 22(4).

MAHOWALD, N., 2011. Aerosol indirect effect on biogeochemical cycles and climate. Science (New York, N.Y.), 334(6057), pp. 794-796.

MAKEPEACE, D.K., SMITH, D.W. and STANLEY, S.J., 1995. Urban stormwater quality: summary of contaminant data. Critical Reviews in Environmental Science and Technology, 25(2), pp. 93-139.

MALVERN INSTRUMENTS, 2007. Scirocco 2000 User Manual. MAN0386 1.0 edn. Worcestershire, UK: Malvern Instruments Ltd.

MARING, H., SAVOIE, D., IZAGUIRRE, M., CUSTALS, L. and REID, J., 2003. Mineral dust aerosol size distribution change during atmospheric transport. Journal of Geophysical Research: Atmospheres, 108(D19).

MARTIN, J. and MEYBECK, M., 1979. Elemental mass-balance of material carried by major world rivers. Marine Chemistry, 7(3), pp. 173-206.

MARTIN, J.H., 1990. Glacial ‐ interglacial CO2 change: The iron hypothesis. Paleoceanography, 5(1), pp. 1-13.

MARTIN, J.H., COALE, K., JOHNSON, K., FITZWATER, S., GORDON, R., TANNER, S., HUNTER, C., ELROD, V., NOWICKI, J. and COLEY, T., 1994. Testing the iron hypothesis in ecosystems of the equatorial Pacific Ocean.

MARTIN, J.H. and FITZWATER, S., 1988. Iron deficiency limits phytoplankton growth in the north-east Pacific subarctic. Nature, 331(3414343), pp. 947-975.

MARTIN, P., LOEFF, M.R., CASSAR, N., VANDROMME, P., D'OVIDIO, F., STEMMANN, L., RENGARAJAN, R., SOARES, M., GONZÁLEZ, H.E. and EBERSBACH, F., 2013. Iron fertilization enhanced net community production but not downward particle flux during the Southern Ocean iron fertilization experiment LOHAFEX. Global Biogeochemical Cycles, 27(3), pp. 871-881.

MCGOWAN, H. and CLARK, A., 2008. Identification of dust transport pathways from Lake Eyre, Australia using Hysplit. Atmospheric Environment, 42(29), pp. 6915-6925.

MCLEOD, S., 1992. Determination of total soil and plant nitrogen using a micro-distillation unit in a continuous flow analyzer. Analytica Chimica Acta, 266(1), pp. 113-117.

MCTAINSH, G. and STRONG, C., 2007. The role of aeolian dust in ecosystems. Geomorphology, 89(1), pp. 39-54.

MEHLICH, A., 1984. Mehlich 3 soil test extractant: A modification of Mehlich 2 extractant. Communications in Soil Science & Plant Analysis, 15(12), pp. 1409-1416.

MÉLANÇON, J., LEVASSEUR, M., LIZOTTE, M., SCARRATT, M., TREMBLAY, J., TORTELL, P., YANG, G., SHI, G., GAO, H. and SEMENIUK, D., 2016. Impact of ocean acidification on phytoplankton assemblage, growth, and DMS production following Fe-dust additions in the NE Pacific high-nutrient, low-chlorophyll waters. Biogeosciences, 13(5), pp. 1677-1692.

MENDEZ, M.J., FUNK, R. and BUSCHIAZZO, D.E., 2011. Field wind erosion measurements with big spring number eight (bsne) and modified wilson and cook (mwac) samplers. Geomorphology, 129(1), pp. 43-48.

MERRITT, D.M. and WOHL, E.E., 2003. Downstream hydraulic geometry and channel adjustment during a flood along an ephemeral, arid-region drainage. Geomorphology, 52(3), pp. 165-180.

MESKHIDZE, N., NENES, A., CHAMEIDES, W.L., LUO, C. and MAHOWALD, N., 2007. Atlantic Southern Ocean productivity: Fertilization from above or below? Global Biogeochemical Cycles, 21(2).

MESSIÉ, M. and CHAVEZ, F.P., 2015. Seasonal regulation of primary production in eastern boundary upwelling systems. Progress in Oceanography, 134, pp. 1-18.

MEYBECK, M., 1982. Carbon, nitrogen, and phosphorus transport by world rivers. Am.J.Sci, 282(4), pp. 401-450.

MICHAELS, A., OLSON, D., SARMIENTO, J., AMMERMAN, J., FANNING, K., JAHNKE, R., KNAP, A., LIPSCHULTZ, F. and PROSPERO, J., 1996. Inputs, losses and transformations of nitrogen and phosphorus in the pelagic North Atlantic Ocean. Nitrogen Cycling in the North Atlantic Ocean and Its Watersheds. Springer, pp. 181-226.

MIDDLETON, N.J. and GOUDIE, A.S., 2001. Saharan dust: sources and trajectories. Transactions of the Institute of British Geographers, 26(2), pp. 165-181.

MILLER, R., TEGEN, I. and PERLWITZ, J., 2004. Surface radiative forcing by soil dust aerosols and the hydrologic cycle. Journal of Geophysical Research: Atmospheres, 109(D4).

MILLS, M.M., RIDAME, C., DAVEY, M., LA ROCHE, J. and GEIDER, R.J., 2004. Iron and phosphorus co-limit nitrogen fixation in the eastern tropical North Atlantic. Nature, 429(6989), pp. 292-294.

MINNETT, P.J., BROWN, O.B., EVANS, R.H., KEY, E.L., KEARNS, E.J., KILPATRICK, K., KUMAR, A., MAILLET, K.A. and SZCZODRAK, G., 2004. Sea-

surface temperature measurements from the Moderate-Resolution Imaging Spectroradiometer (MODIS) on Aqua and Terra, Geoscience and Remote Sensing Symposium, 2004. IGARSS'04. Proceedings. 2004 IEEE International 2004, IEEE, pp. 4576-4579.

MONGER, H. and BESTELMEYER, B., 2006. The soil-geomorphic template and biotic change in arid and semi-arid ecosystems. Journal of Arid Environments, 65(2), pp. 207-218.

MOORE, C., MILLS, M., ARRIGO, K., BERMAN-FRANK, I., BOPP, L., BOYD, P., GALBRAITH, E., GEIDER, R.J., GUIEU, C. and JACCARD, S., 2013. Processes and patterns of oceanic nutrient limitation. Nature Geoscience, 6(9), pp. 701-710.

MOORE, C., MILLS, M.M., MILNE, A., LANGLOIS, R., ACHTERBERG, E.P., LOCHTE, K., GEIDER, R.J. and LA ROCHE, J., 2006. Iron limits primary productivity during spring bloom development in the central North Atlantic. Global Change Biology, 12(4), pp. 626-634.

MOORE, J.K. and DONEY, S.C., 2007. Iron availability limits the ocean nitrogen inventory stabilizing feedbacks between marine denitrification and nitrogen fixation. Global Biogeochemical Cycles, 21(2).

MOORE, L.R., POST, A.F., ROCAP, G. and CHISHOLM, S.W., 2002. Utilization of different nitrogen sources by the marine cyanobacteria Prochlorococcus and Synechococcus. Limnology and Oceanography, 47(4), pp. 989-996.

MOREL, A. and GENTILI, B., 1991. Diffuse reflectance of oceanic waters: its dependence on Sun angle as influenced by the molecular scattering contribution. *Applied Optics,* **30**(30), pp. 4427-4438.

MOREL, F.M., HUDSON, R.J. and PRICE, N.M., 1991. Limitation of productivity by trace metals in the sea. Limnology and Oceanography, 36(8), pp. 1742-1755.

MORIN, E., GRODEK, T., DAHAN, O., BENITO, G., KULLS, C., JACOBY, Y., VAN LANGENHOVE, G., SEELY, M. and ENZEL, Y., 2009. Flood routing and alluvial aquifer recharge along the ephemeral arid Kuiseb River, Namibia. Journal of Hydrology, 368(1), pp. 262-275.

MOULIN, C., LAMBERT, C.E., DULAC, F. and DAYAN, U., 1997. Control of atmospheric export of dust from North Africa by the North Atlantic Oscillation. Nature, 387(6634), pp. 691.

MUHS, D.R., BUDAHN, J.R., SKIPP, G.L. and MCGEEHIN, J.P., 2016. Geochemical evidence for seasonal controls on the transportation of Holocene loess, Matanuska Valley, southern Alaska, USA. Aeolian Research, 21, pp. 61-73.

MYRIOKEFALITAKIS, S., NENES, A., BAKER, A.R., MIHALOPOULOS, N. and KANAKIDOU, M., 2016. Bioavailable atmospheric phosphorous supply to the global ocean: a 3-D global modelling study. Biogeosciences, .

NAKAI, S., HALLIDAY, A.N. and REA, D.K., 1993. Provenance of dust in the Pacific Ocean. Earth and Planetary Science Letters, 119(1), pp. 143-157.

NASA, 2016-last update, EOSDIS Worldview [Homepage of NASA], [Online]. Available: https://worldview.earthdata.nasa.gov [2014-2016, 2016].

NASA, December 31, 2016, 2010-last update, Dust and Hydrogen Sulfide along the Namibian Coast [Homepage of MODIS Rapid Response Team at NASA GSFC], [Online]. Available: http://visibleearth.nasa.gov/view.php?id=443402014].

NASA, 2004-last update, NASA Visible Earth: Dust plumes off Namibia. Available: http://visibleearth.nasa.gov/view.php?id=71329 [2/26/2013, 2013].

NASA, 2003-last update, Visible Earth: Streamers of Dust off Namibia. Available: http://visibleearth.nasa.gov/view.php?id=11657 [2/26/2013, 2013].

NASA, August 9, 2002, 2002-last update, NASA Visible Earth: Dust plumes off Namibia Coast. Available: http://visibleearth.nasa.gov/view.php?id=61656 [2/26/2013, 2013].

NAUD, C.M., POSSELT, D.J. and HEEVER, S.C., 2016. Aerosol optical depth distribution in extratropical cyclones over the Northern Hemisphere oceans. Geophysical Research Letters, 43(19).

NEFF, P.D. and BERTLER, N.A., 2015. Trajectory modeling of modern dust transport to the Southern Ocean and Antarctica. Journal of Geophysical Research: Atmospheres, 120(18), pp. 9303-9322.

NELSON, D.M., TRÉGUER, P., BRZEZINSKI, M.A., LEYNAERT, A. and QUÉGUINER, B., 1995. Production and dissolution of biogenic silica in the ocean: revised global estimates, comparison with regional data and relationship to biogenic sedimentation. Global Biogeochemical Cycles, 9(3), pp. 359-372.

NENES, A., KROM, M., MIHALOPOULOS, N., CAPPELLEN, P.V., SHI, Z., BOUGIATIOTI, A., ZARMPAS, P. and HERUT, B., 2011. Atmospheric acidification of mineral aerosols: a source of bioavailable phosphorus for the oceans. Atmospheric Chemistry and Physics, 11(13), pp. 6265-6272.

NEUER, S., TORRES-PADRÓN, M., GELADO-CABALLERO, M., RUEDA, M., HERNÁNDEZ-BRITO, J., DAVENPORT, R. and WEFER, G., 2004. Dust deposition pulses to the eastern subtropical North Atlantic gyre: Does ocean's biogeochemistry respond. Global Biogeochem.Cycles, 18.

NEUMANN, A., LAHAJNAR, N. and EMEIS, K., 2016. Benthic remineralisation rates in shelf and slope sediments of the northern Benguela upwelling margin. Continental Shelf Research, 113, pp. 47-61.

NEWELL, R.E., KIDSON, J.W., VINCENT, D.G. and BOER, G.J., 1972. General circulation of the tropical atmosphere and interactions with extratropical latitudes.Volume 1, .

NIANG, A., OZER, A. and OZER, P., 2008. Fifty years of landscape evolution in Southwestern Mauritania by means of aerial photos. Journal of Arid Environments, 72(2), pp. 97-107.

NICKLING, W., 1978. Eolian sediment transport during dust storms: Slims River valley, Yukon Territory. Canadian Journal of Earth Sciences, 15(7), pp. 1069-1084.

NICKLING, W. and GILLIES, J., 1993. Dust emission and transport in Mali, West Africa. Sedimentology, 40(5), pp. 859-868.

NICKLING, W., MCTAINSH, G. and LEYS, J., 1999. Dust emissions from the Channel Country of western Queensland, Australia. Zeitschrift fur Geomorphologie Supplementband, , pp. 1-17.

NIELD, J.M., BRYANT, R.G., WIGGS, G.F., KING, J., THOMAS, D.S., ECKARDT, F.D. and WASHINGTON, R., 2015. The dynamism of salt crust patterns on playas. Geology, 43(1), pp. 31-34.

NIELD, J.M., WIGGS, G.F. and SQUIRRELL, R.S., 2011. Aeolian sand strip mobility and protodune development on a drying beach: examining surface moisture and surface roughness patterns measured by terrestrial laser scanning. Earth Surface Processes and Landforms, 36(4), pp. 513-522.

NILSSON, C. and BERGGREN, K., 2000. Alterations of riparian ecosystems caused by river regulation dam operations have caused global-scale ecological changes in riparian ecosystems. How to protect river environments and human needs of rivers remains one of the most important questions of our time. Bioscience, 50(9), pp. 783-792.

NOBLE, A.E., LAMBORG, C.H., OHNEMUS, D.C., LAM, P.J., GOEPFERT, T.J., FRAME, C.H., CASCIOTTI, K.L., DITULLIO, G.R., JENNINGS, J.C. and SAITO, M.A., 2012. Basin-scale inputs of cobalt, iron, and manganese from the Benguela-Angola front to the South Atlantic Ocean.

NOY-MEIR, I., 1973. Desert ecosystems: environment and producers. Annual Review of Ecology and Systematics, , pp. 25-51.

OHDE, T. and SIEGEL, H., 2010. Biological response to coastal upwelling and dust deposition in the area off Northwest Africa. Continental Shelf Research, 30(9), pp. 1108-1119.

OKIN, G.S., BAKER, A.R., TEGEN, I., MAHOWALD, N.M., DENTENER, F.J., DUCE, R.A., GALLOWAY, J.N., HUNTER, K., KANAKIDOU, M. and KUBILAY, N., 2011. Impacts of atmospheric nutrient deposition on marine productivity: Roles of nitrogen, phosphorus, and iron. Global Biogeochemical Cycles, 25(2).

OKIN, G.S., MAHOWALD, N., CHADWICK, O.A. and ARTAXO, P., 2004. Impact of desert dust on the biogeochemistry of phosphorus in terrestrial ecosystems. Global Biogeochemical Cycles, 18(2).

OKITSU, S., 2005. Factors controlling geographical distribution in savanna vegetation in Namibia.

OLIVAREZ, A.M., OWEN, R.M. and REA, D.K., 1991. Geochemistry of eolian dust in Pacific pelagic sediments: Implications for paleoclimatic interpretations. Geochimica et Cosmochimica Acta, 55(8), pp. 2147-2158.

ORCUTT, K.M., LIPSCHULTZ, F., GUNDERSEN, K., ARIMOTO, R., MICHAELS, A.F., KNAP, A.H. and GALLON, J.R., 2001. A seasonal study of the significance of N 2 fixation by Trichodesmium spp. at the Bermuda Atlantic Time-series Study (BATS) site. Deep Sea Research Part II: Topical Studies in Oceanography, 48(8), pp. 1583-1608.

OXFORD INSTRUMENTS ANALYTICAL, 2006. INCA Energy Operator Manual. Issue 2.1. High Wycombe HP12 3SE, UK: Oxford Instruments Analytical.

PASQUINI, A.I., LECOMTE, K.L., PIOVANO, E.L. and DEPETRIS, P.J., 2006. Recent rainfall and runoff variability in central Argentina. Quaternary International, 158(1), pp. 127-139.

PATTON, P.C. and SCHUMM, S.A., 1981. Ephemeral-stream processes: implications for studies of Quaternary valley fills. Quaternary Research, 15(1), pp. 24-43.

PAULY, D. and CHRISTENSEN, V., 1995. Primary production required to sustain global fisheries. Nature, 374(6519), pp. 255-257.

PICHEVIN, L., CREMER, M., GIRAUDEAU, J. and BERTRAND, P., 2005. A 190 ky record of lithogenic grain-size on the Namibian slope: Forging a tight link between past wind-strength and coastal upwelling dynamics. Marine Geology, 218(1), pp. 81-96.

PIKETH, S., ANNEGARN, H. and TYSON, P., 1999. Lower tropospheric aerosol loadings over South Africa: The relative contribution of aeolian dust, industrial emissions, and biomass burning. Journal of Geophysical Research: Atmospheres, 104(D1), pp. 1597-1607.

PIKETH, S., TYSON, P. and STEFFEN, W., 2000. Aeolian transport from southern Africa and iron fertilization of marine biota in the South Indian Ocean. South African Journal of Science, 96(5).

PITCHFORD, J.W. and BRINDLEY, J., 1999. Iron limitation, grazing pressure and oceanic high nutrient-low chlorophyll(HNLC) regions. Journal of Plankton Research, 21(3), pp. 525-547.

POPULATION DIVISION OF THE DEPARTMENT OF ECONOMIC AND SOCIAL AFFAIRS OF THE UNITED NATIONS SECRETARIAT, 2009. World Population Prospects: The 2008 Revision. Highlights. New York: United Nations.

POTTER, C.S., RANDERSON, J.T., FIELD, C.B., MATSON, P.A., VITOUSEK, P.M., MOONEY, H.A. and KLOOSTER, S.A., 1993. Terrestrial ecosystem production: a process model based on global satellite and surface data. Global Biogeochemical Cycles, 7(4).

POULTON, S. and RAISWELL, R., 2002. The low-temperature geochemical cycle of iron: from continental fluxes to marine sediment deposition. American Journal of Science, 302(9), pp. 774-805.

PRESTON-WHYTE, R., DIAB, R. and SOKOLIC, F., 1994. Thermo-topographically induced winds in the boundary layer over the Etosha Pan. South African geographical journal, 76(2), pp. 59-62.

PRICE, N.M., ANDERSEN, L.F. and MOREL, F.M., 1991. Iron and nitrogen nutrition of equatorial Pacific plankton. Deep Sea Research Part A.Oceanographic Research Papers, 38(11), pp. 1361-1378.

PROSPERO, J., 1996. Saharan dust transport over the North Atlantic Ocean and Mediterranean: an overview. The impact of desert dust across the Mediterranean. Springer, pp. 133-151.

PROSPERO, J.M., BONATTI, E., SCHUBERT, C. and CARLSON, T.N., 1970. Dust in the Caribbean atmosphere traced to an African dust storm. Earth and Planetary Science Letters, 9(3), pp. 287-293.

PROSPERO, J.M., GINOUX, P., TORRES, O., NICHOLSON, S.E. and GILL, T.E., 2002. Environmental characterization of global sources of atmospheric soil dust identified with the Nimbus 7 Total Ozone Mapping Spectrometer (TOMS) absorbing aerosol product. Reviews of Geophysics, 40(1).

PULIDO‐VILLENA, E., REROLLE, V. and GUIEU, C., 2010. Transient fertilizing effect of dust in P‐deficient LNLC surface ocean. Geophysical Research Letters, 37(1).

QU, B., GABRIC, A.J., LU, Z., LI, H. and ZHAO, L., 2016. Unusual phytoplankton bloom phenology in the northern Greenland Sea during 2010. Journal of Marine Systems, 164, pp. 144-150.

QUÉGUINER, B., 2013. Iron fertilization and the structure of planktonic communities in high nutrient regions of the Southern Ocean. Deep Sea Research Part II: Topical Studies in Oceanography, 90, pp. 43-54.

RAISWELL, R., TRANTER, M., BENNING, L.G., SIEGERT, M., DE'ATH, R., HUYBRECHTS, P. and PAYNE, T., 2006. Contributions from glacially derived sediment to the global iron (oxyhydr) oxide cycle: implications for iron delivery to the oceans. Geochimica et Cosmochimica Acta, 70(11), pp. 2765-2780.

RASHKI, A., KASKAOUTIS, D., GOUDIE, A. and KAHN, R., 2013. Dryness of ephemeral lakes and consequences for dust activity: the case of the Hamoun drainage basin, southeastern Iran. Science of the Total Environment, 463, pp. 552-564.

RECHE, I., ORTEGA-RETUERTA, E., ROMERA, O., VILLENA, E.P., BAQUERO, R.M. and CASAMAYOR, E.O., 2009. Effect of Saharan dust inputs on bacterial activity and community composition in Mediterranean lakes and reservoirs. Limnology and Oceanography, 54(3), pp. 869-879.

REDFIELD, A.C., 1958. The biological control of chemical factors in the environment. American Scientist, 46(3), pp. 230A-221.

REDFIELD, A.C., 1934. On the proportions of organic derivatives in sea water and their relation to the composition of plankton. University Press of Liverpool James Johnstone memorial volume.

REID, I. and FROSTICK, L., 1987. Flow dynamics and suspended sediment properties in arid zone flash floods. Hydrological Processes, 1(3), pp. 239-253.

REID, I. and FROSTICK, L.E., 1997. Channel form, flows and sediments in deserts. Arid Zone Geomorphology: Processes, Form and Change in Drylands, , pp. 205-229.

REID, I. and LARONNE, J.B., 1995. Bed load sediment transport in an ephemeral stream and a comparison with seasonal and perennial counterparts. Water Resources Research, 31(3), pp. 773-781.

REID, J.S., FLOCCHINI, R.G., CAHILL, T.A., RUTH, R.S. and SALGADO, D.P., 1994. Local meteorological, transport, and source aerosol characteristics of late autumn Owens Lake (dry) dust storms. Atmospheric Environment, 28(9), pp. 1699-1706.

RESANE, T., ANNEGARN, H. and FREIMAN, T., 2004. The day of the white rain: origin of unusual dust deposition in Johannesburg, South Africa. S.Afr.J.Sci, 100(9-10), pp. 483-487.

REYNOLDS, R.L., YOUNT, J.C., REHEIS, M., GOLDSTEIN, H., CHAVEZ, P., FULTON, R., WHITNEY, J., FULLER, C. and FORESTER, R.M., 2007. Dust emission from wet and dry playas in the Mojave Desert, USA. Earth Surface Processes and Landforms, 32(12), pp. 1811-1827.

RIDAME, C., DEKAEZEMACKER, J., GUIEU, C., BONNET, S., L'HELGUEN, S. and MALIEN, F., 2014. Phytoplanktonic response to contrasted Saharan dust deposition events during mesocosm experiments in LNLC environment. Biogeosciences Discuss, 11(753), pp. e796.

RIDAME, C. and GUIEU, C., 2002. Saharan input of phosphate to the oligotrophic water of the open western Mediterranean Sea. Limnology and Oceanography, 47(3), pp. 856-869.

RIDGWELL, A.J., 2003. Implications of the glacial CO2 "iron hypothesis" for Quaternary climate change. Geochemistry Geophysics Geosystems, 4(9), pp. 1076.

RIDGWELL, A.J., 2002. Dust in the Earth system: the biogeochemical linking of land, air and sea. Philosophical transactions.Series A, Mathematical, physical, and engineering sciences, 360(1801), pp. 2905-2924.

RODIER, J., 1985. Aspects of arid zone hydrology. Facets of hydrology, 2, pp. 205-247.

ROSENFELD, D., RUDICH, Y. and LAHAV, R., 2001. Desert dust suppressing precipitation: a possible desertification feedback loop. Proceedings of the National Academy of Sciences of the United States of America, 98(11), pp. 5975-5980.

ROSSI, V., LOPEZ, C., HERNÁNDEZ-GARCÍA, E., SUDRE, J., GARÇON, V. and MOREL, Y., 2009. Surface mixing and biological activity in the four Eastern Boundary Upwelling Systems. arXiv preprint arXiv:0909.0115, .

ROUAULT, M., 2012. Bi‐annual intrusion of tropical water in the northern Benguela upwelling. Geophysical Research Letters, 39(12).

RUIZ-FERNÁNDEZ, A., HILLAIRE-MARCEL, C., GHALEB, B., SOTO-JIMÉNEZ, M. and PÁEZ-OSUNA, F., 2002. Recent sedimentary history of anthropogenic impacts

on the Culiacan River Estuary, northwestern Mexico: geochemical evidence from organic matter and nutrients. Environmental Pollution, 118(3), pp. 365-377.

RUSSELL, B.J., SHELTON, J.P. and WALSH, A., 1957. An atomic-absorption spectrophotometer and its application to the analysis of solutions. Spectrochimica Acta, 8(6), pp. 317E1319-318E2328.

RYDEN, J., SYERS, J. and HARRIS, R., 1974. Phosphorus in runoff and streams. Advances in Agronomy, 25, pp. 1-45.

RYTHER, J.H., 1956. Photosynthesis in the Ocean as a Function of Light Intensity1. Limnology and Oceanography, 1(1), pp. 61-70.

SAÑUDO‐WILHELMY, S., GOBLER, C., OKBAMICHAEL, M. and TAYLOR, G., 2006. Regulation of phytoplankton dynamics by vitamin B12. Geophysical Research Letters, 33(4).

SAVIJÄRVI, H., 2004. Model predictions of coastal winds in a small scale. Tellus A, 56(4), pp. 287-295.

SAYER, A., MUNCHAK, L., HSU, N., LEVY, R., BETTENHAUSEN, C. and JEONG, M., 2014. MODIS Collection 6 aerosol products: Comparison between Aqua's e‐Deep Blue, Dark Target, and "merged" data sets, and usage recommendations. Journal of Geophysical Research: Atmospheres, 119(24).

SCHEPANSKI, K., FLAMANT, C., CHABOUREAU, J., KOCHA, C., BANKS, J., BRINDLEY, H., LAVAYSSE, C., MARNAS, F., PELON, J. and TULET, P., 2013. Characterization of dust emission from alluvial sources using aircraft observations and high‐resolution modeling. Journal of Geophysical Research: Atmospheres, 118(13), pp. 7237-7259.

SCHEUVENS, D., SCHÜTZ, L., KANDLER, K., EBERT, M. and WEINBRUCH, S., 2013. Bulk composition of northern African dust and its source sediments—a compilation. Earth-Science Reviews, 116, pp. 170-194.

SCHOLZ, O., GAWNE, B., EBNER, B. and ELLIS, I., 2002. The effects of drying and re‐flooding on nutrient availability in ephemeral deflation basin lakes in western New South Wales, Australia. River Research and Applications, 18(2), pp. 185-196.

SCHROEDER, J., 1985. Eolian dust in the coastal desert of the Sudan: aggregates cemented by evaporites. Journal of African Earth Sciences (1983), 3(3), pp. 371-380.

SCHROTH, A.W., CRUSIUS, J., SHOLKOVITZ, E.R. and BOSTICK, B.C., 2009. Iron solubility driven by speciation in dust sources to the ocean. Nature Geoscience, 2(5), pp. 337-340.

SCHULZ, M., PROSPERO, J.M., BAKER, A.R., DENTENER, F., ICKES, L., LISS, P.S., MAHOWALD, N.M., NICKOVIC, S., GARCÍA-PANDO, C.P. and RODRÍGUEZ, S., 2012. Atmospheric Transport and Deposition of Mineral Dust to the Ocean: Implications for Research Needs. Environmental science & technology, .

SCHUMM, S.A., 1960. The effect of sediment type on the shape and stratification of some modern fluvial deposits. American Journal of Science, 258(3), pp. 177-184.

SCHÜTZ, L., JAENICKE, R. and PIETREK, H., 1981. Saharan dust transport over the North Atlantic Ocean. Geological Society of America Special Papers, 186, pp. 87-100.

SCHÜTZ, L. and SEBERT, M., 1987. Mineral aerosols and source identification. Journal of Aerosol Science, 18(1), pp. 1-10.

SEARLE, P.L., 1984. The Berthelot or indophenol reaction and its use in the analytical chemistry of nitrogen. A review. Analyst, 109(5), pp. 549-568.

SEDWICK, P.N., CHURCH, T.M., BOWIE, A.R., MARSAY, C.M., USSHER, S.J., ACHILLES, K., LETHABY, P., JOHNSON, R.J., SARIN, M. and MCGILLICUDDY, D.J., 2005. Iron in the Sargasso Sea (Bermuda Atlantic Time‐series Study region) during summer: Eolian imprint, spatiotemporal variability, and ecological implications. Global Biogeochemical Cycles, 19(4).

SEELY, M., HENDERSON, J., HEYNS, P., JACOBSON, P., NAKALE, T., NANTANGA, K. and SCHACHTSCHNEIDER, K., 2003. Ephemeral and endoreic river systems: Relevance and management challenges. Transboundary Rivers, Sovereignty and Development: Hydropolitical Drivers in the Okavango River Basin, , pp. 187-212.

SEELY, M. and LOUW, G., 1980. First approximation of the effects of rainfall on the ecology and energetics of a Namib Desert dune ecosystem. Journal of Arid Environments, 3(1), pp. 25-54.

SHANNON, L.V., 1985. The Benguela ecosystem. I: Evolution of the Benguela physical features and processes. Oceanography and Marine Biology, 23, pp. 105-182.

SHANNON, L. and NELSON, G., 1996. The Benguela: large scale features and processes and system variability. The South Atlantic. Springer, pp. 163-210.

SHAO, Y., 2004. Simplification of a dust emission scheme and comparison with data. Journal of Geophysical Research: Atmospheres, 109(D10).

SHAO, Y. and LU, H., 2000. A simple expression for wind erosion threshold friction velocity. Journal of Geophysical Research: Atmospheres, 105(D17), pp. 22437-22443.

SHAO, Y., RAUPACH, M. and FINDLATER, P., 1993. Effect of saltation bombardment on the entrainment of dust by wind. Journal of Geophysical Research, 98(D7), pp. 12719-12726.

SHARMA, K. and MURTHY, J., 1994. Modelling sediment transport in stream channels in the arid zone of India. Hydrological Processes, 8(6), pp. 567-572.

SHAW, E.C., GABRIC, A.J. and MCTAINSH, G.H., 2008. Impacts of aeolian dust deposition on phytoplankton dynamics in Queensland coastal waters. Marine and freshwater research, 59(11), pp. 951-962.

SHI, N., DUPONT, L.M., BEUG, H. and SCHNEIDER, R., 2000. Correlation between vegetation in southwestern Africa and oceanic upwelling in the past 21,000 years. Quaternary Research, 54(1), pp. 72-80.

SHI, Z., KROM, M.D., BONNEVILLE, S., BAKER, A.R., BRISTOW, C., DRAKE, N., MANN, G., CARSLAW, K., MCQUAID, J.B. and JICKELLS, T., 2011. Influence of chemical weathering and aging of iron oxides on the potential iron solubility of Saharan dust during simulated atmospheric processing. Global Biogeochemical Cycles, 25(2).

SHI, Z., KROM, M.D., BONNEVILLE, S., BAKER, A.R., JICKELLS, T.D. and BENNING, L.G., 2009. Formation of iron nanoparticles and increase in iron reactivity in mineral dust during simulated cloud processing. Environmental science & technology, 43(17), pp. 6592-6596.

SHI, Z., KROM, M.D., BONNEVILLE, S. and BENNING, L.G., 2015. Atmospheric Processing Outside Clouds Increases Soluble Iron in Mineral Dust. Environmental science & technology, 49(3), pp. 1472-1477.

SHI, Z., KROM, M.D., JICKELLS, T.D., BONNEVILLE, S., CARSLAW, K.S., MIHALOPOULOS, N., BAKER, A.R. and BENNING, L.G., 2012. Impacts on iron solubility in the mineral dust by processes in the source region and the atmosphere: A review. Aeolian Research, 5, pp. 21-42.

SHI, D., XU, Y., HOPKINSON, B.M. and MOREL, F.M., 2010. Effect of ocean acidification on iron availability to marine phytoplankton. Science (New York, N.Y.), 327(5966), pp. 676-679.

SIMS, J., SIMARD, R. and JOERN, B., 1998. Phosphorus loss in agricultural drainage: Historical perspective and current research. Journal of environmental quality, 27(2), pp. 277-293.

SINGER, A., ZOBECK, T., POBEREZSKY, L. and ARGAMAN, E., 2003. The PM 10 and PM 2· 5 dust generation potential of soils/sediments in the Southern Aral Sea Basin, Uzbekistan. Journal of Arid Environments, 54(4), pp. 705-728.

SKOULIKIDIS, N. and AMAXIDIS, Y., 2009. Origin and dynamics of dissolved and particulate nutrients in a minimally disturbed Mediterranean river with intermittent flow. Journal of Hydrology, 373(1), pp. 218-229.

SLATER, B., MICHAELIDES, A., SALZMANN, C.G. and LOHMANN, U., 2015. A blue-sky approach to understanding cloud formation. Bulletin of the American Meteorological Society, (2015).

SMITH, R.C. and BAKER, K.S., 1981. Optical properties of the clearest natural waters (200–800 nm). Applied Optics, 20(2), pp. 177-184.

SMITH, R., MASON, T. and WARD, J., 1993. Flash-flood sediments and ichnofacies of the late Pleistocene Homeb Silts, Kuiseb River, Namibia. Sedimentary Geology, 85(1), pp. 579-599.

SOLTANPOUR, P., KHAN, A. and LINDSAY, W., 1976. Factors affecting DTPA‐extractable Zn, Fe, Mn, and Cu from soils 1. Communications in Soil Science & Plant Analysis, 7(9), pp. 797-821.

SONG, K., KANG, H., ZHANG, L. and MITSCH, W.J., 2012. Seasonal and spatial variations of denitrification and denitrifying bacterial community structure in created riverine wetlands. Ecological Engineering, 38(1), pp. 130-134.

SOUKUP, D.A., BUCK, B.J. and HARRIS, W., 2008. Preparing soils for mineralogical analyses. In: A.L. ULERY and L.R. DREES, eds, Methods of Soil Analysis, Part 5 – Mineralogical Methods. Soil Science Society of America, Inc., Madison, Wisconsin, USA, pp. 13-31.

SPERAZZA, M., MOORE, J.N. and HENDRIX, M.S., 2004. High-resolution particle size analysis of naturally occurring very fine-grained sediment through laser diffractometry. Journal of Sedimentary Research, 74(5), pp. 736-743.

STANISTREET, I.G. and STOLLHOFEN, H., 2002. Hoanib River flood deposits of Namib Desert interdunes asanalogues for thin permeability barrier mudstone layers inaeolianite reservoirs. Sedimentology, 49(4), pp. 719-736.

STEAR, W.M., 1985. Comparison of the bedform distribution and dynamics of modern and ancient sandy ephemeral flood deposits in the southwestern Karoo region, South Africa. Sedimentary Geology, 45(3), pp. 209-230.

STEWARD, A.L., VON SCHILLER, D., TOCKNER, K., MARSHALL, J.C. and BUNN, S.E., 2012. When the river runs dry: human and ecological values of dry riverbeds. Frontiers in Ecology and the Environment, 10(4), pp. 202-209.

STOCKDALE, A., KROM, M.D., MORTIMER, R.J., BENNING, L.G., CARSLAW, K.S., HERBERT, R.J., SHI, Z., MYRIOKEFALITAKIS, S., KANAKIDOU, M. and NENES, A., 2016. Understanding the nature of atmospheric acid processing of mineral dusts in supplying bioavailable phosphorus to the oceans. Proceedings of the National Academy of Sciences of the United States of America, 113(51), pp. 14639-14644.

STONE, A. and THOMAS, D., 2013. Casting new light on late Quaternary environmental and palaeohydrological change in the Namib Desert: A review of the application of optically stimulated luminescence in the region. Journal of Arid Environments, 93, pp. 40-58.

STUUT, J.W., PRINS, M.A., SCHNEIDER, R.R., WELTJE, G.J., JANSEN, J.F. and POSTMA, G., 2002. A 300-kyr record of aridity and wind strength in southwestern Africa: inferences from grain-size distributions of sediments on Walvis Ridge, SE Atlantic. Marine Geology, 180(1), pp. 221-233.

SUN, J., ZHANG, M. and LIU, T., 2001. Spatial and temporal characteristics of dust storms in China and its surrounding regions, 1960–1999: Relations to source area and climate. Journal of Geophysical Research: Atmospheres, 106(D10), pp. 10325-10333.

SUNDA, W.G. and HUNTSMAN, S.A., 1995. Cobalt and zinc interreplacement in marine phytoplankton: biological and geochemical implications. Limnology and Oceanography, 40(8), pp. 1404-1417.

SVENDSEN, J., STOLLHOFEN, H., KRAPF, C.B. and STANISTREET, I.G., 2003. Mass and hyperconcentrated flow deposits record dune damming and catastrophic breakthrough of ephemeral rivers, Skeleton Coast Erg, Namibia. Sedimentary Geology, 160(1), pp. 7-31.

SWAP, R., GARSTANG, M., MACKO, S., TYSON, P., MAENHAUT, W., ARTAXO, P., KÅLLBERG, P. and TALBOT, R., 1996. The long-range transport of southern African aerosols to the tropical South Atlantic. JOURNAL OF GEOPHYSICAL RESEARCH-ALL SERIES-, 101, pp. 23,777-23,791.

SWAP, R., GARSTANG, M., GRECO, S., TALBOT, R. and KÅLLBERG, P., 1992. Saharan dust in the Amazon Basin. Tellus B, 44(2), pp. 133-149.

SWEET, J., 1998. Livestock–Coping with drought: Namibia–a case study. Human health, water, livestock, conflict resolution, emergency seed supply, .

SYVITSKI, J.P., 2003. Supply and flux of sediment along hydrological pathways: research for the 21st century. Global and Planetary Change, 39(1), pp. 1-11.

TAGLIABUE, A. and ARRIGO, K.R., 2006. Processes governing the supply of iron to phytoplankton in stratified seas. Journal of Geophysical Research: Oceans, 111(C6).

TAMATAMAH, R.A., HECKY, R.E. and DUTHIE, H., 2005. The atmospheric deposition of phosphorus in Lake Victoria (East Africa). Biogeochemistry, 73(2), pp. 325-344.

TAN, S., LI, J., CHE, H., CHEN, B. and WANG, H., 2017. Transport of East Asian dust storms to the marginal seas of China and the southern North Pacific in spring 2010. Atmospheric Environment, 148, pp. 316-328.

TAN, S., LI, J., GAO, H., WANG, H., CHE, H. and CHEN, B., 2016. Satellite-Observed Transport of Dust to the East China Sea and the North Pacific Subtropical Gyre: Contribution of Dust to the Increase in Chlorophyll during Spring 2010. Atmosphere, 7(11), pp. 152.

TAN, S. and WANG, H., 2014. The transport and deposition of dust and its impact on phytoplankton growth in the yellow sea. Atmospheric Environment, 99, pp. 491-499.

TAN, S., YAO, X., GAO, H., SHI, G. and YUE, X., 2013. Variability in the correlation between Asian dust storms and chlorophyll a concentration from the north to equatorial Pacific. PloS one, 8(2), pp. e57656.

TANAKA, T.Y. and CHIBA, M., 2006. A numerical study of the contributions of dust source regions to the global dust budget. Global and Planetary Change, 52(1), pp. 88-104.

TANG, M., CZICZO, D.J. and GRASSIAN, V.H., 2016. Interactions of Water with Mineral Dust Aerosol: Water Adsorption, Hygroscopicity, Cloud Condensation, and Ice Nucleation. Chemical reviews, 116(7), pp. 4205-4259.

TAYLOR, M., 2000. Determination of total phosphorus in soil using simple Kjeldahl digestion. Communications in Soil Science & Plant Analysis, 31(15-16), pp. 2665-2670.

TAYLOR, S., 1964. Abundance of chemical elements in the continental crust: a new table. Geochimica et Cosmochimica Acta, 28(8), pp. 1273-1285.

TAYLOR, S.R. and MCLENNAN, S.M., 1995. The geochemical evolution of the continental crust. Reviews of Geophysics, 33(2), pp. 241-265.

TEGEN, I., WERNER, M., HARRISON, S. and KOHFELD, K., 2004. Relative importance of climate and land use in determining present and future global soil dust emission. Geophysical Research Letters, 31(5).

TEGEN, I. and FUNG, I., 1994. Modeling of mineral dust in the atmosphere: Sources, transport, and optical thickness. Journal of Geophysical Research: Atmospheres, 99(D11), pp. 22897-22914.

TEGEN, I. and LACIS, A.A., 1996. Modeling of particle size distribution and its influence on the radiative properties of mineral dust aerosol. Journal of Geophysical Research: Atmospheres (1984–2012), 101(D14), pp. 19237-19244.

THOMAS, D.S., KNIGHT, M. and WIGGS, G.F., 2005. Remobilization of southern African desert dune systems by twenty-first century global warming. Nature, 435(7046), pp. 1218-1221.

THOMAS, D.S. and SHAW, P.A., 1991. The Kalahari Environment. Cambridge University Press.

THOMAS, D.G., ed, 2011. Arid Zone Geomorphology - Process, Form and Change in Drylands. 3rd edn. Chichester, West Sussex: Wiley-Blackwell.

THOMAS, D. and TWYMAN, C., 2004. Good or bad rangeland? Hybrid knowledge, science, and local understandings of vegetation dynamics in the Kalahari. Land Degradation & Development, 15(3), pp. 215-231.

TILMAN, D., KILHAM, S.S. and KILHAM, P., 1982. Phytoplankton community ecology: the role of limiting nutrients. Annual Review of Ecology and Systematics, 13, pp. 349-372.

TLHALERWA, K., FREIMAN, M. and PIKETH, S., 2005. Aerosol deposition off the Southern African West Coast by berg winds. South African Geographical Journal, 87(2), pp. 152-161.

TODD, M.C., WASHINGTON, R., MARTINS, J.V., DUBOVIK, O., LIZCANO, G., M'BAINAYEL, S. and ENGELSTAEDTER, S., 2007. Mineral dust emission from the Bodélé Depression nothern Chad, during BoDEx 2005. Journal of Geophysical Research D: Atmospheres, 112(6).

TOGGWEILER, J. and CARSON, S., 1995. What are upwelling systems contributing to the ocean's carbon and nutrient budgets? ENVIRONMENTAL SCIENCES RESEARCH REPORT ES, 18, pp. 337-360.

TOON, O.B., 2003. African dust in Florida clouds. Nature, 424(6949), pp. 623.

TOOTH, S., 2000. Process, form and change in dryland rivers: a review of recent research. Earth-Science Reviews, 51(1), pp. 67-107.

TOOTH, S. and NANSON, G.C., 2000. Equilibrium and nonequilibrium conditions in dryland rivers. Physical Geography, 21(3), pp. 183-211.

TORRENT, J., SCHWERTMANN, U., FECHTER, H. and ALFEREZ, F., 1983. QUANTITATIVE RELATIONSHIPS BETWEEN SOIL COLOR AND HEMATITE CONTENT. Soil Science, 136(6), pp. 354-358.

TSUDA, A., TAKEDA, S., SAITO, H., NISHIOKA, J., NOJIRI, Y., KUDO, I., KIYOSAWA, H., SHIOMOTO, A., IMAI, K., ONO, T., SHIMAMOTO, A., TSUMUNE, D., YOSHIMURA, T., AONO, T., HINUMA, A., KINUGASA, M., SUZUKI, K., SOHRIN, Y., NOIRI, Y., TANI, H., DEGUCHI, Y., TSURUSHIMA, N., OGAWA, H., FUKAMI, K., KUMA, K. and SAINO, T., 2003. A mesoscale iron enrichment in the western subarctic Pacific induces a large centric diatom bloom. Science (New York, N.Y.), 300(5621), pp. 958-961.

TURNER, B.L. and ROMERO, T.E., 2009. Short-term changes in extractable inorganic nutrients during storage of tropical rain forest soils. Soil Science Society of America Journal, 73(6), pp. 1972-1979.

TYRRELL, T., 1999. The relative influences of nitrogen and phosphorus on oceanic primary production. Nature, 400(6744), pp. 525-531.

TYRRELL, T., MARAÑÓN, E., POULTON, A.J., BOWIE, A.R., HARBOUR, D.S. and WOODWARD, E.M.S., 2003. Large-scale latitudinal distribution of Trichodesmium spp. in the Atlantic Ocean. Journal of Plankton Research, 25(4), pp. 405-416.

TYSON, P. and D'ABRETON, P., 1998. Transport and recirculation of aerosols off Southern Africa—macroscale plume structure. Atmospheric Environment, 32(9), pp. 1511-1524.

TYSON, P., GARSTANG, M., SWAP, R., KALLBERG, P. and EDWARDS, M., 1996. An air transport climatology for subtropical southern Africa. International Journal of Climatology, 16(3), pp. 265-291.

TYSON, P. and SEELY, M., 1980. Local winds over the central Namib. South African Geographical Journal, 62(2), pp. 135-150.

UNITED NATIONS DEPARTMENT OF ECONOMIC AND SOCIAL AFFAIRS, 2016. World Statistics Pocketbook 2016 edition. ISBN-13: 978-92-1-161612-5. United Nations Publications, 300 East 42nd Street, New York, NY 10017, USA: United Nations.

UNO, I., EGUCHI, K., YUMIMOTO, K., TAKEMURA, T., SHIMIZU, A., UEMATSU, M., LIU, Z., WANG, Z., HARA, Y. and SUGIMOTO, N., 2009. Asian dust transported one full circuit around the globe. Nature Geoscience, 2(8), pp. 557-560.

VAN LOON, H., 1972. Cloudiness and precipitation in the Southern Hemisphere. Meteorology of the Southern Hemisphere. Springer, pp. 101-111.

VAN WILGEN, B.W. and SCHOLES, R.J., 1997. The vegetation and fire regimes of southern hemisphere Africa. Fire in southern African savannas: ecological and atmospheric perspectives, , pp. 27-46.

VAN WYK, A.E., STRUB, H. and STRUCKMEIR, W.F., 2001. Hydrological Map of Namibia 1:1 000 000. Windhoek: Department of Water Affairs and Geological Survey.

VAUGHAN, N.E. and LENTON, T.M., 2011. A review of climate geoengineering proposals. Climatic Change, 109(3-4), pp. 745-790.

VICKERY, K.J., 2010. Southern African dust sources as identified by multiple space borne sensors. MSc edn. Department of Environmental and Geographical Science: University of Cape Town.

VICKERY, K.J., 2014. The Nature of Pan Sediments: A case study on dust supply from the Makgadikgadi Pans, Botswana.

VICKERY, K.J. and ECKARDT, F.D., 2013. Dust emission controls on the lower Kuiseb River valley, Central Namib. Aeolian Research, 10, pp. 125-133.

VICKERY, K.J., ECKARDT, F.D. and BRYANT, R.G., 2013. A sub ‐ basin scale dust plume source frequency inventory for southern Africa, 2005‐2008. Geophysical Research Letters, 40(19), pp. 5274-5279.

VILES, H.A., 2005. Microclimate and weathering in the central Namib Desert, Namibia. Geomorphology, 67(1), pp. 189-209.

VILJOEN, P., 1989. Spatial distribution and movements of elephants (Loxodonta africana) in the northern Namib Desert region of the Kaokoveld, South West Africa/Namibia. Journal of zoology, 219(1), pp. 1-19.

VISSER, F., GERRINGA, L. and TIMMERMANS, K., 2003. The role of the reactivity and content of iron of aerosol dust on growth rates of two Antarctic diatom species1. Journal of Phycology, 39(6), pp. 1085-1094.

VITOUSEK, P.M. and HOWARTH, R.W., 1991. Nitrogen limitation on land and in the sea: how can it occur? Biogeochemistry, 13(2), pp. 87-115.

VITOUSEK, P.M. and MATSON, P.A., 1993. Agriculture, the global nitrogen cycle, and trace gas flux. Biogeochemistry of Global Change. Springer, pp. 193-208.

VITOUSEK, P.M., PORDER, S., HOULTON, B.Z. and CHADWICK, O.A., 2010. Terrestrial phosphorus limitation: mechanisms, implications, and nitrogen-phosphorus interactions. Ecological Applications, 20(1), pp. 5-15.

VOGEL, J., 1989. Evidence of past climatic change in the Namib Desert. Palaeogeography, Palaeoclimatology, Palaeoecology, 70(4), pp. 355-366.

VOLPE, G., BANZON, V.F., EVANS, R.H., SANTOLERI, R., MARIANO, A.J. and SCIARRA, R., 2009. Satellite observations of the impact of dust in a low ‐ nutrient, low ‐ chlorophyll region: Fertilization or artifact? Global Biogeochemical Cycles, 23(3).

VON HOLDT, J.R., 2013. Lower Kuiseb River sediments and their control on dust emission.

VÖRÖSMARTY, C.J., MEYBECK, M., FEKETE, B., SHARMA, K., GREEN, P. and SYVITSKI, J.P., 2003. Anthropogenic sediment retention: major global impact from registered river impoundments. Global and Planetary Change, 39(1), pp. 169-190.

VOROSMARTY, C.J., GREEN, P., SALISBURY, J. and LAMMERS, R.B., 2000. Global water resources: vulnerability from climate change and population growth. Science (New York, N.Y.), 289(5477), pp. 284-288.

WALDEN, J., WHITE, K.H., KILCOYNE, S.H. and BENTLEY, P.M., 2000. Analyses of iron oxide assemblages within Namib dune sediments using high field remanence measurements (9 T) and Mössbauer analysis. Journal of Quaternary Science, 15(2), pp. 185-195.

WALDEN, J. and WHITE, K., 1997. Investigation of the controls on dune colour in the Namib Sand Sea using mineral magnetic analyses. Earth and Planetary Science Letters, 152(1–4), pp. 187-201.

WALKER, N. and SHILLINGTON, F., 1990. The effect of oceanographic variability on South African weather and climate. South African Journal of Science, 86(7/8/9/10), pp. 382-386.

WALKER, T. and SYERS, J.K., 1976. The fate of phosphorus during pedogenesis. Geoderma, 15(1), pp. 1-19.

WAN, Y. and EL-SWAIFY, S., 1998. Sediment enrichment mechanisms of organic carbon and phosphorus in a well-aggregated Oxisol. Journal of environmental quality, 27(1), pp. 132-138.

WANG, R., BALKANSKI, Y., BOUCHER, O., CIAIS, P., PEÑUELAS, J. and TAO, S., 2015. Significant contribution of combustion-related emissions to the atmospheric phosphorus budget. Nature Geoscience, 8(1), pp. 48-54.

WANG, X., CHANCELLOR, G., EVENSTAD, J., FARNSWORTH, J.E., HASE, A., OLSON, G.M., SREENATH, A. and AGARWAL, J.K., 2009. A novel optical instrument for estimating size segregated aerosol mass concentration in real time. Aerosol Science and Technology, 43(9), pp. 939-950.

WANG, X., XIA, D., WANG, T., XUE, X. and LI, J., 2008. Dust sources in arid and semiarid China and southern Mongolia: impacts of geomorphological setting and surface materials. Geomorphology, 97(3), pp. 583-600.

WARD, D., SALTZ, D. and NGAIRORUE, B.T., 2004. Spatio-temporal rainfall variation and stock management in arid Namibia. Rangeland Ecology & Management, 57(2), pp. 130-140.

WARD, J.D., SEELY, M.K. and LANCASTER, N., 1983. South African Journal of Science, 79, pp. 175.

WASHINGTON, R., TODD, M., LIZCANO, G., TEGEN, I., FLAMANT, C., KOREN, I., GINOUX, P., ENGELSTAEDTER, S., BRISTOW, C. and ZENDER, C., 2006. Links between topography, wind, deflation, lakes and dust: The case of the Bodélé Depression, Chad. Geophysical Research Letters, 33(9), pp. L09401.

WASHINGTON, R., TODD, M., MIDDLETON, N.J. and GOUDIE, A.S., 2003. Dust-storm source areas determined by the total ozone monitoring spectrometer and surface observations. Annals of the Association of American Geographers, 93(2), pp. 297-313.

WASHINGTON, R., BOUET, C., CAUTENET, G., MACKENZIE, E., ASHPOLE, I., ENGELSTAEDTER, S., LIZCANO, G., HENDERSON, G.M., SCHEPANSKI, K. and TEGEN, I., 2009. Dust as a tipping element: the Bodele Depression, Chad. Proceedings of the National Academy of Sciences of the United States of America, 106(49), pp. 20564-20571.

WASHINGTON, R. and TODD, M.C., 2005. Atmospheric controls on mineral dust emission from the Bodélé Depression, Chad: The role of the low level jet. Geophysical Research Letters, 32(17), pp. 1-5.

WEBER, L., VÖLKER, C., SCHARTAU, M. and WOLF ‐ GLADROW, D., 2005. Modeling the speciation and biogeochemistry of iron at the Bermuda Atlantic Time ‐ series Study site. Global Biogeochemical Cycles, 19(1).

WELCH, E.B. and COOKE, G.D., 1995. Internal phosphorus loading in shallow lakes: importance and control. Lake and Reservoir Management, 11(3), pp. 273-281.

WENT, F.W. and WESTERGAARD, M., 1949. Ecology of desert plants. III. Development of plants in the Death Valley National Monument, California. Ecology, , pp. 26-38.

WEST, N.E. and SKUJINS, J., 1978. Nitrogen in desert ecosystems. Dowden, Hutchinson and Ross Inc.

WESTBERRY, T.K. and SIEGEL, D.A., 2006. Spatial and temporal distribution of Trichodesmium blooms in the world's oceans. Global Biogeochemical Cycles, 20(4).

WHITE, K., WALDEN, J., DRAKE, N., ECKARDT, F. and SETTLELL, J., 1997. Mapping the iron oxide content of dune sands, Namib Sand Sea, Namibia, using Landsat Thematic Mapper data. Remote Sensing of Environment, 62(1), pp. 30-39.

WHITE, K., WALDEN, J. and GURNEY, S.D., 2007. Spectral properties, iron oxide content and provenance of Namib dune sands. Geomorphology, 86(3), pp. 219-229.

WIETERS, E.A., KAPLAN, D.M., NAVARRETE, S., SOTOMAYOR, A., LARGIER, J., NIELSEN, K.J. and VELIZ, F., 2003. Alongshore and temporal variability in chlorophyll a concentration in Chilean nearshore waters. Marine Ecology Progress Series, 249, pp. 93-105.

WIGGS, G., BULLARD, J., GARVEY, B. and CASTRO, I., 2002. Interactions between airflow and valley topography with implications for aeolian sediment transport. Physical Geography, 23(5), pp. 366-380.

WIGGS, G.F., 2011. Sediment mobilisation by the wind. Arid Zone Geomorphology: Process, Form and Change in Drylands, Third Edition, , pp. 455-486.

WIGGS, G.F., THOMAS, D.S., BULLARD, J.E. and LIVINGSTONE, I., 1995. Dune mobility and vegetation cover in the southwest Kalahari Desert. Earth Surface Processes and Landforms, 20(6), pp. 515-529.

WIGGS, G. and HOLMES, P., 2011. Dynamic controls on wind erosion and dust generation on west-central Free State agricultural land, South Africa. Earth Surface Processes and Landforms, 36(6), pp. 827-838.

WIJDENES, D.J.O., POESEN, J., VANDEKERCKHOVE, L. and GHESQUIERE, M., 2000. Spatial distribution of gully head activity and sediment supply along an ephemeral channel in a Mediterranean environment. Catena, 39(3), pp. 147-167.

WILKINSON, S.N., HANCOCK, G.J., BARTLEY, R., HAWDON, A.A. and KEEN, R.J., 2013. Using sediment tracing to assess processes and spatial patterns of erosion in grazed rangelands, Burdekin River basin, Australia. Agriculture, Ecosystems & Environment, 180, pp. 90-102.

WILLIAMS, M., HARPER, N., CHAITOVITZ, C., DANSIE, A., DIAZ, R., HEIDEMEIER, J., JIANG, Y., KEMP, M., NAQVI, S. and NERETIN, L., 2011. Hypoxia and Nutrient Reduction in the Coastal Zone: Advice for Prevention, Remediation and Research.

WILSON, C., 2003. Late summer chlorophyll blooms in the oligotrophic North Pacific Subtropical Gyre. Geophysical Research Letters, 30(18).

WINTON, V., EDWARDS, R., DELMONTE, B., ELLIS, A., ANDERSSON, P., BOWIE, A., BERTLER, N., NEFF, P. and TUOHY, A., 2016. Multiple sources of soluble atmospheric iron to Antarctic waters. Global Biogeochemical Cycles, .

WITHERS, P. and JARVIE, H., 2008. Delivery and cycling of phosphorus in rivers: a review. Science of the total environment, 400(1), pp. 379-395.

WOODRUFF, L.L., 1909. The American Society of Zoologists. Science, , pp. 424-438.

WOODWARD, X., KOSTINSKI, A., CHINA, S., MAZZOLENI, C. and CANTRELL, W., 2015. Characterization of dust particles' 3D shape and roughness with nanometer resolution. Aerosol Science and Technology, 49(4), pp. 229-238.

WORDEN, A.Z., FOLLOWS, M.J., GIOVANNONI, S.J., WILKEN, S., ZIMMERMAN, A.E. and KEELING, P.J., 2015. Environmental science. Rethinking the marine carbon cycle: factoring in the multifarious lifestyles of microbes. Science (New York, N.Y.), 347(6223), pp. 1257594.

WRIGHT, A.F. and BAILEY, J.S., 2001. Organic carbon, total carbon, and total nitrogen determinations in soils of variable calcium carbonate contents using a Leco CN-2000 dry combustion analyzer. Communications in Soil Science and Plant Analysis, 32(19-20), pp. 3243-3258.

WU, J., SUNDA, W., BOYLE, E.A. and KARL, D.M., 2000. Phosphate depletion in the western North Atlantic Ocean. Science (New York, N.Y.), 289(5480), pp. 759-762.

XIU, P., THOMAS, A.C. and CHAI, F., 2014. Satellite bio-optical and altimeter comparisons of phytoplankton blooms induced by natural and artificial iron addition in the Gulf of Alaska. Remote Sensing of Environment, 145, pp. 38-46.

YANG, X., POST, W.M., THORNTON, P.E. and JAIN, A., 2013. The distribution of soil phosphorus for global biogeochemical modeling. Biogeosciences, 10(4), pp. 2525-2537.

YI, Y., YANG, Z. and ZHANG, S., 2011. Ecological risk assessment of heavy metals in sediment and human health risk assessment of heavy metals in fishes in the middle and lower reaches of the Yangtze River basin. Environmental Pollution, 159(10), pp. 2575-2585.

YOUNG, R., CARDER, K., BETZER, P., COSTELLO, D., DUCE, R., DITULLIO, G., TINDALE, N., LAWS, E., UEMATSU, M. and MERRILL, J., 1991. Atmospheric iron inputs and primary productivity: Phytoplankton responses in the North Pacific. Global Biogeochemical Cycles, 5(2), pp. 119-134.

YU, H., CHIN, M., YUAN, T., BIAN, H., REMER, L.A., PROSPERO, J.M., OMAR, A., WINKER, D., YANG, Y. and ZHANG, Y., 2015. The Fertilizing Role of African Dust in the Amazon Rainforest: A First Multiyear Assessment Based on CALIPSO Lidar Observations. Geophys.Res.Lett, 42, pp. 10.1002.

ZEGLIN, L.H., DAHM, C.N., BARRETT, J.E., GOOSEFF, M.N., FITPATRICK, S.K. and TAKACS-VESBACH, C.D., 2011. Bacterial community structure along moisture gradients in the parafluvial sediments of two ephemeral desert streams. Microbial ecology, 61(3), pp. 543-556.

ZEHR, J.P. and KUDELA, R.M., 2011. Nitrogen cycle of the open ocean: from genes to ecosystems. Annual Review of Marine Science, 3, pp. 197-225.

ZENDER, C.S., MILLER, R. and TEGEN, I., 2004. Quantifying mineral dust mass budgets: Terminology, constraints, and current estimates. Eos, Transactions American Geophysical Union, 85(48).

ZHANG, M., HE, Z., CALVERT, D., STOFFELLA, P., YANG, X. and LI, Y., 2003. Phosphorus and heavy metal attachment and release in sandy soil aggregate fractions. Soil Science Society of America Journal, 67(4), pp. 1158-1167.

ZHANG, Q. and ZAK, J.C., 1998. Effects of water and nitrogen amendment on soil microbial biomass and fine root production in a semi-arid environment in West Texas. Soil Biology and Biochemistry, 30(1), pp. 39-45.

ZHANG, Y., MAHOWALD, N., SCANZA, R., JOURNET, E., DESBOEUFS, K., ALBANI, S., KOK, J., ZHUANG, G., CHEN, Y. and COHEN, D., 2015. Modeling the global emission, transport and deposition of trace elements associated with mineral dust. Biogeosciences, 12(19), pp. 5771-5792.

ZHU, X., PROSPERO, J. and MILLERO, F.J., 1997. Diel variability of soluble Fe (II) and soluble total Fe in North African dust in the trade winds at Barbados. JOURNAL OF GEOPHYSICAL RESEARCH-ALL SERIES-, 102, pp. 21,297-21,305.

ZHUANG, G., YII, Z. and DUCE, R.A., 1992. Link between iron and sulphur cycles suggested by detection of. Nature, 355, pp. 6.

ZOBECK, T.M., STERK, G., FUNK, R., RAJOT, J.L., STOUT, J.E. and VAN PELT, R.S., 2003. Measurement and data analysis methods for field‐scale wind erosion studies and model validation. Earth Surface Processes and Landforms, 28(11), pp. 1163-1188.

ZOBECK, T.M. and VAN PELT, R.S., 2006. Wind-induced dust generation and transport mechanics on a bare agricultural field. Journal of hazardous materials, 132(1), pp. 26-38.

APPENDICES

Appendix 1 – Paper 5 ……... 300

Appendix 2 – Windblown dust BSNE samples ……... 333

Appendix 3 – Laboratory analyses data …….. 339

Appendix 4 – Sample ID, collection location and maps ……. 346

Appendix 5 – Standard deviation table for duplicate samples …… 357

Appendix 1 – Paper 5

Holocene fluvial valley fill sources of atmospheric mineral dust in the Skeleton Coast, Namibia

David S.G. Thomas[1,2,3]*, Julie A. Durcan[1], Andrew Dansie[1] and Giles F.S. Wiggs[1]

[1]School of Geography and the Environment, University of Oxford, Oxford OX1 3QY, UK

[2]Geography, Archaeology and Environmental Studies, University of the Witwatersrand, Johannesburg, South Africa

[3]Department of Environmental and Geographical Science, University of Cape Town, Rondebosch, South Africa

*Corresponding author david.thomas@ouce.ox.ac.uk

Abstract

Western Namibia is a significant global source of atmospheric mineral dust. We investigate the relationship between dust and source sediments, assessing the sustainability of dust flux. Remote sensing studies (Vickery and Eckhardt, 2013) have highlighted specific ephemeral fluvial systems as important contributors to dust flux, including highlighting sections of valleys that are the origins of dust plumes in the period 2005-8. Little is known however about the specific within-valley dust sediment sources, particularly whether dust is derived from modern ephemeral channel floors or older valley fill sediments, many of which have been reported in the region (Stone and Thomas, 2013). As part of a region-wide analysis of aeolian dust flux, we investigate the sediment properties of

atmospheric dust samples and valley sediments from the Huab valley, one of the principal regional dust sources. Trapped dust samples contain up to 88% very fine sand and silt when collected samples are disaggregated prior to analysis. Valley fill surface samples comprise 80% very fine sand and silt, and the surface of the modern ephemeral channel 30%. Valley fill sediments were sampled at depths up to 3.6m below the present surface and reveal Holocene depositional ages from 0.6± 0.03ka back to 9.79 ± 0.73ka. These sediments contain 30% to 6% very fine sand and silt, with levels decreasing with depth and age. Aeolian bedforms in the valley system (nebkhas on the fill surface and climbing dunes on valley margins) indicate that aeolian processes under the influence of strong seasonal easterly winds likely result in dust being winnowed out of the valley fill surfaces, with sandy bedforms being constructed from the coarser component of the fill sediments. The volume of valley fill sediment suggests dust sourced from Holocene sediments is likely to continue into the future regardless of flow conditions in the modern channel system.

Introduction

The drylands of southern Africa are a major source of atmospheric mineral dust in the southern hemisphere. However, the landscape units from which dust is sourced are highly discrete. The large palaeolake basins of Etosha in Namibia (Hipondoka et al., 2006) and Makgadikgadi in Botswana (Burrough et al., 2009) are the primary sources of southern African seasonal dust emissions today (Bryant 2003, Bryant et al., 2007, Bhattachan et al., 2015). Physically smaller sources, including salt pans and river valleys, are now also identified as

significant contributors to dust flux in the region (Eckardt and Kuring, 2005). These are usually in the form of low level plumes that are identifiable in MODIS and SeaWiFS imagery but not in observational systems such as TOMs, that have tracked higher level plumes and their terrestrial sources (Legrand et al., 2001).

Most significant amongst the smaller-scale sources are the ephemeral valley systems of the northwest Namibian coastal zone (Vickery and Eckardt 2013). The twelve valleys (Figure 1) include the Tsondab and Tsauchab, which trend east-west into, and terminate within, the Namib Sand Sea; the Kuiseb, which forms the northern boundary of the sand sea; and a series of valleys from Swakopmund northwards to the Angolan border that are sourced in the Great Escarpment mountains and run east-west across the Skeleton Coast hyperarid zone to the Atlantic Ocean.

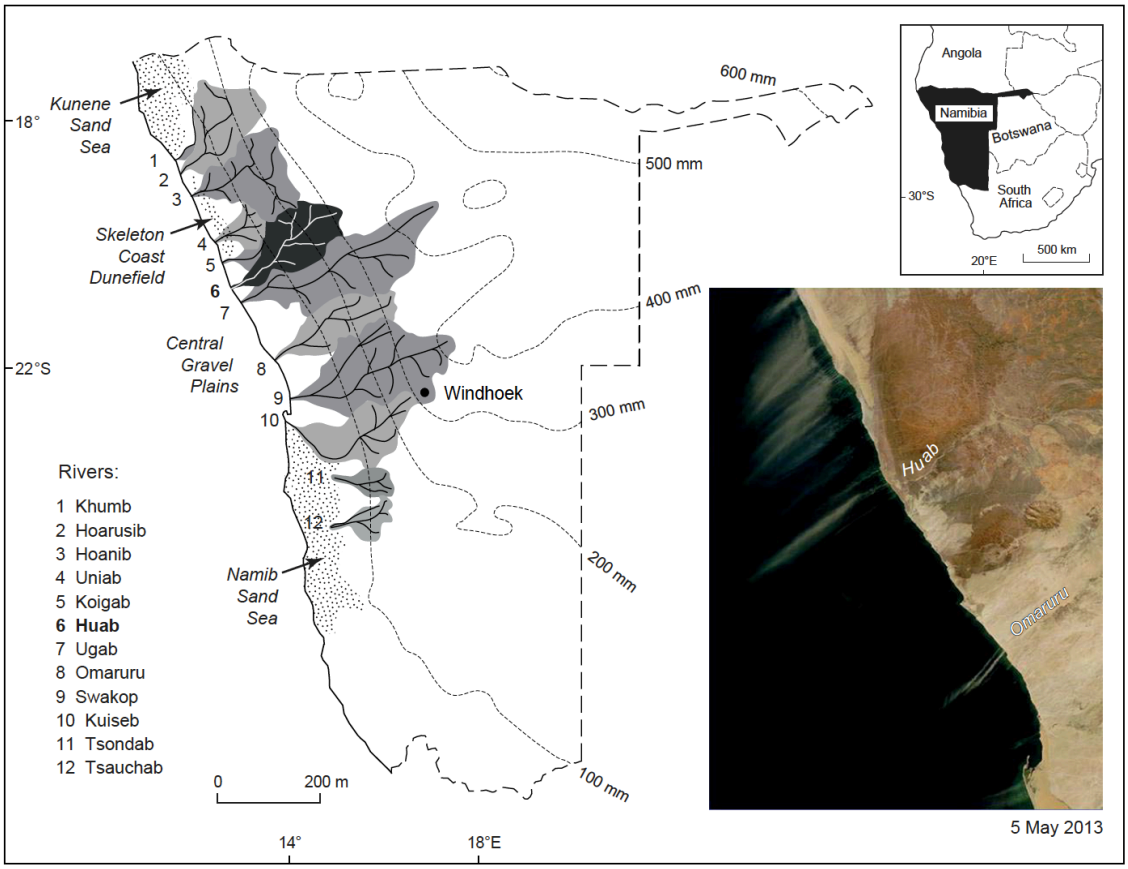


Figure 1. West coast valleys and channel systems of Namibia. Catchments, principle channels, desert sand seas and mean annual isohyets are shown. The Huab catchment is highlighted. Inset MODIS image of dust plumes extending over the Atlantic Ocean on 5 May 2013. The Huab is the source of a particularly extensive plume.

General associations have been drawn between fluvial controls and dust emissions in a wide range of environmental contexts, where water can at different times either inhibit dust entrainment or supply the sediment for deflation (Prospero et al., 2002). Over longer time scales (~10^3-10^5 years), it can be posited that the major global palaeolake dust sources, such as the Bodeli Depression in Chad, may be supply-limited in terms of their ability to emit dust, regardless of favourable atmospheric conditions (Engelstaedter and Washington 2007), because dust is sourced from sediments deposited during wetter late Quaternary phases (e.g. Warren et al., 2007) which is finite in volume.

In southern Africa, marine sediment core records from the SE Atlantic Walvis Ridge (Stuut et al., 2002) have been interpreted as indicating that both precipitation and windiness have controlled levels of dust flux over the last 300ka. The highest volumes of ocean dust deposition occurred during glacial rather than interglacial times, controlled at 10^3-10^4 year timescales principally by the strength of easterly winds rather than precipitation levels in source areas (Stuut et al., 2002). At shorter time scales it may be possible to establish links between fluvial sediment supply and dust emission events. For example, over a twenty year observational period, Bryant (2013) identifies antecedent flooding as a source of sediment input that acts as a positive control on dust flux emissions from Sua Pan, Makgadikgadi. In a study of dust emission events from the Kuiseb Valley,

Namibia, in the period 2005-2008, Vickery and Eckardt (2013) posited a link between ephemeral flow events and subsequent aeolian dust emission.

The last two decades have seen significant advances in the science of mineral dust emissions, with Vickery and Eckardt (2013) proposing that dust emissions from any source are consequential to its exact regional setting. There remain however considerable data gaps in both the atmospheric and surface control aspects of aeolian emission. Allied to the field data collection component of a major research programme focussed on generating the first dust source-area process data tailored to climate modelling needs[14] (Haustein et al., 2015), a series of ongoing investigations are providing new data from Namibian dust-emitting valleys on the relationships between source sediments and dust production (e.g. Dansie et al., 2016 a and b). This paper contributes a further component to this programme, investigating the depositional age of fluvial fills in one of the most heavily monitored systems, the Huab Valley, to address questions of the temporal origins of valley sediments, associations between dust flux and valley deposits, and whether dust flux is ultimately supply-limited. To do this we use both sedimentary data from modern dust and valley sediments, and 2) optically stimulated luminescence (OSL) age data derived from the fluvial valley fill deposits that are exposed through channel incision in the valley (Figure 2).

[14] DO4Models: http://www.geog.ox.ac.uk/research/climate/projects/do4models/

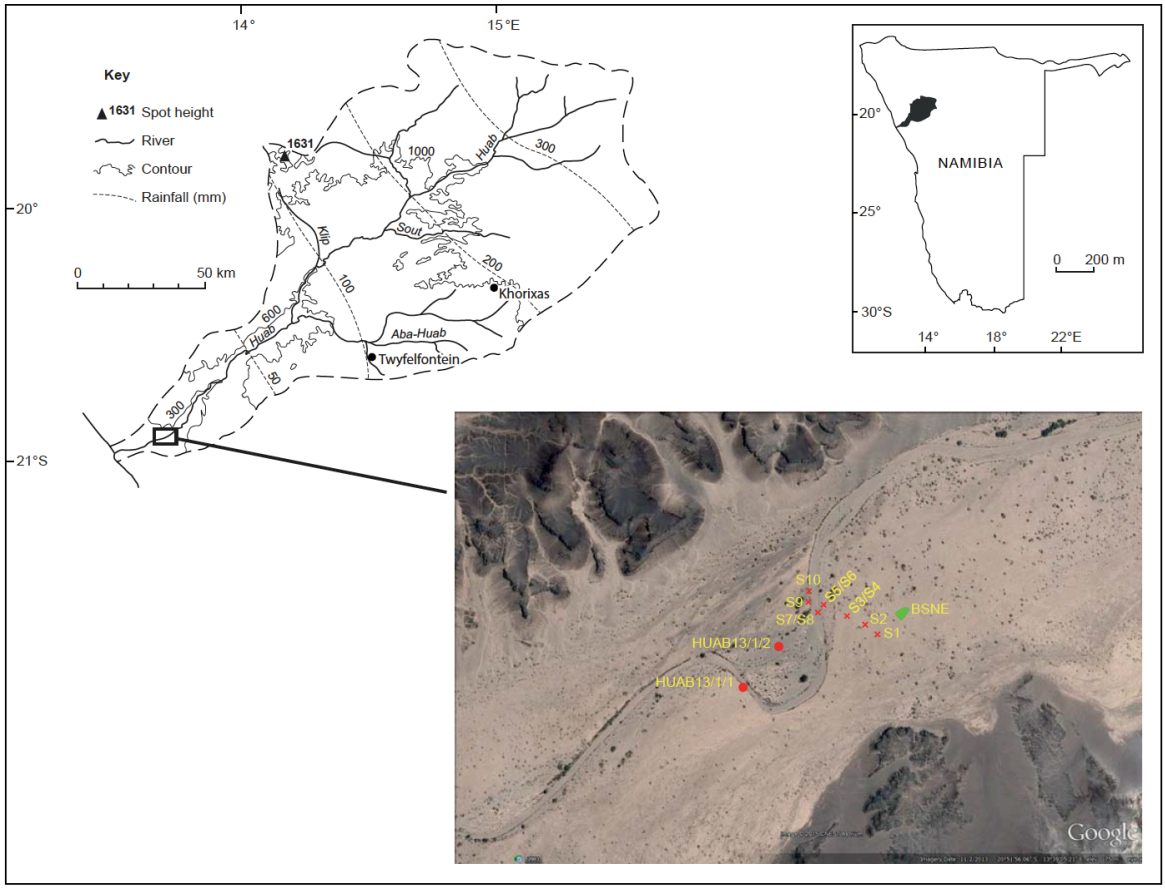


Figure 2. The Huab system showing the location of sediment sample sites used in this paper. Huab13/1 and 13/2 refer to the valley fill sections where samples were collected for OSL dating and S locations refer to the surface samples where S1, S2 and S3 are fill surface samples, S4 is a 10cm depth subsurface sample, S5 and S6 are from the surface of an inner channel terrace and S7, S8, S9 and S10 are modern channel floor samples). The location of the BSNE sampler is also shown.

Background

Skeleton Coast valley systems and fluvial sediments

Today the geomorphic dynamics of the east-west orientated Skeleton Coast valleys are dominated by aeolian processes; evident from nebkha dunes (Figure 3) and wind scour on valley floors, climbing dunes and drapes on valley sides.

These valleys are also regionally-significant sources of aeolian dust. Annually, dust plumes during easterly Berg wind events (which primarily occur in winter months, April-September) extend over the Atlantic Ocean to the west of the Skeleton Coast (Vickery and Eckardt, 2013, Dansie et al., 2016 a and b). Ephemeral fluvial flow occurs in the valleys, driven by summer month (DJFM) precipitation events in the inland escarpment source areas that may exceed 200 mm mean annual rainfall (Stone and Thomas 2013), but with high interannual variability.

Evidence of more significant fluvial flow regimes in the past is provided by extensive valley fill sediments. In some valleys these have been the subject of chronometric investigations and interpretations in the context of late Quaternary changes in precipitation regimes. Dated sequences (summarised in Stone and Thomas, 2013) come from the Khumib, Hoarusib, Hoanib, Kuiseb and Tsauchab valleys (Bourke et al., 2003; Brook et al., 2006; Eitel et al., 2005, 2006; Srivastava et al., 2004, 2005,

2006; Stone et al., 2010) but not the Huab. Various accumulation phases for valley sands and silts have been placed within the c130 ka-0.4 ka period with the majority occurring within the last 40 ka (Stone and Thomas, 2013). Difficulties have ensued in ascribing palaeoclimatic and palaeoenvironmental interpretations to many of these deposits, with some studies attributing silt-sand accumulation to drying conditions (e.g. Marker and Muller, 1978), and others to wetter events (e.g. Srivistava et al., 2006). In part, differences arise because sediments are found in a range of environmental contexts within the valleys, with locational, sedimentary and structural characteristics of deposits now providing a greater

interpretive capacity (Stone and Thomas, 2013). Deposits in more westerly locations in the valley systems are

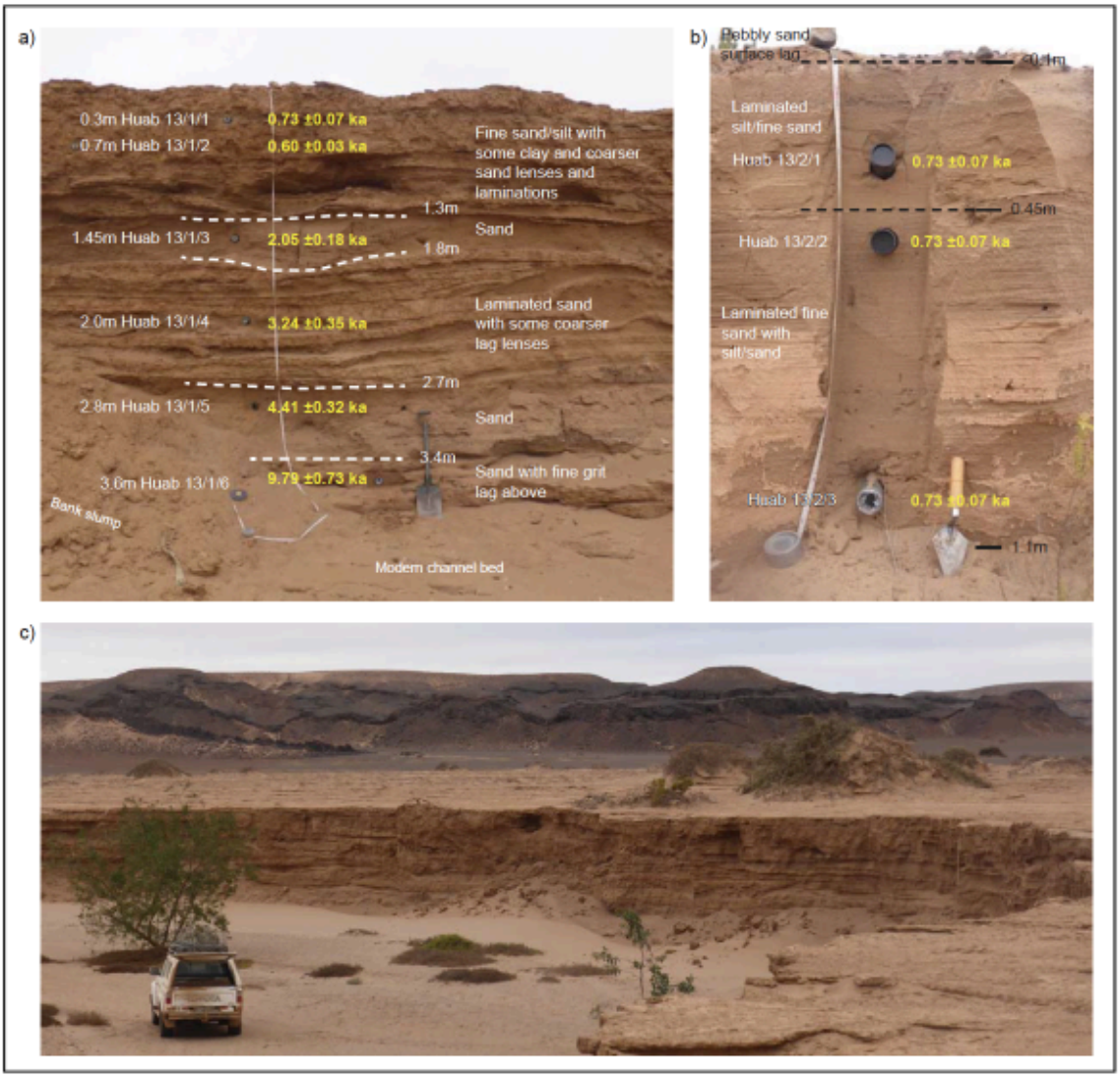


Figure 3. Valley fill sample sites Huab13/1 (a) and Huab13/2 (b). See Figure 2 for locations. c) shows the main channel incision and exposure of valley fill sediments, with nebkha dunes on the upper fill surface in the right of the photograph.

generally slack-water features, indicative of greater flow than under the more semi-arid conditions of today (e.g. Srivastava et al., 2004, 2005, 2006). Deposits in up-valley (eastern) locations are more indicative of flow incompetence, low-energy runoff, and limited transport capacity under drier conditions (e.g. Eitel et

al., 2005). In some situations, these sediments may also be associated with valley-slope loess units (Brunotte et al., 2009).

Individual sedimentary units require careful interpretation with respect to the valley context in which they occur. In this regard, Grodek et al. (2014) used a palaeohydrological approach to investigate valley deposits along a 150km stretch of the middle Kuiseb valley. Their analysis, based on sedimentary data and luminescence dating, identified over forty flood events leading to accumulation during the last 1300 years, but with century and decadal scale phases of increased flood frequency also identified. Using a similar approach, Greenbaum et al. (2014) recorded a similar number of flood event deposits in the Swakop valley, but with accumulation spanning a much longer period, back to 15 ka. Within this record, data are interpreted to suggest that flood magnitudes were at their highest during the transition from warm, dry conditions to the colder and wetter Little Ice Age (700-200 years ago) and in the late 19th to early 20th centuries.

Dust flux and sources

It was noted earlier that data on Namibian dust flux comes at two distinct scales: millennial scale records from oceanic sink data (Stuut et al., 2004) and event-scale remote sensing-derived data for recent decades (e.g. Vickery et al., 2013) that can link dust events to specific source locations. It is this latter approach that has highlighted the Namibian valleys as major dust sources, with 111 plume events from 39 source locations identified from MODIS imagery for the three years from 2005 (Vickery et al., 2013). In terms of frequency, these represent a

third of the total plumes emitted from southern Africa during that period, with the Huab system being one of the major emitting source areas, with 15 plumes in 2005-8 (Vickery, 2010). Nine of these plumes were sourced from a small section of the lower valley, which forms the focus of our subsequent analyses.

Absent to date are data on the sedimentological characteristics of dust-event sediments, and of associated valley deposits. Dansie et al. (2016a and b) show that the surface sediments of the Huab system are neither homogenous in sedimentologically or in their susceptibility to deflation. Therefore, to establish the relationship between the aeolian and fluvial sediment systems, further data on dust sedimentary properties and from fluvial valley fills, are required. These data, along with information on the age of fluvial deposits, can provide the basis for a more holistic understanding of the relationships between fluvial and aeolian sediments in the valleys and on the temporal origins of the material that is being deflated today. In this paper we present data to test these relationships and to address the question of the sustainability of dust flux from the valley systems. We do this specifically in the context of the Huab system, which in 2013 was subject both to field monitoring of dust events and the sediments associated with these events, and to sampling of the valley floor sediments themselves for sedimentary and depositional age determinations. During the 2013 survey season nine notable dust flux events were observed from the section of the valley investigated in this paper, on 1, 2 and 5 May, 11 and 17 of June, and 21, 22, 25 and 30 July. The largest events, in terms of duration and magnitude were those of 5 May, and 21 and 30 July.

Methods

Location

The Huab valley extends for c300 km from the central Highlands of Namibia, through the Great Escarpment (Morin et al., 2009), and flows southwest to the Skeleton Coast, where the channel enters the Atlantic Ocean at 20.910°S, 13.451°E via a small delta. The catchment has an area of 14800 km^2, the seventh largest of the 12 west coast valley systems, and mean annual precipitation through the system ranges from up to 345 mm in the east, where altitudes reach almost 1600 m asl, to almost zero at the coast; 80% of the catchment receives less than 100 mm precipitation (Jacobson et al., 1995, Figure 1). The lower c70 km of the Huab valley is set largely within Karoo (Permo-Carboniferous to Jurassic) glacial sedimentary and volcanic units that form valley sides that can be variable but steep and several hundreds of metres high above the channel floor. Part of the system follows ancient glacial channels (Jacobson et al., 1995) which form the broad valley (up to 2km wide) in which more recent valley fill deposits have accumulated. The middle and upper catchment primarily lies in the metamorphic and igneous rocks, largely granites and gniesses, of the ~2mil yr PreCambrian Kamanjab inlier, set within the Damara Orogen.

Field sampling

Field monitoring stations recording environmental and meteorological data were established at six locations in the lower c30 km of the Huab valley, the section of the system where valley fills have accumulated and from where many dust

plumes are sourced (Vickery, 2010). Monitoring station data were collected during the period April-September 2013. This included Big Spring Number Eight (BSNE) aeolian sediment samplers (Zobeck et al., 2003, Mendez et al., 2011) to capture horizontal sediment flux at 0.25 m (sampler 1), 0.47 m (sampler 2), 0.89 m (sampler 3) and 1.68 m (sampler 4) above the ground surface. These heights were selected to replicate the heights of anemometers in the meteorological station equipment arrays. At these six locations, and additional sampling points through the full length of the Huab system (see Dansie et al., 2016a and b), surface samples were collected in transects across the valley to include valley fill and modern channel sediments. The remainder of this paper utilises data from site H2 (Figure 2) and its immediate vicinity.

Monitoring Station H2 (Figure 2) was located in one of the widest parts of the Huab valley system, 21.3 km from the channel mouth at 20.865^{o}S 13.653^{o}E. Alluvial sediments extend across the 1100 m wide valley floor, upstream from a topographically-induced narrowing of the valley that has acted as a barrier to flow, leading to the extensive accumulation of sediments. The surface of the valley fill shows significant evidence of aeolian activity, in the form of nebkha dunes accumulated around occasional shrubs, and wind scour features. The modern channel has incised into the valley fill, exposing up to 4 m of fill sediments in the channel sides (Figure 3). A secondary channel is further incised into the main meandering channel system, exposing a further 1.1 m of sediments of a secondary inner fill.

A transect across the valley floor at H2 collected surface samples (c200 g each) for particle size and nutrient content from 10 points that embraced the valley fill

surface S1 S2 and S3 in Figure 2), 10 cm subsurface of the valley fill (S4), inner channel terrace (S5, S6) and the modern channel floor (S7, S8, S9, S10) (Dansie et al., 2016a, 2016b). Samples collected for OSL dating from sites Huab13/1 and Huab13/2 also provided subsamples for particle size analyses through the vertical exposures in the main valley fill and the inner fill (Figure 3). Sediment trapped in the BSNE samplers was emptied on a monthly basis (Dansie et al., 2016c) and provided data on the characteristics of the sediment mobilised in dust-raising events in 2013. Samples from the transect and BSNEs were collected in pre-weighed ziplock sample bags. Nine samples for OSL dating were collected in light-proof 15 cm long capped black plastic tubes, which were additionally wrapped in black plastic bags.

Sedimentary analyses

Grain size analyses were undertaken using a Malvern Mastersizer Hydro 2000MU to determine sample particle size ranges of the different sedimentary units in the valley and to identify the proportion of fine material that might be susceptible to aeolian erosion. Samples were 'dry'-analysed (with no disaggregation) following drying and riffling to less than 4g to meet equipment specifications and to standardise the subsamples derived from the different units included in the study. A further subset of samples were also measured 'wet', after standard preparation for disaggregation by digesting overnight in $(NaPO_3)_6$ and four hours on a horizontal shaker before being analysed in the wet dispersal unit to establish the finer silt-sized material present as aggregates within samples.

Age determinations

Samples for OSL dating (Figure 3) were opened and prepared under subdued orange light conditions at the Oxford Luminescence Dating Laboratory, University of Oxford. Sediments were treated with hydrochloric acid and hydrogen peroxide to remove carbonates and organic matter, and sieved to isolate either the 125 – 150 or the 180 – 210 μm grain size fraction. Heavy liquid density separation was carried out to isolate quartz grains and the resulting material was etched using hydrofluoric acid to remove the alpha-irradiated outer surface of the quartz grains and any non-quartz mineral grains still present.

All OSL measurements were made using a Risø TL/OSL luminescence reader. OSL was stimulated using green light-emitting diodes (525 nm) and detected through a bialkali photo multiplier tube fitted with 7.5 mm U340 filters. Equivalent dose (D_e) measurements were made following the single-aliquot regenerative dose (SAR) protocol (Murray and Wintle, 2000; Wintle and Murray, 2006), using a preheat of 220°C for 10 s, a cut-heat of 160°C for 0 s, and luminescence was measured at 125°C for 100 s. Small aliquots of sample were used and a standard set of rejection criteria (e.g. Jacobs et al., 2006) was applied, including the OSL IR depletion ratio of Duller (2003) and the fast ratio of Durcan and Duller (2011) adjusted for stimulation with green diodes. Final D_e determinations were calculated using the central age model (Galbraith et al., 1999) or finite mixture model (Galbraith and Green, 1990), depending on the calculated overdispersion value, after Rodnight et al., (2006). The environmental dose rate was calculated using radionuclide concentrations measured using inductively coupled plasma mass spectrometry, which were converted to dose rates using the attenuation

factors of Guerin et al., (2011) and corrected for attenuation by grain size, chemical etching and a moisture content of 5 ± 2 %. The dose rate contribution from cosmic rays was calculated according to Prescott and Hutton (1994). All dose rates were calculated using the DRAC (v1.1) program of Durcan et al. (2015), available at www.aber.ac.uk/alrl/drac.

Results

Sedimentary data

Dry -analysis particle size data are presented in Table 1 and 2 and Figure 4. Data are mean values for contexts where multiple samples were collected (e.g. the fill surface values in Table 1 and Figure 4 are the means of samples S1, S2 and S3). Aeolian dust is often considered to equate to silt-sized material (2-63 μm) but commonly it includes particles up to ~100-150 μm in diameter (e.g. Hesse and McTainsh, 1999, Wiggs et al., 2003). Grain size data in Tables 1 and 2 are therefore categorized to include the 'very fine sand' and 'fine sand' classes. Medium and coarse sand do, however, also play a function in dust generation, as saltation triggers the expulsion of finer material into the atmosphere (e.g. Rice et al., 1996) during entrainment events, and can break-up protective surface crusts by bombardment.

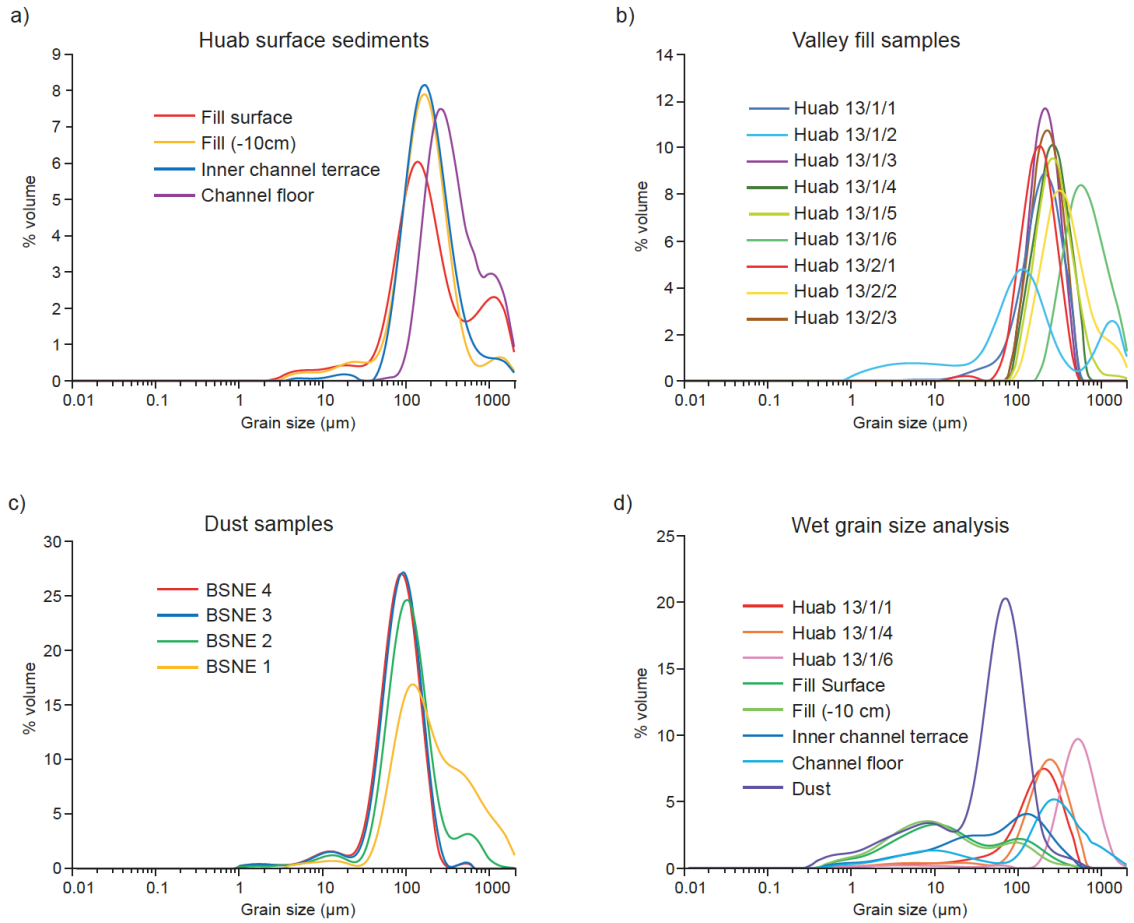


Figure 4. Sediment grain size data for a) surface samples, b) samples from the dated valley fill sections, and c) BSNE sediment samplers. d) Representative wet-analysed samples from the surface, valley fill and BSNE sampler mean values

Figure 4 a and b show that the dry-analysed samples from the valley fill sediments largely display comparable grain size profiles, with distribution curves peaking around 200 µm. Some variability occurs; samples from the modern channel floor are coarser than those from the fill surface, with a modal peak around 350 µm, while the modern fill surface is bimodal in distribution with a second coarser peak at over 1 mm particle diameter. The finer limbs of the two curves (up to the c100 µm modal peak) are directly comparable, but the greater contribution to the total curve of the coarser component of the surface sample

likely reflects a residual lag component resulting from sediment loss through deflation. The BSNE data (mean data from all sampling dates in Table 1 are shown in Figure 4c) show mean value peaks in the 80-100 μm size range, with both an increase in the modal value and an increasing contribution of medium and coarse sand as height of the trap descends. This reflects a greater contribution of saltation, rather than suspended, load closer to the ground surface.

Notwithstanding the commonality in the modal peaks of the majority of samples from the vertical channel bank sections, the data do show some internal variability through the profile (Figure 3b). Sample Huab13/1/2 is bimodal with a secondary peak at 1500 μm, and sample 13/1/6 is significantly coarser than the others, lacking a silt component and peaking at 600 μm. These differences may reflect different sediment loads at separate times of fill deposition; they may however also simply reflect variability within the sedimentary lenses and laminae constituting the units in the section as a whole (Figure 2a).

Table 2 shows that the transported aeolian sediments that contribute to dust flux from the valley comprise both silt and very fine sand fractions with the silt component not exceeding 22%. Dry analysis data show that the upper fill sediments comprise no more than 7% silt (Table 1). Only samples Huab13/1/1, 13/1/2 and 13/2/1 in the vertical section samples contain a silt component (Table 1); the remaining units comprise solely sand-size sediment.

Given the low silt content of the dry-analysed sediments, three samples from the main vertical valley fill section representing upper, middle and lower components (samples Huab13/1/1, 1/3 and 1/6) and the fill surface sample were subjected to

wet grain size analysis, to investigate the presence, in aggregate form, of material finer than sand within the valley and BSNE trap samples (Table 3). Figure 4d shows how on disaggregation, all samples reveal a greater proportion of fine-grained material, with modal peaks of valley fill samples diminishing in height in the 200-500 μm range and more significant limbs in the finer particle sizes emerging.

These data show a significant silt content within both the surface sediment samples and the valley fill samples. When very fine sand and silt contents are considered together, as the potential suspended load (data in right hand column of Tables 1 and 3), the potentially available dust content in valley fill samples increases from 21.22% to 30.82% (Huab13/1/1), 7.91% to 18.58% (Huab13/1/4), and even Huab13/1/6, which had no silt or very fine sand in dry analysis samples, increases to a content of 5.93%. There is clearly a potential future dust load in deeper valley fill sediments, though with variability through the unit.

The collected surface samples also show significant fine sand and silt content increases after disaggregation and wet analysis. This component of the valley-fill surface sample rises from 33.03% to 79.74%, with significant increases evident in the silt + very fine sand content of samples at all locations (Table 3). Interestingly, the silt + very fine sand content of the BSNE samples also increases after disaggregation in analysis, more than doubling (33.18% rising to 69.46%) in the case of the lowermost sampler, BSNE 1, and from 75.27% to 88.44% in the uppermost sampler, BSNE 4.

Age of Huab valley fills

OSL age data are presented in Table 4 and shown in Figure 3. In addition to D_e analysis, dose recovery tests were undertaken on samples Huab13/1/1, 1/6 and 13/2/1 and the ratio of the given to recovered dose was 0.93 ± 0.03, 0.95 ± 0.02 and 0.95 ± 0.04 respectively, demonstrating the suitability of the SAR protocol for D_e measurement. In general, OSL signals measured from this suite of samples were reasonably bright (e.g. Figure 5a) and dominated by the fast component in the initial part of the signal (e.g. Durcan and Duller, 2011). Using the calculations of Heer et al., (2012), the small aliquots used in this study are estimated to consist of ~65 grains per disc, and single grain analyses of samples Huab13/1/1 and -13/2/1 show that 2-3% of grains give a luminescence signal detectable above reader background levels. Therefore, the signal from each aliquot is expected to originate from 1-2 grains on average, which is sufficient for the detection of heterogeneity in the dose distributions. For this suite of samples, overdispersion between 14% and 98% is observed (Table 4), and overdispersion is greater than 37% for all but one sample. Attributing the cause(s) of scatter in dose distributions is challenging, and multiple depositional and post-depositional factors may contribute to the observed heterogeneity in D_es, including incomplete bleaching (e.g. Olley et al., 1998), microdosimetric variability (e.g. Murray and Roberts, 1997) and bioturbation mixing (e.g. Bateman et al., 2003). Given the geomorphological setting, with the sediments likely deposited following transport in flashy desert flow events, heterogeneous bleaching is likely to contribute significantly to the observed spread in data, and the finite mixture model has been used to identify the well-bleached component in the dose distributions.

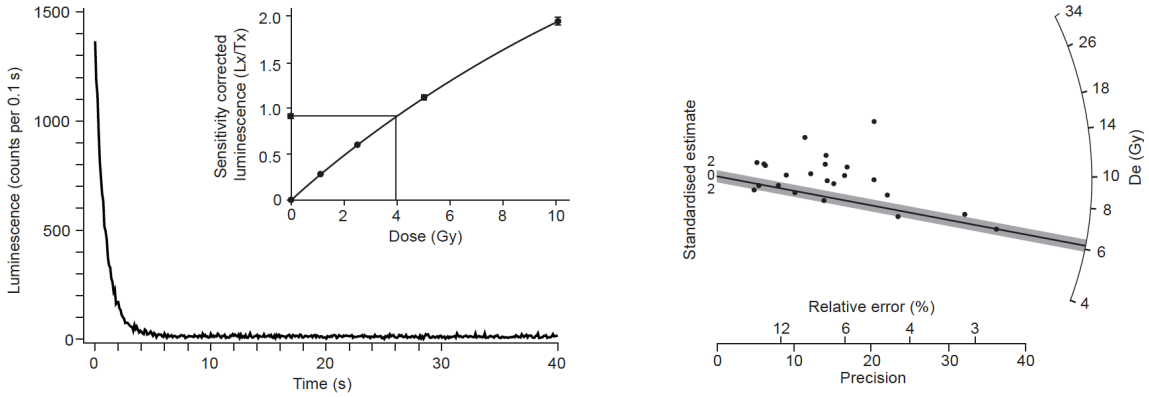


Figure 5. a) An example OSL signal and inset, the dose response for an aliquot of sample Huab13/1/3. The dose response curve has been fitted with an exponential function and that natural, sensitivity corrected luminescence signal (shown by the grey symbol) has been interpolated to give a D_e of 6.87 Gy. b) The dose distribution for the same sample. All points within the grey shaded area are within approximately 2σ of the 6.18 Gy D_e (shown by the solid line).

The calculated OSL ages indicate phases of deposition of alluvial valley fill sediments during the Holocene (Table 4). At site 1, the upper unit dates to within the last millennia, with ages of 0.73 ± 0.07 ka and 0.60 ± 0.03 ka for samples Huab13/1/1 and 13/1/2.. Age increases with depth throughout the rest of the sequence and the OSL dating demonstrates that the majority of the sediments observed have been deposited since the mid-Holocene, with sample Huab13/1/5 towards the base of the unit dated to 4.41 ± 0.32 ka. Sample Huab13/1/6 at the base of the unit was deposited at 9.79 ± 0.73 ka. At site two, samples Huab3/2/1 and 13/2/2 give ages of 0.62 ± 0.04 ka and 0.67 ± 0.06 ka respectively, correlating with the upper part of the sequence at S1. The deepest sample taken from S2, Huab13/2/3, is dated to 1.39 ± 0.10 ka, suggesting the deposition of the valley fill sediments of this unit within the past 1500 years.

Discussion: Sediment supply in the Huab valley and implications for dust emissions

In the Kuiseb valley, modern dust emissions show a temporal relationship to antecedent flood events (Vickery and Eckardt, 2013). We interpret the data and field observations as showing that modern dust emissions in the Huab valley are associated with valley fill sediments that accumulated in the Holocene and not the narrow channels that experience ephemeral fluvial flow today. Further field investigations in other dust-emitting valleys in the area will be needed to establish if this is in fact the situation throughout the region.There is ample very fine sand and silt size material in these deposits, and significant geomorphic evidence of sediment movement by the wind on the fill surfaces at elevations above the modern ephemeral channel. The incised lower channel displays some evidence of modern fluvial flow, but not of significant deposition of new silt-sized sediments derived from upper valley locations.

The OSL chronology of the valley fill sediments does however indicate that, in the last 10 ka at least, deposition in this section of the valley has occurred on multiple occasions. These are likely to be slack water deposits, observed in other Namibian valley contexts (e.g. Srivastava et al., 2004), and this is supported by the fine laminae within the fill sediments and the valley context, upstream from a pinch point in the valley that would act as an impediment to flow, encouraging reductions in transport velocities and subsequent sedimentation. The sedimentary unit appears to extend across the valley at this location, which would also support the notion that ponding has occurred, but confirmation would require supporting data form additional locations in the sedimentary fill. The oldest

sediments exposed in the channel bank section date to 9.79 ± 0.73 ka, but there appears to be no further sedimentary preservation of depositional events until 4.41±0.32 ka. The hiatus in ages between samples 13/1/6 and 13/1/5 may represent a real absence of deposition, spatially variable deposition not recorded at this location, or erosion, likely by deflation of materials in the ck5 year period between the ages. Comparable within-errors early Holocene ages are recorded in the accumulated units in the more northerly upper Hoanib catchment (9.4±0.7 ka, Eitel et al., 2006), and the terminal deposits of the more southerly Tsauchab (9.1 ±1.0 and 9.0 ±1.6 ka, Brook et al., 2006). The Hoanib also records accumulation at 4.9±0.4 ka.

After 4.4 ka, depositional events could be interpreted as occurring with a c.1200 year frequency (Figure 2a) with rounded mean ages 3.2 ka, 2 ka and 0.7 ka in section Huab13/1. The upper two ages (13/1/2 and 13/1/1) at 0.73±0.07 ka and 0.60±0.03 ka are not within one sigma errors, although this needs to be interpreted with caution given the high overdispersion values (Table 4). If these ages were to represent distinct depositional events, then either the frequency of accumulation in the last 700 years has changed from earlier millennia, or the ages from sediments lower in the section are not totally representative of the apparently bounded units that they are derived from. That is, other ages may be derived from within these units were more samples collected for dating. In this respect, the problems reported from aeolian sands by Leighton et al., (2013) with using bounding surfaces as distinct event boundaries may warrant some consideration as relevant to the interpretation of desert fluvial deposits and their depositional chronologies.

Placing these deposits in a regional context, Greenbaum et al. (2014) record several accumulation events in the last millennium within Swakop valley fluvial deposits, including at 0.74±0.19 and 0.74±0.09 ka. In the Kuiseb valley, Grotek et al. (2014) report dated flood deposits at 0.67±0.04 ka and 0.65±0.04 ka within a millennial record of major flood events occurring every 20 to 40 years. These studies suggest that deposits from other floods during the past 1000 years are likely to be recorded within this extensive Huab valley fill unit.

The sediments from the finely laminated inner fill, within the meander of the current Huab channel, were interpreted in the field as representing a second fill phase within the channel incised into the valley-wide deposits. The ages derived from 13/2/1 and 2/2 are almost identical to that of 13/1/2 suggesting that these sediments are not a distinct fill within a cut but are part of the main depositional system.

Only the upper samples from both these vertical sections had a silt-sized component when particle size data were derived through dry sample analysis (Table 1), though very fine sand is prevalent through the deposits within the valley fill. On disaggregation of samples (Table 3), the proportion of silt size material increased significantly demonstrating that appropriate material for wind-suspended transport is available within valley fill sediments. There is variability of the fine content between samples (compare for example the data for Huab13/1/1 and Huab13/1/4). While this may reflect differences in the precise units sampled within the laminae in the fill, there is also the possibility that upper units are enriched by dust fall and infiltration of fines into the surface sediments, it can be noted here too that the fill surface and 10 cm depth samples have higher silt and

very fine sand proportions than the deeper fill units. Indeed, disaggregation may occur during transport events through the effects of saltation bombardment.

The BSNE samples were also subject to dry and wet particle size analyses, with increases in the very fine sand and silt content following. However, it is not possible to determine from the wet and dry analyses of these samples the relative contributions of material transported as aggregates compared with material transported as silts and then subject to post-transport re-aggregation under moist atmospheric conditions. Overall, however, we show that valley fills contain sufficient silt and very fine sand to act as a considerable source of material during deflation events. The silt captured in the BSNE traps is likely to be derived from the mechanical breakdown of aggregates within the sand-size component of the valley fill sediments, through the impact of saltating grains during aeolian transport events. Furthermore, the presence of silt at depth in the valley fills demonstrates the sustainability of this source of atmospheric mineral dust.

Conclusions

This paper has presented the first systematic study of the age of modern aeolian dust flux source sediments. The Namibian west coast valleys represent significant, focussed, sources of aeolian atmospheric dust. In this study, which has centred on the section of the Huab valley that is a major source of dust plumes observed in MODIS imagery, we provide evidence to support a strong relationship between dust sources and Holocene fluvial valley fills. Other aeolian bedforms in the valley system, including nebkha dunes on the valley fill surface

and climbing dunes on valley margins, suggest that aeolian processes occurring under the influence of strong easterly winds generate local sandy bedforms and the emission of dust into the atmosphere. Given the minimum thickness (as exposed in the investigated channel section) of c4 m of valley fill sediments, the likelihood of many metres more beneath the modern channel level, and a record of fluvial depositional events in the mid-Holocene (indicated by the OSL ages), it seems likely that windblown dust events in the Namibian valleys will not be limited by sediment supply in the future. Indeed, our data suggest that the current supply of erodible sediment in the valley-fills would provide ample material to sustain a high frequency of windblown dust events even if fill replenishment events are centuries to millennia apart. This is despite the studied location not recording flood deposits more recent than c.600 years ago. Recent dinvestigations (Grodek et al., 2014, Greenbaum et al., 2014) in two other western Namibian valleys have found evidence of high frequency flood events occurring in the region in recent centuries; further investigations are required to establish if this is the case in the Huab, or whether evidence of events more recent than 600 years ago has been removed from the record by deflation events.

Acknowledgments

We thank other members of the DO4Models project team for contributions to the framing of this study, particularly Richard Washington, Frank Eckardt and Kate Vickery. Fieldwork for this study was conducted as an additional activity during dust and sediment monitoring studies in 2013 that contributed to both

DO4Models, funded by NERC and the Fell Fund (ref121/474), University of Oxford, and the doctoral studies of Andrew Dansie, funded by a Clarendon Scholarship, University of Oxford. Research was carried out under research permit 1788/2013, issued by the Ministry of Environment and Tourism, Namibia.

References

Bateman, M.D., Frederick, C.D, Jaiswal, M.K., Singhvi, A.K., 2003. Investigations into the potential effects of pedoturbation on luminescence dating. Quaternary Science Reviews 22, 1169-1176.

Bhattachan, A. , D'Odorico, P., Okin, G.S. 2015. Biogeochemistry of dust sources in Southern Africa. Journal of Arid Environments 117, 18-27

Bourke, M.C., Child, A., Stokes, S., 2003. Optical age estimates for hyper-arid fluvial deposits at Homeb,Namibia. Quaternary Science Reviews 22, 1099-1103.

Brook, G.A., Srivastava, P., Marais, E., 2006. Characteristics and OSL minimum ages of relict fluvial deposits near Sossus Vlei, Tsauchab River, Namibia, and a regional climate record for the last 30 ka. Journal of Quaternary Science 21, 347-362.

Brunotte, E., Maurer, B., Fischer, P., Lomax, J., Sander, H., 2009. A sequence of fluvial and aeolian deposits (desert loess) and palaeosoils covering the last 60 ka in the Opuwo basin (Kaokoland/Kunene Region, Namibia) based on luminescence dating. Quaternary International 196, 71-85.

Bryant, R.G., 2003. Monitoring hydrological controls on dust emissions: Preliminary observations from Etosha Pan, Namibia. Geographical Journal 169, 131-141.

Bryant, R.G., Bigg, G.R., Mahowald, N.M., Eckardt, F.D., Ross, S.G., 2007. Dust emission response to climate in southern Africa. Journal of Geophysical Research Atmospheres 112, D09207

Bryant, R.G., 2013. Recent advances in our understanding of dust source emission processes. Progress in Physical Geography 37, 397-421.

Burrough S.L., Thomas D.S.G., Bailey, R.M., 2009 Mega-Lake in the Kalahari. A 250 kyr record of Palaeolake Makgadikgadi. Quaternary Science Reviews 28, 1392-1411.

Dansie, A., Wiggs, G.F.S., Thomas, D.S.G., 2016a. Iron and nutrient content of wind-erodible sediment in the dry river valleys of Namibia. Geomorphology, submitted

Dansie, A., Thomas, D.S.G. and Wiggs, G.F.S., 2016b. Spatial variability of nutrients in dust-emitting Namibian ephemeral river catchments. Earth Surface Processes and Landforms, submitted.

Dansie, A., Wiggs, G.F.S., Thomas, D.S.G., 2016c. Iron, phosphorus and nitrogen content of deflated sediments from the Namibian ephemeral river valleys and their potential for ocean fertilization. Aeolian research, in prep.

Duller, G.A.T., 2003. Distinguishing quartz and feldspar in single grain luminescence measurements. Radiation Measurements, 37, 161–165.

Durcan, J.A. and Duller, G.A.T., 2011. The fast ratio: a rapid measure for testing the dominance of the fast component in the initial OSL signal from quartz. Radiation Measurements, 46, 1065-1072.

Durcan, J.A., King, G.E., Duller, G.A.T., 2015. DRAC: Dose rate and age calculator for trapped charge dating. Quaternary Geochronology, 28, 54-61.

Eckardt, F.D., Kuring, N.,2005. SeaWiFS identifies dust sources in the Namib Desert(2005) International Journal of Remote Sensing 26, 4159-4167.

Eitel, B., Kadereit, A., Blümel, W.D., Hüser, K., Kromer, B., 2005. The Amspoort Silts, northern Namib desert (Namibia): formation, age and palaeoclimatic evidence of river-end deposits. Geomorphology 64, 299-314.

Eitel, B., Kadereit, A., Blümel, W.D., Hüser, K., Lomax, J., Hilgers, A., 2006. Environmental changes at the eastern Namib Desert margin before and after the Last Glacial Maximum: new evidence from fluvial deposits in the upper Hoanib River catchment, northwestern Namibia. Palaeogeography, Palaeoclimatology, Palaeoecology 234, 201-222.

Engelstaedter, S.and Washington, R., 2007. Temporal controls on global dust emissions: The role of surface gustiness. Geophysical Research Letters, 34 art. no. L15805,

Galbraith, R.F. and Green, P.F., 1990. Estimating the component ages in a finite mixture. Nuclear Tracks and Radiation Measurements 17, 197-206.

Galbraith, R.F., Roberts, R.G., Laslett, G.M., Yoshida, H., Olley, J.M., 1999. Optical dating of single and multiple grains of quartz from Jinmium rock shelter, northern Australia: part I, experimental design and statistical models. Archaeometry, 41, 339-364.

Guerin, G., Mercier, N., Adamiec, G., 2011. Dose-rate conversion factors: update. Ancient TL, 29, 5-8.

Greenbaum, N., Schwartz, U., Benito, G., Porat, N., Cloete, G.C, Enzel, Y., 2014. Paleohydrology of extraordinary floods along the Swakop River at the margin of the Namib Desert and their paleoclimate implications. Quaternary Science Reviews 103, 153-169.

Grodek, T., Benito, G., Botero, B.A., Jacoby, Y., Porat, N., Haviv, I., Cloete, G., Enzel, Y., 2014. The lasyt millennium largest floods in the hyperarid Kuiseb basin, Namib Desert. Jopurnal of Quaternary science 28, 258-270.

Haustein, K., Washington, R., King, J, Wiggs, G, Thomas, D., Menut, L., 2015. Testing the performance of state-of-the-art dust emission schemes using DO4Models field data. Geoscience Models Development 8, 341-362.

Heer, A.J., Adamiec, G., Moska, P., 2012. How many grains are there on a single aliquot? Ancient TL, 30, 9-16.

Hesse, P., McTainsh, G.M., 1999. Last glacial maximum to early Holocene wind strength in the mid-latitudes of the southern hemisphere from aeolian dust in the Tasman Sea. Quaternary Research 52, 343-349.

Hipondoka, M.H.T., Jousse, H., Kempf, J., Busche, D., 2006. Fossil evidence for perennial lake conditions during the Holocene at Etosha Pan, Namibia. South African Journal of Science 102,93-95.

Jacobs, Z., Duller, G.A.T. and Wintle, A.G., 2006. Interpretation of single grain De distributions and calculation of De. Radiation Measurements 41, 264–277.

Jacobson, P.J., Jacobson, K.N., Seely, M.K., 1995. Ephemeral rivers and their catchments: sustaining people and development in western Namibia. Desert Research Foundation of Namibia.

Legrand, M., Plana-Fattori, A., N'Doumé, C., 2001. Satellite detection of dust using the IR imagery of Meteosat 1. Infrared difference dust index. Journal of Geophysical Research Atmospheres 106, 18251-18274.

Leighton, C.L., Thomas, D.S.G., Bailey, R.M., 2013. Allostratigrapohy and Quaternary dune sediments: Not all bounding surfaces are the same. Aeolian Research 11, 55-60.

Marker, M.E., Müller, D., 1978. Relict vlei silts of the Kuiseb River valley, South West Africa. Madoqua 11, 151-162.

Mendez, M.J., Funk, R., Buschiazzo, D.E, 2011. Field wind erosion measurements with Big Spring Number Eight (BSNE) and Modified Wilson and Cook (MWAC) samplers. Geomorphology 129, 43-48.

Morin, E., Grodek, T., Dahan, O., Benito, G., Kulls, C., Jacoby, Y., Van Langenhove, G., Seely, M., Enzel, Y., 2009. Flood routing and alluvial aquifer recharge along the ephemeral arid Kuiseb River, Namibia. Journal of Hydrology 368, 262-275.

Murray, A.S.,Roberts, R.G., 1997. Determining the burial time of single grains of quartz using optically stimulated luminescence. Earth and Planetary Science Letters 152, 163-180.

Murray, A.S., Wintle, A.G., 2000. Luminescence dating of quartz using an improved singlealiquot regenerative-dose protocol. Radiation Measurements 32, 57-72.

Olley, J., Caitcheon, G., Murray, A.S., 1998. The distribution of apparent dose as determined by optically stimulated luminescence in small aliquots of fluvial quartz: implications for dating young sediments. Quaternary Science Reviews 17, 1033–1040.

Prescott, J.R., Hutton, J.T., 1994. Cosmic ray contributions to dose rates for luminescence and ESR dating: large depths and long-term time variations. Radiation Measurements 3, 497–500.

Prospero, J.M., Ginoux, P., Torres, S., Nicholson, S., Gill, T., 2002. Environmental characterization of global sources of atmospheric soil dust identified with the Nimbus 7 Total Ozone Mapping Spectrometer (TOMS) absorbing aerosol product. Reviews of Geophysics 40, 1-31

Rice, M.A., Willetts, B.B., McEwan, I.K. 1996. Observations of collisions of saltating grains with a granular bed from high-speed cine-film. *Sedimentology* 43, 21-31.

Rodnight, H., Duller, G.A.T., Wintle, A.G., Tooth, S., 2006. Assessing the reproducibility and accuracy of optical dating of fluvial deposits. Quaternary Geochronology 1, 109-120.

Srivastava, P., Brook, G.A., Marais, E., 2004. A Record of fluvial aggradation in the Northern Namib Desert during the Late Quaternary. Zeitschrift fur Geomorphologie, Supplementband 133, 1-18.

Srivastava, P., Brooke, G.A., Marais, E., 2005. Depositional environment and luminescence chronology of the Hoarusib River Clay Castles sediments, northern Namib Desert, Namibia. Catena 59, 187-204.

Srivastava, P., Brook, G.A., Marais, E., Morthekai, P., Singhvi, A.K., 2006. Depositional environment and OSL chronology of the Homeb silt deposits, Kuiseb River, Namibia. Quaternary Research 65, 478-491.

Stone, A.E.C., Thomas, D.S.G. 2013. Casting new light on late Quaternaryenvironmental and palaeohydrological change in the Namib Desert: A review of the application of optically stimulated luminescence in the region. Journal of Arid Environments 93, 40-58.

Stone, A.E.C., Thomas, D.S.G., Viles, H.A., 2010. Late Quaternary palaeohydrological changes in the northern Namib Sand Sea: new chronologies using OSL dating of interdigitated aeolian and water-lain interdune deposits. Palaeogeography, Palaeoclimatology, Palaeoecology 288, 35-53.

Stuut, J.W., Prins, M.A., Schneider, R.R., Weltje, G.J., Fred Jansen, J.H., Postma, G.,2002. A 300-kyr record of aridity and wind strength in southwestern Africa: inferences from grain-size distributions of sediments on Walvis Ridge, SE Atlantic. Marine Geology 180, 221-233.

Stuut, J.B.W., Crosta, X., Schneider, R., van der Borg, K., 2004. Relationship between Antarctic sea ice and southwest African climate during the late Quaternary. Geology 32, 909-912.

Vickery, K.J., 2010. *Southern African dust sources as identified by multiple space borne sensors.* MSc edn. Department of Environmental and Geographical Science: University of Cape Town.

Vickery, K.J. and Eckardt, F.D. 2013. Dust emission controls on the lower Kuiseb River valley, Central Namib. Aeolian Research 10, 125-133.

Wiggs, G.F.S., O'Hara, S.L., Wegerdt, J., van der Meer, J., Small, I., Hubbard, R., 2003. The dynamics and characteristics of aeolian dust in dryland Central Asia: possible impacts on human exposure and repertory health. Geographical Journal 169, 142-157.

Wintle, A.G., Murray, A.S., 2006. A review of quartz optically stimulated luminescence characteristics and their relevance in single-aliquot regeneration dating protocols. Radiation Measurements, 41, 369-391.

Zobeck, T.M., Sterk, G., Funk, R., Rajot, J.L., Stout, J.E., Van Pelt, R.S. 2003. Measurement and data analysis methods for field-scale wind erosion studies and model validation. *Earth Surface Processes and Landforms*, 28, 1163-1188

.

Table **1.** Dry analysis particle size data (% contribution) for valley samples

	% Very Coarse - Medium Coarse Sand (2mm - 250 µm)	% Fine Sand (125 - 250µm)	% Very Fine Sand (63 - 125µm)	% Very Coarse - Coarse Silt (63µm - 16mm)	% Medium- Fine Silt (16µm - 4µm)	%Very Fine Silt (4µm - 2µm)	% Clay (<2µm)	%Total silt + very fine sand
H2 Transect Samples								
Fill Surface	36.52	30.45	22.20	7.22	3.29	0.32	0.00	**33.03**
Fill (-10cm)	28.52	41.20	21.01	6.61	2.66	0.10	0.00	**30.38**
Inner channel terrace	37.30	48.11	13.16	1.03	0.40	0.00	0.00	**14.59**
Channel floor	86.04	12.70	1.08	0.18	0.00	0.00	0.00	**1.26**
Dated valley fill samples								
Huab13/1/1	35.19	43.60	14.90	5.46	0.86	0.00	0.00	**21.22**
Huab13/1/2	25.85	21.95	23.40	13.90	12.58	3.88	2.32	**53.76**
Huab13/1/3	38.21	53.87	7.91	0.00	0.00	0.00	0.00	**7.91**
Huab13/1/4	56.84	38.42	4.75	0.00	0.00	0.00	0.00	**4.75**
Huab13/1/5	60.63	35.68	3.69	0.00	0.00	0.00	0.00	**3.69**
Huab13/1/6	97.61	2.39	0.00	0.00	0.00	0.00	0.00	**0.00**
Huab13/2/1	26.24	52.52	18.98	2.07	0.19	0.00	0.00	**21.24**
Huab13/2/2	75.52	22.93	1.55	0.00	0.00	0.00	0.00	**1.55**
Huab13/2/3	43.67	48.63	7.70	0.00	0.00	0.00	0.00	**7.70**

Table 2. Dry analysis Particle size data (% contribution) for BSNE samples

Sample collection date	**BSNE**	% Very Coarse - Medium Coarse Sand (2mm - 250 µm)	% Fine Sand (125 - 250µm)	% Very Fine Sand (63 - 125µm)	% Very Coarse - Coarse Silt (63µm - 16mm)	% Medium-Fine Silt (16µm - 4µm)	%Very Fine Silt (4µm - 2µm)	% Clay (<2µm)	%Total silt + very fine sand
29/05/13	1	42.51	24.45	24.25	6.61	2.18	0.00	0.00	**33.04**
	2	12.05	27.75	41.98	14.08	3.58	0.57	0.56	**60.21**
	3	1.05	25.76	47.54	20.47	4.54	0.70	0.64	**73.25**
	4	2.79	23.25	46.34	22.31	4.69	0.71	0.62	**74.05**
07/07/13	1	31.36	33.36	27.31	5.81	2.16	0.07	0.00	**35.35**
	2	13.22	33.81	38.34	11.19	3.43	0.44	0.00	**53.40**
	3	2.17	26.16	46.48	20.08	4.50	0.71	0.62	**71.77**
	4	0.04	23.53	48.07	22.91	4.81	0.73	0.64	**76.52**
01/08/13	1	43.60	25.24	23.49	5.98	1.70	0.00	0.00	**31.17**
	2	12.07	28.57	41.86	14.10	2.90	0.45	0.50	**59.31**
	3	2.48	26.23	47.45	19.65	3.60	0.55	0.59	**71.25**
	4	0.91	23.81	48.03	22.90	3.77	0.55	0.59	**75.25**
Collection means	1	39.15	27.68	25.02	6.13	2.01	0.02	0.00	**33.18**
	2	12.45	30.04	40.73	13.13	3.31	0.49	0.35	**57.66**
	3	1.90	26.05	47.16	20.06	4.22	0.66	0.61	**72.10**
	4	1.25	23.53	47.48	22.71	4.42	0.66	0.62	**75.27**

Table 3. Wet analysis (disaggregated) particle size data (% contribution) for selected samples

		% Very Coarse - Medium Coarse Sand (2mm - 250 µm)	% Fine Sand (125 - 250µm)	% Very Fine Sand (63 - 125µm)	% Very Coarse - Coarse Silt (63µm - 16mm)	% Medium-Fine Silt (16µm - 4µm)	%Very Fine Silt (4µm - 2µm)	% Clay (<2µm)	%Total silt + very fine sand
H2 Transect Samples									
Fill Surface		3.14	9.42	11.69	24.82	33.58	9.65	7.69	**79.74**
Fill (-10 cm)		1.92	6.73	10.41	22.49	37.37	11.97	9.10	**82.24**
Inner channel terrace		9.48	20.68	19.45	27.02	14.98	4.18	4.20	**65.63**
Channel floor		46.95	19.81	4.08	8.27	13.65	3.94	3.31	**29.94**
Dated valley fill samples									
Huab13/1/1		29.87	38.20	16.85	8.78	3.95	1.24	1.11	**30.82**
Huab13/1/4		43.74	36.12	9.06	3.66	4.20	1.66	1.56	**18.58**
Huab13/1/6		90.77	3.00	0.53	1.32	2.05	1.03	1.31	**5.93**
Dust									
BSNE collection means	1	7.01	17.91	30.80	20.55	12.90	5.16	5.67	**69.46**
	2	2.07	12.27	36.19	28.94	11.39	4.18	4.95	**80.70**
	3	0.00	7.69	35.71	36.50	11.58	3.81	4.71	**87.60**
	4	0.00	6.98	34.99	38.39	11.38	3.68	4.58	**88.44**

Table 4. OSL age data. Equivalent doses, dose rates, and ages are shown to two decimal places. All calculations were made prior to rounding

Sample (Huab)	Depth (m)	Grain size (μm)	n[a]	σ_d (%)[b]	D_e (Gy)[c]	Beta dose rate (Gy.ka^{-1})	Gamma dose rate (Gy.ka^{-1})	Cosmic dose rate (Gy.ka^{-1})	Environmental dose rate (Gy.ka^{-1})	Age (ka)
13/1/1	0.3	180-210	40 (23)	55 ± 7	2.23 ± 0.16	1.81 ± 0.14	1.03 ± 0.07	0.19 ± 0.02	3.04 ± 0.16	**0.73 ± 0.07**
13/1/2	0.7	125-150	40 (33)	37 ± 3	1.86 ± 0.07	1.84 ± 0.17	1.06 ± 0.12	0.18 ± 0.02	3.08 ± 0.22	**0.60 ± 0.03**
13/1/3	1.5	180-210	40 (23)	51 ± 6	6.18 ± 0.45	1.79 ± 0.14	1.05 ± 0.08	0.17 ± 0.02	3.01 ± 0.16	**2.05 ± 0.18**
13/1/4	2.0	180-210	24 (21)	47 ± 6	8.53 ± 0.79	1.63 ± 0.13	0.86 ± 0.06	0.15 ± 0.02	2.64 ± 0.15	**3.24 ± 0.35**
13/1/5	2.8	180-210	24 (24)	44 ± 5	10.28 ± 0.50	1.42 ± 0.11	0.77 ± 0.05	0.14 ± 0.01	2.33 ± 0.13	**4.41 ± 0.32**
13/1/6	3.6	180-210	24 (19)	14 ± 2	23.68 ± 1.14	1.50 ± 0.12	0.79 ± 0.06	0.12 ± 0.01	2.42 ± 0.14	**9.79 ± 0.73**
13/2/1	0.3	180-210	44 (38)	73 ± 7	2.80 ± 0.14	2.54 ± 0.19	1.81 ± 0.15	0.19 ± 0.02	4.54 ± 0.24	**0.62 ± 0.04**
13/2/2	0.5	180-210	48 (33)	98 ± 1	1.49 ± 0.10	1.37 ± 0.12	0.67 ± 0.05	0.19 ± 0.02	2.23 ± 0.13	**0.67 ± 0.06**
13/2/3	1.0	180-210	38 (34)	97 ± 1	3.82 ± 0.16	1.70 ± 0.14	0.87 ± 0.06	0.18 ± 0.02	2.74 ± 0.16	**1.39 ± 0.10**

[a] The number of measured aliquots is shown, with the number of aliquots passing all rejection criteria and used in age calculation shown in parentheses.

[b] σ_d refers to the overdispersion parameter of Galbraith et al., (1999) used to assess the dose distributions.

[c] The finite mixture model was used for D_e determination for all samples , except HUAB-13-1-6 where the central age model was applied.

Appendix 2 – Windblown dust BSNE samples

Monitoring Station	Collection Date	BSNE	Bag Number	Dry weight of sample (g)	Nutrient Analyses	Grain Size Analyses	
						Wet	Dry
Met-A Huab 1	01/05/13	BSNE 1	SD660	0.3614			
	01/05/13	BSNE 2	SD661	0.1026			
	01/05/13	BSNE 3	SD662	0.0487			
	01/05/13	BSNE 4	SD663	0.0379			
	29/05/13	BSNE 1	SD700	7.9311			
	29/05/13	BSNE 2	SD701	2.1274			
	29/05/13	BSNE 3	SD702	0.7342			
	29/05/13	BSNE 4	SD703	0.4564			
	07/07/13	BSNE 1	1004	5.4580			
	07/07/13	BSNE 2	1005	1.4071			
	07/07/13	BSNE 3	1006	0.6022			
	07/07/13	BSNE 4	1007	0.3122			
	03/08/13	BSNE 1	1076	7.7270			
	03/08/13	BSNE 2	1077	1.9785			
	03/08/13	BSNE 3	1078	0.6429			
	03/08/13	BSNE 4	1079	0.4090			
	15/09/13	BSNE 1	HUAB1 BSNE #1	4.6198			
	15/09/13	BSNE 2	HUAB1 BSNE #2	1.1622			
	15/09/13	BSNE 3	HUAB1 BSNE #3	0.3575			
	15/09/13	BSNE 4	HUAB1 BSNE #4	0.1453			
AWS-1 Huab 2	01/05/13	BSNE 1	SD664	48.7631			x
	01/05/13	BSNE 2	SD665	16.4130			x
	01/05/13	BSNE 3	SD666	8.9948			x
	01/05/13	BSNE 4	SD667	5.5467			x
	29/05/13	BSNE 1	SD704	185.3247	x	x	x
	29/05/13	BSNE 2	SD705	63.3005	x	x	x
	29/05/13	BSNE 3	SD706	32.9290	x	x	x
	29/05/13	BSNE 4	SD707	19.1173	x	x	x
	07/07/13	BSNE 1	1000	296.2833	x	x	x
	07/07/13	BSNE 2	1001	97.5365	x	x	x
	07/07/13	BSNE 3	1002	39.4336	x	x	x
	07/07/13	BSNE 4	1003	20.6411	x	x	x
	01/08/13	BSNE 1	1057	589.3460	x	x	x
	01/08/13	BSNE 2	1058	210.4894	x	x	x
	01/08/13	BSNE 3	1059	113.8029	x	x	x

Monitoring Station	Collection Date	BSNE	Bag Number	Dry weight of sample (g)	Nutrient Analyses	Grain Size Analyses	
						Wet	Dry
AWS-1 Huab 2 (cont.)	01/08/13	BSNE 4	1060	71.7454	x	x	x
	18/09/13	BSNE 1	HUAB2 BSNE #1	162.5285			
	18/09/13	BSNE 2	HUAB2 BSNE #2	44.5874			
	18/09/13	BSNE 3	HUAB2 BSNE #3	15.8847			
	18/09/13	BSNE 4	HUAB2 BSNE #4	7.6654			
Met-C Huab 3	31/05/13	BSNE 1	SD716	63.7028			x
	31/05/13	BSNE 2	SD717	19.7360			x
	31/05/13	BSNE 3	SD718	9.4350			x
	31/05/13	BSNE 4	SD719	5.7091			x
	08/07/13	BSNE 1	1008	73.8531			
	08/07/13	BSNE 2	1009	20.9836			
	08/07/13	BSNE 3	1010	9.4450			
	08/07/13	BSNE 4	1011	5.2974			
	01/08/13	BSNE 1	1064	365.5888	x	x	
	01/08/13	BSNE 2	1065	87.4287	x	x	
	01/08/13	BSNE 3	1066	37.7673	x	x	
	01/08/13	BSNE 4	1067	22.0058	x	x	
	15/09/13	BSNE 1	HUAB3 BSNE #1	29.5674			
	15/09/13	BSNE 2	HUAB3 BSNE #2	9.4193			
	15/09/13	BSNE 3	HUAB3 BSNE #3	4.6186			
	15/09/13	BSNE 4	HUAB3 BSNE #4	2.8230			
Met-B Huab 4	01/05/13	BSNE 1	SD668	28.1475			x
	01/05/13	BSNE 2	SD669	7.6344			x
	01/05/13	BSNE 3	SD670	2.7765			x
	01/05/13	BSNE 4	SD671	1.6348			x
	30/05/13	BSNE 1	SD708	189.2852			x
	30/05/13	BSNE 2	SD709	28.6884			x
	30/05/13	BSNE 3	SD710	5.8783			x
	30/05/13	BSNE 4	SD711	2.3825			x
	08/07/13	BSNE 1	1012	195.3559			
	08/07/13	BSNE 2	1013	36.1760			
	08/07/13	BSNE 3	1014	10.7254			
	08/07/13	BSNE 4	1015	5.6129			
	02/08/13	BSNE 1	1072	274.0779			
	02/08/13	BSNE 2	1073	51.5919			
	02/08/13	BSNE 3	1074	16.4869			
	02/08/13	BSNE 4	1075	9.9148			
	17/09/13	BSNE 1	HUAB4 BSNE #1	113.9922			

Monitoring Station	Collection Date	BSNE	Bag Number	Dry weight of sample (g)	Nutrient Analyses	Grain Size Analyses	
						Wet	Dry
Met-B Huab 4 (cont.)	17/09/13	BSNE 2	HUAB4 BSNE #2	23.0117			
	17/09/13	BSNE 3	HUAB4 BSNE #3	5.2863			
	17/09/13	BSNE 4	HUAB4 BSNE #4	3.6355			
Met-G Huab 5	01/05/13	BSNE 1	SD672	7.5731			x
	01/05/13	BSNE 2	SD673	2.0534			x
	01/05/13	BSNE 3	SD674	0.9903			x
	01/05/13	BSNE 4	SD675	0.6251			x
	30/05/13	BSNE 1	SD712	212.6876			x
	30/05/13	BSNE 2	SD713	51.4032			x
	30/05/13	BSNE 3	SD714	25.0516			x
	30/05/13	BSNE 4	SD715	12.4825			x
	09/07/13	BSNE 1	1016	80.4146			
	09/07/13	BSNE 2	1017	23.7276			
	09/07/13	BSNE 3	1018	12.5811			
	09/07/13	BSNE 4	1019	6.1968			
	02/08/13	BSNE 1	1068	224.7356			
	02/08/13	BSNE 2	1069	56.8396			
	02/08/13	BSNE 3	1070	28.1019			
	02/08/13	BSNE 4	1071	11.5892			
	17/09/13	BSNE 1	HUAB5 BSNE #1	48.0571			
	17/09/13	BSNE 2	HUAB5 BSNE #2	15.7089			
	17/09/13	BSNE 3	HUAB5 BSNE #3	8.7930			
	17/09/13	BSNE 4	HUAB5 BSNE #4	4.6746			
Davis-A44 Huab 6	31/05/13	BSNE 1	SD720	340.8800	x	x	x
	31/05/13	BSNE 2	SD721	154.7800	x	x	x
	31/05/13	BSNE 3	SD722	85.1024	x	x	x
	31/05/13	BSNE 4	SD723	46.7694	x	x	x
	09/07/13	BSNE 1	1020	347.3591			
	09/07/13	BSNE 2	1021	13.1722			
	09/07/13	BSNE 3	1022	1.8102			
	09/07/13	BSNE 4	1023	0.9920			
	03/08/13	BSNE 1	1080	680.1438	x	x	x
	03/08/13	BSNE 2	1081	64.4059	x	x	x
	03/08/13	BSNE 3	1082	30.3113	x	x	x
	03/08/13	BSNE 4	1083	16.9855	x	x	x
Huab 6	19/09/13	BSNE 1	HUAB 6 BSNE#1	19.2300			
	19/09/13	BSNE 2	HUAB 6 BSNE#2	2.2994			
	19/09/13	BSNE 3	HUAB 6 BSNE#3	0.9725			

Monitoring Station	Collection Date	BSNE	Bag Number	Dry weight of sample (g)	Nutrient Analyses	Grain Size Analyses	
						Wet	Dry
(cont.)	19/09/13	BSNE 4	HUAB 6 BSNE#4	0.3977			
AWS-2 Kuiseb 1	02/05/13	BSNE 1	SD676	0.1336			
	02/05/13	BSNE 2	SD677	0.0818			
	02/05/13	BSNE 3	SD678	0.0559			
	02/05/13	BSNE 4	SD679	0.0432			
	24/05/13	BSNE 1	SD658	7.1792			x
	24/05/13	BSNE 2	SD659	4.5283			x
	24/05/13	BSNE 3	SD689	3.2969			x
	24/05/13	BSNE 4	SD690	2.4100			x
	13/07/13	BSNE 1	1024	4.8887			
	13/07/13	BSNE 2	1025	2.4676			
	13/07/13	BSNE 3	1026	1.4727			
	13/07/13	BSNE 4	1027	0.7518			
	07/08/13	BSNE 1	1084	2.3637			
	07/08/13	BSNE 2	1085	1.5013			
	07/08/13	BSNE 3	1086	1.0653			
	07/08/13	BSNE 4	1087	0.7795			
	23/09/13	BSNE 1	1135	0.6050			
	23/09/13	BSNE 2	1136	0.4486			
	23/09/13	BSNE 3	1137	0.3858			
	23/09/13	BSNE 4	1138	0.3408			
AWS-3 Tsauchab 1	04/05/13	BSNE 1	SD685	92.1842			x
	04/05/13	BSNE 2	SD686	17.4413			x
	04/05/13	BSNE 3	SD687	7.3301			x
	04/05/13	BSNE 4	SD688	3.8822			x
	26/05/13	BSNE 1	SD695	51.6376			x
	26/05/13	BSNE 2	SD696	10.8663			x
	26/05/13	BSNE 3	SD697	4.6066			x
	26/05/13	BSNE 4	SD698	2.5810			x
	16/07/13	BSNE 1	1036	85.5443			
	16/07/13	BSNE 2	1037	18.3314			
	16/07/13	BSNE 3	1038	8.4669			
	16/07/13	BSNE 4	1039	4.9230			
	27/07/13	BSNE 1	1045	34.9565			
	27/07/13	BSNE 2	1046	6.8795			
	27/07/13	BSNE 3	1047	3.3240			
	27/07/13	BSNE 4	1048	1.8260			
	08/08/13	BSNE 1	1188	217.8877			

Monitoring Station	Collection Date	BSNE	Bag Number	Dry weight of sample (g)	Nutrient Analyses	Grain Size Analyses	
						Wet	Dry
AWS-3 Tsauchab 1 (cont.)	08/08/13	BSNE 2	1189	42.5341			
	08/08/13	BSNE 3	1190	18.1879			
	08/08/13	BSNE 4	1191	10.2650			
	24/09/13	BSNE 1	1150	36.0989			
	24/09/13	BSNE 2	1151	9.0177			
	24/09/13	BSNE 3	1152	4.2308			
	24/09/13	BSNE 4	1153	2.3088			
Met-F Tsauchab 2	04/05/13	BSNE 1	SD681	16.5707			x
	04/05/13	BSNE 2	SD682	6.6546			x
	04/05/13	BSNE 3	SD683	3.7035			x
	04/05/13	BSNE 4	SD684	1.9447			x
	26/05/13	BSNE 1,2,3,4	SD699	107.4858	x	x	x
	16/07/13	BSNE 1	1032	99.2272			
	16/07/13	BSNE 2	1033	32.2773			
	16/07/13	BSNE 3	1034	15.4838			
	16/07/13	BSNE 4	1035	7.2773			
	27/07/13	BSNE 1	1049	24.6539			
	27/07/13	BSNE 2	1050	8.4689			
	27/07/13	BSNE 3	1051	3.8747			
	27/07/13	BSNE 4	1052	1.8014			
	08/08/13	BSNE 1	1088	101.0221			
	08/08/13	BSNE 2	1089	34.5367			
	08/08/13	BSNE 3	1185	16.0708			
	08/08/13	BSNE 4	1186	7.4993			
	24/09/13	BSNE 1	1139	14.9124			
	24/09/13	BSNE 2	1140	5.1278			
	24/09/13	BSNE 3	1141	2.7239			
	24/09/13	BSNE 4	1142	1.2924			
Met-E Tsauchab 3	03/05/13	BSNE 1,2,3,4	SD680	0.0378			
	26/05/13	BSNE 1	SD691	0.8009			
	26/05/13	BSNE 2	SD692	0.5427			
	26/05/13	BSNE 3	SD693	0.4214			
	26/05/13	BSNE 4	SD694	0.3627			
	15/07/13	BSNE 1	1028	1.5255			
	15/07/13	BSNE 2	1029	1.0513			
	15/07/13	BSNE 3	1030	0.8348			
	15/07/13	BSNE 4	1031	0.6253			
	28/07/13	BSNE 1	1053	0.2154			

Monitoring Station	Collection Date	BSNE	Bag Number	Dry weight of sample (g)	Nutrient Analyses	Grain Size Analyses	
						Wet	Dry
Met-E Tsauchab 3 (cont.)	28/07/13	BSNE 2	1054	0.1714			
	28/07/13	BSNE 3	1055	0.1779			
	28/07/13	BSNE 4	1056	0.1305			
	09/08/13	BSNE 1	1187	1.5306			
	09/08/13	BSNE 2	1192	1.0522			
	09/08/13	BSNE 3	1193	0.9308			
	09/08/13	BSNE 4	1194	0.7511			
	25/09/13	BSNE 1	1154	0.1089			
	25/09/13	BSNE 2	1155	0.0937			
	25/09/13	BSNE 3	1156	0.0063			
	25/09/13	BSNE 4	1157	0.0357			

Appendix 3 – Laboratory analyses of surface sediments and BSNE samples (raw data, laboratory repeats highlighted)

	Sample ID	Lab #	pH	Mehlich P (ppm)	Fe (ppm)	NH_4^+ (ppm)	$N0_3^-$ (ppm)	Total N (ppm)	Total P (ppm)
Tsauchab Cross-section Samples	LSS1	32	9.2	9.2	3.6	1.9	1.0	148	226
	LSS2	33	7.8	55.6	17.0	17.1	17.1	1803	722
	LSS3	34	8.0	31.1		1.9	10.7	722	408
	LSS3	35	8.3	27.5	2.4	1.3	9.4	381	265
	LSS4	36	7.9	65.0	23.3	12.5	8.1	1492	542
	LSS5	37	8.5	9.7	3.4	13.1	12.6	239	217
	LSS6	38	7.8	39.7	18.3	23.9	13.9	2039	604
	LSS7	39	8.5	49.6	7.9	4.1	2.3	1093	558
	LSS8	40	8.3	10.0	3.1	2.9	6.9	164	401
	LSS9	41	8.7	26.5	2.0	1.7	1.7	228	403
	LSS10	42	8.1	51.2	9.5	8.1	4.7	1256	644
	LSS11	43	8.6	10.0	3.3	3.9	2.3	144	381
	AWS3.01	44	8.5	2.8	5.0	6.2	3.0	188	263
	AWS3.02	45	8.3	4.2	4.2	6.7	5.9	183	264
	AWS3.03	46	8.1	3.9	3.1	7.1	4.3	189	235
	AWS3.04	47	7.8	54.5	20.7	14.2	8.5	1604	472
	AWS3.05	48	8.6	61.3	37.3	14.8	6.1	2215	574
	AWS3.06	49	8.2	6.6	2.8	10.6	5.8	228	204
	AWS3.07	50	8.7	3.1	3.2	7.4	8.4	238	196
	AWS3.08	51	8.7	2.3	3.8	7.1	2.7	161	202
	AWS3.09	52	9.1	3.1	2.8	3.8	0.6	79	112
	AWS3.10	53	8.1	2.1	2.0	3.5	0.9	75	152
	MetF.1	1	8.43	72.1	12.7	13.0	6.6	1552	576
	MetF.1	2	8.30	65.2	10.3	14.5	6.9	1314	513
	MetF.2	3	8.35	5.3	3.8	6.0	6.9	294	223
	MetF.3	4	7.80	99.8	14.9	5.8	189.3	2056	853
	MetF.4	5	8.49	8.2	3.4	5.4	4.1	261	190
	MetF.5	6	8.24	38.6	13.8	19.2	2.4	1130	541
	MetF.5	7	8.30	21.1	5.5	9.4	2.5	499	308
Huab Cross-section Samples	AWS1.1	98	8.2	80.0	11.1	6.6	8.4	730	906
	AWS1.2	99	8.6	63.6		5.3	3.9	501	785
	AWS1.2	100	8.4	48.2	4.9	3.1	3.7	218	562
	AWS1.3	101	8.2	89.1	8.1	12.3	84.0	846	917
	AWS1.4	102	8.0	39.6	2.2	2.2	57.2	223	448
	AWS1.5	103	8.7	71.9	19.1	4.5	41.1	967	681
	AWS1.6	104	8.9	39.6	4.2	2.3	7.0	171	433

	Sample ID	Lab #	pH	Mehlich P (ppm)	Fe (ppm)	NH_4^+ (ppm)	$N0_3^-$ (ppm)	Total N (ppm)	Total P (ppm)
Huab Cross-section Samples (cont.)	AWS1.7	105	9.1	29.2	3.7	0.6	1.2	65	523
	AWS1.8	106	7.8	76.9	18.8	11.7	27.5	1169	918
	AWS1.9	107	8.9	19.8	3.8	1.4	3.2	69	324
	AWS1.9	108	8.6	23.8	3.5	0.9	3.0	49	315
	AWS1.10	109	9.0	23.0	3.6	0.9	2.6	43	266
	METG.1	110	7.9	46.4	13.0	1.3	8.2	268	586
	METG.2	111	7.8	58.0	18.4	2.8	16.8	666	759
	METG.3	112	7.6	21.7	4.5	1.4	8.0	105	347
	METG.4	113	7.5	44.4	3.2	0.7	20.9	115	509
	METG.5	114	7.5	43.7	3.3	0.3	56.2	128	579
	UH1	115	8.8	13.8	3.5	0.4	1.9	87	324
	UH2	116	8.9	13.1	3.4	0.6	3.1	91	338
	UH3	117	8.9	36.1	3.8	1.2	0.9	222	481
	UH4	118	9.4	36.0	3.5	0.5	1.0	158	433
	UH5	119	8.9	40.0	2.6	0.3	1.9	118	342
	UH6	120	9.3	43.1	2.8	0.4	0.8	130	427
	UH7	121	9.2	39.5	3.1	0.5	0.8	134	450
	UH08	122	9.3	41.2	2.2	0.5	1.9	152	441
	UH09	123	9.3	41.5	3.2	0.5	0.6	147	433
	UH10	124	9.2	34.7	2.0	0.3	1.4	172	465
	HB1	125	8.5	17.1	7.6	0.7	9.3	145	381
	HB2	126	8.2	24.2	4.5	0.8	2.2	131	384
	HB3	127	8.4	47.5	5.5	0.6	3.4	172	523
	HB4	128	8.2	79.4	17.7	0.9	17.1	251	619
	HB5	129	8.5	30.8	13.9	1.1	133.4	314	476
	HB5	130	8.6	42.9	9.8	0.5	81.4	212	534
	HB6	131	8.5	47.2	9.4	0.6	41.0	205	534
	HC1	132	7.4	86.0	7.5	7.4	159.4	1009	632
	HC2	133	7.4	89.3	10.8	6.0	88.8	1336	697
	HC3	134	7.9	91.0	7.6	6.5	63.3	993	732
	HC3	135	7.6	94.5	10.9	5.8	254.0	1362	685
	HC.4	29	8.07	75.8	11.4	5.9	101.1	786	720
	HC.4	30	8.09	77.4	11.4	4.8	98.6	782	729
	HC.5	31	7.93	90.9	9.9	7.2	136.7	1168	736
Upper Catchment Samples	TUW001	1	7.4	83.0	14.0	22.4	5.2	1068	525
	TUW001	2	7.8	72.8	11.6	10.7	5.7	766	532
	TUW002	3	6.6	17.9	6.9	2.6	1.8	603	405
	TUW007	4	6.4	28.1	7.0	19.4	4.1	511	250
	TUT008	5	6.4	5.4	6.8	4.1	4.7	621	285
	TUW009	6	6.9	18.9	4.5	2.3	1.0	541	292
	TUT010	7	7.2	3.8	5.1	1.5	1.4	530	417

	Sample ID	Lab #	pH	Mehlich P (ppm)	Fe (ppm)	NH_4^+ (ppm)	$N0_3^-$ (ppm)	Total N (ppm)	Total P (ppm)
Upper Catchment Samples (cont.)	TUT011	8	7.4	10.8	9.5	4.2	3.5	465	250
	TUW012	9	7.0	29.3	4.7	7.0	1.8	659	396
	ZR016	10	7.9	21.3	12.8	31.8	4.5	1217	362
	TRT020	11	7.7	10.9	3.5	1.8	7.5	409	314
	TR025	12	8.1	7.2	9.0	17.2	6.0	492	317
	TR026	13	8.3	18.1	37.0	20.1	4.0	1185	381
	TR026	14	8.0	8.5	32.3	23.4	4.8	948	370
	TUW027	15	8.4	31.9	2.5	4.5	0.9	432	240
	TR028	16	8.1	3.2	5.6	3.0	2.2	342	299
	TR030	17	8.7	2.9	3.2	1.4	9.1	259	364
	TUW032	18	7.6	30.6	3.0	6.2	6.3	709	326
	TUT033	19	8.5	11.7	3.5	2.1	2.7	300	283
	TUT035	20	7.6	20.8	3.7	7.5	9.4	686	282
	TUW036	21	7.7	64.9	3.5	3.0	2.3	413	323
	TUT037	22	8.3	2.0	1.7	6.6	3.6	441	197
	TUW038	23	7.9	35.0	3.6	4.7	2.0	622	286
	TUT039	24	8.4	13.6	2.9	1.8	4.9	417	236
	TUT040	25	7.8	2.3	7.4	12.7	8.3	859	300
	TUT040	26	8.0	6.4	5.4	11.8	11.6	947	293
	TR041	27	8.1	2.1	6.7	11.9	5.1	572	315
	TR042	28	7.9	2.2	40.1	17.4	24.7	1670	314
	TR042	29	7.6	3.6	28.5	14.0	18.2	1193	317
	TR044	30	8.0	31.0	20.4	12.6	8.5	1828	505
	TR044	31	7.7	13.9	10.2	8.0	6.7	871	387
	AHUW03	54	8.2	16.5	1.7	3.9	1.4	260	395
	AHUW014	55	7.5	36.3	2.5	3.5	4.2	268	177
	HR015	56	7.2	49.7	6.7	8.3	132.8	1543	511
	HR015	57	7.3	58.6	15.9	5.2	88.3	795	363
	HR016	58		92.8		7.8	142.8	1889	444
	HR016	59	7.5	98.9	4.2	4.5	70.9	773	405
	HR017	60	7.7	98.2	3.9	3.9	6.9	616	739
	HR018	61	8.3	26.6	3.4	7.0	3.0	125	283
	HR019	62		57.4	11.6	12.2	16.0	1012	391
	HR019	63	7.9	33.0	7.5	6.6	5.4	475	311
	HR031	64		40.7	7.7	6.3	4.0	673	314
	HR031	65	7.8	30.9	7.4	7.1	5.9	605	334
	HRT032	66	7.8	13.6	2.8	3.2	2.8	98	110
	HR033	67	8.0	13.9	2.4	0.9	3.4	101	137
	HR034	68	8.1	26.3	3.4	1.4	5.7	162	144
	HR035	69	7.9	74.9	31.2	4.7	37.1	1013	496
	HR036	70	8.2	6.9	1.9	0.6	2.5	97	90

	Sample ID	Lab #	pH	Mehlich P (ppm)	Fe (ppm)	NH_4^+ (ppm)	$N0_3^-$ (ppm)	Total N (ppm)	Total P (ppm)
Upper Catchment Samples (cont.)	HUW040	71	7.6	28.0	3.5	3.9	6.2	536	134
	HUT046	72	7.7	32.4	4.9	3.2	17.1	806	419
	HUW047	73	7.2	51.1	6.8	15.8	8.9	1370	377
	HUW051	74	7.9	9.2	2.3	3.9	8.6	1626	223
	HUW052	75	7.6	52.5	3.9	10.1	11.6	1567	622
	HUW053	76	8.0	97.0	4.0	2.8	6.2	1116	379
	HUW055	77	7.3	79.5	41.4	12.9	39.4	3561	580
	HUT057	78	7.7	36.6	7.4	9.6	16.5	1180	521
	HUT057	79	7.8	31.8	5.9	12.1	11.1	776	498
	HUW058	80	7.7	42.6	27.8	27.5	20.1	2156	779
	HUW058	81	7.8	66.9	25.3	29.7	25.2	2027	658
	HUT059	82	8.2	27.6	2.6	4.4	7.0	215	174
	HUW060	83	8.2	44.7	3.1	6.6	10.4	210	203
	HR064	84	7.8	52.5	16.8	14.2	36.0	631	557
	HR065	85	8.6	23.9	5.2	7.9	3.7	189	443
	HR066	86	8.4	23.5	3.6	5.8	4.4	90	284
	HR067	87	7.8	54.2	48.4	46.9	5.2	1693	769
	HR067	88	7.7	54.0	48.0	32.6	4.6	1181	653
	AH075	89	8.1	17.4	2.2	1.7	2.0	106	246
	AH076	90	7.7	107	27.4	47.1	6.0	2846	796
	AH076	91	7.5	74.9	26.1	25.5	5.5	1930	606
	HR077	92	8.4	26.4	4.4	5.1	2.6	131	280
	HR078	93	7.8	75.9	30.5	20.0	24.5	1554	808
	HR078	94	8.0	62.4	28.8	12.8	16.5	1047	726
	HR079	95	8.1	36.2	9.1	4.6	5.9	301	475
	HUW040.2 (duplicate)	96	8.0	23.9	3.3	2.3	4.1	413	182
	HUW060.2 (duplicate)	97	8.0	35.4	2.7	1.5	4.0	163	180
	HUW049	9	7.92	23.6	6.0	8.1	4.2	787	177
	HUW044	10	7.94	94.1	7.2	4.3	8.3	1019	553
	HUW045	11	7.71	30.8	4.7	5.8	6.0	753	260
	AHUW063	12	8.19	69.7	2.9	8.0	1.7	392	414
	HUW090	13	7.32	72.3	5.6	6.9	3.4	622	770
	HUW089	14	7.15	58.3	7.5	5.5	2.4	545	456
	HR094	15	8.47	43.4	5.0	2.1	44.5	164	466
	HR093	16	8.15	45.1	1.3	2.7	138.8	255	356
	HR080	17	8.17	66.7	54.7	37.4	12.5	1653	768
	KUW001	136	6.4	25.2	17.0	6.5	5.2	1095	403
	KUT002	137	8.0	13.2	5.6	2.1	3.3	425	239
	KUW009	138		31.9	9.5	6.5	4.4	1033	286
	KUW009	139	6.6	30.9	8.2	10.2	9.9	1608	283

	Sample ID	Lab #	pH	Mehlich P (ppm)	Fe (ppm)	NH_4^+ (ppm)	$N0_3^-$ (ppm)	Total N (ppm)	Total P (ppm)
Upper Catchment Samples (cont.)	KUW011	140	5.8	17.3	18.0	6.8	1.9	900	582
	KUT014	141	8.0	12.6	7.6	4.1	1.8	673	493
	KR015	142	8.6	9.7	6.0	2.1	3.0	261	368
	KR016	143	8.4	11.0	5.0	3.2	2.3	283	286
	KUW017	144	7.0	13.0	6.1	9.5	3.4	489	440
	KUT018	145	7.8	10.8	4.0	4.5	1.5	254	490
	KUW019	146	6.3	40.3	11.2	5.5	1.6	755	670
	KUW020	147	6.7	37.4	6.3	3.3	2.1	661	578
	KUW021	148	6.2	69.9	13.6	10.8	5.3	901	717
	KUT024	149	7.9	32.5	9.3	4.5	16.7	360	525
	KUT026	150	8.8	12.4	1.5	1.6	2.2	81	216
	KUT027	151	8.0	56.8	4.5	7.7	7.6	447	674
	KUW030	152	8.1	71.9	2.8	3.6	3.5	466	536
	KUT032	153	8.6	16.0	1.9	2.1	3.8	195	186
	KUT033	154	8.3	26.3	5.1	1.3	7.7	260	483
	KUT036	155	8.0	45.3	17.6	8.0	19.7	672	487
	KUW038	156	8.5	21.1	1.8	1.6	2.6	258	222
	KR040	157	9.5	9.9	4.8	0.5	2.7	141	414
	KR041	158	7.3	121	27.4	12.4	33.8	1881	757
	KT043	159	7.7	42.2	5.6	2.6	13.7	636	521
	KT044	160	7.8	44.8	10.7	2.9	7.6	582	453
	KT045	161	8.6	12.8	3.8	1.2	4.2	158	362
	KT046	162	8.0	20.4	6.2	0.7	1.8	248	541
	KR049	163	9.4	14.1	2.4	0.1	1.4	65	268
	KR050	164		101	56.7	6.1	25.4	1355	869
	KR050	165	8.0	58.3	21.3	9.2	27.2	467	557
	KR051	166	7.3	80.5	56.7	9.6	27.9	2042	787
	KR051	167	7.4	67.2	45.8	6.1	14.5	1462	697
	KR052	168	8.5	10.5	4.2	0.6	1.6	121	297
	KT053	169	8.4	33.0	1.3	0.4	313.2	427	654
	KT054	170	7.8	55.8	2.2	0.4	266.9	325	587
	KR055	171	8.1	82.5	39.3	1.3	62.2	1280	796
	KR055	172	8.3	72.6	27.2	0.8	35.4	750	658
	KUW020.2 (duplicate)	173	6.7	34.2	6.3	2.3	2.4	585	640
	KUT027	174	7.9	58.8	4.8	7.0	8.8	432	770
	KR040.2 (Duplicate)	175	9.5	9.6	4.8	0.6	2.3	145	671
	KT053	176	8.4	33.8	1.3	0.1	320.0	426	639
	KUT056	1	7.73	61.4	10.9	19.7	39.4	1029	799
	KUW057	2	7.82	17.0	1.5	4.9	9.0	166	301
	KUT058	3	8.42	21.4	2.6	1.2	2.9	101	426

	Sample ID	Lab #	pH	Mehlich P (ppm)	Fe (ppm)	NH_4^+ (ppm)	$N0_3^-$ (ppm)	Total N (ppm)	Total P (ppm)
Upper Catchment Samples (cont.)	KRCAN02	177	7.9	76.8	40.8	9.2	13.6	998	780
	KRCAN003	178	8.3	32.8	2.1	1.8	7.7	220	416
	GR001	179	8.4	11.5	7.4	0.8	24.1	170	297
	GR002	180	8.8	11.9	4.0	0.6	7.8	165	328
	GRUW004	181	8.0	47.9	4.2	1.8	1.6	622	535
	GUW006	182	7.4	5.5	4.4	1.4	0.8	270	200
	GUW009	183	7.9	75.8	4.5	2.7	3.7	791	424
	GUT011	184	6.1	66.4	167.2	23.2	60.0	2439	616
	GUT011	185	6.2	76.1	153.7	24.0	42.4	3096	765
	GUT013	186	8.3	9.0	4.7	9.5	3.3	537	255
	GUW014	187	7.1	22.5	6.4	5.2	1.0	410	380
	GUW007	4	7.87	27.1	4.5	7.2	1.8	430	261
	GUW008	5	8.24	33.0	5.7	4.9	1.5	387	272
	GUT010	6	7.68	94.3	18.1	8.5	2.4	880	470
	GUW012	7	7.94	10.4	6.8	2.2	1.2	727	548
	GUT011	8			160.7				
	D19	18	8.94	221	13.3	6.4	57.6	1979	942
	D20	19	8.18	70.1	4.3	8.2	10.5	680	615
	D18	20	7.90	59.8	20.5	5.2	35.3	662	726
	GPC33	21	7.95	6.6	1.7	3.9	79.0	184	448
	RF1-2	22	8.92	101	38.1	5.6	11.2	1774	643
	RF1-3	23	7.74	173	43.6	6.1	78.4	2567	870
	RF1-12	24	8.00	109	15.1	8.6	77.5	1132	687
	RF4-12	25	7.95	57.1	51.9	9.6	16.0	1198	544
	RF4-12	26	7.81	58.3	42.7	8.1	40.9	1243	570
	RAC4-11	27	8.75	8.3	5.2	1.9	1.1	94	278
	RF4-10	28	8.17	29.4	14.9	6.6	3.2	568	420
Etosha Samples	ET01	8	9.89	60.8	1.8	1.4	48.3	1052	230
	ET02	9	9.90	65.5	1.5	1.3	63.8	869	202
	ET03	10	9.06	39.0	0.2	1.1	421.7	563	262
	ET04	11	9.69	5.9	0.3	0.7	242.6	376	256
	ET05	12	9.26	8.3	0.3	1.1	274.8	576	149
	ET06	13	9.93	3.2	1.0	0.9	218.6	606	204
Sua Pan Samples	GW Sua 8	188	8.9	13.8	0.4	0.6	42.2	367	196
	GWSua 25	189	9.0	8.9	0.4	0.5	8.8	585	132
	GWSua 26	190	8.8	11.3	0.4	0.4	13.4	485	154
	GWSua 28	191	9.7	19.8	0.4	0.2	15.6	524	160
BSNE Samples	SD704	14	8.59	44.5	5.9	6.0	11.5	428	555
	SD705	15	8.75	41.3	6.6	8.0	10.4	327	566
	SD706	16	8.82	40.3	10.0	11.9	12.6	368	588
	SD707	17	8.84	40.0	1.4	13.9	12.0	380	615

	Sample ID	Lab #	pH	Mehlich P (ppm)	Fe (ppm)	NH_4^+ (ppm)	$N0_3^-$ (ppm)	Total N (ppm)	Total P (ppm)
BSNE Samples (cont.)	1000	18	8.53	42.4	5.6	5.5	14.5	332	529
	1001	19	8.50	42.6	5.8	5.5	10.5	330	580
	1002	20	8.47	42.9	9.5	7.9	7.2	371	618
	1003	21	8.56	40.1	13.9	10.2	5.4	325	596
	1057	22	8.65	41.5	6.4	5.8	16.2	351	582
	1058	23	8.63	42.7	5.9	4.2	11.8	346	627
	1059	24	8.58	43.9	6.1	4.0	11.2	336	631
	1060	25	8.63	43.1	6.1	4.1	11.5	348	628
	1080	26	7.75	38.8	8.3	2.3	28.8	356	899
	1081	27	7.34	46.3	1.6	10.0	76.6	677	703
	1082	28	7.36	57.3	1.4	24.5	139.6	1032	763
	1083	29	7.50	53.0	1.3	18.3	96.7	967	760
	1064	30	8.98	48.3	6.3	4.2	18.3	349	563
	1065	31	8.90	46.7	8.0	4.3	17.9	335	603
	1066	32	8.87	45.4	6.4	4.3	16.3	327	651
	1067	33	8.93	44.4	10.9	4.7	14.9	341	614
	SD699	34	9.52	9.9	5.5	6.7	22.9	454	297
	SD720	35	6.80	59.6	0.6	26.9	196.0	1044	778
	SD721	36	7.09	57.7	0.6	35.2	177.7	1021	718
	SD722	37	7.25	55.8	1.4	45.2	156.3	920	645
	SD723	38	7.73	59.5	0.7	22.1	183.3	854	693
Laboratory Repeats		QC 32	9.52	7.4	4.1	1.6	1.8	180	260
		6		19.5	4.6	1.9	0.9		
		48		62.9	38.3	14.0	5.8		
		88/94		59.1	29.7	30.2	4.1		
		128		83.5	18.3	0.8	16.7		
		157		10.3	4.6	0.4	2.2		
		177		78.4	42.4	8.7	13.9		260
		QC 5	8.29	32.1	5.3	5.1	1.5	390	720
		QC 17	8.16	69.2	54.5	36.7	13.0	1519	241
		QC 27	8.75	8.3	5.4	1.8	1.0	94	
		QC 13	9.92	3.4	1.2	0.6	216.2	577	206
		QC 35	6.80	60.6	0.5	26.6	194.0	1006	749

Appendix 4 – Surface sediment sample ID, collection location and date (maps provided following table)

River Valley	Sample ID	Latitude	Longitude	Collection Date
Kuiseb	KUW001	-22.598002	16.867734	07/18/2013
Kuiseb	KUT002	-22.606896	16.84014	07/18/2013
Kuiseb	KUW003	-22.608168	16.835514	07/18/2013
Kuiseb	KUW004	-22.611701	16.738587	07/18/2013
Kuiseb	KUT005	-22.605351	16.715784	07/18/2013
Kuiseb	KUT006	-22.604823	16.71594	07/18/2013
Kuiseb	KUW007	-22.631513	16.677275	07/18/2013
Kuiseb	KUW008	-22.678604	16.605548	07/18/2013
Kuiseb	KUW009	-22.709387	16.493391	07/18/2013
Kuiseb	KUW009-DUP	-22.709387	16.493391	07/18/2013
Kuiseb	KUW010	-22.76868	16.484287	07/18/2013
Kuiseb	KUW011	-22.789299	16.501156	07/18/2013
Kuiseb	KR012	-22.805728	16.526683	07/18/2013
Kuiseb	KUW013	-22.927987	16.49521	07/19/2013
Kuiseb	KUT014	-22.932997	16.498885	07/19/2013
Kuiseb	KR015	-23.025357	16.345734	07/19/2013
Kuiseb	KR016	-23.024369	16.345945	07/19/2013
Kuiseb	KUW017	-23.007413	16.307108	07/19/2013
Kuiseb	KUT018	-23.053387	16.147091	07/19/2013
Kuiseb	KUW018	-23.053016	16.14725	07/19/2014
Kuiseb	KUW20	-23.053042	16.146986	07/19/2013
Kuiseb	KUW20-DUP	-23.053042	16.146986	07/19/2013
Kuiseb	KUW021	-23.075618	16.036445	07/19/2013
Kuiseb	KUW022	-23.07736	15.924099	07/19/2013
Kuiseb	KUT023	-23.078502	15.913854	07/19/2013
Kuiseb	KUT024	-23.078541	15.913829	07/19/2013
Kuiseb	KUT025	-23.089404	15.863555	07/19/2013
Kuiseb	KUT026	-23.067579	15.780486	07/19/2013
Kuiseb	KUT027	-23.067682	15.780314	07/19/2013
Kuiseb	KUT028	-23.067223	15.780978	07/19/2013
Kuiseb	KUW029	-23.065613	15.674727	07/19/2013
Kuiseb	KUW030	-23.098935	15.600611	07/19/2013
Kuiseb	KUW031	-23.220913	15.588923	07/19/2013
Kuiseb	KUT031	-23.220551	15.589403	07/19/2013

River Valley	Sample ID	Latitude	Longitude	Collection Date
Kuiseb	KUT033	-23.370389	15.692002	07/20/2013
Kuiseb	KUT034	-23.364324	15.689676	07/20/2013
Kuiseb	KUT035	-23.362704	15.688613	07/20/2013
Kuiseb	KUT036	-23.357927	15.68723	07/20/2013
Kuiseb	KUT037	-23.35427	15.684994	07/20/2013
Kuiseb	KUW038	-23.347798	15.68057	07/20/2013
Kuiseb	KUW039	-23.343659	15.67858	07/20/2013
Kuiseb	KR040	-23.305082	15.772258	07/20/2013
Kuiseb	KR040-DUP	-23.305082	15.772258	07/20/2013
Kuiseb	KR041	-23.305096	15.771807	07/20/2013
Kuiseb	GR001	-23.484111	15.76831	07/20/2013
Kuiseb	GR002	-23.482489	15.765809	07/20/2013
Kuiseb	GR003	-23.482477	15.762725	07/20/2013
Kuiseb	GUW004	-23.653079	16.159765	07/21/2013
Kuiseb	GUT005	-23.653469	16.160701	07/21/2013
Kuiseb	GUW006	-23.622689	16.25932	07/21/2013
Kuiseb	GUW007	-23.624584	16.347589	07/21/2013
Kuiseb	GUW008	-23.572327	16.433887	07/21/2013
Kuiseb	GUW009	-23.507399	16.476606	07/21/2013
Kuiseb	GUT010	-23.391958	16.510813	07/21/2013
Kuiseb	GUT011	-23.307241	16.51102	07/21/2013
Kuiseb	GUT011-DUP	-23.307241	16.51102	07/21/2013
Kuiseb	GUW012	-23.316958	16.476855	07/21/2013
Kuiseb	GUT013	-23.318407	16.44726	07/21/2013
Kuiseb	GUW014	-23.327889	16.348064	07/21/2013
Kuiseb	KT043	-23.253796	16.313976	07/21/2013
Kuiseb	KT044	-23.24763	16.300015	07/21/2013
Kuiseb	KT045	-23.245671	16.229932	07/21/2013
Kuiseb	KT046	-23.245757	16.229676	07/21/2013
Kuiseb	KUT047	-23.318991	16.034742	07/21/2013
Kuiseb	KUW048	-23.357773	15.990681	07/21/2013
Kuiseb	KR049	-23.504561	14.973641	07/24/2013
Kuiseb	KR050	-23.503876	14.974164	07/24/2013
Kuiseb	KR050-DUP	-23.503876	14.974164	07/24/2013
Kuiseb	KR051	-23.503755	14.974179	07/24/2013
Kuiseb	KR052	-23.503371	14.974396	07/24/2013
Kuiseb	KT053	-23.443505	14.959238	07/24/2013
Kuiseb	KT054	-23.442744	14.95898	07/24/2013
Kuiseb	KR055	-23.362512	14.891435	07/24/2013
Kuiseb	KUT056	GPS point 145		01/09/2013

River Valley	Sample ID	Latitude	Longitude	Collection Date
Kuiseb	KUW057	GPS point 144		01/09/2013
Kuiseb	KUT058	GPS point 143		01/09/2013
Kuiseb	KTCAN01	-23.553359	15.584767	08/24/2013
Kuiseb	KRCAN02	-23.551755	15.579386	08/24/2013
Kuiseb	KRCAN003	-23.524763	15.534885	08/24/2013
Huab	AH01	-20.546269	14.401198	08/12/2013
Huab	AH02	-20.546206	14.40118	08/12/2013
Huab	AHUW03	-20.563519	14.402106	08/12/2013
Huab	AHUT04	-20.576464	14.399612	08/12/2013
Huab	AHUT05	-20.467508	14.346205	08/12/2013
Huab	AHUT06	-20.444116	14.349217	08/12/2013
Huab	AHUW07	-20.443664	14.349093	08/12/2013
Huab	AHUT08	-20.434971	14.410401	08/12/2013
Huab	AHUW09	-20.435132	14.410744	08/12/2013
Huab	AHUT10	-20.422907	14.512895	08/12/2013
Huab	AHUT11	-20.422878	14.512925	08/12/2013
Huab	AHUW12	-20.422793	14.513158	08/12/2013
Huab	AHUW13	-20.398823	14.58789	08/12/2013
Huab	AHUW14	-20.33685	14.516836	08/12/2013
Huab	HR015	-20.182559	14.403747	08/13/2013
Huab	HR016	-20.183302	14.404315	08/13/2013
Huab	HR017	-20.18367	14.404911	08/13/2013
Huab	HUT017	-20.182037	14.334273	08/13/2013
Huab	HR018	-20.202934	14.338064	08/13/2013
Huab	HR019	-20.202934	14.338064	08/13/2013
Huab	HR20	-20.165295	14.448528	08/13/2013
Huab	HR20-DUP	-20.165295	14.448528	08/13/2013
Huab	HR021	-20.157238	14.51018	08/13/2013
Huab	HR023	-20.146151	14.533074	08/13/2013
Huab	HR022	-20.146173	14.533163	08/13/2013
Huab	HR024	-20.141357	14.543464	08/13/2013
Huab	HR025	-20.141487	14.543451	08/13/2013
Huab	HR026	-20.141195	14.543516	08/13/2013
Huab	HRT027	-20.139845	14.5535	08/13/2013
Huab	HRT028	-20.139689	14.553341	08/13/2013
Huab	HR029	-20.136083	14.549038	08/13/2013
Huab	HR030	-20.136022	14.549052	08/13/2013
Huab	HR031	-20.115515	14.581296	08/13/2013
Huab	HRT032	-20.030415	14.637739	08/14/2013
Huab	HR033	-20.032506	14.636162	08/14/2013

River Valley	Sample ID	Latitude	Longitude	Collection Date
Huab	HR034	-20.032668	14.637623	08/14/2013
Huab	HR035	-20.032604	14.637621	08/14/2013
Huab	HR036	-20.015134	14.699253	08/14/2013
Huab	HR037	-20.016598	14.699072	08/14/2013
Huab	HR038	-19.987458	14.743334	08/14/2013
Huab	HUW039	-20.045451	14.959787	08/14/2013
Huab	HUW040	-20.083642	15.058012	08/14/2013
Huab	HUW040-DUP	-20.083642	15.058012	08/14/2013
Huab	HRUW041	-20.203572	15.01257	08/14/2013
Huab	HUT042	-20.032105	15.000758	08/14/2013
Huab	HR043	-19.917306	14.951266	08/14/2013
Huab	HUW044	-19.916381	14.95135	08/14/2013
Huab	HUW045	-19.789397	14.846892	08/14/2013
Huab	HUT046	-19.679512	15.083747	08/14/2013
Huab	HUW047	-19.679125	15.083408	08/14/2013
Huab	HR048	-19.770347	15.236724	08/14/2013
Huab	HUW049	-19.769923	15.236462	08/14/2013
Huab	HUW050	-19.81966	15.506732	08/14/2013
Huab	HUW051	-19.649232	15.521795	08/14/2013
Huab	HUW052	-20.235793	15.419973	08/17/2013
Huab	HUW053	-20.256397	15.299108	08/17/2013
Huab	HUW054	-20.364602	15.093406	08/17/2013
Huab	HUW056	-20.466118	15.003305	08/18/2013
Huab	HUT055	-20.466563	15.002879	08/18/2013
Huab	HUT057	-20.532218	14.923915	08/18/2013
Huab	HUW058	-20.542423	14.916446	08/18/2013
Huab	HUT059	-20.624433	14.569288	08/18/2013
Huab	HUW060	-20.624975	14.569097	08/18/2013
Huab	HUW060-DUP	-20.624975	14.569097	08/18/2013
Huab	AH061	-20.545684	14.499276	08/18/2013
Huab	AH062	-20.545696	14.499259	08/18/2013
Huab	AHUW063	-20.523281	14.396719	08/18/2013
Huab	HR064	-20.348477	14.190616	08/18/2013
Huab	HR065	-20.348483	14.190604	08/18/2013
Huab	HR066	-20.485385	14.152857	08/19/2013
Huab	HR067	-20.485562	14.152808	08/19/2013
Huab	AH068	-20.461919	14.165661	08/19/2013
Huab	AH069	-20.461993	14.165596	08/19/2013
Huab	AH070	-20.461952	14.165237	08/19/2013
Huab	HT071	-20.433133	14.164267	08/19/2013

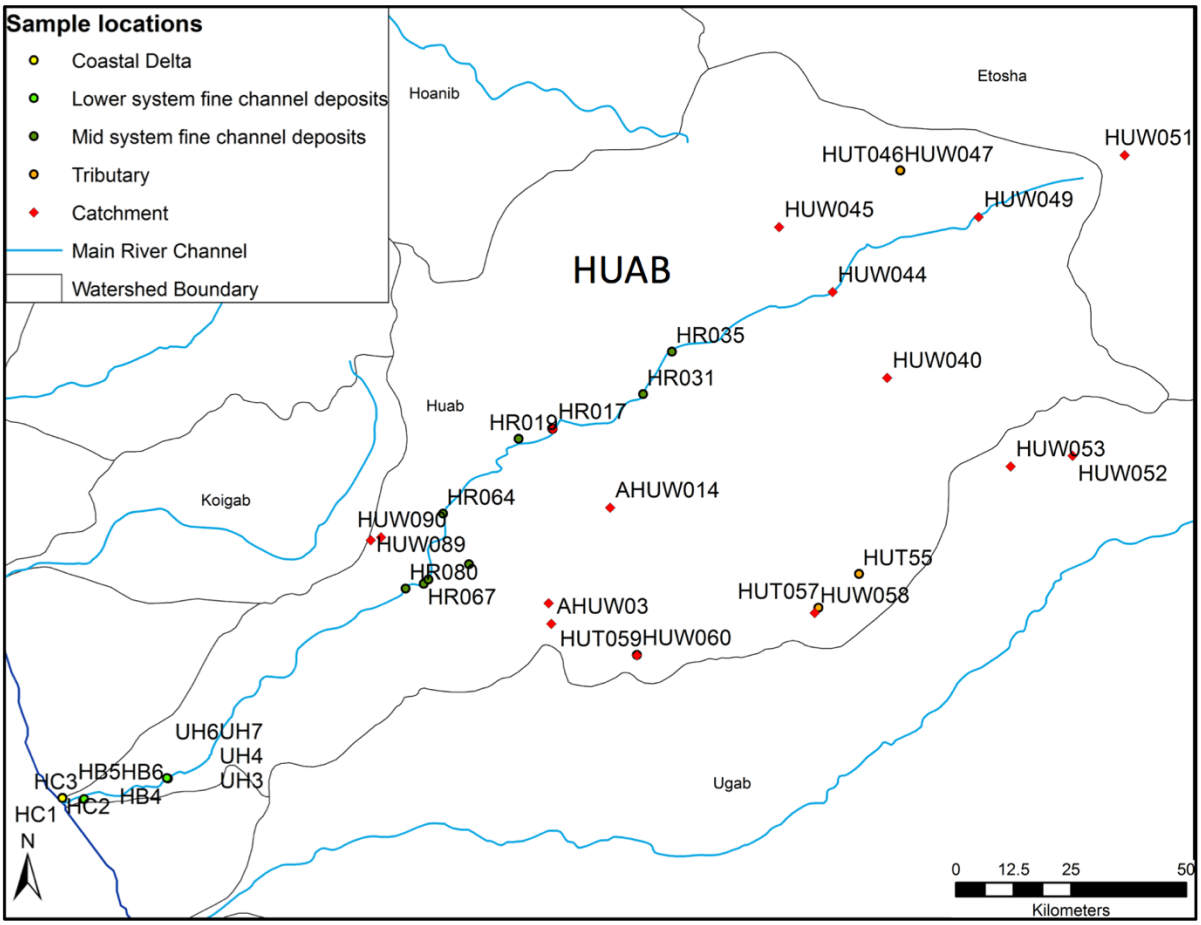
River Valley	Sample ID	Latitude	Longitude	Collection Date
Huab	HR072	-20.432238	14.164735	08/19/2013
Huab	AH073	-20.470959	14.181844	08/19/2013
Huab	AH074	-20.471357	14.181164	08/19/2013
Huab	AH075	-20.44755	14.241314	08/19/2013
Huab	AH076	-20.447492	14.241513	08/19/2013
Huab	HR077	-20.477033	14.162966	08/19/2013
Huab	HR078	-20.477372	14.162347	08/19/2013
Huab	HR079	-20.477384	14.162349	08/19/2013
Huab	HR080	-20.49479	14.117472	08/19/2013
Huab	HT081	-20.428628	14.085725	08/19/2013
Huab	HR082	-20.538101	14.035741	08/20/2013
Huab	HR083	-20.538068	14.035808	08/20/2013
Huab	HUT084	-20.538475	14.014764	08/20/2013
Huab	HUT085	-20.488955	14.020764	08/20/2013
Huab	HUT086	-20.464354	14.027182	08/20/2013
Huab	HUW087	-20.462414	14.029224	08/20/2013
Huab	HUT088	-20.456323	14.032815	08/20/2013
Huab	HUW089	-20.400292	14.049635	08/20/2013
Huab	HUW090	-20.394872	14.069866	08/20/2013
Huab	HR091	-20.86444	13.65073	18/09/2013
Huab	HR092	-20.89993	13.5092	17/09/2013
Huab	HR093	-20.89993	13.5092	17/09/2013
Huab	HR094	-20.89993	13.5092	17/09/2013
Huab	HR095	-20.90544	13.48993	17/09/2013
Huab	HR096	-20.90544	13.48993	17/09/2013
Huab (H1 transect)	UH1	-20.82413	13.730744	04/25/2013
Huab (H1 transect)	UH2	-20.824039	13.730794	04/25/2013
Huab (H1 transect)	UH3	-20.824033	13.730567	04/25/2013
Huab (H1 transect)	UH4	-20.822994	13.729961	04/25/2013
Huab (H1 transect)	UH5	-20.822994	13.729961	04/25/2013
Huab (H1 transect)	UH6	-20.822258	13.729867	04/25/2013
Huab (H1 transect)	UH7	-20.821186	13.7297	04/25/2013
Huab (H1 transect)	UH8	-20.821186	13.7297	04/25/2013
Huab (H1	UH9	-20.820911	13.729569	04/25/2013

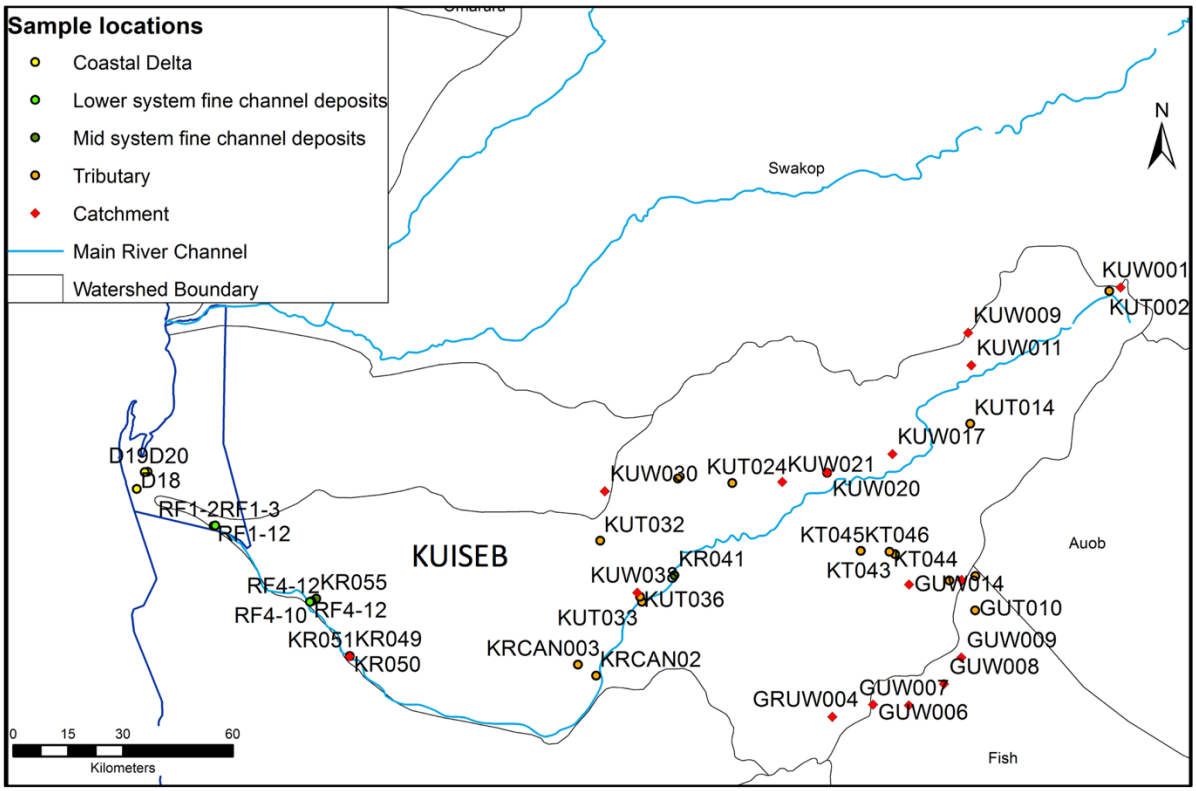
River Valley	Sample ID	Latitude	Longitude	Collection Date
transect)				
Huab (H1 transect)	UH10	-20.820911	13.729569	04/25/2013
Huab (H2 transect)	AWS1.1	-20.865619	13.653467	04/28/2013
Huab (H2 transect)	AWS1.2	-20.865397	13.653397	04/28/2013
Huab (H2 transect)	AWS1.3	20°51'56.54"S	20°51'56.54"S	04/28/2013
Huab (H2 transect)	AWS1.4	20°51'56.54"S	20°51'56.54"S	04/28/2013
Huab (H2 transect)	AWS1.5	-20.864658	13.651519	04/28/2013
Huab (H2 transect)	AWS1.6	-20.864658	13.651519	04/28/2013
Huab (H2 transect)	AWS1.7	-20.864611	13.651294	04/28/2013
Huab (H2 transect)	AWS1.8	-20.864611	13.651294	04/28/2013
Huab (H2 transect)	AWS1.9	-20.864561	13.651136	04/28/2013
Huab (H2 transect)	AWS1.10	-20.864539	13.651056	04/28/2013
Huab (H4 transect)	HB1	-20.897556	13.534142	04/26/2013
Huab (H4 transect)	HB2	-20.89755	13.534192	04/26/2013
Huab (H4 transect)	HB3	-20.897553	13.534258	04/26/2013
Huab (H4 transect)	HB4	-20.898353	13.534914	04/26/2013
Huab (H4 transect)	HB5	-20.900175	13.538033	04/26/2013
Huab (H4 transect)	HB6	-20.900242	13.538019	04/26/2013
Huab (H5 Transect)	G.1	-20.905484	13.489905	04/26/2013
Huab (H5 Transect)	G.2	-20.905497	13.489905	04/26/2013
Huab (H5 Transect)	G.3	-20.905299	13.489864	04/26/2013
Huab (H5 Transect)	G.4	-20.906431	13.489682	04/26/2013
Huab	G.5	-20.906622	13.489746	04/26/2013

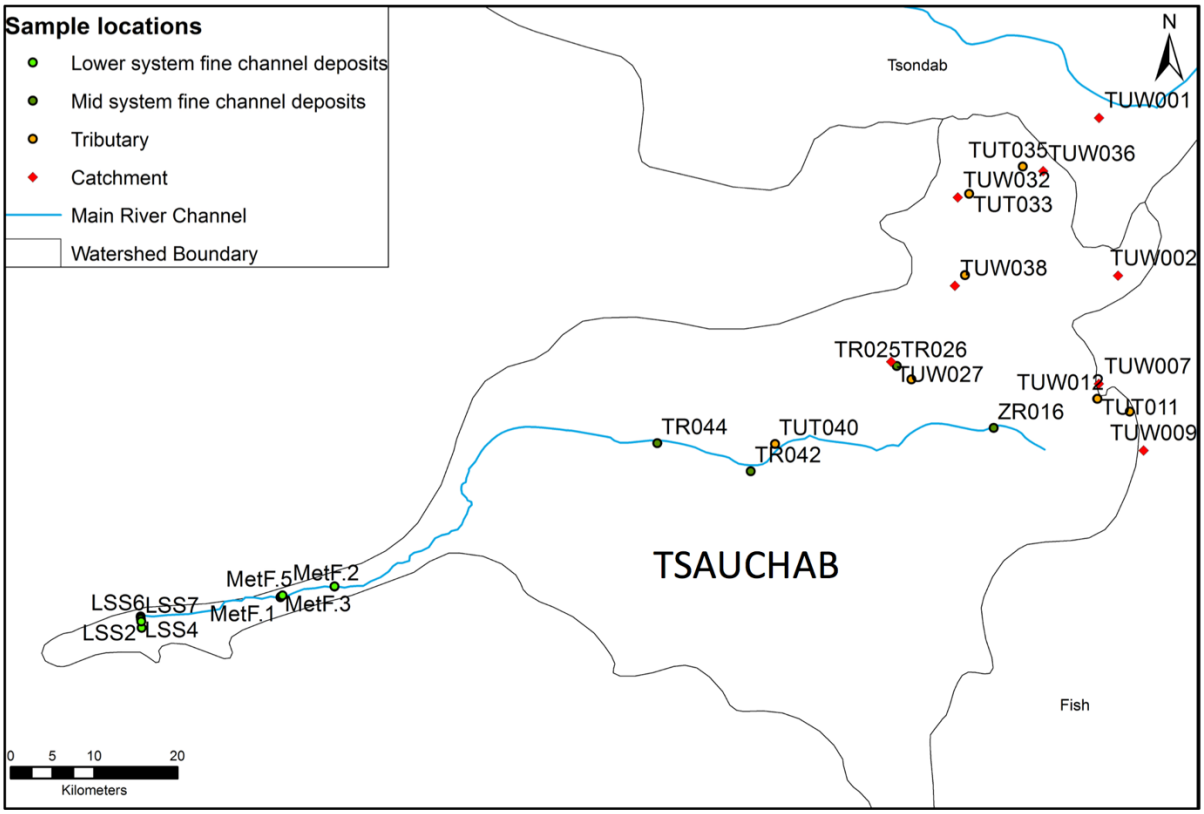
River Valley	Sample ID	Latitude	Longitude	Collection Date
(H5 Transect)				
Huab (H6 Transect)	HC.1	-20.903685	13.447185	04/28/2013
Huab (H6 Transect)	HC.2	-20.903685	13.447185	04/28/2013
Huab (H6 Transect)	HC.3	-20.903537	13.447341	04/28/2013
Huab (H6 Transect)	HC.4	-20.903409	13.447496	04/28/2013
Huab (H6 Transect)	HC.5	-20.903242	13.44774	04/28/2013
Tsauchab	TUW001	-24.179046	16.388642	08/22/2013
Tsauchab	TUW002	-24.349173	16.40899	08/22/2013
Tsauchab	TUT003	-24.351679	16.409152	08/22/2013
Tsauchab	TUT004	-24.361785	16.410734	08/22/2013
Tsauchab	TUW005	-24.366318	16.411241	08/22/2013
Tsauchab	TUT006	-24.433051	16.385612	08/22/2013
Tsauchab	TUW007	-24.465477	16.388428	08/22/2013
Tsauchab	TUT008	-24.495548	16.421776	08/22/2013
Tsauchab	TUW009	-24.537299	16.436693	08/22/2013
Tsauchab	TUT010	-24.481723	16.386649	08/22/2013
Tsauchab	TUT011	-24.481789	16.386681	08/22/2013
Tsauchab	TUT012	-24.481782	16.386751	08/22/2013
Tsauchab	TUT013	-24.495381	16.296798	08/22/2013
Tsauchab	TUT014	-24.495417	16.296856	08/22/2013
Tsauchab	ZR015	-24.513073	16.275027	08/22/2013
Tsauchab	ZR016	-24.51323	16.275112	08/22/2013
Tsauchab	ZRUW017	-24.514743	16.276186	08/22/2013
Tsauchab	ZR018	-24.521626	16.291179	08/22/2013
Tsauchab	ZR019	-24.521654	16.291113	08/22/2013
Tsauchab	TRT021	-24.46085	16.186395	08/22/2013
Tsauchab	TRT020	-24.460918	16.186313	08/22/2013
Tsauchab	TRT020-DUP	-24.460918	16.186313	08/22/2013
Tsauchab	TRT022	-24.458979	16.184562	08/22/2013
Tsauchab	TRT023	-24.459131	16.184471	08/22/2013
Tsauchab	TUW024	-24.459309	16.184622	08/22/2013
Tsauchab	TR025	-24.446376	16.170509	08/22/2013
Tsauchab	TR026	-24.446445	16.170583	08/22/2013
Tsauchab	TUW027	-24.441753	16.164587	08/22/2013
Tsauchab	TR028	-24.528469	16.070193	08/22/2013
Tsauchab	TR029	-24.529111	16.069774	08/22/2013

River Valley	Sample ID	Latitude	Longitude	Collection Date
Tsauchab	TR030	-24.530021	16.067744	08/22/2013
Tsauchab	TUT031	-24.265503	16.239989	08/23/2013
Tsauchab	TUW032	-24.264902	16.23633	08/23/2013
Tsauchab	TUT033	-24.261015	16.248558	08/23/2013
Tsauchab	TUW034	-24.237193	16.297421	08/23/2013
Tsauchab	TUT035	-24.231465	16.306459	08/23/2013
Tsauchab	TUW036	-24.236356	16.32828	08/23/2013
Tsauchab	TUT037	-24.348591	16.244112	08/23/2013
Tsauchab	TUW038	-24.360046	16.23319	08/23/2013
Tsauchab	TUT039	-24.530389	16.0394	08/23/2013
Tsauchab	TUT040	-24.5304	16.039335	08/23/2013
Tsauchab	TUT040-DUP	-24.5304	16.039335	08/23/2013
Tsauchab	TR041	-24.560081	16.01333	08/23/2013
Tsauchab	TR042	-24.559777	16.013309	08/23/2013
Tsauchab	TR043	-24.529253	15.912591	08/23/2013
Tsauchab	TR044	-24.529585	15.912539	08/23/2013
Tsauchab (T1 transect)	AWS3.01	-24.684657	15.564924	05/02/2013
Tsauchab (T1 transect)	AWS3.02	-24.68426	15.564845	05/02/2013
Tsauchab (T1 transect)	AWS3.03	-24.68411	15.564798	05/02/2013
Tsauchab (T1 transect)	AWS3.04	-24.684008	15.564767	05/02/2013
Tsauchab (T1 transect)	AWS3.05	-24.68392	15.564698	05/02/2013
Tsauchab (T1 transect)	AWS3.06	-24.683696	15.564722	05/02/2013
Tsauchab (T1 transect)	AWS3.07	-24.683426	15.564763	05/02/2013
Tsauchab (T1 transect)	AWS3.08	-24.683167	15.564766	05/02/2013
Tsauchab (T1 transect)	AWS3.09	-24.680696	15.56713	05/02/2013
Tsauchab (T1 transect)	AWS3.10	-24.680489	15.566838	05/02/2013
Tsauchab (T2 transect)	METF1AD	-24.695704	15.506436	05/04/2013
Tsauchab (T2 transect)	METF2AD	-24.69561	15.506484	05/04/2013
Tsauchab (T2 transect)	METF3AD	-24.695051	15.506872	05/04/2013

River Valley	Sample ID	Latitude	Longitude	Collection Date
Tsauchab (T2 transect)	METF4AD	-24.694574	15.507478	05/04/2013
Tsauchab (T2 transect)	METF5AD	-24.693603	15.508707	05/04/2013
Tsauchab (T3 transect)	LSS1	-24.7157	15.355565	05/03/2013
Tsauchab (T3 transect)	LSS2	-24.71632	15.355704	05/03/2013
Tsauchab (T3 transect)	LSS3	-24.71632	15.355704	05/03/2013
Tsauchab (T3 transect)	LSS3	-24.71632	15.355704	05/03/2013
Tsauchab (T3 transect)	LSS4	-24.716866	15.355784	05/03/2013
Tsauchab (T3 transect)	LSS5	-24.717192	15.355823	05/03/2013
Tsauchab (T3 transect)	LSS6	-24.719014	15.356085	05/03/2013
Tsauchab (T3 transect)	LSS7	-24.721644	15.356408	05/03/2013
Tsauchab (T3 transect)	LSS8	-24.723779	15.356778	05/04/2013
Tsauchab (T3 transect)	LSS9	-24.72458	15.356866	05/04/2013
Tsauchab (T3 transect)	LSS10	-24.728414	15.356882	05/04/2013
Tsauchab (T3 transect)	LSS11	-24.729553	15.356972	05/04/2013


Sample locations
Coastal Delta
Lower system fine channel deposits
Mid system fine channel deposits
Tributary
Catchment
Main River Channel
Watershed Boundary
Hoanib
Etosha
HUAB
Huab
Koigab
Ugab
HUW051
HUT046HUW047
HUW045
HUW049
HUW044
HR035
HR031
HUW040
HR019
HR017
HUW053
HUW052
HR064
AHUW014
HUW090
HUW089
HR080
HR067
HUT55
HUT057HUW058
AHUW03
HUT059HUW060
UH6UH7
UH4
UH3
HC3
HB5HB6
HB4
HC2
HC1
N
0 12.5 25 50
Kilometers


Sample locations
Coastal Delta
Lower system fine channel deposits
Mid system fine channel deposits
Tributary
Catchment
Main River Channel
Watershed Boundary
Swakop
KUISEB
Auob
Fish
N
KUW001
KUT002
KUW009
KUW011
KUT014
KUW017
D19D20
D18
KUW030
KUT024KUW021
KUW020
RF1-2RF1-3
RF1-12
KUT032
KT045KT046
KT043
KT044
KR041
KUW038
GUW014
RF4-12KR055
RF4-10
RF4-12
KUT036
GUT010
KUT033
KR051KR049
KR050
KRCAN003
KRCAN02
GUW009
GUW008
GRUW004
GUW007
GUW006
0 15 30 60
Kilometers


Sample locations
Lower system fine channel deposits
Mid system fine channel deposits
Tributary
Catchment
Main River Channel
Watershed Boundary
N
Tsondab
TUW001
TUT035
TUW036
TUW032
TUT033
TUW038
TUW002
TR025
TR026
TUW027
TUW012
TUW007
TUT011
ZR016
TR044
TUT040
TR042
TUW009
TSAUCHAB
MetF.5
MetF.2
LSS6
LSS7
MetF.1
MetF.3
LSS2
LSS4
Fish
0 5 10 20
Kilometers

Appendix 5 – Standard deviation table for duplicate samples as shown in Figures 23, 24, 25 and 26

Laboratory Duplicates							
Sample ID	**Mehlich P (ppm)**	**Fe (ppm)**	**NH4-N (ppm)**	**N03-N (ppm)**	**Total N (ppm)**	**Total P (ppm)**	**pH**
T9	18.90	4.52	2.31	1.00	541.18	292.34	-
T9 Lab Duplicate	19.50	4.62	1.91	0.93	-	-	-
TS3.5	61.30	37.35	14.80	6.10	2215.32	574.41	-
TS3.5 Lab Duplicate	62.90	38.25	13.95	5.83	-	-	-
H67/H68	54.00	28.79	32.60	4.60	1180.56	653.01	-
H67/H68 Lab Duplicate	59.10	29.71	30.17	4.07	-	-	-
HS4.4	79.40	17.67	0.89	17.05	250.57	618.86	-
HS4.4 Lab Duplicate	83.50	18.27	0.84	16.73	-	-	-
K40	9.94	4.79	0.50	2.70	140.58	414.26	-
K40 Lab Duplicate	10.30	4.56	0.40	2.22	-	-	-
K2	76.80	40.82	9.15	13.58	997.74	780.11	-
K2 Lab Duplicate	78.40	42.42	8.65	13.91	-	-	-
E6	3.16	0.99	0.88	218.58	606.48	203.99	9.93
E6 Lab Duplicate	3.39	1.17	0.57	216.20	577.38	206.41	9.92
SD720	59.60	0.60	26.85	196.04	1043.79	778.39	6.80
SD720 Lab Duplicate	60.60	0.55	26.62	193.95	1006.37	749.12	6.80
T3.1	7.64	4.24	1.04	1.87	223.86	273.99	9.47
T3.1 Lab Duplicate	7.39	4.06	1.59	1.75	180.17	260.40	9.52
G8	33.00	5.67	4.93	1.50	386.76	271.68	8.24
G8 Lab Duplicate	32.10	5.25	5.08	1.49	389.77	260.17	8.29
H80	66.70	54.71	37.38	12.54	1652.58	767.98	8.29
H80 Lab Duplicate	69.20	54.49	36.73	12.96	1518.78	719.52	8.16
K4.11	8.34	5.22	1.92	1.05	93.75	277.94	8.75
K4.11 Lab Duplicate	8.30	5.40	1.78	0.98	94.37	241.08	8.75
Standard Deviation between Laboratory Duplicates							
Sample ID	**Mehlich P**	**Fe**	**NH4-N**	**N03-N**	**Total N**	**Total P**	**pH**
T9	0.42	0.07	0.28	0.05	-	-	-
TS3.5	1.13	0.64	0.60	0.19	-	-	-
H67/H68	3.61	0.66	1.72	0.37	-	-	-
HS4.4	2.90	0.43	0.04	0.23	-	-	-
K40	0.25	0.16	0.07	0.34	-	-	-
K2	1.13	1.13	0.35	0.23	-	-	-
E6	0.16	0.13	0.22	1.68	20.57	1.71	0.01
SD720	0.71	0.04	0.16	1.48	26.46	20.69	0.00
T3.1	0.18	0.12	0.39	0.08	30.89	9.61	0.04

Laboratory Duplicates							
Sample ID	**Mehlich P (ppm)**	**Fe (ppm)**	**NH4-N (ppm)**	**N03-N (ppm)**	**Total N (ppm)**	**Total P (ppm)**	**pH**
G8	0.64	0.30	0.11	0.01	2.13	8.13	0.04
H80	1.77	0.15	0.46	0.30	94.61	34.26	0.09
K4.11	0.03	0.13	0.10	0.05	0.44	26.07	0.00

Field Duplicates							
Sample ID	**Mehlich P (ppm)**	**Fe (ppm)**	**NH4-N (ppm)**	**N03-N (ppm)**	**Total N (ppm)**	**Total P (ppm)**	**pH**
KUT027	56.80	4.45	7.70	7.64	446.52	674.45	7.98
KUT027 Field duplicate	58.80	4.80	7.00	8.83	432.18	770.43	7.93
KUW020	37.40	6.29	3.26	2.06	661.26	578.08	6.73
KUW020.2 Field duplicate	34.20	6.34	2.29	2.44	584.92	639.62	6.67
HUW040	28.00	3.50	3.90	6.20	535.55	134.44	7.60
HUW040.2 Field duplicate	23.90	3.31	2.34	4.10	412.70	182.42	7.97
HUW060	44.70	3.06	6.60	10.40	210.40	202.79	8.17
HUW060.2 Field duplicate	35.40	2.67	1.52	3.95	162.80	179.82	8.02
KR040	9.94	4.79	0.50	2.70	140.58	414.26	9.53
KR040.2 Field duplicate	9.62	4.82	0.64	2.29	145.08	670.74	9.48
Standard Deviation between Field Duplicates							
KUT027	1.41	0.25	0.49	0.84	10.14	67.87	0.04
KUW020	2.26	0.04	0.69	0.27	53.98	43.52	0.04
HUW040	2.90	0.14	1.10	1.48	86.87	33.93	0.26
HUW060	6.58	0.28	3.59	4.56	33.66	16.24	0.11
KR040	0.23	0.02	0.10	0.29	3.19	181.36	0.04